

Controlling Macromolecular and Supramolecular Architectures based on Poly(2-oxazoline)s



Victor R. de la Rosa

Controlling Macromolecular and Supramolecular Architectures based on Poly(2-oxazoline)s

by

Victor R. de la Rosa

Presented to the Faculty of Sciences, Ghent University,
in partial fulfillment of the requirements for the degree of

Doctor of Philosophy

Ghent University, December 2014

Promotor: Prof. Richard Hoogenboom



Controlling Macromolecular and Supramolecular Architectures based on Poly(2-oxazoline)s

The research presented in this thesis has been financed by the Bijzonder Onderzoeksfonds (BOF), Ghent University.

Members of the examination committee (*reading committee):

Prof. Dr. Richard Hoogenboom (Ghent University, BE)

Prof. Dr. Patrice Woisel* (University of Lille, FR)

Prof. Dr. Filip Du Prez* (Ghent University, BE)

Dr. Laetitia Mespouille* (University of Mons, BE)

Prof. Dr. Jan van Hest (Radboud Universiteit Nijmegen, NL)

Prof. Dr. Annemieke Madder (Ghent University, BE)

Prof. Dr. Bruno De Geest (Ghent University, BE)

Table of Contents

Chapter 1. Poly(2-oxazoline)s as versatile platform in biomedicine and supramolecular chemistry

1.1 Introduction: The inspiring power of nature	1
1.2 Poly(2-oxazoline)s	3
1.3 Poly(2-oxazoline)s as materials for biomedical applications	4
1.3.1 Biocompatibility of PAOx	6
1.3.2. Poly(2-oxazoline)s as polymer therapeutics	6
1.3.3 Hydrogels.....	12
1.3.4 Surface modification: controlling protein and cell adhesion.....	13
1.3.5 PAOx as matrix excipient for drug formulation	16
1.3.6 Conclusions.....	17
1.4 Smart polymeric materials	17
1.4.1 Lower critical solution temperature (LCST)	17
1.4.2 Thermoresponsive polymers.....	18
1.4.3 Smart systems based on polymers and supramolecular chemistry	24
1.5 Aim and outline of the thesis	29
1.6 References	31

Chapter 2. Controlling the hydrolysis of (co)poly(2-alkyl/aryl-2-oxazoline)s

2.1 Introduction.....	39
2.1.1 Hydrolysis of poly(2-oxazoline)s: kinetic considerations.....	42
2.2 Fast and accurate partial hydrolysis of poly(2-ethyl-2-oxazoline) into tailored linear polyethylenimine copolymers	43
2.2.1 Introduction	43
2.2.2 Synthesis and characterization of PEOx-OH.....	43
2.2.3 Accelerating PEOx hydrolysis: hydrolysis kinetics of poly(2-ethyl-2-oxazoline) at elevated temperatures	44
2.2.4 Controlling PEOx hydrolysis by variation of acid concentration.....	48
2.2.5 Conclusions.....	49
2.3 Enhanced Selectivity for the Hydrolysis of block copoly(2-oxazoline)s in ethanol-water resulting in linear poly(ethyleneimine) copolymers.....	51
2.3.1 Introduction	51
2.3.2 Synthesis of PAOx homopolymers and block-copolymers.....	51
2.3.3 Hydrolysis kinetics of homo poly(2-oxazoline)s	52

2.3.4 Hydrolysis kinetics of block copoly(2-oxazoline)s.....	55
2.3.5 Conclusions.....	57
2.4 Experimental Section	57
2.5 References.....	61

Chapter 3. Synthesis and micellization behavior of poly(2-oxazoline)-polycarbonate block copolymers

3.1 Introduction.....	63
3.2 Poly(2-ethyl-2-oxazoline) synthesis optimization.....	64
3.3 Synthesis of poly(2-ethyl-2-oxazoline)- <i>b</i> -poly(carbonate) copolymers.....	70
3.4 Poly(2-ethyl-2-oxazoline)- <i>b</i> -poly(carbonate) self-assembly	73
3.4.1 PEtOx ₂₄ - <i>b</i> -PC block copolymers.....	74
3.4.2 PEtOx ₄₃ - <i>b</i> -PC block copolymers.....	76
3.5 Conclusions.....	80
3.6 Experimental Section	81
3.7 References and notes.....	83

Chapter 4. Colorimetric Logic Gates Based on Novel Poly(2-alkyl-2-Oxazoline) Coated Gold Nanoparticles

4.1 Introduction.....	86
4.2 Synthesis and characterization of xanthate-functionalized poly(2-alkyl-2-oxazoline)s	87
4.3 Synthesis and characterization of poly(2-alkyl-2-oxazoline) coated AuNPs	89
4.4 Evaluation of the temperature responsiveness of poly(2-alkyl-2-oxazoline) coated AuNPs.....	94
4.5 Colirimetric logic gates based on poly(2-alkyl-2-oxazoline) coated AuNPs.....	98
4.6 Conclusions.....	99
4.7 Experimental Section	99
4.8 References.....	102

Chapter 5. Tuning temperature responsive polymers by supramolecular interactions

5.1 Introduction.....	104
5.2 Poly(2-ethyl-2-oxazoline)- <i>ran</i> -poly(2-nonyl-2-oxazoline) synthesis.....	106
5.3 Influence of different supramolecular hosts on the solubility properties of poly(2-ethyl-2-oxazoline)- <i>ran</i> -poly(2-nonyl-2-oxazoline)s.....	107
5.3.1 Cyclodextrins as supramolecular host molecules.....	107
5.3.2 Turbidimetry Experiments.....	109
5.3.3 Alpha-cyclodextrin	110

5.3.4 Effect of the Supramolecular Host: Hydroxypropyl-alpha-cyclodextrin, Hydroxypropyl-beta-cyclodextrin and Curcubit[7]uril.....	115
5.4 Influence of nonyl side chain content: poly(2-ethyl-2-oxazoline)- <i>ran</i> -poly(2-nonyl-2-oxazoline) containing 20% nonyl chains	120
5.5 Highly hydrophobic copolymers: poly(2-ethyl-2-oxazoline)- <i>ran</i> -poly(2-nonyl-2-oxazoline) containing 25% and 30% nonyl chains.....	123
5.6 Poly(2-ethyl-2-oxazoline)- <i>ran</i> -poly(2-nonyl-2-oxazoline): influence of polymer length.....	125
5.7 Conclusions.....	126
5.8 Experimental Section	126
5.9 References.....	129
Chapter 6. Solution Polymeric Temperature Sensors with Long-Term Memory Function	
6.1 Introduction.....	132
6.2 Poly(2-ethyl-2-oxazoline) ₆₂ - <i>ran</i> -poly(2-nonyl-2-oxazoline) ₂₉ synthesis	133
6.3 Poly(2-ethyl-2-oxazoline) ₆₂ - <i>ran</i> -poly(2-nonyl-2-oxazoline) ₂₉ host-guest complexation with hydroxypropyl-alpha-cyclodextrin.....	133
6.4 Poly(2-ethyl-2-oxazoline) ₆₂ - <i>ran</i> -poly(2-nonyl-2-oxazoline) ₂₉ host-guest complexation with hydroxypropyl-beta-cyclodextrins.....	139
6.5 A different polymeric supramolecular system: PNIPAM-naphtalene - Blue Box	144
6.6 Conclusions.....	146
6.7 Experimental Section	147
6.8 References.....	149
Conclusions and outlook	151
Nederlandse samenvatting	155
About the author	158
Publication list	159
Acknowledgements/Agradecimientos	161

Poly(2-oxazoline)s as versatile platform in biomedicine and supramolecular chemistry

1.1 Introduction: The inspiring power of nature

The ability of nature to achieve an immense number of complex tasks with an extreme level of precision and efficiency has always intrigued humanity. The strength of the silk in a spider web, the capacity of our eye lenses to change their focus (without a large number of moving parts, knobs and gearwheels, such as in any modern camera), or the ability of plants to obtain energy from sunlight, are some of the most typical examples that have fascinated mankind throughout history. With the advent of modern analytical techniques, and the advances in chemical and biological sciences during the last century, a deep understanding of the molecular components that make life and its marvels possible has been achieved, and now we are able to look deeper and deeper into the seemingly black box that used to constitute a living organism.

Every constituting cell of a living organism requires the production and transportation of energy, machinery, and to establish a logistics and communication network, both within itself and with its surroundings (see Figure 1.1.1). Moreover, the cell needs to store an enormous amount of information that describes how all these activities need to be done. In addition, these tasks need to be performed at the nanoscale, and in harmony with the other 10^{14} cells that, in the case of the human body, constitute the living organism. The success of nature is demonstrated by the ubiquity of life, that spans across the planet thriving in a wide variety of circumstances, even in apparently inhabitable environments.^[1]

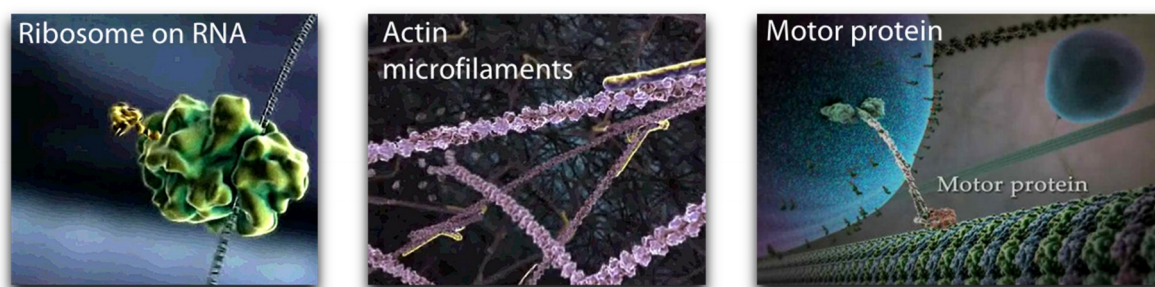


Figure 1.1.1. *Some examples of natural polymeric systems driven by supramolecular interactions. Ribosomes constitute an example of specific supramolecular host-guest interactions. Actin microfilaments are an example of a supramolecular polymer, and can be seen as the highways that*

Parts of this chapter have been published in:

de la Rosa, V. R. *J. Mater. Sci. Mater. Med.*, **2014**, *25*, 1211-1225.

de la Rosa, V. R.; Bouten, P. J. M.; Hoogenboom, R. *Macromol. Chem. Phys.*, **2012**, *213*, 2669-2673.

provide structure and organize the logistics of a cell. Motor proteins transport liposomes with a variety of cargos over the actin filaments connecting the different cell organelles, and constitute an example of responsive supramolecular interactions. Source: Harvard educational movie: The inner life of a cell (Qiagen Technologies).

After billions of years of evolution, the platform that nature has found to accomplish all the complex tasks required to sustain life is based on linear chains of poly(nucleotide)s, such as RNA or DNA, and poly(amino acid)s. Polymer chains, after all, make possible the construction of these complex architectures at the nanoscale, the molecular machines behind life, shaped by intermolecular forces, such as hydrogen-bonding, π - π stacking, dipole-dipole, Coulombic, or hydrophobic interactions. These structures interact with each other and with the environment through supramolecular forces, such as the docking process of a ribosome on an RNA strain, or the movement of a liposome transporting cargo across the cell through actin microfilaments (which themselves constitute an example of a supramolecular polymer).

It would be naïve for us to pretend the achievement of this level of control at the molecular level, especially considering the time frame in which nature developed these complex and fascinating systems. However, the expansion of technology and scientific knowledge is allowing us to translate this fascination into inspiration for the development of new materials able to take advantage of nature's strategies to perform complex tasks at the nanoscale. Following nature's steps, polymers, and their supramolecular interactions with other macromolecules, represent a good starting point for this new development.^[2] Recent progress in the development of controlled polymerization techniques has enabled the synthesis of well-defined polymers with almost any desired architecture, therefore allowing control on the resulting nanostructures.^[3] For instance, coming back to our first examples of nature's success stories, polymeric hydrogels have been used to construct microlenses with the ability to focus without the need of any moving part, but upon the application of external stimuli. Furthermore, the use of stimuli-responsive hydrogels has led to liquid lenses able to focus autonomously,^[4] with applications in sensing, medical diagnostics, and lab-on-a-chip technologies.^[5] In addition, the conversion of light into energy, exhibited by photosynthetic organisms, is also benefiting from polymer science, with organic solar cells based on conducting polymers, such as poly(thiophene)s, close to becoming cost-effective.^[6]

On the other hand, the information storage capability of poly(nucleic acid)s has been proposed as a real alternative in the near future for archiving large volumes of information that are now stored in a digital format.^[7] In addition, the development of molecular and polymeric logic gates, that perform the tasks allocated to transistors (the working principle of any computer), could signify a paradigm shift on how computers will operate in the future, especially when applied to life sciences.^[8-10]

There is therefore no doubt that nature is a powerful source of inspiration, especially for the chemist, to develop new materials with unprecedented properties. In the present thesis, we have focused our efforts in two main distinct, although interconnected, objectives. First, the control on the synthesis of polymers, in particular poly(2-oxazoline)s and polyethyleneimines, especially aimed for applications in the biomedical field, and the study of their self-assembly behavior in aqueous medium (Chapters 2 and 3). Specifically, the synthesized polymers may be utilized as drug and gene-delivery carriers for novel advanced therapies, as will be discussed in the next part of this chapter. Secondly, we have investigated the stimuli-responsive properties of poly(2-oxazoline)-based systems in aqueous medium, and their supramolecular interplay with other macromolecules in solution. These systems result in supramolecular logic-gates (Chapter 4) and sensors (Chapter 5) with, in some cases, the ability of storing information (Chapter 6). An overview

of the state-of-the-art regarding stimuli-responsive polymeric materials and their interplay with supramolecular chemistry is given in the second part of this introductory chapter.

1.2 Poly(2-oxazoline)s

Firstly reported in the 1960s by four independent research groups,^[11-14] the field of poly(2-oxazoline)s, or poly(N-acyl ethyleneimine)s, experienced a rapid growth, with a rush to publish that was extended during the 15 years thereafter. During the 1980s and 1990s, the research on poly(2-oxazoline)s decelerated just to experience a renewed growth at the dawn of the new millennium, together with the advent of novel research and application areas, especially in the biomedical field. Structurally similar to natural poly(peptide)s, poly(2-alkyl/aryl-2-oxazoline)s (PAOx) feature a backbone composed of tertiary amides that suppress interactions with proteins and, as a result, they are not recognized by the immune system. This so-called stealth behavior, together with their structural and functionalization possibilities, accounts for PAOx resurgence in the new millennium.

PAOx are readily obtained via the cationic ring-opening polymerization (CROP) of 2-oxazolines,^[15-17] as depicted in **Figure 1.2.1**.

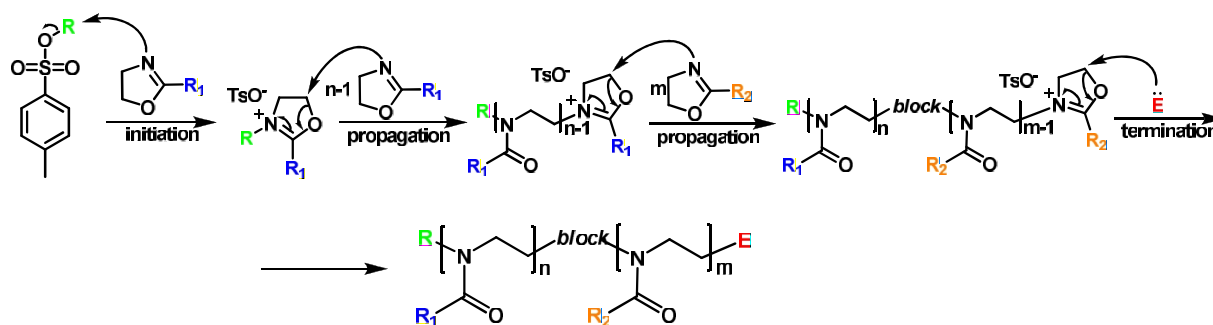


Figure 1.2.1. *Living Cationic Ring Opening Polymerization (CROP) of 2-oxazolines. Both alpha and omega termini can be functionalized by the selection of initiator (tosylate in the scheme) and terminating agent (a nucleophile). Well defined block copolymers are attainable by successive monomer addition, resulting in polymers with very low dispersity values (typically $\bar{D} = 1.05 - 1.30$).*

Telechelic functional polymers are accessible by selection of the initiator (alkyl halides,^[18] acid halides,^[19] (pluri)tosylates,^[20] (pluri)triflates,^[21] (pluri)nosylates,^[22]...) and terminating agent (a nucleophile)^[23-26] in a one pot fashion, while the side chains are tunable by modification of the 2-substituent of the 2-oxazoline monomer, allowing to control the hydrophilicity and lower critical solution temperature (LCST) behavior of the polymer (see **Figure 1.2.2**).^[27-31]

Furthermore, the living character of the CROP of 2-oxazolines allows the synthesis of well-defined statistical and block copolymers by sequential monomer addition in a one-pot fashion, and therefore the design of complex multifunctional architectures^[22, 32-38] and the tuning of the (thermo)responsive properties of the final polymer. These qualities situate PAOx in an exceptional position to become the basic tool for devising complex smart materials.^[39-48] In addition, the straightforward attachment of functional and reactive groups to both chain termini and to the polymer side groups, together with PAOx biocompatibility, makes this polymer class an ideal platform for the development of polymer therapeutics and biomaterials.^[49-52]

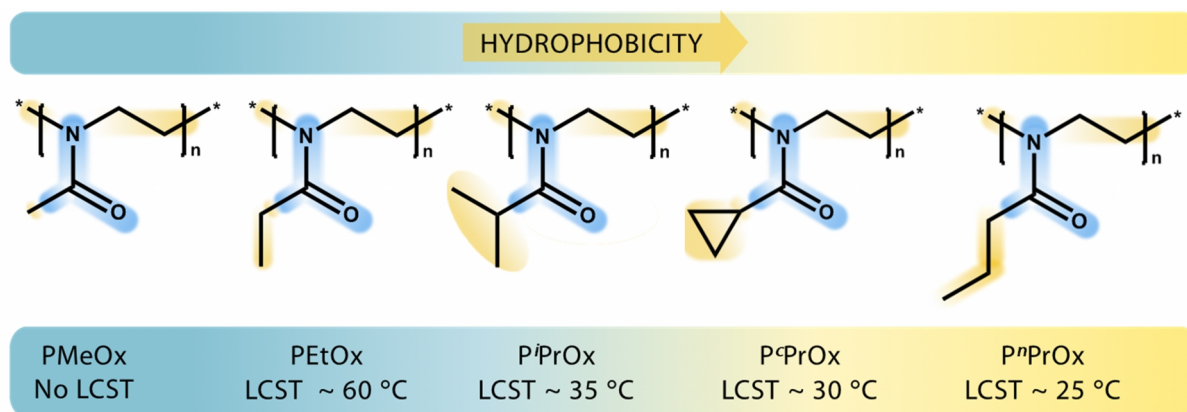


Figure 1.2.2. Series of poly(2-alkyl-2-oxazoline)s, displaying their amphiphilic character and their structural analogy to polypeptides. The lower critical solution temperature (LCST) can be finely tuned by copolymerization. P^oPrOx and PⁿPrOx are structural isomers and potential alternatives of poly(*N*-isopropylacrylamide) (PNIPAAm, LCST = 32 °C), considered as the gold standard of LCST polymers, especially for biomedical applications.

Finally, the use of microwave synthesizers^[32, 33] has revolutionized the polymerization of 2-oxazolines,^[34-38] reducing reaction times from hours to minutes or even seconds, and allowing for high-throughput combinatorial polymer synthesis^[39] and the subsequent exploration of structure–property relationships.^[29, 40, 41]

The next part of this thesis aims to summarize the most recent research on PAOx in biomedicine and life sciences, trying to give a global vision of PAOx as a platform for novel biomedical applications and materials, by highlighting the breakthroughs in the last years.

1.3 Poly(2-oxazoline)s as materials for biomedical applications

The last few decades have seen significant expansion of polymer chemistry into the biomedical field, as Staudinger and Ringsdorf already envisioned many decades ago.^[42-44] The interface between polymer science and medicine has evolved and expanded through a plethora of new scientific research areas such as polymeric biomaterials, tissue engineering, implant technology, and polymer therapeutics. The medicine of the new millennium requires selective and responsive materials that allow for personalized highly effective treatments. Conferring these features, typical of natural systems, to synthetic materials requires supramolecular platforms that provide a wide range of well-defined architectures and a high degree of functionalization.

Polymers constitute the platform of choice for this new development, especially since the advent of living and controlled polymerization techniques affording highly defined materials and offering the synthetic tools necessary to build the required complex systems.^[45-47]

In the framework of the proteomic era,^[48] polymers have been mainly utilized in combination with proteins for different medical applications, constituting the majority of the approved polymer-containing drugs to date.^[49] Poly(ethylene glycol) (PEG, or PEO) is the most widespread used polymer in biomedicine, being used mainly to increase half-life and immunogenicity of proteins,^[50, 51] and has had a tremendous impact^[52, 53] economically as well as clinically. Since the milestone approval of Adagen in 1990, a full dozen PEG-based products have been approved and are clinically in use today.^[54, 55] Although PEG remains the gold-standard in polymer based biomedical applications, based on its low dispersity (\bar{D}), biocompatibility and stealth behavior, it has some drawbacks and limitations. The development of anti-PEG antibodies has been

repeatedly observed in some patients,^[56, 57] including 25 % of patients never treated with PEG drugs (due to its ubiquity in cosmetics, and food additives), and is suggested to be responsible for the accelerated blood clearance of PEG conjugates after multiple injections.^[58-60] In addition, the polyether backbone of PEG is prone to oxidative degradation representing strong drawbacks especially for long term applications as antifouling surfaces for implants^[61] and probable induction of PEG-mediated complement activation has been recently reported^[62-64] (for comprehensive reviews on the drawbacks of PEG the reader is directed to Refs.^[65, 66]). In addition, the profuse number of patents protecting a variety of compositions and applications of PEG-based formulations hinders further research and development on novel therapies.

These PEG disadvantages are, however, strongly overwhelmed by its advantageous properties as evidenced by the large number of PEG-based biomedical products that have been approved by the U.S. Food and Drug Administration (FDA) and the European Medicines Agency (EMA).^[53, 65, 67] PEG's success has paved the way for the current development of the next generation of polymeric biomaterials, which have improved properties and greater versatility to meet the new challenges in medicine and the requirements in drug loading, responsiveness, and diverse architectural possibilities.^[68-70]

PAOx constitute a possible candidate to overcome the pitfalls of PEG while retaining the required features, such as biocompatibility, stealth behavior, low dispersity, responsiveness, high functionalization possibilities, and high versatility attainable by copolymerization, for a polymeric platform for novel biomedical applications.^[47, 71-74] In particular, poly(2-methyl-2-oxazoline) (PMeOx) and poly(2-ethyl-2-oxazoline) (PEtOx) have been demonstrated to be biocompatible and non-cytotoxic based on several independent *in vitro* cell viability and *in vivo* studies.^[75-78] PMeOx and PEtOx have similar stealth behavior as PEG^[79, 80] while offering advantageous properties such as thermo-responsiveness, low viscosity and high stability.^[75, 81]

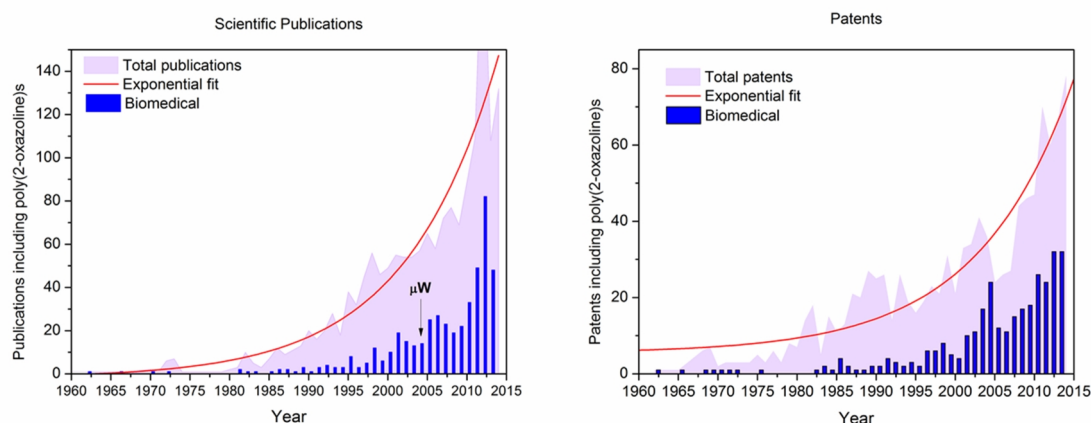


Figure 1.3.1. Number of scientific publications (left) and filed patents (right) on poly(2-oxazoline)s, indicating the introduction of the microwave-assisted synthesis of PAOx. An exponential increase in both scientific publications and patents is observed, especially in the ones related to the biomedical field which accounts for almost 50% of all patents filed during the last 10 years. (Source: Scifinder).

It is noteworthy that PAOx are experiencing an exponential growth in patent registration (see Figure 1.3.1) where the share of bio-related applications is increasing each year (over one-third of all patents involving PAOx in the twenty first century were related to biomedical applications, in contrast to a marginal fraction in the early 1990s). This blooming in patent registration has occurred while PAOx is still not approved by the FDA for medical purposes (currently, only PEtOx is approved by the FDA as an indirect food additive). Nevertheless, on view of the great potential

of this type of polymers, companies and research institutions are taking positions while the number of pre-clinical evaluations on effectiveness and toxicokinetics is growing. This extended body of data based on *in vitro* studies and subsequently on animal models is necessary to access the three-stage process implemented by the U.S. FDA and the EMA in the EU, that usually requires 5–10 years to be completed for a particular product. In fact, Serina Therapeutics Inc. (Alabama, USA) is, since its foundation in 2007, developing a drug-delivery system based on PAOx. Their main pipelines are directed towards new PAOx-based drug carriers for restless leg syndrome, cancer and Parkinson's disease, the latter imminently entering Phase I Clinical Trials.^[82] PAOx approval for medical use will definitely trigger an even more rapid development of PAOx-based biomaterials and their introduction in the market.

1.3.1. Biocompatibility of PAOx

PAOx constitute a versatile polymer platform that allows the construction of complex polymeric architectures with tunable physicochemical properties in a defined manner, representing an ideal candidate for biomedical applications. It is therefore of major importance to assess the biocompatibility of PAOx and their fate in the human body, especially since they are not biodegradable. Good cytocompatibility has been found *in vitro* for PAOx based polymers of different topologies,^[77, 81, 83, 84] while exhibiting similar stealth behavior as PEG due to their peptidomimetic structure.^[85, 86] In addition, PAOx exhibit significantly higher chemical stability as a result of the lower polarization of the *N*- vicinal C-H bond respect to the *O*- vicinal C-H bond present in PEG,^[87] rendering PAOx a potent alternative to PEG for long term applications such as coatings for sensors and implants, as reviewed in section 1.3.4.

Biodistribution studies with radiolabeled 5 kDa PMeOx and PEtOx have demonstrated very rapid blood clearance (mostly after the first renal passage) and remarkably low uptake in the organs of the reticuloendotheliary system.^[76, 88]

In vivo toxicity was assessed by repeated intravenous injections (rats) of 10 and 20 kDa PEtOx showing no adverse effects in the range of concentrations studied (from 500 to 2000 mg/kg), as reported by Viegas. *et al.*^[75] Furthermore, long term exposure to a PAOx-based hydrogel for intraocular drug delivery was recently demonstrated to maintain morphology and function in rabbit retina.^[89]

Although further in-depth research is still necessary, especially *in vivo*, to verify the safety of PAOx for clinical use, the available data is very promising and the excellent biodistribution profile of PAOx, together with their high chemical stability and versatility justifies their consideration as emerging polymeric platform for biomedical applications.

1.3.2. Poly(2-oxazoline)s as Polymer Therapeutics

The term "polymer therapeutics" encompasses polymeric drugs, polymer-drug conjugates, polymer-protein conjugates, polymeric micelles that serve as drug carriers, and polyplexes or non-viral vectors for gene delivery.^[49, 70, 90]

Due to their biocompatibility, architectural and functional diversity, PAOx have been explored as a polymer platform in all the fields of polymer therapeutics, as recently reviewed by Luxenhofer, Jordan *et al.*^[91] In view of this recent review, only a brief summary will be given here of the state of the art of PAOx as polymer therapeutics.

1.3.2.1. PAOx-Protein Conjugates

Protein therapeutics play a major role in medicine and continue their expansion since the first recombinant protein therapeutic, human insulin, was introduced 30 years ago.^[48] The main limitations related to the first generation of these biopharmaceuticals involve suboptimal pharmacokinetics, physicochemical instability, immunogenicity, short elimination half-life, and toxicity. Conjugation of the protein with PEG has demonstrated to be a successful strategy to overcome these issues and in fact led to the first polymer-based biopharmaceutical ever marketed (Adagen, as discussed earlier) being followed by other PEGylated proteins which have later become blockbuster drugs.^[51] The focus on PEGylation eclipsed further research on the development of PAOx-protein conjugates until the new millennium when PAOXylation has received a renewed attention. The PAOXylation of a number of proteins like trypsin, catalase, serum albumin, insulin or uricase has yielded conjugates with similar performance as PEGylated conjugates. Veronese *et al.*^[80] conjugated N-Hydroxysuccinimide (NHS) functionalized 5 kDa PEtOx to trypsin in order to assess the steric influence of the attached polymer chains to the enzyme activity towards substrates of different molecular weight. The activity of the conjugate was in line with analogous PEG-based conjugates, both partially losing activity towards large substrates. More recently, a similar synthetic strategy was applied for the conjugation of a series of model enzymes, namely uricase, catalase, and ribonuclease, observing conjugates that retained high enzymatic activity.^[75] In addition, the authors tested the ability of 5 and 10 kDa PEtOx and PEG to camouflage the immunogenicity of BSA in rabbits for a period of 72 days (see Figure 1.3.2a); both conjugates yielded significantly lower immunological response, especially for the larger conjugates, and slightly better performance for PEtOx over PEG. Furthermore, both *in vivo* activity and pharmacodynamics of PAOXylated proteins were studied by means of a PEtOx 10kDa insulin conjugate in rats (see Figure 1.3.2b). The conjugate lowered the blood glucose levels in a similar extent as free insulin but, whereas insulin activity reversed after 2h, PEtOx insulin kept the blood glucose lowering effect for 8 h, indicating that PEtOx protected insulin from rapid clearance and proteolysis.

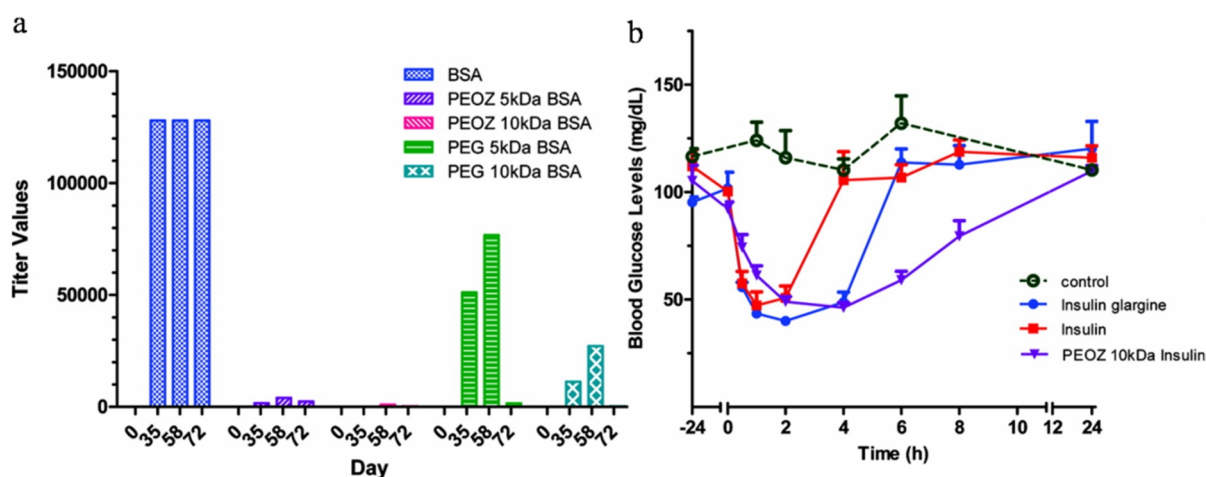


Figure 1.3.2. a) Relative immunogenicity of BSA, PEG BSA, and PEtOx BSA in rabbits treated as measured by anti-BSA antibody levels. Animals with treated with immune booster on days 1, 14, 28, and 42. PAOx had a slightly higher attenuation of BSA immunogenicity than PEG at each molecular weight tested. b) Effect of subcutaneous injection of insulin, insulin glargine, and PEtOx 10 kDa insulin on the blood glucose levels in male Sprague-Dawley rats (dose = 10 U/kg; n = 4; mean \pm SEM). (Adapted with permission from ref. ^[75]. Copyright 2011, American Chemical Society).

Mero *et al.*, studied the influence of the PAOx attachment site on the conjugate activity by conjugating 5 to 20 kDa PEOx to granulocyte colony stimulating factor (G-CSF) via a NHS-activated PEOx chemical strategy and an enzymatic mediated one, using TGase; the attachment site was determined to be the terminal amino group or the Gln-135 residue, depending respectively whether the chemical or the enzymatic mediated conjugation was used.^[92] Importantly, high biological activities of both conjugates were demonstrated both in vitro and in vivo (rats), regardless of polymer length and attachment site, supporting the utilization of PEOx as a substitute to PEG in protein conjugation.

To improve the efficacy of protein conjugates and enhance cellular delivery and transport of drugs, Kabanov *et al.* used a NHS synthetic strategy to conjugate amphiphilic PAOx copolymers to horseradish peroxidase (HRP) using both nondegradable and disulfide-bearing linkers that are cleaved in the reductive environment of the cytosol.^[93] The hydrophilic block was composed of PEOx or PEOx, whereas poly(2-*n*-butyl-2-oxazoline) (PBOx) constituted the hydrophobic block. P(MeOx-*b*-PBOx), and P(EtOx-*b*-BOx) conjugates retained up to 90% of the HRP activity while significantly enhanced cellular uptake was found in MDCK and Caco-2 cells (3 to 6 fold) compared to unmodified protein. Random copolymers and PEOx homopolymer conjugates did not increase cellular uptake, as the hydrophobic block appears to assist the transport of the lipophilic protein across the cellular wall. The straightforward synthesis of PAOx block-copolymers, allowing fast screening of different polymeric constructs, will certainly lead to the development of improved PAOx protein vectors in the future.

1.3.2.2. Vectors for gene delivery

Gene therapy has been regarded as the last revolution in medicine, to treat genetic inherited diseases, or acquired ones as cancer, being the first gene therapy already approved in the European Union.^[94] Viral vectors have demonstrated to be efficient gene carriers, although concerns about their in vivo side-effects have directed research towards safer alternatives such as polymeric systems for gene delivery, or polyplexes.^[95-97] Polyplexes are formed by interaction of a positively charged polymer with the phosphate anions present along the genetic material (see Figure 1.3.3), providing protection and enabling passage through the cell membrane.^[98, 99]

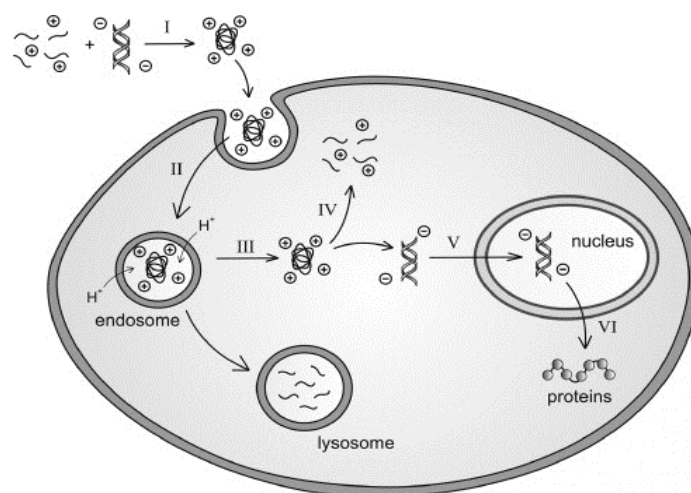


Figure 1.3.3. Barriers to gene delivery—Design requirements for gene delivery systems include the ability to (I) package therapeutic genes; (II) gain entry into cells; (III) escape the endo-lysosomal pathway; (IV) effect DNA/vector release; (V) traffic through the cytoplasm and into the nucleus; (VI) enable gene expression; and (VII) remain biocompatible. (Reprinted from ref.^[100] with permission of Elsevier).

Branched polyethyleneimine (PEI) has been regarded as the gold standard in gene transfection^[100]; however, high cytotoxicity has been found in vivo, hindering its broad application as non-viral gene carrier. Linear PEI has demonstrated to partially overcome the cytotoxicity issues of its branched counterpart^[101, 102] and it can be obtained in a facile manner from acidic or basic hydrolysis of PAOx.^[103, 104] Thomas, Klivanov, *et al.* used linear PEI obtained from the hydrolysis of commercial PEOx to deliver DNA to mice lungs with a 200-fold specificity; furthermore, the authors used the obtained polyplexes to deliver siRNA to treat influenza-infected mice reducing the virus titer by 94%, which is over the accepted 90% necessary to effectively cure a patient from a life-threatening infection.^[105]

Importantly, PAOx hydrolysis yields well defined PEI with diverse architectures, enabling the optimization of the resulting gene carrier,^[106] and the recent advances on PAOx selective and partial hydrolysis are expected to further expand the possibilities of PEI-PAOx copolymers.^[107, 108] Hsiue *et al.* connected partially hydrolyzed PEOx to a PEOx chain via a disulfide linkage, obtaining high levels of transfection to HeLa cells and strongly reducing the cytotoxicity related to pure PEI.^[109] However, higher polymer/DNA ratios were needed to form stable polyplexes. In a similar approach, Breunig and coworkers recently reported the synthesis of thiol-terminated PMeOx of different lengths that were used to build a library of redox cleavable PEI-SS-PEG block copolymers, and subsequently study their structure-property relationships as gene carriers. Nearly neutral, compact and stable polyplexes were obtained with PEI lengths of 3 kDa or more. The cytotoxicity of the polyplexes bearing long PEI blocks was partially circumvented by using high molecular weight PEG domains. Interestingly, when stable linkers were used to connect both blocks, the transfection ability of the polyplexes was lost, indicating that intracellular cleavage of the PEG domain is necessary for the transfection process.^[110]

A different strategy for obtaining protected polyplexes with low cytotoxicity was developed by Lümman *et al.* based on PMeOx grafted on poly(L-lysine) (PLL). Good transfection efficiencies were obtained in COS-7 cells at grafting densities around 10%, and the PLL-*g*-PMeOx-DNA condensates displayed excellent stability against serum and DNase digestion.^[111]

Finally, Grayson and Cortez recently synthesized circular PEI by cyclization of a propargyl initiated and azido terminated PEOx telechelic polymer and subsequent acid hydrolysis. Initial results show substantial improvement in gene transfection with cyclic PEIs in comparison with exact linear analogs, probably due to the increased charge density of the more compact circular polycation.^[112, 113]

1.3.2.3. PAOx-drug conjugates

Polymer-drug conjugates have been explored as a strategy to improve drug solubility, specific targeting by the inclusion of homing moieties in the polymer chain, especially interesting in regenerative medicine, or to improve cancer treatment by exploiting the enhanced permeability and retention (EPR) effect.^[114] In addition, different APIs can be incorporated into a single polymeric structure, allowing their simultaneous delivery to the target tissue, opening new horizons in the field of combination therapy.^[115] Moreover, polymer-drug conjugates create an added value to pre-existing pharmaceuticals, a very interesting outcome, also from an economical point of view.

The great opportunities offered by PAOx in the development of polymer-drug conjugates are mostly yet to be explored and only a limited number of examples can be found in literature (see ref.^[91]). Nevertheless, Serina Therapeutics Inc. has developed several PAOx-drug conjugates for Parkinson's disease and restless leg syndrome, in addition to folate-terminated PAOx bearing

anticancer drugs along the polymer backbone. These formulations are expected to enter clinical trials shortly, after very promising preclinical results.^[82]

1.3.2.4. PAOx-based micellar systems

Micelles formed by self-assembly of amphiphilic block copolymers have been extensively explored as drug carriers, an alternative to polymer-drug conjugates, and increasingly complex constructs can be found in literature.^[116-118] Micellar systems are advantageous since they have the capability of transporting high loadings of poorly soluble drugs, a challenge in cancer treatment; moreover, micelles can feature both passive and active targeting, as they accumulate in the tumor site by the EPR effect and also serve as a platform for targeting groups, as seen in Figure 1.3.4.

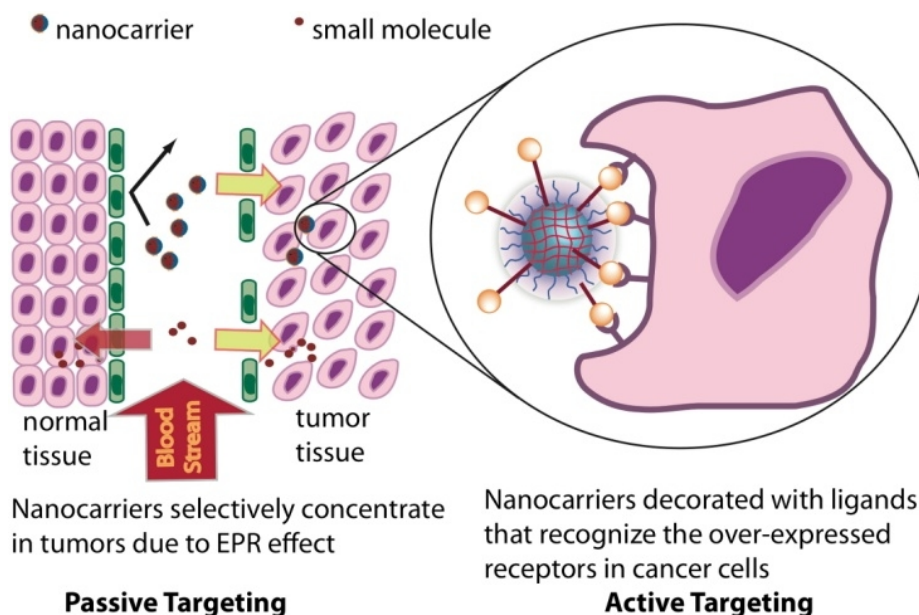


Figure 1.3.4. Representation displaying the concept of passive targeting through EPR effect and active targeting via inclusion of homing moieties (reprinted from ref.^[119] by permission of Elsevier).

The use of these nanocarrier systems thus increases blood circulation times and the overall efficacy of drugs, significantly lowering their side effects and the required administered quantities.^[120, 121] In addition, the cargo is not chemically bound to the polymeric system, and multiple drug or protein formulations can be loaded in a straightforward manner, facilitating combination therapy, personalized treatments, and simplifying regulatory approval matters since the cargo is not chemically modified.

PAOx permit high definition in polymer structure and composition, together with a straightforward synthesis of block-copolymers of finely tuned hydrophilicity,^[122, 123] thus allowing the rational design of micelles with controlled properties, such as size, critical micelle concentration, and drug release properties.

In a pioneering work, Meier and coworkers observed the formation of stable polymersomes in diluted aqueous solutions of PMeOx-PDMS-PMeOx ABA triblock copolymers, controlling the vesicle size from 50 to 300 nm.^[124] Similar copolymers were later utilized for the encapsulation of different proteins and drugs as trypsin,^[125] pravastatin^[126] or trypanosome vivax nucleoside hydrolase (TvNH).^[127] The authors turned the low permeability typical of polymersomes into an opportunity for reconstituting natural membrane proteins in the polymersome shell.^[128] In the first example, the membrane protein OmpF was embedded in a PMeOx-PDMS-PMeOx copolymer-based polymersome leading to a therapeutic nanoreactor capable to hydrolyze the prodrug 2-

fluoroadenisine and release 2-fluoroadenine, a cytotoxic molecule. Since its introduction,^[124, 127] this concept has been widely explored for diverse biomedical and/or biotechnological applications (see Figure 1.3.5).^[129]

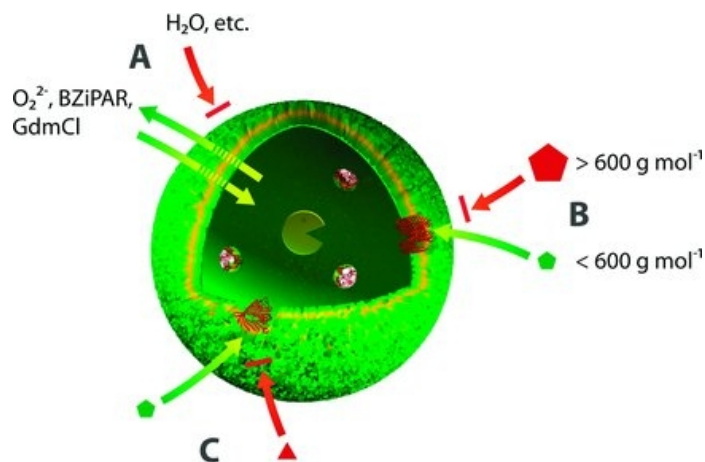


Figure 1.3.5. *Illustration of selective access to PMeOx-b-PDMS-b-PMeOx polymersomes. A) The membrane itself shows permeability to a small number of molecules only. B,C) Selective access into and egress out of the inner cavity can be achieved by reconstitution of membrane proteins in the block copolymer membrane. Most of the proteins give rise to size selective channels, e.g., OmpF (specific transport of nucleosides) (B), others are substrate specific, e.g., Tsx (specific transport of nucleosides and nucleotides) (C).*^[129] (Copyright Wiley, 2011)

Micelles formed by poly(2-phenyl-2-oxazoline) (PPhOx) as the hydrophobic domain together with PMeOx as hydrophilic part have been studied in detail,^[130, 131] and have been recently used by Tiller *et al.* as ABA-triblock copolymers for the development of large polymersomes that can be used to entrap functional molecules.^[123]

As discussed above, one of the most problematic issues in cancer treatment is the poor solubility of many very effective anti-cancer drugs and the need for combination therapy to effectively tackle tumors, and particularly the inherently resistant “tumor initiating cells”,^[132] requiring high capacity drug delivery vehicles. Kabanov, Luxenhofer and coworkers prepared a series of micelles comprising PMeOx and PBUOx as the hydrophobic block in an ABA-triblock copolymer architecture. Subsequently, the solubilization capacities of the micelles were tested with a number of well known, poorly soluble anti-cancer drugs; loading capacities as high as 17 wt. % were found for Cyclosporin A and Amphotericin B. Moreover, formulations entrapping Paclitaxel (PTX) could consist of up to 45 wt. % of the drug, reducing the amount of excipient used by nearly one order of magnitude in comparison with the clinically used formulation Abraxane™ and outperforming all alternative formulations. In addition, very low toxicity and complement activation was found *in vitro*.^[133] PBUOx appears to supply the right balance between hydrophobicity and polarity (from the amide group) to establish Van der Waals as well as dipole-dipole and hydrogen-bonding interactions with the polar moieties and H-bond donors of the drug molecules. Therefore, similar micelle compositions (P(MeOx₄₀-*b*-PBUOx₂₁-*b*-PMeOx₃₄), $\bar{D} = 1.14$) were used to prepare binary and ternary drug formulations for multidrug cancer chemotherapy. Some of the drugs explored were PTX, 17-allylamino-17-demethoxygeldanamycin (17-AAG), etoposide (ETO), and bortezomib (BTZ). Interestingly, the inclusion of various drugs as ETO or BTZ together with PTX or 17-AAG in the same micelle, enhanced the formulation stability and definition in comparison to single-drug loaded micelles. The drug loading capacities went up to 50 wt.%, and strong synergies were found dependent on the drug combination and ratios in MCF-7, PC-3, HepG2 and MDA-MB-231 cancer cells.^[134] The nature of the synergistic effects found is still not well understood and further research

will be necessary in order to optimize future multidrug formulations. In addition, the reported micellar systems still have not benefited from the versatility of PAOx synthesis, as the inclusion of targeting groups or stimuli-responsive domains would further increase the efficacy of PAOx-based micellar systems. For a recent summary of the drugs formulated in PAOx-based micelles, and other applications based on PAOx micellar systems see ref.^[91].

1.3.3 Hydrogels

Hydrogels typically are cross-linked polymeric materials capable of entrapping large amounts of water and feature characteristics that resemble those of biological soft tissues finding applications in controlled drug delivery or tri-dimensional tissue culture, and tissue engineering.^[135] PAOx allow total control over the polymer composition and reactive monomers can be located throughout the polymer chain affording, after cross-linking, the materialization of a pre-designed structure and architecture. This feature, together with the biocompatibility, stealth behavior, and stability properties already discussed, make PAOx ideal candidates for the development of hydrogels. Wiesbrock *et al.* prepared a series of 32 PAOx-based hydrogels allowing to finely tune the swelling degree while exhibiting for the first time stimuli-triggered compound release (see Figure 1.3.6).

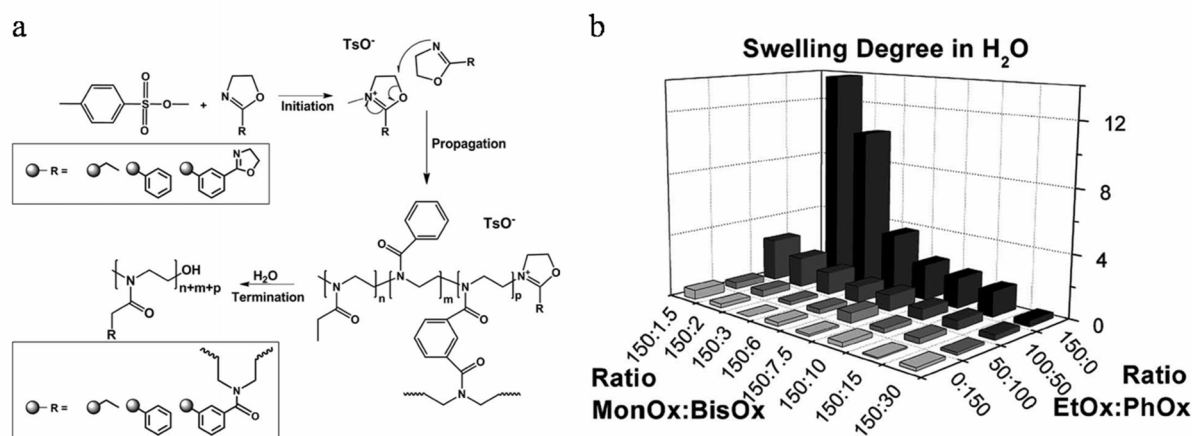


Figure 1.3.6. a) Mechanism of the living cationic ring-opening copolymerization of EtOx, PhOx, and PBO, yielding cross-linked hydrogels of the composition $pEtOx_m-pPhOx_n-pPBO_q$. b) Maximum swelling degrees of the 32 $pEtOx_m-pPhOx_n-pPBO_q$ -based hydrogels constituting the small compound library in water. (Adapted from ref.^[136] with permission of WILEY-VCH Verlag GmbH & Co. KGaA).

The library could be prepared in a straightforward manner by microwave polymerization of MeOx, PhOx, and a bifunctional oxazoline monomer.^[136] Recently, Dargaville, Hoogenboom and coworkers copolymerized MeOx or EtOx with 2-(dec-9-enyl)-2-oxazoline (DecEnOx), and subsequently formed a hydrogel with dithiol molecules by thiol-ene photochemistry. The authors incorporated a hydrolytically cleavable crosslinker obtaining degradable hydrogels, with potential applications in biomedicine.^[137, 138] Finally, Hsiue, Hwang and coworkers prepared a PEtOx-*b*-P(ϵ -caprolactone)-*b*-PEtOx that exhibited a reversible sol-gel transition between room temperature (sol) and physiological temperature (gel) and used it as intraocular depot of bevacizumab. The biocompatibility and biodegradability found make this hydrogel a potential candidate for a long term sustained drug release carrier.^[89]

Very recently, Gatt Technologies B.V.^[139] developed a tissue adhesive medical product based on PEtOx with side-chain NHS-activated esters.^[140] The PAOx based surgical tape benefits from PAOx structural versatility to tailor the strength, flexibility and degradability properties of the final product.^[141]

The main synthetic strategies available for obtaining PAOx-based hydrogels as well as a comprehensive overview of the recent literature can be found in refs.^[138, 142]

1.3.4 Surface modification: controlling protein and cell adhesion

Devices such as catheters, blood vessel grafts, pacemaker leads, artificial heart valves, vascular stents, joint implants, as well as haemodialysis, and oxygenator membranes have improved and enlarged the life of millions of people. However, bio-fouling of proteins, cells, or bacteria on the surface of such devices and implants represents a major healthcare problem and requires the use of prophylactic systemic medication and, in some cases, painkiller and antibiotic treatment.^[143] This negatively impacts the quality of life of patients while producing high costs.

Thus, there is a need for coatings that prevent infection, are not prone to biofouling, and render the device surface undetectable by proteins or microorganisms in a biological medium,^[144] also referred to as a “stealth surface”.^[145] Hydrophilic surfaces with low values of surface-water interfacial energy exhibit resistance to protein and microbial adhesion;^[146, 147] therefore, surfaces coated with hydrophilic polymers, mainly PEG, have been used for the development of stealth surfaces. PMeOx appears as a promising material in implant and biosensor technologies thanks to its biocompatibility, high hydrophilicity and superior chemical stability,^[75, 85, 87] a must in implant technology where PEG has showed important shortcomings, particularly for long-term *in vivo* applications.^[148, 149] Recently, De Geest, Hoogenboom *et al.* found that PEOx is stable towards hydrolysis in biological relevant conditions (acidic conditions and/or in the presence of enzymes) and furthermore the PEOx hydrolysis does not lead to breakage of the polymer chains. In addition, even up to 10% hydrolysis of PEOx yields polymers with no relevant changes in material properties nor cytotoxicity.^[150]

Different methods have been reported to attach PAOx to different surfaces conferring them their fascinating properties. The diversity of architectures, hydrophilicity levels, and functionalities offered by PAOx permits the development of antifouling and antimicrobial surfaces, responsive surfaces, or biosensors. Therefore *PAOXylation* of surfaces has a dynamic future ahead for devising novel medical implants and devices.

1.3.4.1 Not-covalently grafted poly(2-oxazoline)s

The first use of PMeOx to develop protein-repellent surfaces was explored by Textor, Konradi, Pidhatika *et al.* who grafted PMeOx chains to a poly(L-lysine) (PLL) backbone obtaining graft-copolymers that were subsequently deposited onto Nb₂O₅-coated silicon wafers by virtue of electrostatic interactions. The authors used a simple dip-and-rinse procedure, and characterized the surfaces by high-resolution X-ray photoelectron spectroscopy (XPS).^[151, 152] The formed PMeOx brush was repeatedly exposed to full human serum and no significant mass uptake was observed, indicating that protein adsorption was below the detection limit of the instrument (2 ng/cm²), equaling the excellent protein-repellent properties of the benchmark PEG. In a follow-up study, the authors improved the stability of the PMeOx-PLL linkage and demonstrated the microbial anti-fouling properties of the graft-copolymers (Figure 1.3.7).^[153]

The optimum polymeric composition was found to be PLL (20 kDa)-*g*-PMeOx (4 kDa) with a PMeOx grafting density of $\alpha = 0.33$, as the resulting thin film prevented adsorption of proteins as well as bacteria independently of the presence of fimbriae.

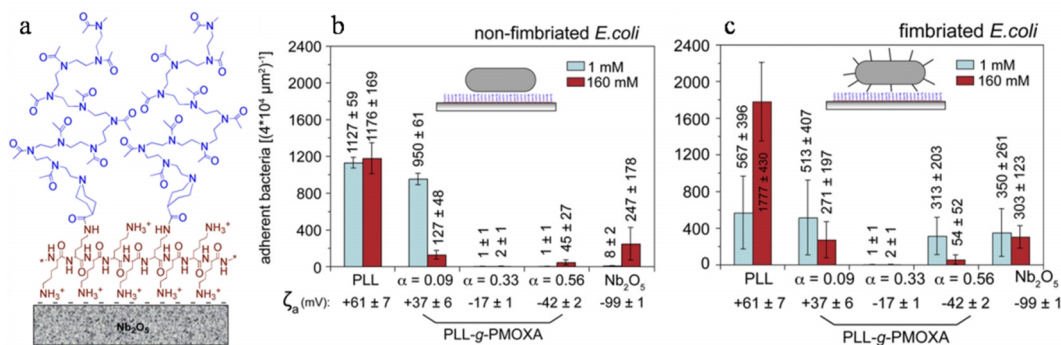


Figure 1.3.7. a) Scheme of the macromolecular architecture of PLL-g-PMeOx copolymer film assembled on a niobia surface. b) Average numbers of non-fimbriated and c) fimbriated *E. coli* bacteria adhered on 4 10⁴ mm² area after incubation in a protein-free buffer medium of either 1 mM or 160 mM ionic strength present on the different model surfaces: bare niobia and niobia coated with PLL and PLL-g-PMeOx with different grafting densities [PMeOx/Lys] ($\alpha = 0.09, 0.33, \text{ and } 0.56$). (Adapted from Ref.^[153] by permission of Elsevier).

While these studies demonstrated the outstanding performance of PMeOx as anti bio-fouling material, Pidhatika *et al.* recently reported a comparative study on the stability of PEG and PMeOx brush coatings.^[87] Upon exposure to physiological solution in presence of an oxidant (H₂O₂), PMeOx-g-PLL copolymer films were found to be very stable losing only 10-20% of the initial mass and remaining largely resistant to protein adsorption. In stark contrast, analogous PEG graft films revealed a large mass loss of 40-60% that strongly diminished their anti-fouling properties.

1.3.4.2 Covalently grafted poly(2-oxazoline)s

Another approach for the immobilization of PAOx on surfaces relies on covalent instead of electrostatic interactions to obtain more stable coatings for long-term implants. Rhe *et al.* explored the use of PEtOx (Mw ca. 400kDa) for the development of heart valves from biological sources. Ten different high molecular weight hydrophilic polymers were photochemically attached to glassy surfaces via UV irradiation of polymer-covered monolayers of a benzophenone derivative, and the final characteristics of the surfaces compared.^[154] PEtOx covered surfaces exhibited excellent surface coverage promoting the formation of a dense layer of healthy human endothelial cells. Consequently, very high molecular weight PEtOx covalently bound to biologic tissue constitutes a promising approach for achieving cellular coverage of biomaterials, as was confirmed in a further report.^[155]

PEtOx of diverse molecular weights were also photochemically immobilized by Wang, Yan, *et al.* to produce thin films as protein-resistant surfaces on silicon wafers and gold slides.^[156] Their method based on photocoupling with activated perfluorophenyl azide afforded surfaces with different thicknesses and sufficient grafting density to avoid unspecific protein adsorption. Furthermore, the use of amorphous PEtOx instead of semi-crystalline PEG facilitated the access to high quality thin films by spin coating used for the development of specific protein sensors.

Jordan and Ulman presented a more defined grafting-from polymerization method via surface induced polymerization using self-assembled monolayers (SAMs) as surface bonded initiation sites on gold surfaces.^[157] This approach affords a high grafting density on the surface and therefore was later utilized by Zhang, Jordan *et al.* for the modification of glassy and carbonaceous surfaces with highly crowded PAOx bottle-brush brushes (BBBs).^[158, 159] Firstly, the BBB backbone was formed by living anionic or free-radical polymerization of 2-isoprenyl-2-oxazoline (PIPOx). Next, by addition of methyl triflate, a poly(2-isopropenyl-2-oxazolium triflate) macroinitiator was obtained. Finally, the macroinitiator was used to polymerize various 2-oxazolines, affording the BBBs. This strategy

allowed the authors to screen the influence of polymer length, side chain composition, and end-group functionality on the antifouling capabilities of the modified substrate (see scheme in Figure 1.3.8a). While the end-group function had a slight effect on the protein-repellant properties of the coatings, the PAOx composition and chain length had a great impact on fibronectin (Fn) and cell adhesion. Hydrophilic PAOx with sufficiently long side chains ($m > 10$) rendered surfaces highly resistant to protein adsorption ($\leq 6 \text{ ng/cm}^2$), regardless of the surface, indicating that it was efficiently covered by the PAOx-BBB. To screen the initial cell adhesion properties of the PAOx-BBBs, coated surfaces were treated with Fn in PBS at pH = 7.4 and 37 °C, and subsequently seeded with Human Umbilical Vein Endothelial Cells (HUVEC). After being cultured for up to 24 h, the samples were fixed, stained, and examined by fluorescence microscopy as displayed in Figure 1.3.8.

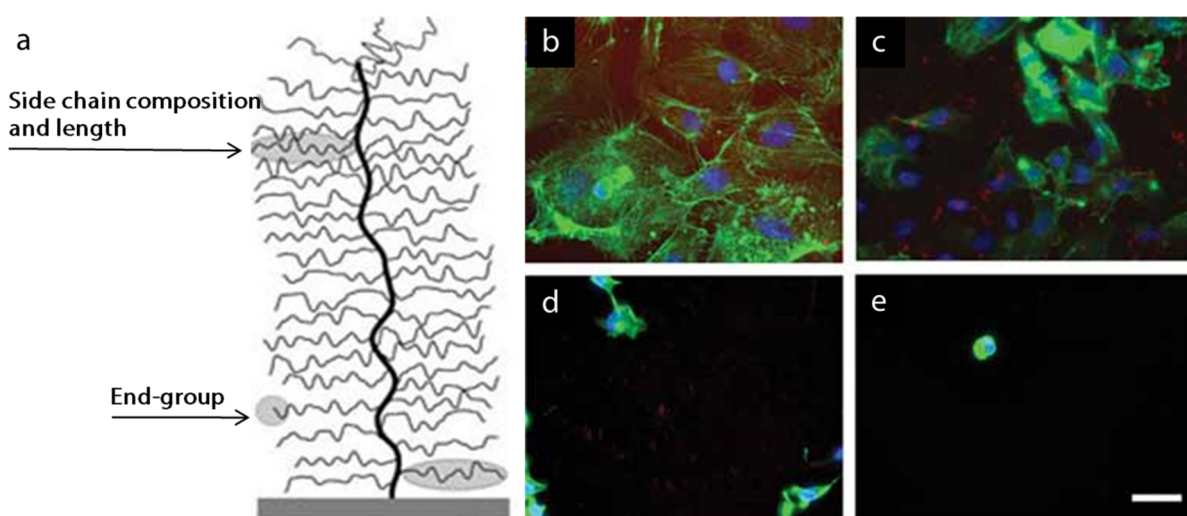


Figure 1.3.8. a) Schematic representation of the PAOx-BBBs. b-e) Examples of cell adhesion on the different PAOx-BBBs pre-exposed to Fn investigated by fluorescence microscopy. In correlation to the amount of adsorbed Fn, different degrees of cell adhesion can be observed: (b) very good cell adhesion with highly spread cells on P^rPrOx with more hydrophobic side chains, (c) reduced cell adhesion with fewer spread cells on P^{Me}Ox-Boc, (d) almost suppressed cell adhesion with few and mostly unspread or highly elongated cells on P^{Me}Ox-OH, (e) no cell adhesion on protein-repellent P^{Me}Ox. [Labeling: Fn (red), actin (green), and nuclei (blue). Scale bar: 50 μm]. (Adapted from ref.^[159] with permission of WILEY-VCH Verlag GmbH & Co. KGaA).

The lipophilic P^rPrOx-based BBBs (note that adhesion tests were performed at 37 °C, which is almost 20 °C above the P^rPrOx-BBB cloud point temperature) promoted the development of healthy cells, in contrast to the highly hydrophilic P^{Me}Ox that efficiently suppressed cell adhesion.

The novel preparation of thermoresponsive PAOx-BBBs in solution and the modulation of their cloud points^[27] augurs further developments in PAOx-based functional antifouling coatings that exploit the responsive behavior of this polymer class.

The so far reviewed systems are based on preventing protein and bacteria adhesion, and are referred to as biopassive coatings. However, PAOx have also successfully been used in the design of bioactive polymer surfaces that prevent microbial infection of the biomaterial by actively interacting with and killing bacteria.^[160-162] Waschinsky, Tiller *et al.* attached a *N,N*-dimethyldodecylammonium (DDA) biocidal moiety to a P^{Me}Ox chain with a polymerizable acrylate end group.^[163, 164] The activity against *Staphylococcus Aureus* was tested on a polymer-grafted surface, revealing that the P^{Me}Ox-based system kills bacteria in contact; no leaching of the

biocidal group was observed and activity was maintained even after 45 days of washing, constituting a promising approach for developing long-term stable antimicrobial surfaces.

To avoid overloading of the surfaces with bacterial debris and a loss of antibacterial activity, Bieser, Tiller *et al.* explored the development of self-polishing surfaces based on DDA grafted to a cellulose backbone *via* a PEtOx spacer. The biodegradable coating was applied to glassy surfaces exhibiting an antimicrobial efficacy of 99.9% against *S. Aureus* and degraded after application of the enzyme cellulase, expressed by many microorganisms, thus refreshing the surface when overloaded.^[165]

Agrawal, Rueda, Stamm *et al.* have recently proposed a grafting to approach for the development of PAOx-grafted brushes on silicon substrates. First, polyglycidyl methacrylate (PGMA) was spin-coated on silicon wafers as an anchoring layer and subsequently a thin film of carboxyl functionalized poly(2-isopropyl-2-oxazoline) (PⁱPrOx) was grafted on the surface (see Figure 1.3.9). The resulting PⁱPrOx brush was used for the stabilization of gold nanoparticles (Au NPs) to proof the usability of these PAOx-based brushes for the immobilization of inorganic NPs with great potential in sensing and biomedical applications such as in bio-implants.^[166, 167]

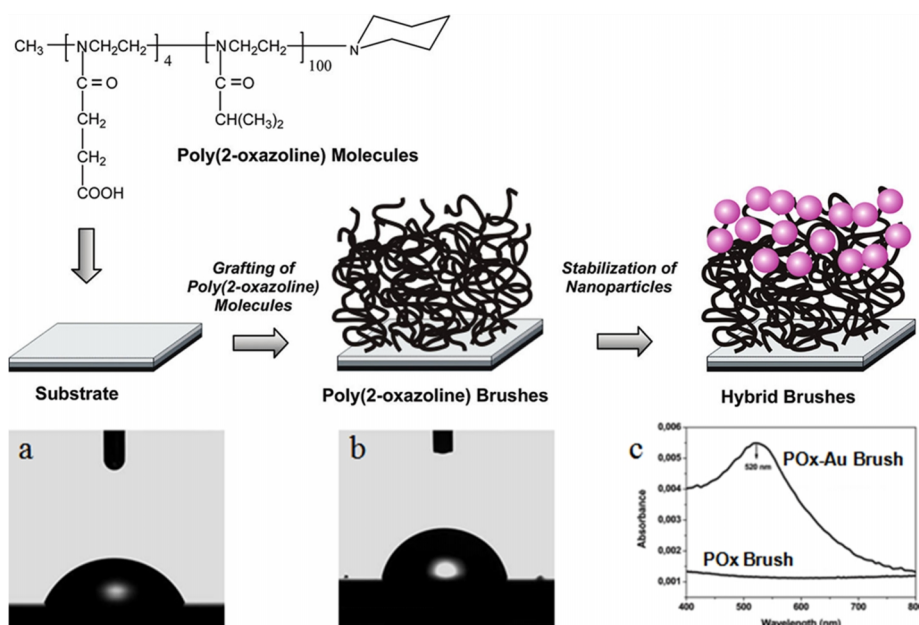


Figure 1.3.9. Top: Schematic Presentation of the Fabrication of Poly(2-Oxazoline) Brushes and Stabilization of NPs thereon. Below: Static water contact angle measurements on (a) PGMA coated and (c) PGMA and subsequently poly(2-isopropyl-2-oxazoline) brushes modified silicon wafers. c) UV-vis spectra of poly(2-isopropyl-2-oxazoline) brushes with immobilized Au NPs. (Adapted with permission from ref.^[168] Copyright 2012, American Chemical Society).

1.3.5 PAOx as matrix excipient for drug formulation

Recently, De Geest, Hoogenboom *et al.* explored the use of PEtOx as a matrix excipient to formulate drugs for oral dosage, as preliminary studies on the stability and toxicity of PEtOx in the gastrointestinal tract have been very promising.^[150] PEtOx with molecular weights ranging from 50 to 200 kDa were used to prepare solid solutions of drugs with different water solubility, decreasing the dissolution rate of hydrophilic drugs and allowing the complete uptake of hydrophobic ones, that otherwise only partially dissolve.^[169, 170] The dissolution rate could be reduced by increasing

the PEtOx molecular weight, opening the path towards optimized PAOx-based formulations that achieve the goal of near-linear, daylong drug release profiles.

1.3.6. Conclusions

The myriad of different possibilities offered by PAOx for devising materials that impact a broad variety of biomedical applications is unique for this polymer class. While waiting for regulatory approval, PAOx have already demonstrated excellent biocompatibility and stability properties in a large number of studies. Thanks to their structural and functional diversity, and the high control and definition that the CROP of oxazolines offers, they constitute a very attractive polymer class to serve as a platform for the development of polymer therapeutics and biomaterials. This is supported by the flourishing amount of academic research and patents being materialized in the last decade, together with the first commercial applications that are expected to enter clinical trials in the coming years.

1.4 Smart polymeric materials

In the past, the interest on materials was focused on the search of a composition that would confer the properties of interest (corrosion resistance, hardness, color...) to a certain device or machine, and would change as little as possible in time. If different properties were needed, then different materials were assembled together.

However, the paradigm is now evolving towards the search of materials that, far from being fixed and static, can actively perform tasks and adapt to the environment. The natural world is replete with examples of these materials, such as the bacterial flagellum that drives the bacterium towards the nutrients, our muscles which contract on release of calcium ions from the nerve terminals, or the lens that changes its focal length when your gaze shifts from the page to the horizon. All these systems are based on a combination of polypeptide chains or proteins. This kind of materials, that are able to respond or adapt to changes in the environment, has been regarded to as intelligent or smart materials. The key difference with any other artificial material that responds to environmental changes (such as the thermal expansion of a metal) is that smart materials react to changes by design. Responsive polymeric materials that undergo a phase transition in response to external stimuli are perhaps the smart materials with most parallels with natural systems, and they have attracted much scientific interest.^[171, 172]

The triggering event that induces the phase-changing event might be originated by a chemical or biological agent,^[173, 174] the rise or fall in temperature,^[175] electromagnetic radiation,^[176-178] pH,^[179-181] ionic strength,^[182, 183] the arrival of a magnetic^[184, 185] or electrical impulse,^[186] or the application of mechanical forces,^[187] to enumerate some examples. The specific response of the material can also be manifold, and changes can be induced in the surface properties of the material,^[174] its shape,^[188] its interaction with light,^[187, 189] or its solubility properties.^[190] In particular, thermoresponsive polymers, with the ability to respond to changes in temperature, have led to the development of a vast number of applications in areas spanning construction,^[191, 192] water management,^[193] separation sciences,^[194, 195] shape memory materials,^[196] and biomedicine,^[197] and allow the development of smart soluble materials or smart fluids. Most of such polymeric materials that undergo a solubility phase transition in response to a change in temperature exhibit a lower critical solution temperature (LCST).^[198]

1.4.1. Lower critical solution temperature (LCST)

The behavior of a polymer in solution reflects the balance of positive and negative interactions with the surrounding solvent molecules. In aqueous solutions, the role of solvent-solvent interactions is particularly strong, as a result of the partially ordered structure of water. The particularities of this solvent^[199] and its capacity to direct the conformation of the biological molecules are in fact responsible for the occurrence of life on Earth. Polymers exhibiting a LCST behavior establish a network of hydrogen-bonds with surrounding water molecules, that arrange around the polymer polar groups forming clathrate-like structures. The established hydrogen-bonds result in a favorable exothermic enthalpy contribution ($\Delta H < 0$), driving the dissolution of the polymer. However, the clathrate structures formed also lead to an unfavorable entropy of mixing (negative ΔS), term that increases its importance along with temperature. Beyond a certain critical temperature value, regarded as LCST, the entropic term predominates, and the difference in the Gibbs free energy (ΔG) becomes positive, resulting in phase separation.^[175]

$$\Delta G = \Delta H - T\Delta S$$

Equation 1.3.1.

Since the phase transition temperature depends on polymer concentration, a complete phase diagram of polymer concentration has to be measured to determine the LCST. In addition, the phase transition temperature is also dependent on the polymer molecular weight, usually being lowered with increasing polymer length.^[200] Nevertheless, in most cases polymer concentration is kept fixed, or varied within a small range, and therefore cloud point temperature (T_{CP}) values are reported. Figure 1.4.1 shows a representation of the temperature-induced phase transition of LCST polymers in aqueous solution.

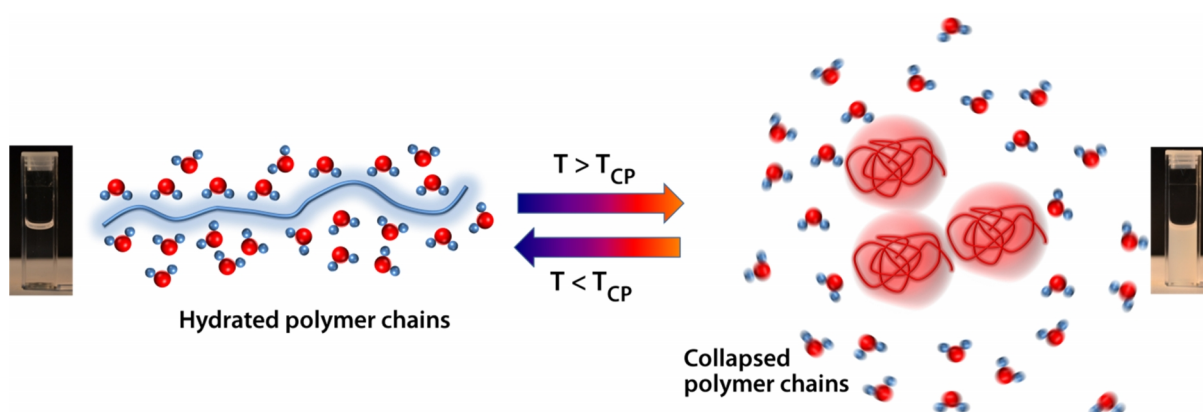


Figure 1.4.1. *Schematic representation of the lower critical solution temperature (LCST) reversible transition of polymers in water. At temperatures below the cloud point, the polymer chains are hydrated, resulting in a clear solution (left). Temperatures below the T_{CP} causes the entropy-driven hydrophobic collapse and aggregation of the polymer chains and the release of the solvation water molecules to the bulk water, leading to a cloudy solution (right).*

1.4.2 Thermoresponsive polymers

Polymers with LCST behavior exhibit a structural hydrophobic-hydrophilic balance consisting of polar groups, to establish hydrogen-bonding with water molecules, and apolar groups, to stabilize hydrophobic interactions in the polymer globular state.^[201, 202] Since the discovery of its thermoresponsive properties more than 50 years ago, poly(*N*-isopropylacrylamide) (PNIPAAm, LCST ≈ 32 °C) continuous being the most studied LCST polymer, mainly due to the robustness of its phase transition temperature that has low dependence on polymer length, concentration and

environmental pH.^[175, 203-205] Nevertheless, considering the high potential of these thermoresponsive materials, in combination with PNIPAAm drawbacks, there is a growing number of applications based on a variety of alternative polymers. PNIPAAm downsides are mainly related to its tendency to vitrify in the collapsed state, due to the formation of intramolecular hydrogen bonds, and its high glass transition temperature that result in hysteresis of its thermal solubility transition.^[206, 207] Among the alternatives investigated, polymers based on ethylene/propylene oxide (PEO-PPO, LCST \approx 20 - 85 °C,^[208] oligo(ethylene glycol) (meth)acrylates (OEG(M)A, LCST \approx 15 - 90 °C),^[209] *N,N*-diethylacrylamide (DEAM, LCST \approx 32 - 34 °C),^[210] methylvinylether (MVE, LCST \approx 37 °C),^[211, 212] *N*-vinylcaprolactam (NVCl, LCST \approx 32 °C),^[213, 214] 2-hydroxyalkyl (meth)acrylates (HE(M)A, HP(M)A)^[215, 216] and 2-alkyl-2-oxazolines^[29] are among the most widely studied.^[217] Considering the recent comprehensive reviews on thermoresponsive polymers, only a brief introduction on some selected polymers and applications will be given here.^[218, 219]

1.4.2.1 Tuning the polymer transition temperature

As has been previously indicated, the LCST behavior of a polymer relies on the subtle balance of hydrophobicity and hydrophilicity. Modification of this balance can then be used to manipulate the phase transition temperature, and therefore tune the LCST to the desired temperature value.

In particular, poly(oligo(ethylene glycol) (meth)acrylate)s (POEG(M)A)s consisting of a poly(meth)acrylate backbone with pendant oligo(ethylene glycol) side chains, allow easy tunability of the T_{CP} by variation of the number of ethylene glycol units.^[220] This has been shown for POEGMAs, where the T_{CP} can be tuned by variation of the polymer chain end functionality^[221] and, especially, by copolymerization of OEGMAs with short and long oligo(ethylene glycol) chains (that increase or lower the T_{CP} , respectively).^[222] Importantly, the low T_g of POEGMAs has been shown to suppress the hysteresis observed in the phase transition of PNIPAAm or PNVCl,^[223] which have a much higher T_g (\approx 140 - 150 °C), therefore presenting themselves as attractive alternatives to these widespread polymers for the design of smart materials.^[224]

Alternatively, poly(oligo ethylene glycol acrylate)s (POEGAs), exhibiting a more flexible and less hydrophilic poly(acrylate) backbone, have also been investigated as useful thermoresponsive polymers with tunable T_{CP} s, in analogy with POEGMAs. Indeed, copolymerization of oligo ethylene glycol acrylates with similar monomers such as hydrophilic hydroxyethyl and hydropropyl (meth)acrylates, and hydrophobic 2-methoxyalkylacrylates give access to copolymers with T_{CP} s tunable from 0 to 100 °C.^[215, 225]

Finally, as introduced in the beginning of this chapter, poly(2-alkyl/aryl-2-oxazoline)s (PAOx) exhibit high composition and structural versatility and allow straightforward functionalization.^[122, 226-229] PAOx permit the variation of the polymer side chain hydrophilicity by gradually tuning the length of the alkyl chain in the 2-oxazoline monomer.^[27-31] Whereas poly(2-methyl-2-oxazoline) (PMeOx) is a highly hydrophilic water soluble polymer, the extra methylene unit in the side chain of poly(2-ethyl-2-oxazoline) (PEtOx) already induces a LCST phase transition, at *ca.* 60 °C.^[230, 231] Polymers based on 2-propyl-2-oxazoline (PrOx) have become the most interesting for biomedical applications, as their T_{CP} is close to body temperature and can be easily tuned by variation of the propyl group structure (*i.e.* *n*-propyl, *iso*-propyl, and cyclopropyl) and as such have been extensively studied.^[232-235]

Combination of different 2-oxazoline monomers affords thermoresponsive PAOx with tunable LCST. For instance, copolymerization of EtOx and *n*PrOx results in PEtOx-*co*-P^{*n*}PrOx copolymers with transition temperatures tunable over the entire range from *ca.* 25 to 100 °C depending on the ratio of both monomers. Interestingly, the T_{CP} has a similar concentration dependence as that of

PNIPAAm and, due to the low T_g of these copolymers (< 45 °C) and the absence of intermolecular H-bonding in the collapsed state, no hysteresis is observed.^[29] In addition, similar control over the copolymer T_{CP} has been recently reported by combination of EtOx with Φ PrOx, that affords copolymers with higher T_g s in the range of 45 to 55 °C maintaining only a minor hysteresis (see Figure 1.4.2).^[31]

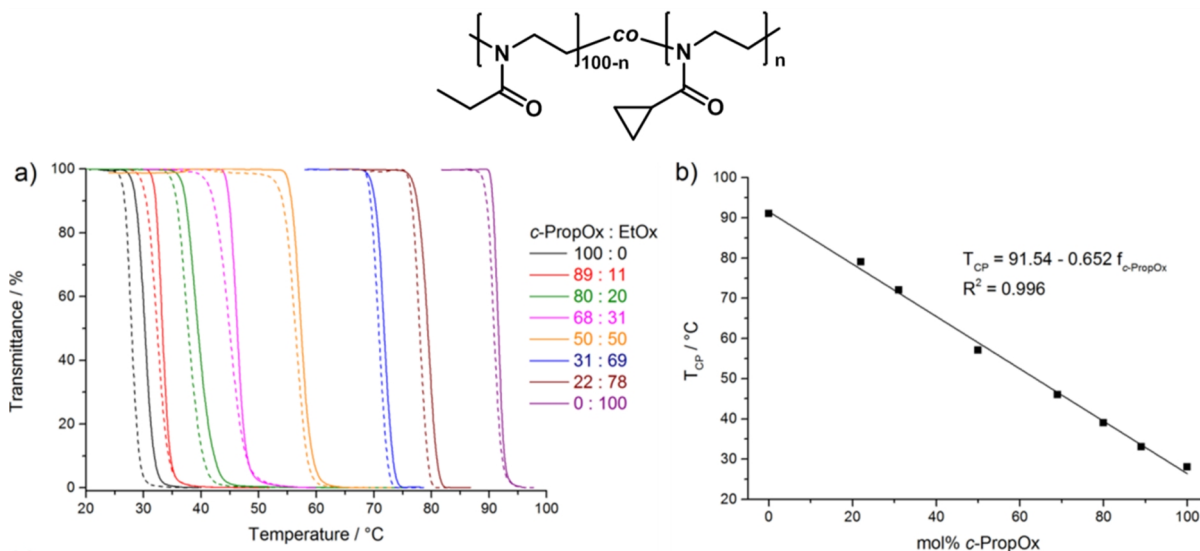


Figure 1.4.2. (a) Transmittance curves during heating (solid lines) and cooling (dashed lines) scans of *P*(Φ Pro PAOx-grad-EtOx) copolymers in milli-Q water at a concentration of 5 mg mL⁻¹ and a heating/cooling rate of 1K min⁻¹. (b) Relationship between cloud point temperature (T_{CP}), defined as point of 50% transmittance during second heating cycle, and copolymer composition.^[31]

1.4.2.2 Selected applications of thermoresponsive polymers

The most intuitive application of thermoresponsive polymers is the use of their phase transition as a means to measure the temperature in solution. Monitoring temperature variations at the cellular level will contribute to the improvement of the recently developed nanomaterials for targeted delivery of chemotherapeutics. Considering the low spatial resolution of conventional thermometers (up to 10 μ m), the development of molecular thermometers to be used as intracellular temperature mapping constitutes a field of great interest.^[236-238] In this context, Uchiyama *et al.* developed a fluorescent polymeric thermometer able to measure intracellular temperature fluctuations with a resolution of 0.18–0.58 °C within the range of 29–39 °C.^[239]

As seen in Figure 1.4.3, the sensor was based on three parts: a thermo-responsive poly-*N*-*n*-propylacrylamide (NNPAM) component, a fluorescent *N*-[2-[(7-*N,N*-dimethylaminosulfonyl)-2,1,3-benzoxadiazol-4-yl](methyl)amino]ethyl-*N*-methylacrylamide (DBD-AA), and an ionic potassium 3-sulfopropyl acrylate (SPA) component. The copolymer was prepared by free radical polymerization with AIBN as radical initiator. The mechanism of action of the thermometer is based on the fluorescence of the DBD-AA unit, that is quenched by neighboring water molecules. At higher temperatures, the PNNPAM sequence shrinks due to the LCST behavior of the polymer, resulting in the release of water molecules and strong fluorescence from the DBD-AA units. The ionic SPA moieties increase the hydrophilicity of the copolymer to prevent further aggregation within a cell. Temperature was determined by fluorescent lifetime spectroscopy, *i.e.* by correlating the fluorescent decay time of the dye. The temperature sensor provided insights on the different temperatures within the different cell organelles, that are also dependent on the current phase of the cell cycle.

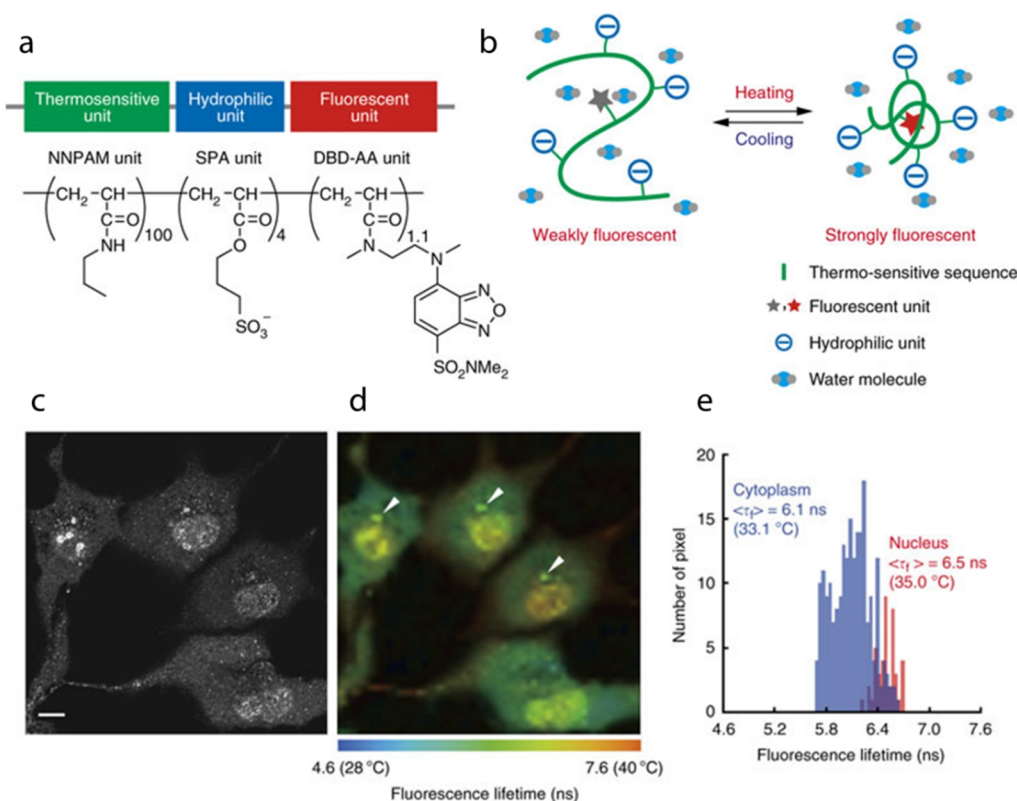


Figure 1.4.3. a) Chemical structure of the polymeric thermometer. b) Scheme representing the working mechanism of the thermometer. c) Confocal fluorescence image and d) fluorescence lifetime image of living COS7 cells with the polymeric thermometer. The standard error in determining the temperature was 0.38 °C. e) Histograms of the fluorescence lifetime in the nucleus and in the cytoplasm in a representative cell (the leftmost cell in a). As can be seen, the highest temperature was found in the nucleus of the cell. (Adapted from ref.^[239]).

Besides the simple coil-to-globule transition schematized in Figure 1.4.1, thermoresponsive polymers give rise to a wide range of nanoparticle architectures in solution, depending on their structure (homopolymers, block- or graft-copolymers, cross-linked networks, *etc.*) and composition. In addition, they can be grafted to surfaces, membranes, or particles, further expanding the application possibilities of the resulting smart-materials (see Figure 1.4.4). In the following, a brief introduction on this immense research topic will be given, highlighting some of the applications in which thermoresponsive polymers have proven their enormous potential.

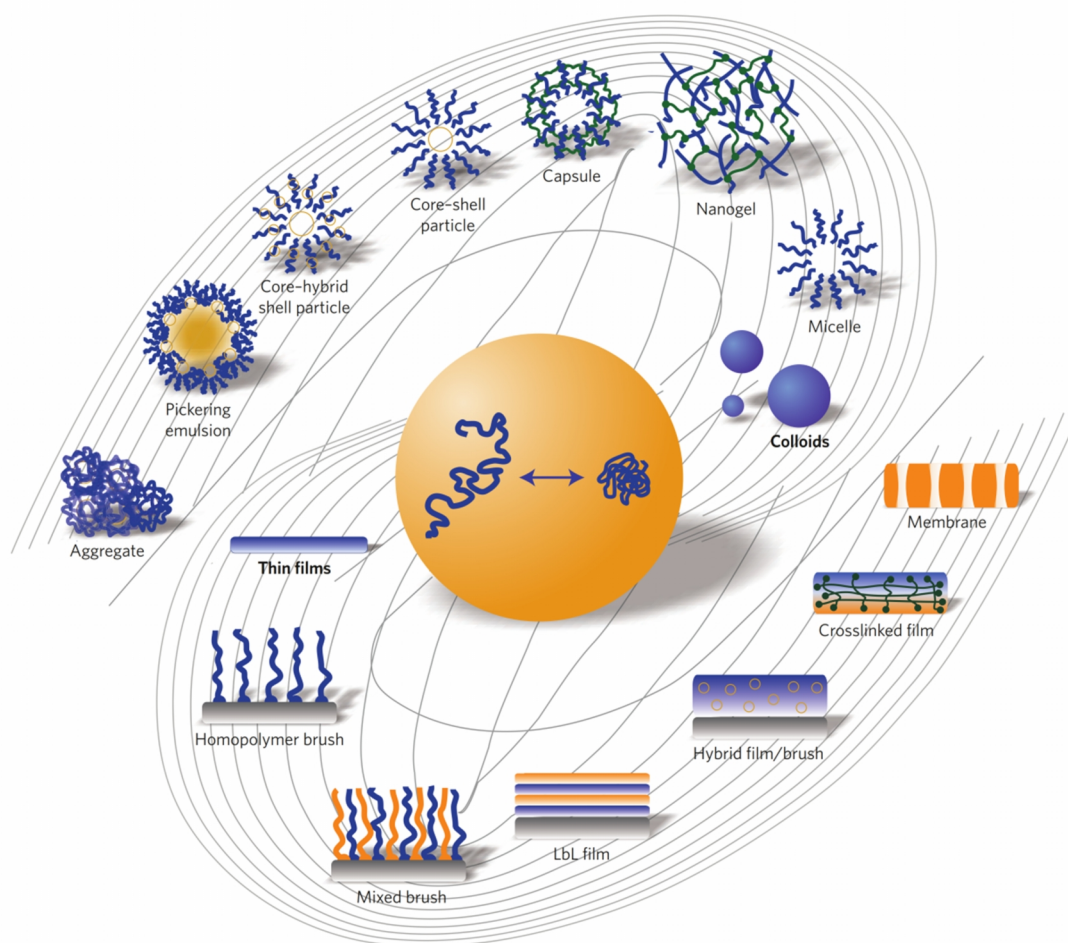


Figure 1.4.4. Overview of the wide range of nanostructured architectures based on stimuli-responsive polymer materials. These polymers can present themselves in polymer brushes, multilayered films made of different polymers, hybrid systems that combine polymers and inorganic particles, thin films of polymer network or hydrogels, or grafted on membranes that exhibit channels/pores. In solution, thermoresponsive polymers form nanoparticles such as micelles, nanogels, capsules and vesicles.^[171]

The combination of thermoresponsive polymers together with hydrophilic polymer domains, allows the conversion of the thermal stimulus into the formation of ordered self-assembled nanostructures in solution, as illustrated in Figure 1.4.5.^[197, 240]

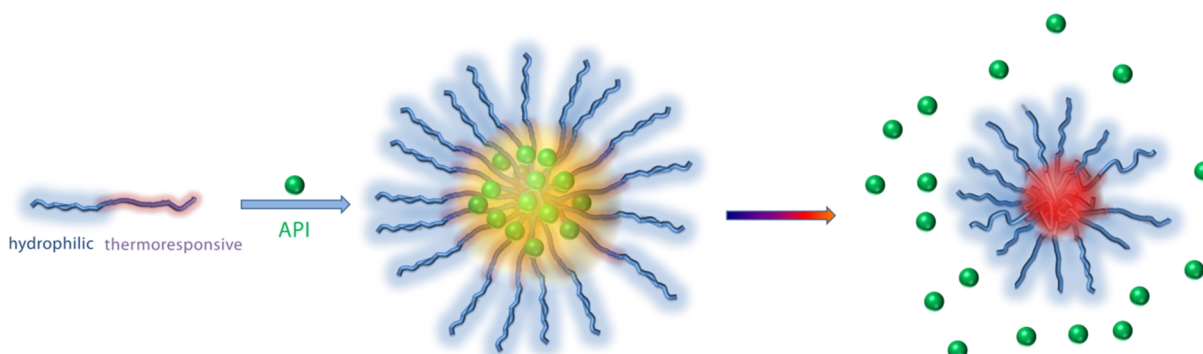


Figure 1.4.5 Schematic representation of the micelle formation of a copolymer containing both a hydrophilic and a thermoresponsive domain. A hydrophobic API can be loaded inside the micelle and its release profile governed by the environmental temperature.

The most common self-assembled structures are micelles and polymersomes, that find many applications in cosmetics and biomedical sciences.^[241] The active pharmaceutical ingredient can be loaded inside a micelle formed by copolymers containing a highly hydrophilic block and a thermoresponsive block. When temperature increases further beyond the T_{CP} , the thermoresponsive block further dehydrates into compact aggregates leading to a burst release of the API.^[242] These kind of responsive systems are of interest in cancer and targeted therapies, and examples include PNIPAAm-poly(lactic acid) (PNIPAAm-PLA) star-block copolymers loaded with methotrexate,^[243] and camptothecin,^[244] dexamethasone-loaded PLA-*g*-PNIPAAm-copoly(hydroxyethyl methacrylate),^[245] or doxorubicin-loaded PCL-*b*-PEO-*b*-PNIPAAm. Interestingly, the temperature-triggered doxorubicin release profile was proved to be controlled by the composition of the polymer.^[246]

An extra layer of complexity can be introduced by utilizing multiresponsive copolymers that exhibit two distinct LCST transitions that could be used for sequential release of several cargos with different affinities for each polymer domain. These systems have been developed based on poly(2-dimethylaminoethyl methacrylate) (PDMAEMA) together with PNIPAAm^[247] and P(NVCL),^[248] or with ethylene oxide based-polymers,^[202] and PAOx.^[28, 208]

The controlled-release profile enabled by thermoresponsive polymers has been applied in the development of polymeric hydrogels as controlled drug release matrices, allowing on-off release profiles in response to a stepwise temperature change.^[249] The drug is trapped in the cross-linked polymeric hydrogel, and is progressively released as the hydrogel volume contracts due to the temperature-induced collapse of the polymer.^[250, 251]

The volumetric contraction experienced by thermoresponsive polymers upon temperature-induced aggregation can also be used to control the permeability of membranes, or function as valves in microfluidic systems. As an example, Keurentjes *et al.*^[252] grafted PNIPAAm onto a poly(ethylene terephthalate) microfiltration membrane, resulting in a hydrogel graft layer. Since a UV-photografting method was used, both the location and amount of hydrogel could be tuned by the amount of cross-linker employed. A solution of bovine serum albumin (BSA) was stored in one side of the membrane, where the polymer chains grafted on the membrane pores hindered the diffusion of the macromolecule. Upon temperature increase beyond the T_{CP} , the PNIPAAm chains collapsed, opening the pores and allowing the passage of the BSA. As the polymer LCST transition is a reversible process, the membrane could be reversibly switched enabling controlled-delivery.

This technology is of great interest in the development of valves for smart microfluidic systems,^[253-255] as miniaturized pumps,^[256] or in liquid lenses with autonomous focusing,^[4] or sensors,^[257] with great potential in lab-on-a-chip technologies.^[258] The possibilities offered by thermoresponsive hydrogels thus assure a wide range of new applications based on these systems still to come.^[259]

The LCST transition of thermoresponsive polymers grafted to surfaces has also been exploited to tune the hydrophilicity of the surface, that remains hydrophilic at low temperatures and shifts to hydrophobic at temperatures beyond the LCST. This property has found great success in the development of cell-culture carriers^[260] that allow on-demand immobilization and release of bioactive molecules, and can be applied *e.g.* in the transplantation of cell sheets, which can be recovered without any defects.^[261, 262]

Finally, grafting of thermoresponsive polymers to noble metal nanoparticles has been found as an ideal manner to both stabilize the nanoparticle by the steric protection of the polymer brush, and also to translate the LCST transition of the polymer into a shift in the absorption band of the

nanoparticle,^[189] resulting in highly sensitive temperature and biological sensing systems.^[214, 263-265] In Chapter 4, we will implement this interesting property for the development of colorimetric logic gates based on thermoresponsive PAOx grafted onto gold nanoparticles.

In addition, the conjugation of photo-thermal or magento-thermal properties of the nanoparticles with the thermoresponsive properties of the polymer brush allows triggering the LCST transition by application of light or an oscillating magnetic field.^[266] This strategy has been applied for the *in vivo* targeted release of a drug cargo entrapped within the polymer brush upon application of non-invasive stimuli like near-infrared irradiation.^[267]

1.4.3. Smart systems based on polymers and supramolecular chemistry

As defined by Jean Marie Lehn almost 25 years ago, supramolecular chemistry, the chemistry beyond the molecule, is the designed chemistry of the intermolecular bond, just as molecular chemistry is that of the chemical bond.^[268] This relatively young area of science lays at the intersection of chemistry, physics and biology, and its wide horizons continue to be a source of challenges and inspiration for the chemist. Non covalent interactions are indeed the primary driving force of nature to direct the self-assembly of biomacromolecules into the wide variety of architectures that configure the world of the living organisms at the nanoscale. The incorporation of non-covalent interactions in synthetic polymer systems therefore appears as a powerful approach to confer qualities and properties typical of natural systems to artificial structures. The specificity of the enzyme lock and key principle can be mimicked via supramolecular interactions *via* host-guest chemistry enabling the control on the polymer structure and properties in a reversible and adaptive manner.^[269-276]

Hereby, we will discuss some of the recent advances of the combination of polymer and supramolecular chemistry to obtain thermoresponsive materials that benefit from interactions with other macromolecules resulting in responsive and adaptive smart materials. In view of the recent reviews available covering this fast growing field of research,^[277-281] only a brief introduction will be given here, with special emphasis on thermoresponsive polymeric systems modulated by supramolecular host-guest interactions.

1.4.3.1 Modulating polymeric architectures by supramolecular interactions

As previously seen in part 1.4.2, variation of the polymer structure by copolymerization or grafting allows the tuning of its solubility and self-assembly properties in solution. The incorporation of supramolecular host or guest moieties into a polymer offers a reversible handle for functionalization via non-covalent chemistry, affording adaptive and versatile structures. Inspired by nature's supramolecular systems, hydrogen-bonding, π - π stacking, dipole-dipole, Coulombic, or hydrophobic interactions have been utilized to direct the self-assembly of polymer chains in solution, and to modulate the polymer response to external stimuli.^[282, 283] In addition, the supramolecular information embedded in the host/guest moieties attached to the polymer chain enables specific molecular recognition that can be governed, just as natural systems, by the temperature, ionic strength, pH or other stimuli in solution.

In virtue of the reversibility of intermolecular forces, besides offering a high level of control on polymer conformation, supramolecular chemistry also offers the ability to switch it on demand.

Controlling the helicity of polymers, in analogy to poly(nucleic acid)s or poly(amino acid)s, affords materials of interest in data storage, optical devices, and liquid crystals for displays, and nicely illustrates the potential of combining polymer and supramolecular chemistry.^[284, 285] A nice example was developed by Kakuchi *et al.*, who synthesized a poly(4'-ethynylbenzo-15-crown-5)

conjugated polymer furnished with crown ethers that established host-guest interactions with several amino acids in a chloroform/acetonitrile (1/1, v/v) solvent mixture. These interactions directed the formation of a one-handed helical configuration of the polymer chains, as determined by circular dichroism, whose sense was dictated by the chirality of the amino acid guest. The formation of 2:1 crown-ether – amino acid host-guest complexes induces a conformational change in the polymer chain that modulates the binding affinity for further host-guest complex formation. This cooperative binding effect is directly related to the presence of multiple supramolecular moieties in a polymer chain, and is behind the interesting properties that arise when coupling polymers to supramolecular interactions. This recognition is manifested in this case by a sharp shift of the induced circular dichroism in the presence of the amino acid guest at $-30\text{ }^{\circ}\text{C}$, indicating host-guest complexation, and at $30\text{ }^{\circ}\text{C}$, indicating host-guest disassembly (see Figure 1.4.6). Interestingly, varying temperature allows to modulate the strength of the host-guest complex^[286] that, due to the cooperative nature of the binding, permits full on-off switching of the polymer chain chirality.^[287, 288]

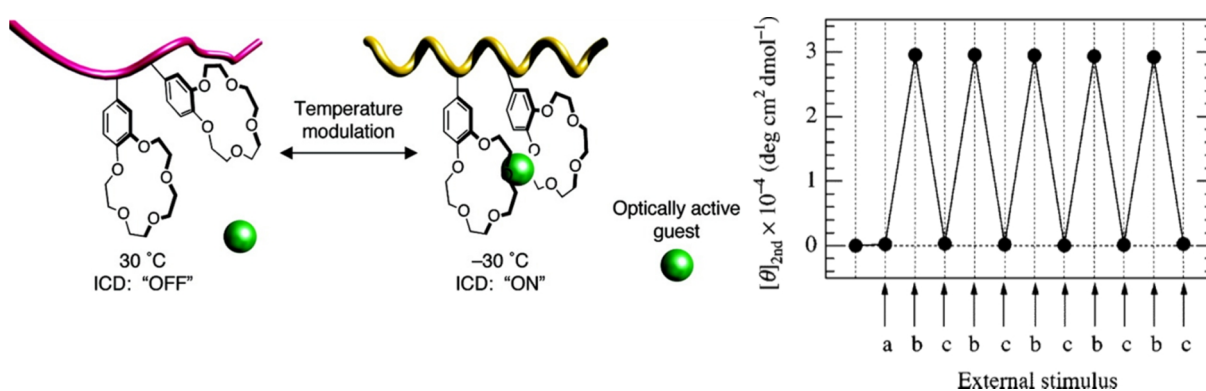


Figure 1.4.6. Left: Schematic illustration of the macromolecular helicity induction of poly(4'-ethynylbenzo-15-crown-5) driven by the host-guest complexation with an optically active guest (*l*-Phenylglycine) and the thermoresponsive on-off switching of an induced circular dichroism (ICD) based on the construction and collapse of the one-handed helical structure. Right: Plots of the $[\theta]_{2nd}$ values of the polymer upon continuous external stimuli. The first plot is the $[\theta]_{2nd}$ value for a polymer solution in chloroform/acetonitrile (1/1, v/v) at $30\text{ }^{\circ}\text{C}$. The stimuli (a–c) represent the addition of 1.0 equiv. of *l*-Pgly-HClO₄ at $30\text{ }^{\circ}\text{C}$ (a), changing temperature to $-30\text{ }^{\circ}\text{C}$ (b), and changing temperature to $30\text{ }^{\circ}\text{C}$ (c).^[288]

Other examples based on beta-cyclodextrin functionalized polymers have been reported, and allow for visual observation of the helicity changes with temperature, and in the presence of competitive guests.^[289]

The formation of graft and block copolymers through supramolecular chemistry represents a convenient methodology to modulate polymer self-assembly in solution, and to confer responsive properties to the nanostructures.^[290-292] Woisel, Cook *et al.* have demonstrated the potential of specific host-guest interactions to control micelle formation of a tetrathiafulvalene (TTF) end-functionalized PNIPAAm amphiphilic polymer.^[293] Using Nile red as a molecular fluorescent probe, the formation of micelles containing a TTF core was confirmed by fluorescence studies. The micelles could be disassembled by oxidation of TTF and, interestingly, by the addition of a suitable host macromolecule such as randomly-methylated beta cyclodextrin (RAMEB) or cyclobis(paraquat-*p*-phenylene) (CBPQT⁴⁺) that formed inclusion complexes with TTF rendering it hydrophilic. Micelles disrupted by the formation of TTF-RAMEB complexes could be reformed by addition of adamantanol as a competitive guest for RAMEB.^[294] Similar examples of micelle

formation/deformation by supramolecular interactions have been reported based on poly(2-oxazoline)s terminated with an alkylic chain as guest and cyclodextrins as host.^[295, 296]

A similar strategy was applied for the preparation of thermoresponsive double-hydrophilic di-block copolymers, by host-guest interaction between CBPQT⁴⁺ - terminated PNIPAAm and TTF-terminated PEG or poly(*N,N*-dimethylacrylamide) (PDMA). The formation of the supramolecular block copolymer was confirmed by 2D diffusion-ordered spectroscopy (DOSY) ¹H NMR spectroscopy, isothermal titration calorimetry. UV-Vis spectroscopy also proved the binding by the appearance of a green color and an absorption band at around 800 nm, both originated from the donor-acceptor interactions between the π -electron-deficient cavity of the CBPQT⁴⁺ unit and the π -electron-rich TTF moiety. Interestingly, the host-guest complexes, and thus the di-block copolymer structure, remained stable upon the temperature-triggered collapse of the PNIPAAm thermoresponsive domain.^[297]

As seen in the aforementioned example, the incorporation of suitable host and guest units in the polymer chain ends allows the straightforward formation of supramolecular block and miktoarm copolymers.^[279, 292, 298, 299] As an illustrative example, multiresponsive double hydrophilic block copolymers were formed *via* host-guest complexation between terminal beta cyclodextrin (β CD) and adamantane (AD) moieties present in PNIPAAm (β CD-PNIPAAm) and poly(2-(diethylamino)ethyl methacrylate) (AD-PDEA) homopolymers. The two homopolymers orthogonally self-assembled into supramolecular PNIPAAm-*b*-PDEA copolymers, as confirmed by 2D nuclear Overhauser effect spectroscopy (NOESY). The supramolecular copolymer exhibited a "schizophrenic" self-assembling behavior in aqueous solution. Specifically, at room temperature and pH < 6, it existed as unimers, whereas it formed PDEA core micelles with PNIPAAm coronas at pH > 8 due to the deprotonation of the PDEA block. Furthermore, vesicular nanostructures with collapsed PNIPAAm bilayers and solvated inner/outer PDEA coronas formed at temperatures above the LCST of PNIPAAm at pH 4. The thermo- and pH-induced morphological transitions were fully reversible.^[300]

In analogy to end-functionalized host/guest polymers, incorporation of supramolecular motifs across the polymer backbone render supramolecular graft copolymers with tunable micellization behavior.^[301-303] In addition, responsive hyperbranched polymeric structures and dendrimers can be realized by incorporation of multiple supramolecular moieties onto the polymer. Similarly as with other copolymer architectures, the assembly/disassembly of the hyperbranched structures can be controlled by the addition of a competitive guest,^[304-306] or other stimuli.^[307, 308]

1.4.3.2 Tuning polymer stimuli-responsiveness *via* supramolecular chemistry

Besides the impact on polymer morphology in solution, the combination of supramolecular hosts with thermoresponsive polymers allows to finely tune the polymer transition temperature. In addition, sensitivity towards additional stimuli can be introduced by using stimuli-responsive host-guest systems. Amphiphilic host molecules, such as cyclodextrins, featuring a hydrophilic outer shell and a hydrophobic cavity, complexate with hydrophobic guests present in a thermoresponsive polymer, thereby increasing its T_{CP} . Many examples have been reported on complexation of cyclodextrins with end-group functionalized thermoresponsive polymers, including PNIPAAm-azo dye,^[309] PNIPAAm-vinylcyclopropane,^[310] or poly(*N,N*-diethylacrylamide)-4-alkylphenol with methylated β CDs.^[210] As expected, T_{CP} variations were found to be dependent on the excess of cyclodextrin host added, and typically increased by less than 5 K, although a T_{CP} increase of close to 10 K was observed in a *tert*-butyl phenyl-terminated poly(*N,N*-diethylacrylamide) (PDEAAm) thermoresponsive polymer in the presence of 2 equivalents of methylated- β CD. The addition of an

excess of 1-adamantylamine as competitive guest reduced the cloud point temperature to an intermediate temperature between that of the free polymer and the polymer-cyclodextrin ensemble.^[311]

In an interesting study, the T_{CP} of a 1,5-dialkoxynaphthalene-terminated PNIPAAm solution, could be tuned by the addition of CBPQT⁴⁺, that forms a host-guest complex with the electron-rich dialkoxynaphthalene unit, similarly as seen previously with TTF. Upon addition of one equivalent of CBPQT⁴⁺, the T_{CP} increased from *ca.* 28 °C to 34 °C, due to host-guest complex formation. In contrast with the behavior observed with TTF, in this case the dialkoxynaphthalene-CBPQT⁴⁺ host-guest complexes were broken upon thermal collapse of the PNIPAAm chain. This was demonstrated by the disappearance of the purple color characteristic of the dialkoxynaphthalene-CBPQT⁴⁺ donor-acceptor complex, and despite the large association constant of the host-guest couple ($K_a > 10^5 \text{ M}^{-1}$, as determined by ITC). The breakage of the host-guest complex was further confirmed by UV-Vis and ¹H NMR spectroscopy.^[312]

The disruption of the host-guest complexes upon the temperature-induced collapse of the copolymer was also observed for a thermosensitive cationic diblock copolymer composed by PNIPAAm-*b*-poly(3-acrylamidopropyl)trimethylammonium chloride (PNIPAAm₂₄-*b*-PAMPTAM(+)₉). Gamma cyclodextrin (γ CD) was found to thread around the PNIPAAm polymer backbone forming pseudopolyrotaxanes. Increasing temperature to 40 °C, beyond the PNIPAAm LCST, induced the dethreading of the γ CD molecules, as observed by steady-state fluorescence spectroscopy.^[313]

The incorporation of hydrophobic host units throughout the polymer backbone, multiplies the hydrophilicity gain upon host-guest complex formation thus leading to much larger increases in the polymer cloud point temperature. Recently, Ritter *et al.* reported the thermoresponsive behavior of a copolymer containing 2-methacrylamido-caprolactam and *N,N*-dimethylacrylamide in a 0.7 : 0.3 molar ratio obtained by free radical copolymerization. The copolymer T_{CP} was determined to be 34 °C by turbidimetry, and increased to 47 °C upon addition of 1.5 equivalents of methylated- β CD. The authors confirmed the cyclodextrin-caprolactam inclusion complex formation by 2D Rotating frame nuclear Overhauser effect spectroscopy (ROESY) NMR, and the 1 : 1 stoichiometry by a Job's plot. However, no correlation between host concentration and T_{CP} was given.^[314]

In another recent account,^[315] free radical polymerization of NIPAAm, *N,N*-dimethylacrylamide (DMA), and a cholic acid-based methacrylate monomer (CA) resulted in a P(NIPAA₇₅-*co*-DMAA₂₅-*co*-CA₂) statistical copolymer with a $T_{CP} \approx 22$ °C. Titration with different amounts of β CD produced an increase in the copolymer T_{CP} due to host guest complexation between the CA pendant groups and β CD (see Figure 1.4.7).

The authors studied the size of the aggregates formed upon collapse of the polymer chains, observing that the size of the aggregates was reduced when a large excess of β CD was present (200 – 300 nm), in relation with the aggregates formed upon collapse of the free polymer (> 600 nm). This possibly indicates incomplete breakage of the host-guest complexes. When adamantane carboxylate (AD) was added as a competitive guest, the T_{CP} could be brought back to the original value of the free polymer. Although the T_{CP} of the copolymer- β CD ensemble increased with the concentration of β CD, up to 10 equivalents of the cavitand are necessary to increase the T_{CP} to 31 °C. Similar results were obtained in another study performed on a copolymer comprising PNIPAAm and different levels of substitution with adamantane- and dodecyl-*N*-substituted acrylamide monomers.^[316]

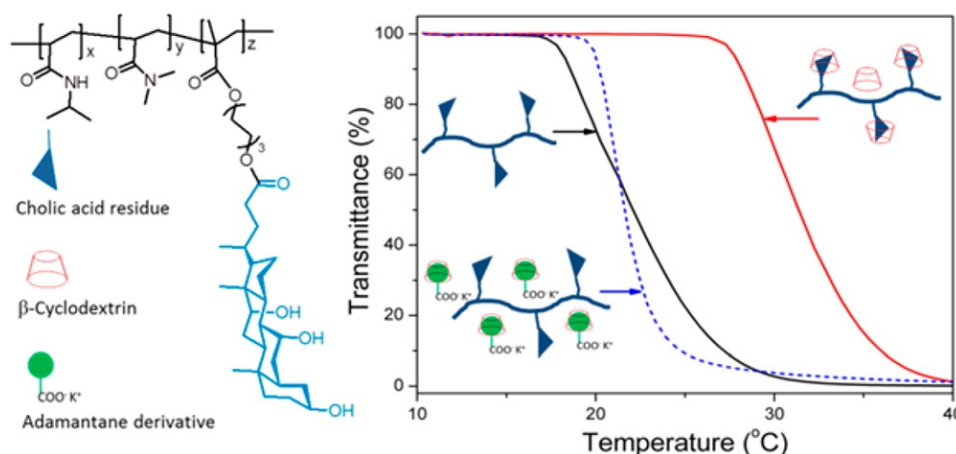


Figure 1.4.7. Turbidimetry studies of a $P(\text{NIPAA}_{75}\text{-co-DMAA}_{25}\text{-co-CA}_2)$ copolymer, and effect of βCD . The T_{CP} of the copolymer gradually increase with the addition of βCD , due to the complexation of the cholic acid guest with the βCD host. The increase of the T_{CP} may be reversed by the addition of a competing guest molecule, potassium 1-adamantylcarboxylate. Polymer concentration: 2 mg mL^{-1} . Heating rate: 1 K min^{-1} .^[315]

As expected, the influence of the supramolecular host was larger on the polymers containing a higher content of alkyl substituents. The addition of 3 equivalents of hydroxypropylated- βCD (HP βCD) to a PNIPAAm-C12 copolymer containing 4.4 % C12 produced an increase in the T_{CP} of 9 K. In Chapter 5, we will see that increasing the alkyl chain hydrophobic content in a similar amphiphilic copolymer based on PAOx, together with the rational selection of cavitand, results in a much broader tunability of the T_{CP} .

Naturally, not only the number but also the nature of the hydrophobic units decorating the polymer needs to be considered to assess the influence of supramolecular complexation on the thermoresponsive properties of the copolymer. In a recent contribution, the LCST behavior of a $P(\text{NIPAAm}_{195})$ copolymer bearing 5 dialkoxynaphthalene units across the polymer backbone was reported, and the effect of inclusion complex formation with CBPQT^{4+} evaluated.^[317] The polymer T_{CP} could be varied from $\approx 20 \text{ }^\circ\text{C}$ to $\approx 32 \text{ }^\circ\text{C}$ upon addition of stoichiometric amounts of CBPQT^{4+} in relation to dialkoxynaphthalene moieties. Interestingly, a hysteresis spanning the whole solubility range was found for the copolymer - CBPQT^{4+} stoichiometric mixture. Due to the high hydrophobicity of the dialkoxynaphthalene side chains, this large hysteresis was found to be stable in time, and applicable to the development of temperature sensors with memory. This system with unprecedented properties will be discussed in full detail in Chapter 6.

As introduced earlier, the incorporation of responsive guests in the polymer structure enables the modulation of their interactions with host macromolecules in solution, affording multi-stimuli responsive systems. A nice illustration of this multi-stimuli responsiveness is provided by the alpha cyclodextrin (αCD)-azobenzene host-guest couple; while the association constant between αCD and *trans*-azo derivatives is $K_a \approx 10^4 \text{ M}^{-1}$,^[318] the *cis*-azo obtained by UV irradiation of the *trans* form yields complexes with $K_a \approx 10^1 \text{ M}^{-1}$.^[319] The ability to control the host-guest complexation of αCD and azobenzene-functional polymers has been extensively investigated by Harada for the preparation of supramolecular hydrogels with a reversible sol-gel transition controlled by UV irradiation and other supramolecular systems, including a photoresponsive artificial muscle.^[278, 320-322]

One example of modulation of a polymer LCST by light irradiation has been realized in a system comprising a poly(*N,N*-dimethylacrylamide-*co-N*-4-phenylazophenyl acrylamide) (PDMAA-*co*-

PAPA) thermoresponsive copolymer and α CD. The copolymer containing 11.3 wt.% of azo groups, exhibited a LCST of 29 °C, that increases up to 45.5 °C upon addition of one equivalent of α CD. Irradiation with 365 nm UV light for 40 min. reduced the LCST to \approx 40 °C as a consequence of the *trans* to *cis* conversion of the azo groups, and the consequent breakage of the azo- α CD inclusion complexes. The relatively small drop in T_{CP} upon irradiation was ascribed to the lower hydrophobicity of the *cis* azo derivative, leading to an increase in T_{CP} in relation with the *trans* form.^[323] The dependence of the azo group conformation with cloud point temperature has also been found in PNIPAAm-based copolymers where it is highly affected by the solvent composition.^[324]

1.4.4 Conclusions

Thermoresponsive polymers constitute a polymer type with a wide range of applications, as they bring together structure and function, therefore resulting in smart-materials of interest in applications ranging from construction, to microfluidics, lab-on-a-chip technologies or biomedical sciences. The polymer morphology in solution and its response to temperature can be tuned by combining different hydrophilic and hydrophobic units in the polymer composition.

In addition, supramolecular chemistry has been proven to be a valuable strategy to modulate the conformation of polymer chains and their self-assembly behavior in solution resulting in complex adaptive structures. Moreover, the transition temperature of thermoresponsive polymers can be finely tuned in a reversible and adaptive manner by the incorporation of suitable supramolecular host molecules. In Chapter 5, the potential of host-guest interactions to modulate the LCST behavior of amphiphilic PAOx, will be explored. The appropriate combination of copolymer composition and supramolecular host will allow tuning the T_{CP} of the copolymers across a temperature range well beyond what has been realized in the reported systems. Furthermore, in Chapter 6, the ability of thermoresponsive polymers in combination with supramolecular hosts to remain in the collapsed state upon temperature-triggered aggregation will be explored, leading to temperature sensors able to store thermal information.

1.5 Aim and outline of the thesis

The evolution of human civilization is based on finding new materials and devising new tools to control the environment. The paradigm that prevailed throughout history was creating materials adapted to a specific function that would be as immutable as possible from the outside world. In a way, mankind was thus walking against the natural forces. However, our current understanding of nature and the chemistry behind its marvels, is rapidly shifting this paradigm towards a more subtle and intelligent approach. Now, we focus our efforts not on immobile materials adapted to a function, but on materials that embrace the function and can adapt to an evolving environment.

The development of living and controlled polymerization techniques has empowered us with the necessary tools to realize these responsive functional materials, in analogy to the strategies found in natural systems. Controlling the synthesis of defined polymers allows us to establish structure-property relationships to drive the polymeric chains into functional conformations at the nanoscale, in analogy to natural polymers, such as proteins and DNA. The biomedical field has been the first scientific area taking advantage from these new polymer-based materials, as has been reviewed in the introductory chapter of this thesis. As has been seen, poly(2-alkyl/aryl-2-oxazoline)s (PAOx) will have a preeminent role to play in this new rapid development, and research has already resulted in chemistries to produce safer implants, more effective tablets,

convenient tissue tapes, or advanced targeted therapies, some of them soon to be realized in the first commercial products.

Notwithstanding the importance of devising new applications and functionalities, screening recent PAOx literature reveals the scarcity of recent papers devoted to the detailed study of polymer synthesis and its effect on composition or molecular weight distribution. This is especially evident in literature regarding PEI synthesis. Therefore, in the course of this thesis, the synthesis and functionalization of PAOx have been studied in detail, with the aim of optimizing their preparation in a fast and reproducible manner. In addition, the synthesis of PEI from the selective or partial hydrolysis of PAOx has been investigated, resulting in useful methodologies to obtain vectors for gene-delivery and to facilitate the expansion of the PAOx structural and functional versatility. These topics are covered in Chapters 2 and 3 of this thesis.

As stated earlier, understanding the structure-property relationships that dictate polymer conformational changes into complex architectures at the nanoscale is of major importance to develop responsive and functional materials. Therefore, in Chapter 3, the composition of amphiphilic block copolymers based on PAOx-polycarbonates, the latter chosen as biodegradable polymer block, is varied to modulate their self-assembly in solution. A wide range of morphologies were obtained, from star-shaped to crew-cut micelles and polymersomes, the structure-property relationships were investigated to enable rational design of novel vehicles for drug delivery or diagnostics.

The second part of this thesis focuses on the development of smart materials that are able to respond to environmental changes in solution. In Chapter 4, a new functionalization strategy was developed to enable straightforward grafting of PAOx onto gold surfaces, with potential uses in the development of highly sensitive sensing devices. These novel PAOx were used to synthesize PAOx-gold nanoparticle (AuNP) hybrids that exhibited dual responsiveness to temperature and to the presence of electrolytes in solution, resulting in colorimetric logic gates. Importantly, the responsiveness and thermal trigger input signal could be tuned by variation of the PAOx composition.

The ability of PAOx to respond to temperature was further exploited in combination with supramolecular hosts in aqueous solution. Surprisingly, to the best of our knowledge there is no systematic study dedicated to the modulation of a thermoresponsive polymer phase transition temperature by using supramolecular host-guest interactions. The reported systems generally utilize ill-defined polymers synthesized by free-radical polymerization, which hampers the establishment of structure-property relationships, and do not include detailed evaluation of the influence of the macromolecular host on the self-assembly behavior of the system. To shed light onto this fascinating field, we performed a systematic study of the thermoresponsive properties of a series of well-defined PAOx amphiphilic copolymers in combination with various macromolecular hosts. The temperature triggered transition temperature of the copolymers could be tuned in an extraordinarily broad temperature range. More importantly, these detailed investigations allowed us to establish structure-property relationships that permit the control on the reversibility of the transition, and to record thermal information in the supramolecular structures. This research, in which the synergy of polymer and supramolecular chemistry is highlighted, is covered in Chapters 5 and 6 of the thesis.

1.6 References

- [1] L.-H. Lin, P.-L. Wang, D. Rumble, J. Lippmann-Pipke, E. Boice, L. M. Pratt, B. S. Lollar, E. L. Brodie, T. C. Hazen, G. L. Andersen, T. Z. DeSantis, D. P. Moser, D. Kershaw, T. C. Onstott, *Science* **2006**, *314*, 479.
- [2] L. Ionov, in *Intelligent Stimuli-Responsive Materials*, John Wiley & Sons, Inc., **2013**, pp. 1.
- [3] T. P. Lodge, *Science* **2008**, *321*, 50.
- [4] L. Dong, A. K. Agarwal, D. J. Beebe, H. Jiang, *Nature* **2006**, *442*, 551.
- [5] O. Mudanyali, E. McLeod, W. Luo, A. Greenbaum, A. F. Coskun, Y. Hennequin, C. P. Allier, A. Ozcan, *Nat. Photon.* **2013**, *7*, 240.
- [6] X. Guo, N. Zhou, S. J. Lou, J. Smith, D. B. Tice, J. W. Hennek, R. P. Ortiz, J. T. L. Navarrete, S. Li, J. Strzalka, L. X. Chen, R. P. H. Chang, A. Facchetti, T. J. Marks, *Nat. Photon.* **2013**, *7*, 825.
- [7] N. Goldman, P. Bertone, S. Chen, C. Dessimoz, E. M. LeProust, B. Sipo, E. Birney, *Nature* **2013**, *494*, 77.
- [8] F. Pu, E. Ju, J. Ren, X. Qu, *Adv. Mater.* **2014**, *26*, 1111.
- [9] D. Gentili, P. Sonar, F. Liscio, T. Cramer, L. Ferlauto, F. Leonardi, S. Milita, A. Dodabalapur, M. Cavallini, *Nano Lett.* **2013**, *13*, 3643.
- [10] A. P. de Silva, in *Supramol. Chem.*, John Wiley & Sons, Ltd, **2012**.
- [11] T. Kagiya, S. Narisawa, T. Maeda, K. Fukui, *Journal of Polymer Science Part B: Polymer Letters* **1966**, *4*, 441.
- [12] W. Seeliger, E. Aufderhaar, W. Diepers, R. Feinauer, R. Nehring, W. Thier, H. Hellmann, *Angew. Chem. Int. Ed. Engl.* **1966**, *5*, 875.
- [13] D. A. Tomalia, D. P. Sheetz, *J. Polym. Sci., Part A1: Polym. Chem.* **1966**, *4*, 2253.
- [14] A. Levy, M. Litt, *J. Polym. Sci., Part A1: Polym. Chem.* **1968**, *6*, 63.
- [15] K. Aoi, M. Okada, *Prog. Polym. Sci.* **1996**, *21*, 151.
- [16] S. Kobayashi, in *Polymer Science: A Comprehensive Reference* (Ed.: K. M. Möller), Elsevier, Amsterdam, **2012**, pp. 397.
- [17] R. Hoogenboom, in *Handbook of Ring-Opening Polymerization* (Eds.: D. P., C. O., R. J.-M.), Wiley-VCH Verlag GmbH & Co. KGaA, Weinheim, Germany, **2009**, pp. 141.
- [18] S. Kobayashi, H. Uyama, Y. Narita, J. Ishiyama, *Macromolecules* **1992**, *25*, 3232.
- [19] R. M. Paulus, C. R. Becer, R. Hoogenboom, U. S. Schubert, *Macromol. Chem. Phys.* **2008**, *209*, 794.
- [20] R. Hoogenboom, M. W. M. Fijten, G. Kickelbick, U. S. Schubert, *Beilstein J. Org. Chem.* **2010**, *6*, 773.
- [21] R. Luxenhofer, M. Bezen, R. Jordan, *Macromol. Rapid Commun.* **2008**, *29*, 1509.
- [22] A. Kowalczyk, J. Kronek, K. Bosowska, B. Trzebicka, A. Dworak, *Polym. Int.* **2011**, *60*, 1001.
- [23] M. A. Tasdelen, M. U. Kahveci, Y. Yagci, *Prog. Polym. Sci.* **2011**, *36*, 455.
- [24] M. Glassner, K. Kempe, U. S. Schubert, R. Hoogenboom, C. Barner-Kowollik, *Chem. Commun.* **2011**, *47*, 10620.
- [25] G. Volet, T.-X. Lav, J. Babinot, C. Amiel, *Macromol. Chem. Phys.* **2011**, *212*, 118.
- [26] G. David, V. Alupe, B. C. Simionescu, *Eur. Polym. J.* **2001**, *37*, 1353.
- [27] N. Zhang, R. Luxenhofer, R. Jordan, *Macromol. Chem. Phys.* **2012**, *213*, 1963.
- [28] L. T. T. Trinh, H. M. L. Lambermont-Thijs, U. S. Schubert, R. Hoogenboom, A.-L. Kjøniksen, *Macromolecules* **2012**, *45*, 4337.
- [29] R. Hoogenboom, H. M. L. Thijs, M. J. H. C. Jochems, B. M. van Lankvelt, M. W. M. Fijten, U. S. Schubert, *Chem. Commun.* **2008**, 5758.
- [30] M. M. Bloksma, R. M. Paulus, H. P. C. van Kuringen, F. van der Woerd, H. M. L. Lambermont-Thijs, U. S. Schubert, R. Hoogenboom, *Macromol. Rapid Commun.* **2011**, *33*, 92.
- [31] M. Glassner, K. Lava, V. R. de la Rosa, R. Hoogenboom, *J. Polym. Sci., Part A: Polym. Chem.* **2014**, *52*, 3118.
- [32] D. Bogdal, in *Polymer Science: A Comprehensive Reference* (Ed.: K. M. Möller), Elsevier, Amsterdam, **2012**, pp. 981.
- [33] A. Sosnik, G. Gotelli, G. A. Abraham, *Prog. Polym. Sci.* **2011**, *36*, 1050.
- [34] F. Wiesbrock, R. Hoogenboom, M. Leenen, S. F. G. M. van Nispen, M. van der Loop, C. H. Abeln, A. M. J. van den Berg, U. S. Schubert, *Macromolecules* **2005**, *38*, 7957.
- [35] F. Wiesbrock, R. Hoogenboom, M. A. M. Leenen, M. A. R. Meier, U. S. Schubert, *Macromolecules* **2005**, *38*, 5025.
- [36] R. Hoogenboom, M. W. M. Fijten, H. M. L. Thijs, B. M. van Lankvelt, U. S. Schubert, *Des. Monomers Polym.* **2005**, *8*, 659.
- [37] R. Hoogenboom, M. W. M. Fijten, R. M. Paulus, H. M. L. Thijs, S. Hoepfener, G. Kickelbick, U. S. Schubert, *Polymer* **2006**, *47*, 75.
- [38] R. Hoogenboom, U. S. Schubert, *Macromol. Rapid Commun.* **2007**, *28*, 368.
- [39] R. Hoogenboom, M. W. M. Fijten, S. Wijnans, A. M. J. van den Berg, H. M. L. Thijs, U. S. Schubert, *J. Comb. Chem.* **2006**, *8*, 145.

- [40] J. M. Kranenburg, C. A. Tweedie, R. Hoogenboom, F. Wiesbrock, H. M. L. Thijs, C. E. Hendriks, K. J. Van Vliet, U. S. Schubert, *J. Mater. Chem.* **2007**, *17*, 2713.
- [41] M. W. M. Fijten, J. M. Kranenburg, H. M. L. Thijs, R. M. Paulus, B. M. van Lankvelt, J. de Hullu, M. Springintveld, D. J. G. Thielen, C. A. Tweedie, R. Hoogenboom, K. J. Van Vliet, U. S. Schubert, *Macromolecules* **2007**, *40*, 5879.
- [42] *Nobel lecture: macromolecular chemistry*, <http://www.nobelprize.org>
- [43] H. Ringsdorf, *Angew. Chem. Int. Ed.* **2004**, *43*, 1064.
- [44] H. Ringsdorf, *J. Polym. Sci., Polym. Sym.* **1975**, *51*, 135.
- [45] R. Haag, F. Kratz, *Angew. Chem. Int. Ed.* **2006**, *45*, 1198.
- [46] A. Lendlein, A. T. Neffe, *Macromol. Biosci.* **2013**, *13*, 1633.
- [47] H. Schlaad, R. Hoogenboom, *Macromol. Rapid Commun.* **2012**, *33*, 1593.
- [48] B. Leader, Q. J. Baca, D. E. Golan, *Nat. Rev. Drug Discov.* **2008**, *7*, 21.
- [49] R. Duncan, *Nat Rev Drug Discov* **2003**, *2*, 347.
- [50] P. Caliceti, F. M. Veronese, *Adv. Drug Delivery Rev.* **2003**, *55*, 1261.
- [51] S. Jevševar, M. Kunstelj, V. G. Porekar, *Biotechnol. J.* **2010**, *5*, 113.
- [52] F. M. Veronese, G. Pasut, *Drug Discovery Today* **2005**, *10*, 1451.
- [53] G. Pasut, F. M. Veronese, *J. Control. Release* **2012**, *161*, 461.
- [54] Y. Levy, M. S. Hershfield, C. Fernandez-Mejia, S. H. Polmar, D. Scudiero, M. Berger, R. U. Sorensen, *J. Pediatr.* **1988**, *113*, 312.
- [55] S. N. S. Alconcel, A. S. Baas, H. D. Maynard, *Polym. Chem.* **2011**, *2*, 1442.
- [56] J. K. Armstrong, G. Hempel, S. Koling, L. S. Chan, T. Fisher, H. J. Meiselman, G. Garratty, *Cancer* **2007**, *110*, 103.
- [57] T. Tagami, K. Nakamura, T. Shimizu, N. Yamazaki, T. Ishida, H. Kiwada, *J. Control. Release* **2010**, *142*, 160.
- [58] Y. Zhao, C. Wang, L. Wang, Q. Yang, W. Tang, Z. She, Y. Deng, *Eur. J. Pharm. Biopharm.* **2012**, *81*, 506.
- [59] Y. Ma, Q. Yang, L. Wang, X. Zhou, Y. Zhao, Y. Deng, *Eur. J. Pharm. Sci.* **2012**, *45*, 539.
- [60] T. Suzuki, M. Ichihara, K. Hyodo, E. Yamamoto, T. Ishida, H. Kiwada, H. Ishihara, H. Kikuchi, *Int. J. Pharm.* **2012**, *436*, 636.
- [61] Y. Arima, M. Toda, H. Iwata, *Biomaterials* **2008**, *29*, 551.
- [62] S. M. Moghimi, A. C. Hunter, C. M. Dadswell, S. Savay, C. R. Alving, J. Szebeni, *Biochimica et Biophysica Acta (BBA) - Molecular Basis of Disease* **2004**, *1689*, 103.
- [63] I. Hamad, A. C. Hunter, J. Szebeni, S. M. Moghimi, *Mol. Immunol.* **2008**, *46*, 225.
- [64] Z. He, J. Liu, L. Du, *Nanoscale* **2014**, *6*, 9017.
- [65] K. Knop, R. Hoogenboom, D. Fischer, U. S. Schubert, *Angew. Chem. Int. Ed.* **2010**, *49*, 6288.
- [66] M. Barz, R. Luxenhofer, R. Zentel, M. J. Vicent, *Polym. Chem.* **2011**, *2*, 1900.
- [67] PEGylated protein drugs: basic science and clinical applications
- [68] E. Fleige, M. A. Quadir, R. Haag, *Adv. Drug Delivery Rev.* **2012**, *64*, 866.
- [69] J. S. Lee, J. Feijen, *J. Control. Release* **2012**, *161*, 473.
- [70] R. Duncan, M. J. Vicent, *Adv. Drug Delivery Rev.* **2013**, *65*, 60.
- [71] N. Adams, U. S. Schubert, *Adv. Drug Delivery Rev.* **2007**, *59*, 1504.
- [72] R. Hoogenboom, H. Schlaad, *Polymers* **2011**, *3*, 467.
- [73] H. Schlaad, C. Diehl, A. Gress, M. Meyer, A. L. Demirel, Y. Nur, A. Bertin, *Macromol. Rapid Commun.* **2010**, *31*, 511.
- [74] V. R. de la Rosa, *J. Mater. Sci.: Mater. Med.* **2014**, *25*, 1211.
- [75] T. X. Viegas, M. D. Bentley, J. M. Harris, Z. Fang, K. Yoon, B. Dizman, R. Weimer, A. Mero, G. Pasut, F. M. Veronese, *Bioconjugate Chem.* **2011**, *22*, 976.
- [76] F. C. Gaertner, R. Luxenhofer, B. Blechert, R. Jordan, M. Essler, *J. Control. Release* **2007**, *119*, 291.
- [77] R. Luxenhofer, G. Sahay, A. Schulz, D. Alakhova, T. K. Bronich, R. Jordan, A. V. Kabanov, *J. Control. Release* **2011**, *153*, 73.
- [78] J. Kronek, E. Paulovičová, L. Paulovičová, Z. Kroneková, J. Luston, *Biocompatibility and Immunocompatibility Assessment of Poly(2-Oxazolines), Practical Applications in Biomedical Engineering*, InTech., available from www.intechopen.com/books, **2013**.
- [79] M. C. Woodle, C. M. Engbers, S. Zalipsky, *Bioconjugate Chem.* **1994**, *5*, 493.
- [80] A. Mero, G. Pasut, L. D. Via, M. W. M. Fijten, U. S. Schubert, R. Hoogenboom, F. M. Veronese, *J. Control. Release* **2008**, *125*, 87.
- [81] M. Bauer, C. Lautenschlaeger, K. Kempe, L. Tauhardt, U. S. Schubert, D. Fischer, *Macromol. Biosci.* **2012**, *12*, 986.
- [82] SER-214, A novel polymer conjugated Rotigotine formulation affords greatly extended duration of anti-Parkinsonian effect and enhanced plasma exposure following a single administration in rodents and primates

- [83] X. Wang, X. Li, Y. Li, Y. Zhou, C. Fan, W. Li, S. Ma, Y. Fan, Y. Huang, N. Li, Y. Liu, *Acta Biomaterialia* **2011**, *7*, 4149.
- [84] J. Kronek, Z. Kroneková, J. Lustoň, E. Paulovičová, L. Paulovičová, B. Mendrek, *J. Mater. Sci.: Mater. Med.* **2011**, *22*, 1725.
- [85] R. Konradi, C. Acikgoz, M. Textor, *Macromol. Rapid Commun.* **2012**, *33*, 1663.
- [86] S. Zalipsky, C. B. Hansen, J. M. Oaks, T. M. Allen, *J. Pharm. Sci.* **1996**, *85*, 133.
- [87] B. Pidhatika, M. Rodenstein, Y. Chen, E. Rakhmatullina, A. Mühlebach, C. Acikgöz, M. Textor, R. Konradi, *Biointerphases* **2012**, *7*.
- [88] P. Goddard, L. E. Hutchinson, J. Brown, L. J. Brookman, *J. Control. Release* **1989**, *10*, 5.
- [89] C.-H. Wang, Y.-S. Hwang, P.-R. Chiang, C.-R. Shen, W.-H. Hong, G.-H. Hsiue, *Biomacromolecules* **2011**, *13*, 40.
- [90] R. Duncan, *Curr. Opin. Biotechnol.* **2011**, *22*, 492.
- [91] R. Luxenhofer, Y. Han, A. Schulz, J. Tong, Z. He, A. V. Kabanov, R. Jordan, *Macromol. Rapid Commun.* **2012**, *33*, 1613.
- [92] A. Mero, Z. Fang, G. Pasut, F. M. Veronese, T. X. Viegas, *J. Control. Release* **2012**, *159*, 353.
- [93] J. Tong, R. Luxenhofer, X. Yi, R. Jordan, A. V. Kabanov, *Mol. Pharm.* **2010**, *7*, 984.
- [94] *European Medicines Agency. Summary of the European public assessment report (EPAR) for Glybera.*
- [95] E. Marshall, *Science* **1999**, *286*, 2244.
- [96] N. Boyce, *Nature* **2001**, *414*, 677.
- [97] E. Check, *Nature* **2002**, *420*, 116.
- [98] M. Morille, C. Passirani, A. Vonarbourg, A. Clavreul, J.-P. Benoit, *Biomaterials* **2008**, *29*, 3477.
- [99] S. O'Rorke, M. Keeney, A. Pandit, *Prog. Polym. Sci.* **2010**, *35*, 441.
- [100] S. Y. Wong, J. M. Pelet, D. Putnam, *Prog. Polym. Sci.* **2007**, *32*, 799.
- [101] M. A. Gosselin, W. Guo, R. J. Lee, *Bioconjugate Chem.* **2001**, *12*, 989.
- [102] M. Breunig, U. Lungwitz, R. Liebl, C. Fontanari, J. Klar, A. Kurtz, T. Blunk, A. Goepferich, *J. Gene Med.* **2005**, *7*, 1287.
- [103] B. Brissault, A. Kichler, C. Guis, C. Leborgne, O. Danos, H. Cheradame, *Bioconjugate Chem.* **2003**, *14*, 581.
- [104] H. M. L. Lambermont-Thijs, F. S. van der Woerd, A. Baumgaertel, L. Bonami, F. E. Du Prez, U. S. Schubert, R. Hoogenboom, *Macromolecules* **2009**, *43*, 927.
- [105] M. Thomas, J. J. Lu, Q. Ge, C. Zhang, J. Chen, A. M. Klibanov, *Proc. Natl. Acad. Sci. U. S. A.* **2005**, *102*, 5679.
- [106] J. H. Jeong, S. H. Song, D. W. Lim, H. Lee, T. G. Park, *J. Control. Release* **2001**, *73*, 391.
- [107] V. R. de la Rosa, E. Bauwens, B. D. Monnery, B. G. De Geest, R. Hoogenboom, *Polym. Chem.* **2014**, *5*, 4957.
- [108] H. P. C. van Kuringen, V. R. de la Rosa, M. W. M. Fijten, J. P. A. Heuts, R. Hoogenboom, *Macromol. Rapid Commun.* **2012**, *33*, 827.
- [109] G.-H. Hsiue, H.-Z. Chiang, C.-H. Wang, T.-M. Juang, *Bioconjugate Chem.* **2006**, *17*, 781.
- [110] S. Bauhuber, R. Liebl, L. Tomasetti, R. Rachel, A. Goepferich, M. Breunig, *J. Control. Release* **2012**, *162*, 446.
- [111] T. von Erlach, S. Zwicker, B. Pidhatika, R. Konradi, M. Textor, H. Hall, T. Lühmann, *Biomaterials* **2011**, *32*, 5291.
- [112] S. M. Grayson, *Polym. Prepr. (Am. Chem. Soc., Div. Polym. Chem.)* **2012**, *53*, 370.
- [113] S. Grayson, M. Cortez, *Polyplex Gene Delivery Vectors, Vol. WO 2011/116371*, I. Patent, **2011**.
- [114] F. Canal, J. Sanchis, M. J. Vicent, *Curr. Opin. Biotechnol.* **2011**, *22*, 894.
- [115] F. Greco, M. J. Vicent, *Adv. Drug Delivery Rev.* **2009**, *61*, 1203.
- [116] H. Wei, R.-X. Zhuo, X.-Z. Zhang, *Prog. Polym. Sci.* **2013**, *38*, 503.
- [117] Z. L. Tyrrell, Y. Shen, M. Radosz, *Prog. Polym. Sci.* **2010**, *35*, 1128.
- [118] A. Kowalczyk, R. Trzcinska, B. Trzebicka, A. H. E. Müller, A. Dworak, C. B. Tsvetanov, *Prog. Polym. Sci.* **2014**, *39*, 43.
- [119] R. T. Chacko, J. Ventura, J. Zhuang, S. Thayumanavan, *Adv. Drug Delivery Rev.* **2012**, *64*, 836.
- [120] Y. Matsumura, K. Kataoka, *Cancer Sci.* **2009**, *100*, 572.
- [121] O. Onaca, R. Enea, D. W. Hughes, W. Meier, *Macromol. Biosci.* **2009**, *9*, 129.
- [122] R. Hoogenboom, F. Wiesbrock, M. A. M. Leenen, H. M. L. Thijs, H. Huang, C.-A. Fustin, P. Guillet, J.-F. Gohy, U. S. Schubert, *Macromolecules* **2007**, *40*, 2837.
- [123] C. Krumm, C. P. Fik, M. Meuris, G. J. Dropalla, H. Geltenpoth, A. Sickmann, J. C. Tiller, *Macromol. Rapid Commun.* **2012**, *33*, 1677.
- [124] C. Nardin, S. Thoeni, J. Widmer, M. Winterhalter, W. Meier, *Chem. Commun.* **2000**, 1433.
- [125] N. Ben-Haim, P. Broz, S. Marsch, W. Meier, P. Hunziker, *Nano Lett.* **2008**, *8*, 1368.

- [126] P. Broz, N. Ben-Haim, M. Grzelakowski, S. Marsch, W. Meier, P. Hunziker, *J. Cardiovasc. Pharmacol.* **2008**, *51*, 246.
- [127] A. Ranquin, W. Versées, W. Meier, J. Steyaert, P. Van Gelder, *Nano Lett.* **2005**, *5*, 2220.
- [128] W. Meier, C. Nardin, M. Winterhalter, *Angew. Chem. Int. Ed.* **2000**, *39*, 4599.
- [129] K. Renggli, P. Baumann, K. Langowska, O. Onaca, N. Bruns, W. Meier, *Adv. Funct. Mater.* **2011**, *21*, 1241.
- [130] B. Trzebicka, N. Koseva, V. Mitova, A. Dworak, *Polymer* **2010**, *51*, 2486.
- [131] Y. Milonaki, E. Kaditi, S. Pispas, C. Demetzos, *J. Polym. Sci., Part A: Polym. Chem.* **2012**, *50*, 1226.
- [132] A. Persidis, *Nat. Biotech.* **1999**, *17*, 94.
- [133] R. Luxenhofer, A. Schulz, C. Roques, S. Li, T. K. Bronich, E. V. Batrakova, R. Jordan, A. V. Kabanov, *Biomaterials* **2010**, *31*, 4972.
- [134] Y. Han, Z. He, A. Schulz, T. K. Bronich, R. Jordan, R. Luxenhofer, A. V. Kabanov, *Mol. Pharm.* **2012**, *9*, 2302.
- [135] M. P. Lutolf, *Nat. Mater.* **2009**, *8*, 451.
- [136] A. M. Kelly, A. Hecke, B. Wirnsberger, F. Wiesbrock, *Macromol. Rapid Commun.* **2011**, n/a.
- [137] T. R. Dargaville, R. Forster, B. L. Farrugia, K. Kempe, L. Voorhaar, U. S. Schubert, R. Hoogenboom, *Macromol. Rapid Commun.* **2012**, *33*, 1695.
- [138] T. R. Dargaville, B. G. Hollier, A. Shokoohmand, R. Hoogenboom, *Cell Adh. Migr.* **2014**, *8*, 88.
- [139] GATT Technologies BV, Last accessed: September 2014. <http://www.gatt-tech.com/technology>
- [140] P. J. M. Bouten, M. Zonjee, J. Bender, S. T. K. Yauw, H. van Goor, J. C. M. van Hest, R. Hoogenboom, *Prog. Polym. Sci.* **2014**, *39*, 1375.
- [141] R. Hoogenboom, *Polyoxazoline polymers and methods for their preparation, conjugates of these polymers and medical uses thereof*, Universiteit Gent, Bender Analytical Holding B.V., **2013**.
- [142] A. M. Kelly, F. Wiesbrock, *Macromol. Rapid Commun.* **2012**, *33*, 1632.
- [143] J. L. Del Pozo, R. Patel, *N. Engl. J. Med.* **2009**, *361*, 787.
- [144] C. Werner, M. F. Maitz, C. Sperling, *J. Mater. Chem.* **2007**, *17*, 3376.
- [145] S. Krishnan, C. J. Weinman, C. K. Ober, *J. Mater. Chem.* **2008**, *18*, 3405.
- [146] E. A. Vogler, *Adv. Colloid Interface Sci.* **1998**, *74*, 69.
- [147] Water in Biomaterials Surface Science
- [148] A. Roosjen, J. de Vries, H. C. van der Mei, W. Norde, H. J. Busscher, *J. Biomed. Mater. Res. Part B Appl. Biomater.* **2005**, *73B*, 347.
- [149] S. Bozzini, P. Petrini, M. C. Tanzi, S. Zürcher, S. Tosatti, *Langmuir* **2009**, *26*, 6529.
- [150] H. P. C. Van Kuringen, J. Lenoir, E. Adriaens, J. Bender, B. G. De Geest, R. Hoogenboom, *Macromol. Biosci.* **2012**, *12*, 1114.
- [151] R. Konradi, B. Pidhatika, A. Mühlebach, M. Textor, *Langmuir* **2008**, *24*, 613.
- [152] B. Pidhatika, J. Iler, V. Vogel, R. Konradi, *CHIMIA International Journal for Chemistry* **2008**, *62*, 264.
- [153] B. Pidhatika, J. Möller, E. M. Benetti, R. Konradi, E. Rakhmatullina, A. Mühlebach, R. Zimmermann, C. Werner, V. Vogel, M. Textor, *Biomaterials* **2010**, *31*, 9462.
- [154] B.-J. Chang, O. Prucker, E. Groh, A. Wallrath, M. Dahm, J. Rühle, *Colloids Surf., A* **2002**, *198–200*, 519.
- [155] H. Murata, B. J. Chang, O. Prucker, M. Dahm, J. Rühle, *Surf. Sci.* **2004**, *570*, 111.
- [156] H. Wang, L. Li, Q. Tong, M. Yan, *ACS Appl. Mater. Interfaces* **2011**, *3*, 3463.
- [157] R. Jordan, A. Ulman, *J. Am. Chem. Soc.* **1998**, *120*, 243.
- [158] N. Zhang, M. Steenackers, R. Luxenhofer, R. Jordan, *Macromolecules* **2009**, *42*, 5345.
- [159] N. Zhang, T. Pompe, I. Amin, R. Luxenhofer, C. Werner, R. Jordan, *Macromol. Biosci.* **2012**, *12*, 926.
- [160] M. Charnley, M. Textor, C. Acikgoz, *React. Funct. Polym.* **2011**, *71*, 329.
- [161] F. Siedenbiedel, J. C. Tiller, *Polymers* **2012**, *4*, 46.
- [162] C. P. Fik, C. Krumm, C. Muennig, T. I. Baur, U. Salz, T. Bock, J. C. Tiller, *Biomacromolecules* **2011**, *13*, 165.
- [163] C. J. Waschinski, V. Herdes, F. Schueler, J. C. Tiller, *Macromol. Biosci.* **2005**, *5*, 149.
- [164] C. J. Waschinski, J. Zimmermann, U. Salz, R. Hutzler, G. Sadowski, J. C. Tiller, *Adv. Mater.* **2008**, *20*, 104.
- [165] A. M. Bieser, Y. Thomann, J. C. Tiller, *Macromol. Biosci.* **2011**, *11*, 111.
- [166] S. Phadtare, V. P. Vinod, K. Mukhopadhyay, A. Kumar, M. Rao, R. V. Chaudhari, M. Sastry, *Biotechnol. Bioeng.* **2004**, *85*, 629.
- [167] I. Tokarev, I. Tokareva, V. Gopishetty, E. Katz, S. Minko, *Adv. Mater.* **2010**, *22*, 1412.
- [168] M. Agrawal, J. C. Rueda, P. Uhlmann, M. Müller, F. Simon, M. Stamm, *ACS Appl. Mater. Interfaces* **2012**, *4*, 1357.
- [169] J. C. M. E. Bender, R. Hoogenboom, P. A. A. Van Vliet, *Drug delivery system comprising polyoxazoline and a bioactive agent*, Bender Analytical Holding B.V., **2011**.
- [170] B. Claeys, A. Vervaeck, C. Vervaeet, J. P. Remon, R. Hoogenboom, B. G. De Geest, *Macromol. Rapid Commun.* **2012**, *33*, 1701.

- [171] M. A. C. Stuart, W. T. S. Huck, J. Genzer, M. Muller, C. Ober, M. Stamm, G. B. Sukhorukov, I. Szleifer, V. V. Tsukruk, M. Urban, F. Winnik, S. Zauscher, I. Luzinov, S. Minko, *Nat Mater* **2010**, *9*, 101.
- [172] E. S. Gil, S. M. Hudson, *Prog. Polym. Sci.* **2004**, *29*, 1173.
- [173] K. T. Kim, J. J. L. M. Cornelissen, R. J. M. Nolte, J. C. M. v. Hest, *J. Am. Chem. Soc.* **2009**, *131*, 13908.
- [174] G. Qing, X. Wang, H. Fuchs, T. Sun, *J. Am. Chem. Soc.* **2009**, *131*, 8370.
- [175] H. G. Schild, *Prog. Polym. Sci.* **1992**, *17*, 163.
- [176] S. R. Sershen, S. L. Westcott, N. J. Halas, J. L. West, *J Biomed Mater Res* **2000**, *51*, 293.
- [177] Designing light responsive bistable arches for rapid, remotely triggered actuation
- [178] M. Burnworth, L. Tang, J. R. Kumpfer, A. J. Duncan, F. L. Beyer, G. L. Fiore, S. J. Rowan, C. Weder, *Nature* **2011**, *472*, 334.
- [179] S. Dai, P. Ravi, K. C. Tam, *Soft Matter* **2008**, *4*, 435.
- [180] Y. Kotsuchibashi, Y. Wang, Y.-J. Kim, M. Ebara, T. Aoyagi, R. Narain, *ACS Appl. Mater. Interfaces* **2013**, *5*, 10004.
- [181] Y. Liu, W. Wang, J. Yang, C. Zhou, J. Sun, *Asian J. Pharm. Sci.* **2013**, *8*, 159.
- [182] M. M. Bloksma, D. J. Bakker, C. Weber, R. Hoogenboom, U. S. Schubert, *Macromol. Rapid Commun.* **2010**, *31*, 724.
- [183] T. Wu, P. Gong, I. Szleifer, P. Vlček, V. Šubr, J. Genzer, *Macromolecules* **2007**, *40*, 8756.
- [184] H. Huang, S. Delikanli, H. Zeng, D. M. Ferkey, A. Pralle, *Nat Nano* **2010**, *5*, 602.
- [185] R. Hergt, R. Hiergeist, I. Hilger, W. A. Kaiser, Y. Lapatnikov, S. Margel, U. Richter, *J. Magn. Magn. Mater.* **2004**, *270*, 345.
- [186] K. C. Wood, N. S. Zacharia, D. J. Schmidt, S. N. Wrightman, B. J. Andaya, P. T. Hammond, *Proc. Natl. Acad. Sci. U. S. A.* **2008**, *105*, 2280.
- [187] D. A. Davis, A. Hamilton, J. Yang, L. D. Cremar, D. Van Gough, S. L. Potisek, M. T. Ong, P. V. Braun, T. J. Martinez, S. R. White, J. S. Moore, N. R. Sottos, *Nature* **2009**, *459*, 68.
- [188] C. L. van Oosten, C. W. M. Bastiaansen, D. J. Broer, *Nat Mater* **2009**, *8*, 677.
- [189] R. Contreras-Cáceres, A. Sánchez-Iglesias, M. Karg, I. Pastoriza-Santos, J. Pérez-Juste, J. Pacifico, T. Hellweg, A. Fernández-Barbero, L. M. Liz-Marzán, *Adv. Mater.* **2008**, *20*, 1666.
- [190] J. T. F. Keurentjes, M. F. Kemmere, H. Bruinewoud, M. A. M. E. Vertommen, S. A. Rovers, R. Hoogenboom, L. F. S. Stemkens, F. L. A. M. A. Péters, N. J. C. Tielen, D. T. A. van Asseldonk, A. F. Gabriel, E. A. Joosten, M. A. E. Marcus, *Angew. Chem.* **2009**, *121*, 10051.
- [191] J. Zhang, G. Pu, M. R. Dubay, Y. Zhao, S. J. Severtson, *J. Mater. Chem. C* **2013**, *1*, 1080.
- [192] A. C. Rotzetter, C. M. Schumacher, S. B. Bubenhofer, R. N. Grass, L. C. Gerber, M. Zeltner, W. J. Stark, *Adv Mater* **2012**, *24*, 5352.
- [193] H. Yang, H. Zhu, M. M. R. M. Hendrix, N. J. H. G. M. Lousberg, G. de With, A. C. C. Esteves, J. H. Xin, *Adv. Mater.* **2013**, *25*, 1150.
- [194] A. Kikuchi, T. Okano, *Prog. Polym. Sci.* **2002**, *27*, 1165.
- [195] I. Tan, F. Roohi, M.-M. Titirici, *Anal. Methods* **2011**, *4*, 34
- [196] T. Defize, R. Riva, J.-M. Raquez, P. Dubois, C. Jérôme, M. Alexandre, *Macromol. Rapid Commun.* **2011**, *32*, 1264.
- [197] M. A. Ward, T. K. Georgiou, *Polymers* **2011**, *3*, 1215.
- [198] R. Hoogenboom, in *Complex Macromolecular Architectures*, John Wiley & Sons (Asia) Pte Ltd, **2011**, pp. 685.
- [199] F. Franks, D. Eagland, *CRC Crit Rev Biochem* **1975**, *3*, 165.
- [200] C. Diab, Y. Akiyama, K. Kataoka, F. M. Winnik, *Macromolecules* **2004**, *37*, 2556.
- [201] D. Kuckling, H.-J. P. Adler, K.-F. Arndt, L. Ling, W. D. Habicher, *Macromol. Chem. Phys.* **2000**, *201*, 273.
- [202] C. Weber, R. Hoogenboom, U. S. Schubert, *Prog. Polym. Sci.* **2012**, *37*, 686.
- [203] A. Pranzetti, J. A. Preece, P. M. Mendes, in *Intelligent Stimuli-Responsive Materials*, John Wiley & Sons, Inc., **2013**, pp. 377.
- [204] M. Islam, A. Ahiabu, X. Li, M. Serpe, *Sensors* **2014**, *14*, 8984.
- [205] T. Lopez-Leon, J. L. Ortega-Vinuesa, D. Bastos-Gonzalez, A. Elaissari, *J. Colloid Interface Sci.* **2014**, *426*, 300.
- [206] X. Qiu, M. Li, C. M. S. Kwan, C. Wu, *J. Polym. Sci., Part B: Polym. Phys.* **1998**, *36*, 1501.
- [207] H. Cheng, L. Shen, C. Wu, *Macromolecules* **2006**, *39*, 2325.
- [208] C. Weber, C. Remzi Becer, W. Guenther, R. Hoogenboom, U. S. Schubert, *Macromolecules* **2009**, *43*, 160.
- [209] G. Vancoillie, D. Frank, R. Hoogenboom, *Prog. Polym. Sci.* **2014**, *39*, 1074.
- [210] S. Reinelt, D. Steinke, H. Ritter, *Beilstein J. Org. Chem.* **2014**, *10*, 680.
- [211] E. Moreno, J. Schwartz, E. Larraneta, P. A. Nguewa, C. Sanmartin, M. Agueros, J. M. Irache, S. Espuelas, *Int. J. Pharm.* **2014**, *459*, 1.
- [212] N. Willet, S. Gabriel, C. Jerome, F. E. Du Prez, A.-S. Duwez, *Soft Matter* **2014**, *10*, 7256.
- [213] K. Van Durme, S. Verbrughe, F. E. Du Prez, B. Van Mele, *Macromolecules* **2004**, *37*, 1054.

- [214] M. Beija, J.-D. Marty, M. Destarac, *Chem. Commun.* **2011**, 47, 2826.
- [215] R. Hoogenboom, D. Popescu, W. Steinhauer, H. Keul, M. Moller, *Macromol. Rapid Commun.* **2009**, 30, 2042.
- [216] R. Hoogenboom, A.-M. Zorn, H. Keul, C. Barner-Kowollik, M. Moeller, *Polym. Chem.* **2012**, 3, 335.
- [217] R. Hoogenboom, in *Smart Polymers and their Applications* (Eds.: M. R. Aguilar, J. S. Román), Woodhead Publishing, **2014**, pp. 15.
- [218] D. Roy, W. L. A. Brooks, B. S. Sumerlin, *Chem. Soc. Rev.* **2013**, 42, 7214.
- [219] R. Liu, M. Fraylich, B. Saunders, *Colloid. Polym. Sci.* **2009**, 287, 627.
- [220] S. Han, M. Hagiwara, T. Ishizone, *Macromolecules* **2003**, 36, 8312.
- [221] T. Ishizone, A. Seki, M. Hagiwara, S. Han, H. Yokoyama, A. Oyane, A. Deffieux, S. Carlotti, *Macromolecules* **2008**, 41, 2963.
- [222] J.-F. Lutz, A. Hoth, *Macromolecules* **2005**, 39, 893.
- [223] J.-F. Lutz, Ö. Akdemir, A. Hoth, *J. Am. Chem. Soc.* **2006**, 128, 13046.
- [224] J.-F. Lutz, *Adv. Mater.* **2011**, 23, 2237.
- [225] W. Steinhauer, R. Hoogenboom, H. Keul, M. Moeller, *Macromolecules* **2010**, 43, 7041.
- [226] C. R. Becer, R. M. Paulus, S. Höppener, R. Hoogenboom, C.-A. Fustin, J.-F. Gohy, U. S. Schubert, *Macromolecules* **2008**, 41, 5210.
- [227] K. Kempe, T. Neuwirth, J. Czaplowska, M. Gottschaldt, R. Hoogenboom, U. S. Schubert, *Polym. Chem.* **2011**, 2, 1737.
- [228] R. Hoogenboom, *Angew. Chem. Int. Ed.* **2009**, 48, 7978.
- [229] E. Rossegger, V. Schenk, F. Wiesbrock, *Polymers* **2013**, 5, 956.
- [230] P. Lin, C. Clash, E. M. Pearce, T. K. Kwei, M. A. Aponte, *J. Polym. Sci., Part B: Polym. Phys.* **1988**, 26, 603.
- [231] D. Christova, R. Velichkova, W. Loos, E. J. Goethals, F. D. Prez, *Polymer* **2003**, 44, 2255.
- [232] J.-S. Park, K. Kataoka, *Macromolecules* **2006**, 39, 6622.
- [233] J.-S. Park, K. Kataoka, *Macromolecules* **2007**, 40, 3599.
- [234] H. Uyama, S. Kobayashi, *Chem. Lett.* **1992**, 21, 1643.
- [235] M. M. Bloksma, C. Weber, I. Y. Perevyazko, A. Kuse, A. Baumgärtel, A. Vollrath, R. Hoogenboom, U. S. Schubert, *Macromolecules* **2011**, 44, 4057.
- [236] K. M. McCabe, M. Hernandez, *Pediatr. Res.* **2010**, 67, 469.
- [237] J. Lee, N. A. Kotov, *Nano Today* **2007**, 2, 48.
- [238] C. Gota, K. Okabe, T. Funatsu, Y. Harada, S. Uchiyama, *J. Am. Chem. Soc.* **2009**, 131, 2766.
- [239] K. Okabe, N. Inada, C. Gota, Y. Harada, T. Funatsu, S. Uchiyama, *Nat. Commun.* **2012**, 3, 705.
- [240] L. Luo, A. Eisenberg, *Langmuir* **2001**, 17, 6804.
- [241] J. Hu, *Adaptive and Functional Polymers, Textiles and Their Applications* Imperial College Press, London, **2011**.
- [242] Y.-M. Liu, W. Wu, X.-J. Ju, W. Wang, R. Xie, C.-L. Mou, W.-C. Zheng, Z. Liu, L.-Y. Chu, *RSC Advances* **2014**, 4, 46568.
- [243] H. Wei, X.-Z. Zhang, W.-Q. Chen, S.-X. Cheng, R.-X. Zhuo, *Journal of Biomedical Materials Research Part A* **2007**, 83A, 980.
- [244] Y.-L. Luo, X.-L. Yang, F. Xu, Y.-S. Chen, Z.-M. Ren-Ting, *J. Appl. Polym. Sci.* **2013**, 130, 4137.
- [245] T. M. Quynh, M. Yoneyama, Y. Maki, T. Dobashi, *J. Appl. Polym. Sci.* **2012**, 123, 2368.
- [246] P. Sun, Y. Zhang, L. Shi, Z. Gan, *Macromol. Biosci.* **2010**, 10, 621.
- [247] J. Xu, S. Luo, W. Shi, S. Liu, *Langmuir* **2005**, 22, 989.
- [248] M. Karesoja, E. Karjalainen, S. Hietala, H. Tenhu, *J. Phys. Chem. B* **2014**, 118, 10776.
- [249] R. Pelton, *Adv. Colloid Interface Sci.* **2000**, 85, 1.
- [250] M. S. H. Akash, K. Rehman, S. Chen, *Polymer Reviews* **2014**, 54, 573.
- [251] L. Klouda, A. G. Mikos, *Eur. J. Pharm. Biopharm.* **2008**, 68, 34.
- [252] M. A. M. E. Vertommen, H.-J. L. Cornelissen, C. H. J. T. Dietz, R. Hoogenboom, M. F. Kemmere, J. T. F. Keurentjes, *J. Membr. Sci.* **2008**, 322, 243.
- [253] Y. S. Park, Y. Ito, Y. Imanishi, *Langmuir* **1998**, 14, 910.
- [254] E. J. Geiger, A. P. Pisano, F. Svec, *J. MEMS* **2010**, 19, 944
- [255] Nanopatterning and Nanoscale Devices for Biological Applications
- [256] A. K. Agarwal, S. S. Sridharamurthy, D. J. Beebe, J. Hongrui, *J. MEMS* **2005**, 14, 1409.
- [257] C. Comminges, S. Frasca, M. Sutterlin, E. Wischerhoff, A. Laschewsky, U. Wollenberger, *RSC Advances* **2014**, 4, 43092.
- [258] S. Camou, H. Fujita, T. Fujii, *Lab on a Chip* **2003**, 3, 40.
- [259] S.-k. Ahn, R. M. Kasi, S.-C. Kim, N. Sharma, Y. Zhou, *Soft Matter* **2008**, 4, 1151.
- [260] A. K. A. S. Brun-Graeppe, C. Richard, M. Bessodes, D. Scherman, O.-W. Merten, *Prog. Polym. Sci.* **2010**, 35, 1311.
- [261] D. Schmaljohann, *Adv. Drug Delivery Rev.* **2006**, 58, 1655.
- [262] A. Kubota, K. Nishida, M. Yamato, J. Yang, A. Kikuchi, T. Okano, Y. Tano, *Biomaterials* **2006**, 27, 3639.

- [263] J. Shan, M. Nuopponen, H. Jiang, E. Kauppinen, H. Tenhu, *Macromolecules* **2003**, *36*, 4526.
- [264] K. Kusolkamabot, P. Sae-ung, N. Niamnont, K. Wongravee, M. Sukwattanasinitt, V. P. Hoven, *Langmuir* **2013**, *29*, 12317.
- [265] C. Boyer, M. R. Whittaker, M. Luzon, T. P. Davis, *Macromolecules* **2009**, *42*, 6917.
- [266] I. Robinson, C. Alexander, L. D. Tung, D. G. Fernig, N. T. K. Thanh, *J. Magn. Magn. Mater.* **2009**, *321*, 1421.
- [267] Z. Zhang, J. Wang, X. Nie, T. Wen, Y. Ji, X. Wu, Y. Zhao, C. Chen, *J. Am. Chem. Soc.* **2014**, *136*, 7317.
- [268] J.-M. Lehn, *Angew. Chem. Int. Ed. Engl.* **1990**, *29*, 1304.
- [269] P. Cordier, F. Tournilhac, C. Soulie-Ziakovic, L. Leibler, *Nature* **2008**, *451*, 977.
- [270] A. Harada, J. Li, M. Kamachi, *Nature* **1992**, *356*, 325.
- [271] A. Harada, K. Kataoka, *Macromolecules* **1995**, *28*, 5294.
- [272] J. H. K. K. Hirschberg, L. Brunsveld, A. Ramzi, J. A. J. M. Vekemans, R. P. Sijbesma, E. W. Meijer, *Nature* **2000**, *407*, 167.
- [273] F. M. Raymo, J. F. Stoddart, *Chem. Rev.* **1999**, *99*, 1643.
- [274] T. Shimizu, M. Masuda, H. Minamikawa, *Chem. Rev.* **2005**, *105*, 1401.
- [275] M. Steinhart, in *Self-Assembled Nanomaterials II, Vol. 220* (Ed.: T. Shimizu), Springer Berlin Heidelberg, **2008**, pp. 123.
- [276] L. Brunsveld, B. J. B. Folmer, E. W. Meijer, R. P. Sijbesma, *Chem. Rev.* **2001**, *101*, 4071.
- [277] A. Harada, A. Hashidzume, H. Yamaguchi, Y. Takashima, *Chem. Rev.* **2009**, *109*, 5974.
- [278] A. Harada, Y. Takashima, H. Yamaguchi, *Chem. Soc. Rev.* **2009**, *38*, 875.
- [279] B. V. K. J. Schmidt, M. Hetzer, H. Ritter, C. Barner-Kowollik, *Prog. Polym. Sci.* **2014**, *39*, 235.
- [280] J. Hu, S. Liu, *Macromolecules* **2010**, *43*, 8315.
- [281] J. Hu, S. Liu, *Acc. Chem. Res.* **2014**, *47*, 2084.
- [282] C. Cheng, X.-J. Han, Z.-Q. Dong, Y. Liu, B.-J. Li, S. Zhang, *Macromol. Rapid Commun.* **2011**, *32*, 1965.
- [283] Y. Liu, D. Zhao, R. Ma, D. a. Xiong, Y. An, L. Shi, *Polymer* **2009**, *50*, 855.
- [284] B. Nowacki, H. Oh, C. Zanlorenzi, H. Jee, A. Baev, P. N. Prasad, L. Akcelrud, *Macromolecules* **2013**, *46*, 7158.
- [285] E. Yashima, K. Maeda, *Macromolecules* **2007**, *41*, 3.
- [286] T. Vidil, F. Tournilhac, L. Leibler, *Polym. Chem.* **2013**, *4*, 1323.
- [287] R. Sakai, T. Kakuchi, *Macromol. Symp.* **2007**, *249-250*, 81.
- [288] R. Sakai, I. Otsuka, T. Satoh, R. Kakuchi, H. Kaga, T. Kakuchi, *Macromolecules* **2006**, *39*, 4032.
- [289] E. Yashima, K. Maeda, O. Sato, *J. Am. Chem. Soc.* **2001**, *123*, 8159.
- [290] H. Hofmeier, A. El-ghayoury, A. P. H. J. Schenning, U. S. Schubert, *Chem. Commun.* **2004**, 318.
- [291] H. Hofmeier, R. Hoogenboom, M. E. L. Wouters, U. S. Schubert, *J. Am. Chem. Soc.* **2005**, *127*, 2913.
- [292] H.-X. Zhao, D.-S. Guo, L.-H. Wang, H. Qian, Y. Liu, *Chem. Commun.* **2012**, *48*, 11319.
- [293] J. Bigot, B. Charleux, G. Cooke, F. Delattre, D. Fournier, J. Lyskawa, L. Sambe, F. Stoffelbach, P. Woisel, *J. Am. Chem. Soc.* **2010**, *132*, 10796.
- [294] L. n. Sambe, F. o. Stoffelbach, J. Lyskawa, F. o. Delattre, D. Fournier, L. Bouteiller, B. Charleux, G. Cooke, P. Woisel, *Macromolecules* **2011**, *44*, 6532.
- [295] G. Volet, V. Chanthavong, V. Wintgens, C. Amiel, *Macromolecules* **2005**, *38*, 5190.
- [296] G. Volet, A.-C. L. Deschamps, C. Amiel, *J. Polym. Sci., Part A: Polym. Chem.* **2010**, *48*, 2477.
- [297] L. Sambe, F. Stoffelbach, K. Poltorak, J. Lyskawa, A. Malfait, M. Bria, G. Cooke, P. Woisel, *Macromol. Rapid Commun.* **2014**, *35*, 498.
- [298] X. Wang, J. Li, X. Jia, C. Li, *Polym. Chem.* **2013**, *4*, 3998.
- [299] B. V. K. J. Schmidt, M. Hetzer, H. Ritter, C. Barner-Kowollik, *Polym. Chem.* **2012**, *3*, 3064.
- [300] H. Liu, Y. Zhang, J. Hu, C. Li, S. Liu, *Macromol. Chem. Phys.* **2009**, *210*, 2125.
- [301] F. Sakai, G. Chen, M. Jiang, *Polym. Chem.* **2012**, *3*, 954.
- [302] F. Szillat, B. V. K. J. Schmidt, A. Hubert, C. Barner-Kowollik, H. Ritter, *Macromol. Rapid Commun.* **2014**, *35*, 1293.
- [303] Y. Li, H. Guo, Y. Zhang, J. Zheng, J. Gan, X. Guan, M. Lu, *RSC Advances* **2014**, *4*, 17768.
- [304] M. Adeli, M. Kalantari, Z. Zarnega, R. Kabiri, *RSC Advances* **2012**, *2*, 2756.
- [305] Z. Ge, H. Liu, Y. Zhang, S. Liu, *Macromol. Rapid Commun.* **2011**, *32*, 68.
- [306] J. Yan, X. Zhang, X. Zhang, K. Liu, W. Li, P. Wu, A. Zhang, *Macromol. Chem. Phys.* **2012**, *213*, 2003.
- [307] Y. Liu, C. Yu, H. Jin, B. Jiang, X. Zhu, Y. Zhou, Z. Lu, D. Yan, *J. Am. Chem. Soc.* **2013**, *135*, 4765.
- [308] J. Yan, X. Zhang, W. Li, X. Zhang, K. Liu, P. Wu, A. Zhang, *Soft Matter* **2012**, *8*, 6371.
- [309] G. Maatz, A. Maciollek, H. Ritter, *Beilstein J. Org. Chem.* **2012**, *8*, 1929.
- [310] H. Ritter, J. Cheng, M. Tabatabai, *Beilstein J. Org. Chem.* **2012**, *8*, 1528.
- [311] B. V. K. J. Schmidt, M. Hetzer, H. Ritter, C. Barner-Kowollik, *Macromol. Rapid Commun.* **2013**, *34*, 1306.
- [312] J. Bigot, M. Bria, S. T. Caldwell, F. Cazaux, A. Cooper, B. Charleux, G. Cooke, B. Fitzpatrick, D. Fournier, J. Lyskawa, M. Nutley, F. Stoffelbach, P. Woisel, *Chem. Commun. (Cambridge, U. K.)* **2009**, *0*, 5266.

- [313] G. Lazzara, G. Olofsson, V. Alfredsson, K. Zhu, B. Nystrom, K. Schillen, *Soft Matter* **2012**, *8*, 5043.
- [314] A. Burkhart, H. Ritter, *Beilstein J. Org. Chem.* **2014**, *10*, 1951.
- [315] Y.-G. Jia, X. X. Zhu, *Langmuir* **2014**.
- [316] V. Wintgens, M. Charles, F. Allouache, C. Amiel, *Macromol. Chem. Phys.* **2005**, *206*, 1853.
- [317] L. Sambe, V. R. de La Rosa, K. Belal, F. Stoffelbach, J. Lyskawa, F. Delattre, M. Bria, G. Cooke, R. Hoogenboom, P. Woisel, *Angew. Chem. Int. Ed.* **2014**, *53*, 5044.
- [318] M. V. Rekharsky, Y. Inoue, *Chem. Rev.* **1998**, *98*, 1875.
- [319] I. Tomatsu, A. Hashizume, A. Harada, *J. Am. Chem. Soc.* **2006**, *128*, 2226.
- [320] A. Harada, *Acc. Chem. Res.* **2001**, *34*, 456.
- [321] S. Tamesue, Y. Takashima, H. Yamaguchi, S. Shinkai, A. Harada, *Angew. Chem. Int. Ed.* **2010**, *49*, 7461.
- [322] Y. Takashima, S. Hatanaka, M. Otsubo, M. Nakahata, T. Kakuta, A. Hashizume, H. Yamaguchi, A. Harada, *Nat. Commun.* **2012**, *3*, 1270.
- [323] C. Luo, F. Zuo, X. Ding, Z. Zheng, X. Cheng, Y. Peng, *J. Appl. Polym. Sci.* **2008**, *107*, 2118.
- [324] J. He, L. Tremblay, S. Lacelle, Y. Zhao, *Polym. Chem.* **2014**, *5*, 5403.

Controlling the hydrolysis of (co)poly(2-alkyl/aryl-2-oxazoline)s

The ability of merging the properties of poly(2-alkyl/aryl-2-oxazoline)s (PAOx) and poly(ethyleneimine) (PEI) is of high interest for various applications, including gene delivery, biosensors, hydrogels and switchable surfaces and nanoparticles. Moreover, the diverse end group functionality attainable in the cationic ring-opening polymerization of 2-oxazolines highly extends the application potential of such copolymers. In the present research, efficient strategies for the controlled and selective hydrolysis of (co)poly(2-oxazoline)s are developed, opening the path towards a wide range of block or statistical poly(2-oxazoline-*co*-ethylene imine) (PAOx-PEI) copolymers with tunable properties.

2.1 Introduction

Cationic ring opening polymerization (CROP) of 2-alkyl/aryl-2-oxazolines affords poly(2-alkyl/aryl-2-oxazoline)s (PAOx) with a narrow molecular weight distribution, tunable properties and excellent biocompatibility,^[1] mostly documented for the water-soluble poly(2-methyl-2-oxazoline) (PMeOx) and poly(2-ethyl-2-oxazoline) (PEtOx), and ascribed to their structural analogy with polypeptides.^[2] Telechelic polymers are readily obtained by selection of initiator (typically alkyl halides, (pluri)tosylates, (pluri)nosylates, etc.) and end-capping agent (a nucleophile)^[3], while side-chains can be tuned by modification of the 2-substituent of the 2-oxazoline monomer.^[4] Block copolymers can be obtained by sequential one-pot monomer addition, as a result of the living character of the CROP of 2-oxazolines. The use of microwave synthesizers has exerted a tremendous impact on the polymerization of 2-oxazolines by reducing the polymerization times to minutes or even seconds, thus allowing for high-throughput polymer synthesis and a systematic study of structure-property relationships.^[5,6] Therefore, PAOx have become a promising candidate for a variety of biomedical applications,^[7-10] exhibiting higher synthetic versatility than the ubiquitous poly(ethylene glycol) (PEG).^[11,12]

Furthermore, the hydrolysis of PAOx renders linear poly[(2-oxazoline)-*co*-ethylenimine] (PAOx-*co*-PEI) copolymers or, if the process is brought to full conversion, in linear polyethyleneimine (L-PEI), constituting the main method to synthesize well defined L-PEI with interesting solubility properties due to its crystallinity and pH responsiveness (see Figure 2.1.1).^[13-15]

Parts of this chapter have been published in: de la Rosa, V. R.; Bauwens, E.; Monnery, B. D.; De Geest, B. G.; Hoogenboom, R. *Polymer Chemistry*, **2014**, *17*, 4957-4964.
van Kuringen, H. P. C.; de la Rosa, V. R.; Fijten, M. W. M.; Heuts, J. P. A.; Hoogenboom, R. *Macromolecular Rapid Communications*, **2012**, *33*, 827-832.

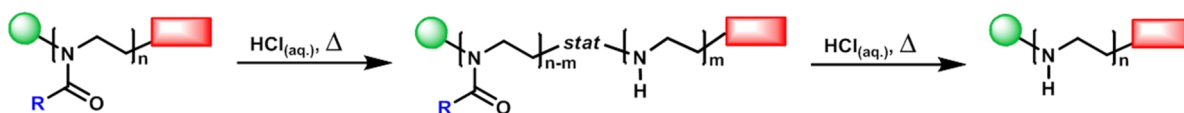


Figure 2.1.1. *Partial acid hydrolysis of poly(2-alkyl/aryl-2-oxazoline)s yielding PAOx-PEI random copolymers. By controlling reaction time or acid concentration, full hydrolysis of PAOx yielding L-PEI can be achieved. Polymer end-group functionalities, such as targeting groups or fluorescent probes, can be easily introduced in the resulting L-PEI during the synthesis of the PAOx precursor.*

The introduction of secondary amines throughout the PAOx backbone in PAOx-*co*-PEI copolymers also offers a reactive handle for further modification by post-polymerization functionalization, further expanding PAOx synthetic versatility and polymer architectures attainable.^[16-19] For instance, PAOx graft copolymers can be readily synthesized by terminating living PAOx chains with the secondary amines present in PAOx-*co*-PEI copolymers.^[20] These secondary amines can also be used as cross-linking points, resulting in pH-responsive hydrogels and nanogels for biomedical applications, as recently reported by Lecommandoux *et al.*^[21]

As seen in the aforementioned applications, control over the hydrolysis degree is crucial to tailor the properties of the final PAOx-*co*-PEI materials. Since first reported by Saegusa over 40 years ago,^[13] the synthesis of L-PEI *via* PAOx hydrolysis has been performed under strong acidic or alkaline conditions exhibiting pseudo-first order kinetics, with a direct correlation between acid or base concentration and hydrolysis rate.

Acidic conditions were found to be preferred as they afford a faster and more controlled hydrolysis process by assuring total solubility of the formed PEI domains that are protonated at low pH.^[22] Moreover, size exclusion chromatography (SEC; using hexafluoroisopropanol (HFIP) as eluent) revealed degradation during basic hydrolysis.^[23] Typically, the hydrolysis is performed under reflux conditions with concentrated HCl_{aq} (usually 6 M), and the extent of hydrolysis can be controlled by the reaction time. However, under these conditions, small fluctuations in temperature and reaction time can result in large variations on the final degree of hydrolysis, thereby strongly impairing reproducibility.

Despite the research undertaken, the main limitation for the partial hydrolysis of PAOx remains the difficulty to obtain accurate and reproducible hydrolysis degrees over the whole hydrolysis range, especially over short reaction times.^[24] In the first part of this chapter, the optimization of the hydrolysis conditions is described. The hydrolysis process has been greatly accelerated by increasing reaction temperature and, importantly, the degree of hydrolysis is accurately controlled by varying the acid concentration.

Fast and robust synthesis of PEtOx-PEI copolymers

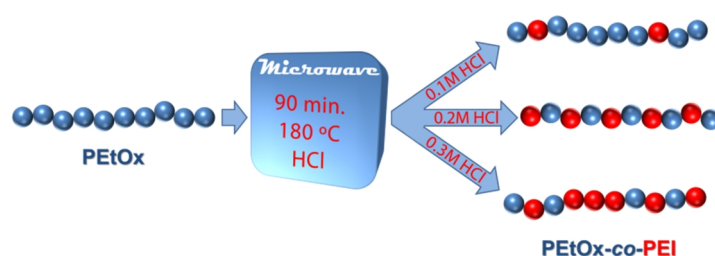


Figure 2.1.2. *The hydrolysis of PEtOx is accelerated by increasing temperature to 180 °C, which was found to yield the optimal results with regard to speed and control over the final copolymer structure.*

In addition, control over the desired degree of hydrolysis of PEtOx was obtained by selecting the appropriate HCl concentration.

Besides the new synthetic opportunities opened by the introduction of secondary amines across the polymer backbone in partially hydrolyzed PAOx, PEI constitutes a polymer with a wide range of applications, especially in life-sciences. L-PEI obtained from the full hydrolysis of PAOx has been widely studied as a successful non-viral vector for gene delivery, outperforming the gold standard branched-PEI in terms of toxicity,^[25-31] and in other biomedical applications such as component in dental cements.^[32] In fact, some of the commercially available L-PEIs (ExGen500, jetPEI®) already reached clinical trials, including treatments for bladder carcinoma and HIV disease.^[27,33]

The partial hydrolysis of PAOx results in PAOx-co-PEI copolymers that encompass both the interesting properties of PAOx and PEI while being less cytotoxic than L-PEI. These copolymers are also responsive to external stimuli such as temperature and pH^[23, 34] finding a variety of applications in biomedicine, such as aqueous self-assembly, micellar catalysis, or drug delivery.^[14, 35] Indeed, the conjunction of PEI domains with stealth polymers such as PAOx or PEG has demonstrated to meet the DNA and RNA transfection efficiency of the commercial L-PEI, while reducing cytotoxicity and facilitating the introduction of targeting moieties for localized gene therapy (Figure 2.1.3).^[36-41]

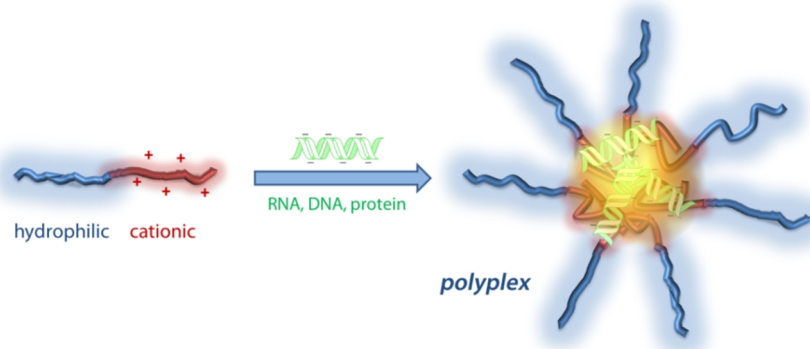


Figure 2.1.3. *Block copolymers containing a hydrophilic stealth polymer, such as PEtOx, and a cationic L-PEI domain, interact with poly(nucleic acids) resulting in efficient formation of polymer-poly(nucleic acid) complexes or polyplexes with improved biocompatibility.*

Consequently, the direct preparation of such L-PEI conjugates via selective hydrolysis of PAOx block copolymers is of high interest, representing an elegant approach in the pursue of improved gene delivery systems benefiting from the tunable properties and biocompatibility of PAOx. Therefore, detailed investigations of the hydrolysis of different PAOx are required aiming for double hydrophilic PEI-PAOx statistical and copolymers with blocky character by straightforward selective hydrolysis of hydrophilic PAOx copolymers; previous reports on selective PAOx hydrolysis all included a hydrophobic PAOx block.¹⁹⁻²¹

In the second part of this chapter, we describe the development of a new methodology that provides control and selectivity over the partial hydrolysis of (co)poly(2-oxazoline)s. PEtOx-co-PEI quasi-block copolymers are successfully obtained by controlling the characteristics of the solvent used in the hydrolysis of hydrophilic block-copoly(2-oxazoline)s (see Figure 2.1.4).

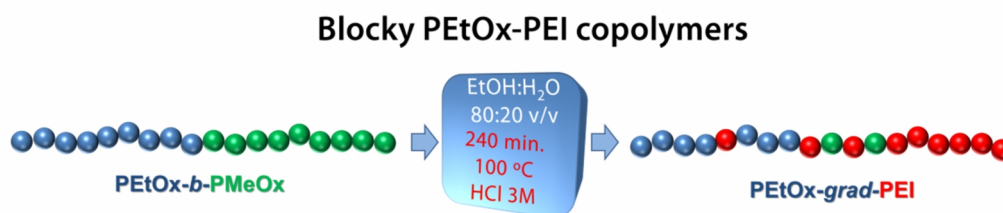


Figure 2.1.4. PEtOx-co-PEI copolymers with a blocky character are obtained in a straightforward manner by tuning the composition of the ethanol : water binary solvent system employed.

2.1.1. Hydrolysis of poly(2-oxazoline)s: kinetic considerations

The mechanism of the acid-catalyzed hydrolysis of PAOx is analogous to that of a monomeric amide, and has been found to be independent on the length of the polymer chain, indicating that all amide groups in the PAOx side chain are equally accessible.^[22, 34] The mechanism of the acid-catalyzed hydrolysis of PAOx is shown in Figure 2.1.5.^[42]

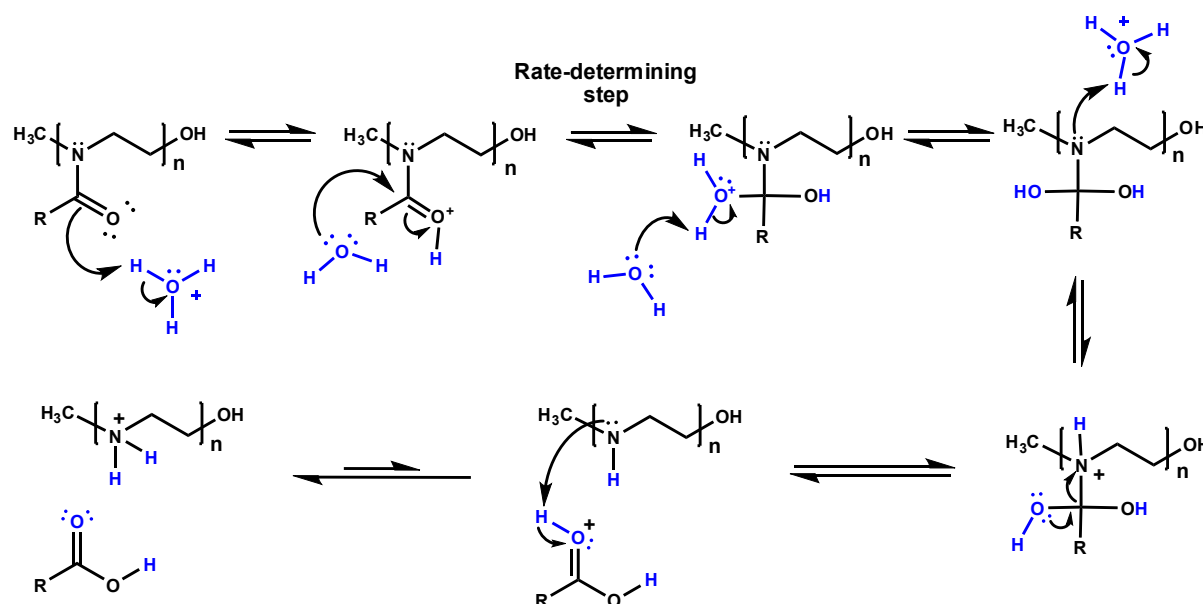


Figure 2.1.5. Mechanism for the acid-catalyzed hydrolysis of poly(2-oxazoline)s.

The reaction occurs as a four-step process. First, the acid protonates the carbonyl oxygen, which increases the susceptibility of the carbonyl carbon to nucleophilic addition. The second and rate-determining step is the nucleophilic attack of a water molecule to the carbon atom of the amide group. During this process, a proton is transferred to the water phase. In a separate step, the protonation of the intermediate nitrogen atom occurs. Protonation on nitrogen is favored as this is a stronger base in comparison with the OH group. Both protonation by a hydronium ion or *via* dissociation of a water molecule are possible. Finally, the C-N bond is cleaved releasing the ethyleneimine unit and the corresponding carboxylic acid resulting from the PAOx side chain. One proton is released in this last step, which can be captured by the ethyleneimine secondary amine.

In excess of acid, the reaction follows pseudo first-order kinetics, and the rate constant is given by the following equation:

$$\text{hydrolysis rate} = k_h[A][H^+] = k'_h[A] \quad \text{Equation 2.1.1.}$$

Where k is the rate constant, $[A]$ and $[H^+]$ the amide and acid concentration, respectively, and k'_h the pseudo-first order rate constant.

In the present work, the amide concentration was kept fixed to 0.48 M for all hydrolysis reactions, and the acid used was HCl_{aq} . In part 2.2. of this chapter, acid concentration was varied from a small excess (1.0 M) to sub-stoichiometric amounts. As we shall see, acid concentration has a major impact on the hydrolysis process. In part 2.3., the acid concentration was kept in large excess, at 3.0 M.

2.2 Fast and accurate partial hydrolysis of poly(2-ethyl-2-oxazoline) into tailored linear polyethylenimine copolymers

2.2.1. Introduction

As has been previously introduced, partial hydrolysis of poly(2-oxazoline) homopolymers yields poly[(2-oxazoline)-*co*-(ethylenimine)] statistical copolymers that are of interest for a broad range of applications. These range from switchable surfaces,^[43] nanoparticles and hydrogels,^[21, 31] to gene delivery and biosensors.^[20, 35, 38] However, the main limitation for the partial hydrolysis of PAOx remains the difficulty to obtain accurate and reproducible hydrolysis degrees over the whole hydrolysis range, especially over short reaction times.^[24]

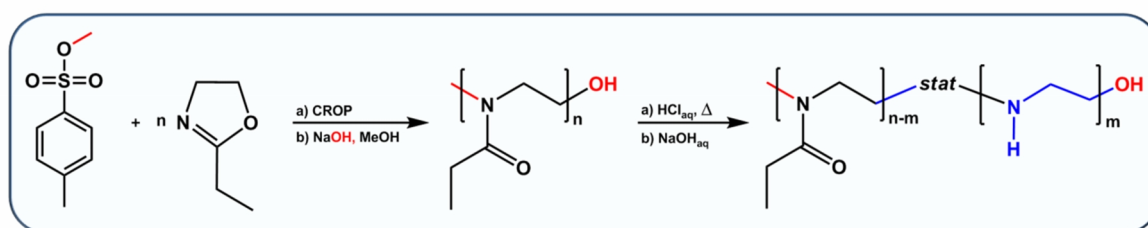


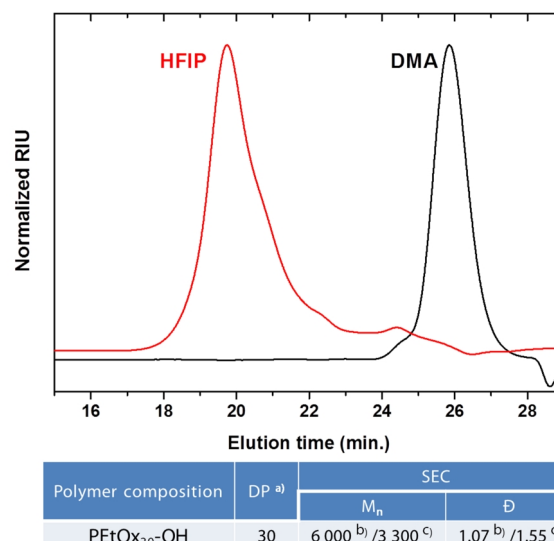
Figure 2.2.1. General scheme for the cationic ring-opening polymerization of 2-ethyl-2-oxazoline initiated by methyl tosylate and terminated by $-OH$, followed by partial hydrolysis in $HCl_{(aq)}$.

In this part of the chapter, we report on defining optimal conditions to achieve tailored PEtOx-*co*-PEI copolymers in a fast and reproducible way, utilizing high temperatures and controlled acidic conditions.

2.2.2. Synthesis and characterization of PEtOx-OH

To confirm that the hydrolysis conditions are independent on the length of the PEtOx polymer, we performed all the hydrolysis experiments on a well-defined PEtOx 3 kDa synthesized in our laboratories, and on a polydisperse commercial PEtOx 50 kDa. The results were analogous for both polymers, therefore we will only discuss the results concerning the well-defined PEtOx 3 kDa.

Figure 2.2.2. Characterization data of the synthesized PEtOx₃₀-OH polymer. ^{a)} Calculated by 1H -NMR spectroscopy in $CDCl_3$. SEC eluent: ^{b)} N,N -



dimethylacetamide, calibrated against poly(methyl methacrylate) standards. ^d*Hexafluoroisopropanol, calibrated against polystyrene standards.*

2.2.3. Accelerating PEtOx hydrolysis: hydrolysis kinetics of poly(2-ethyl-2-oxazoline) at elevated temperatures

The use of a microwave synthesizer allows performing PEtOx hydrolysis at higher temperatures, and can reduce reaction times to an order of minutes. Recently, the full hydrolysis of PEtOx to obtain pure L-PEI was optimized by Schubert *et al.* using high acid concentration (3M) and a temperature slightly beyond reflux conditions (130 °C), by means of a microwave synthesizer.^[15] In the current research, we aimed to control fast partial hydrolysis of PEtOx. Therefore, milder acidic conditions, *i.e.* 1.0 M HCl concentration, and higher temperatures were utilized. In order to ascertain the maximum temperature at which the hydrolysis of PEtOx can be performed, without compromising the polymer integrity, PEtOx solutions were heated for different times at temperatures ranging from 100 °C to 220 °C under microwave irradiation.

The obtained PEtOx-*co*-PEI copolymers were basidified with NaOH_(aq) and the conversion from PEtOx to PEI was calculated based on ¹H-nuclear magnetic resonance (¹H-NMR) spectroscopy. Figure 2.2.3 shows the ¹H-NMR spectrum of the PEtOx₃₀-OH hydrolyzed in this study and a typical spectrum obtained after its partial hydrolysis.

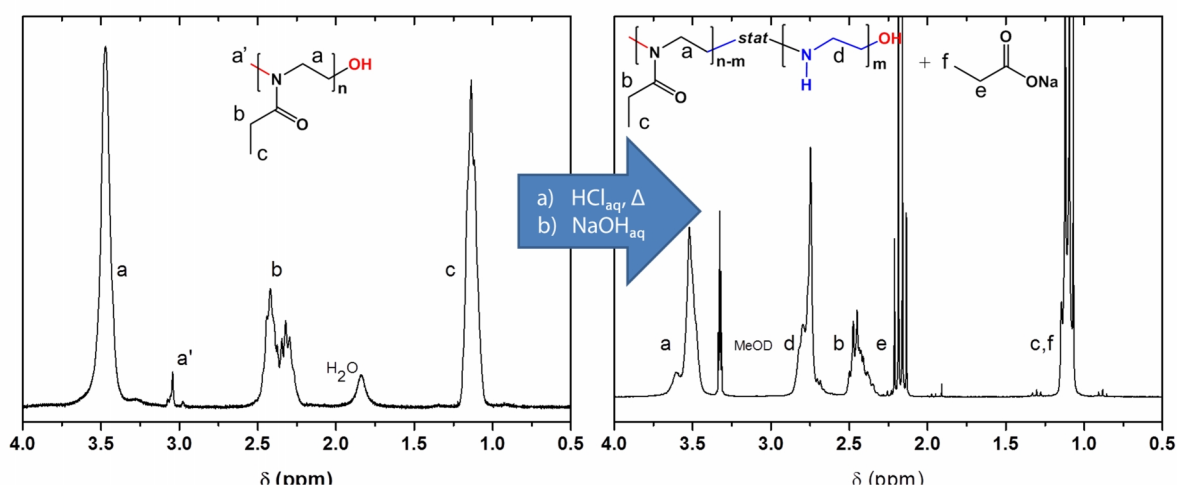


Figure 2.2.3. ¹H-NMR spectra of poly(2-ethyl-2-oxazoline) 3 kDa in CDCl₃ before hydrolysis (left) and after 20 min, hydrolysis at 140 °C (54% hydrolysis conversion), measured in CD₃OD.

The hydrolysis conversion is calculated from the ¹H-NMR spectra of the obtained PEtOx-*co*-PEI copolymers in deuterated methanol. Besides the signals of PEtOx and PEI, the signals of the sodium propionate released upon hydrolysis and addition of NaOH are present.

The calculation method used for determining the conversion is based on the integral values (*I*) of the PAOx and PEI backbones, as displayed in the following equations:

$$\% \text{ Conversion PEtOx} = \frac{I[\text{PEI backbone}]}{I[\text{PEI backbone}] + I[\text{PEtOx backbone}]} \times 100 \quad \text{Equation 2.2.1.}$$

$$\% \text{ Conversion PEtOx} = \frac{I[\text{PEI backbone}]}{2(I[\text{EtOx CH}_2]) + I[\text{PEI backbone}]} \times 100 \quad \text{Equation 2.2.2.}$$

The conversion values calculated from these equations were always found to differ by less than 5%, and the average value is reported. Figure 2.2.4. displays the evolution of the ¹H-NMR spectra

with the hydrolysis time at 140 °C, where the progressive conversion of EtOx units into ethyleneimine (EI) and sodium propionate is observed.

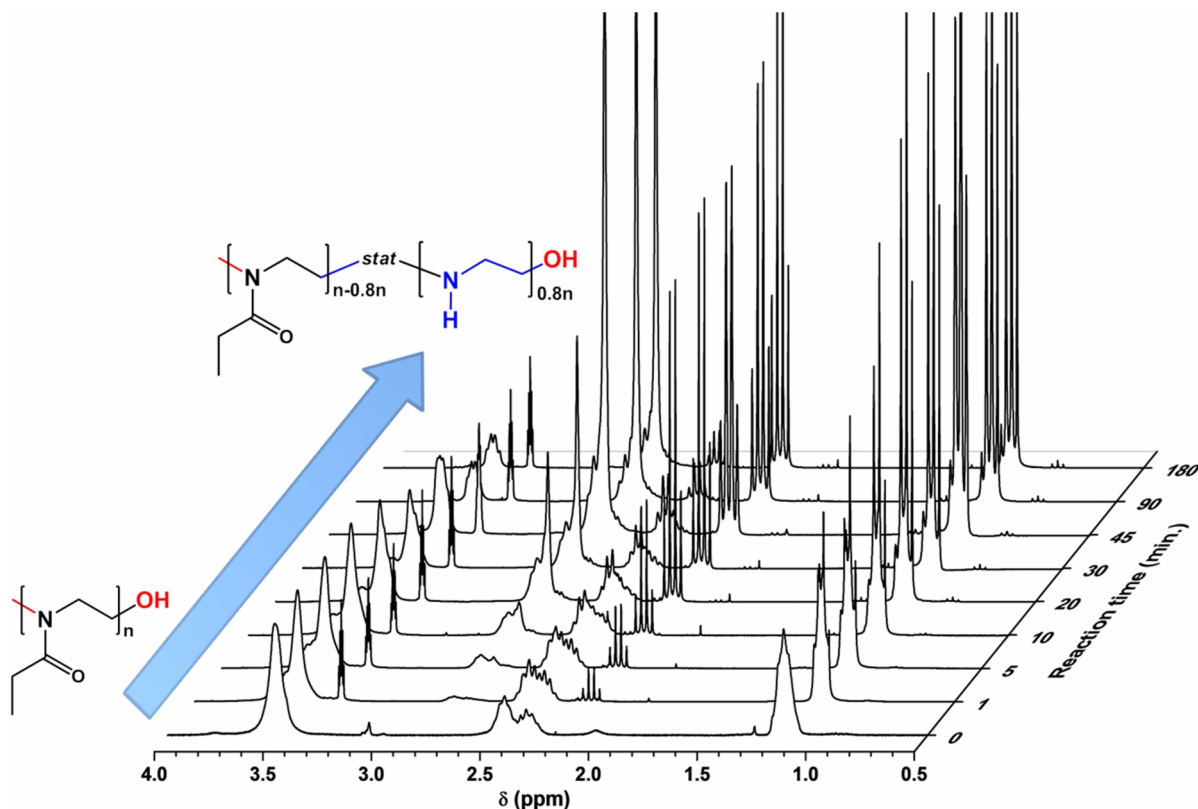


Figure 2.2.4. Series of $^1\text{H-NMR}$ spectra in CD_3OD corresponding to the hydrolysis of PEtOx 3 kDa in 1.0 M $\text{HCl}_{(\text{aq})}$ at 140 °C. $[A] = \text{amide concentration} = 0.48 \text{ M}$. The spectra were normalized to the signal corresponding to deuterated methanol.

Temperature was found to strongly impact the hydrolysis kinetics of PEtOx, sharply accelerating the hydrolysis rate even when heating only 20 °C above reflux conditions (see Figure 2.2.5). Increasing reaction temperature thus constitutes an effective way to hydrolyze PEtOx under much milder acidic conditions than previously reported, namely 1.0 M HCl instead of 6 M HCl.

As described in part 2.1.1., the hydrolysis of PEtOx has been shown to follow a pseudo-first order kinetics mechanism, where hydronium ions act as a catalyst and thus their concentration remains *quasi* constant during the hydrolysis.^[34] However, in the current research the kinetic plot deviates from linearity leveling-off after *ca.* 80% conversion, as shown in Figure 2.2.5.b. This observation can be ascribed to the protonation of the ethylene imine units formed during the hydrolysis, reducing the availability of hydronium ions to catalyze the reaction, and consequently decreasing the reaction rate. This effect of a lower concentration of hydronium ions directly results from integrating the pseudo-first order rate law:

$$-\frac{d[A]_0}{dt} = k_h [H^+] [A] \quad \text{Equation 2.2.3.}$$

$$\text{Conversion} \propto \ln \left(\frac{[A]_0}{[A]_t} \right) = k_h [H^+] t \quad \text{Equation 2.2.4.}$$

Where: initial amide concentration, $[A]_0 = 0.48 \text{ M}$. k_h : hydrolysis rate constant ($\text{L mol}^{-1} \text{ s}^{-1}$), $[H^+]_0 = 1.0 \text{ M}$, $t = \text{time (seconds)}$.

This hydronium depletion upon PEtOx hydrolysis has not been previously observed as a deviation from linear first order kinetics since former reports made use of a large HCl excess, thereby masking the effect of amine protonation. In the present study, the HCl concentration (1.0 M) was just beyond twice the PEtOx amide concentration (0.48 M) and thus, the loss of hydronium ions by protonation of the amines has a significant effect on the hydrolysis kinetics.

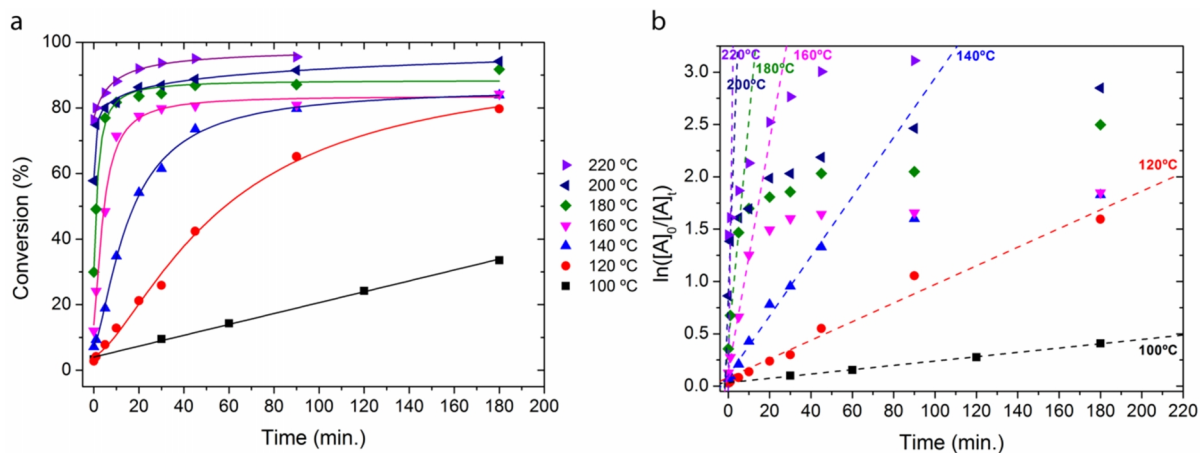


Figure 2.2.5. a) Conversion versus time plot for the hydrolysis of PEtOx 3 kDa at temperatures ranging from reflux conditions to 220 °C. [HCl] = 1.0 M. Increasing temperature greatly accelerates the hydrolysis rate. b) Corresponding first order kinetic plot. The deviation from linearity beyond 80% conversion ($\ln([A]_0/[A])_t = 1.6$) can be ascribed to the protonation of the formed ethylenimine units and the consequent decrease of free protons available to catalyze the hydrolysis.

To quantify these experimental results, the initial linear part of the kinetic plots was fitted and the apparent hydrolysis rate constant (k_h^{app}) was calculated for each temperature by using Equation 2.2.4. The obtained k_h^{app} values permit the calculation of the thermodynamical parameters associated with the hydrolysis process, by using the Arrhenius equation:

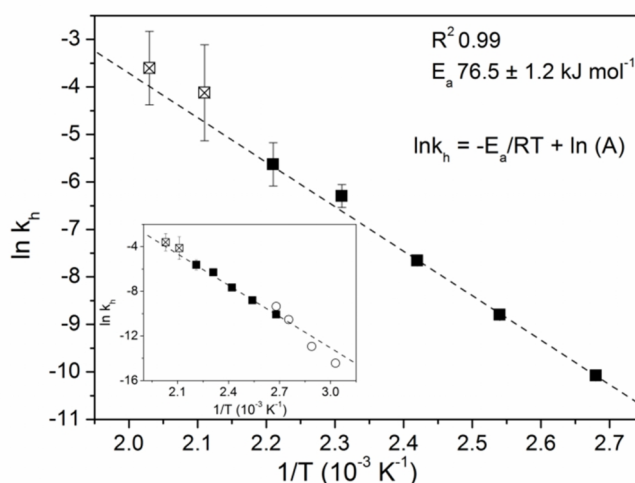
$$k_h^{app} (\text{l mol}^{-1} \text{s}^{-1}) = A e^{-E_a/RT} \quad \text{Equation 2.2.5.}$$

$$\ln(k_h^{app}) = \ln\left(\frac{A}{\text{M}^{-1} \text{s}^{-1}}\right) - \frac{E_a}{R} \frac{1}{T} \quad \text{Equation 2.2.6.}$$

Where A is the frequency factor, E_a the activation energy (J mol^{-1}), R the gas constant ($\text{J K}^{-1} \text{mol}^{-1}$) and T the temperature (K).

Figure 2.2.6. shows the corresponding Arrhenius plot (Equation 2.2.6) from which a value of $76 \pm 1 \text{ kJ mol}^{-1}$ for the activation energy (E_a) was calculated. These k_h^{app} are in good agreement with previously reported values* for hydrolysis studies performed at lower temperatures (from 57 to 100 °C) and a high acid concentration of 6 M.^[24]

Figure 2.2.6. Arrhenius plot for the acid hydrolysis of PEtOx 3 kDa (1 M HCl_(aq)) at



* It should be noted that the previously reported k_h values were found to be 10^3 times lower than reported,^[24] likely due to a typographic error.

temperatures ranging from 100 °C to 220 °C. The data points corresponding to 200 °C and 220 °C (⊠) were not considered for the calculation of the E_a , as the polymer degrades at these temperatures (*vide infra*). The inset includes previously reported data^[24] (○) obtained at temperatures from 57 °C to 100 °C with $[HCl] = 5.8 M$, and is in good agreement with the current results.

SEC in hexafluoroisopropanol, which was recently found to be an excellent eluent for L-PEI,^[34] was used to investigate the influence of temperature on the structural integrity of the obtained PEtOx-co-PEI copolymers. PEI has a larger hydrodynamic volume than PEtOx in HFIP and consequently the retention time and molecular weight calculated for PEtOx-co-PEI copolymers increases with the degree of hydrolysis. Figure 2.2.7 displays the evolution of the measured number average molecular weight (M_n) with the hydrolysis conversion at different temperatures. It should be noted that the absolute M_n values at 120, 160, and 200 °C are higher than those obtained by hydrolysis at 140, 180 and 220 °C, which can be ascribed to a change in the SEC system (possible variation in trifluoroacetate salt concentration) and recalibration in between these two series of experiments.

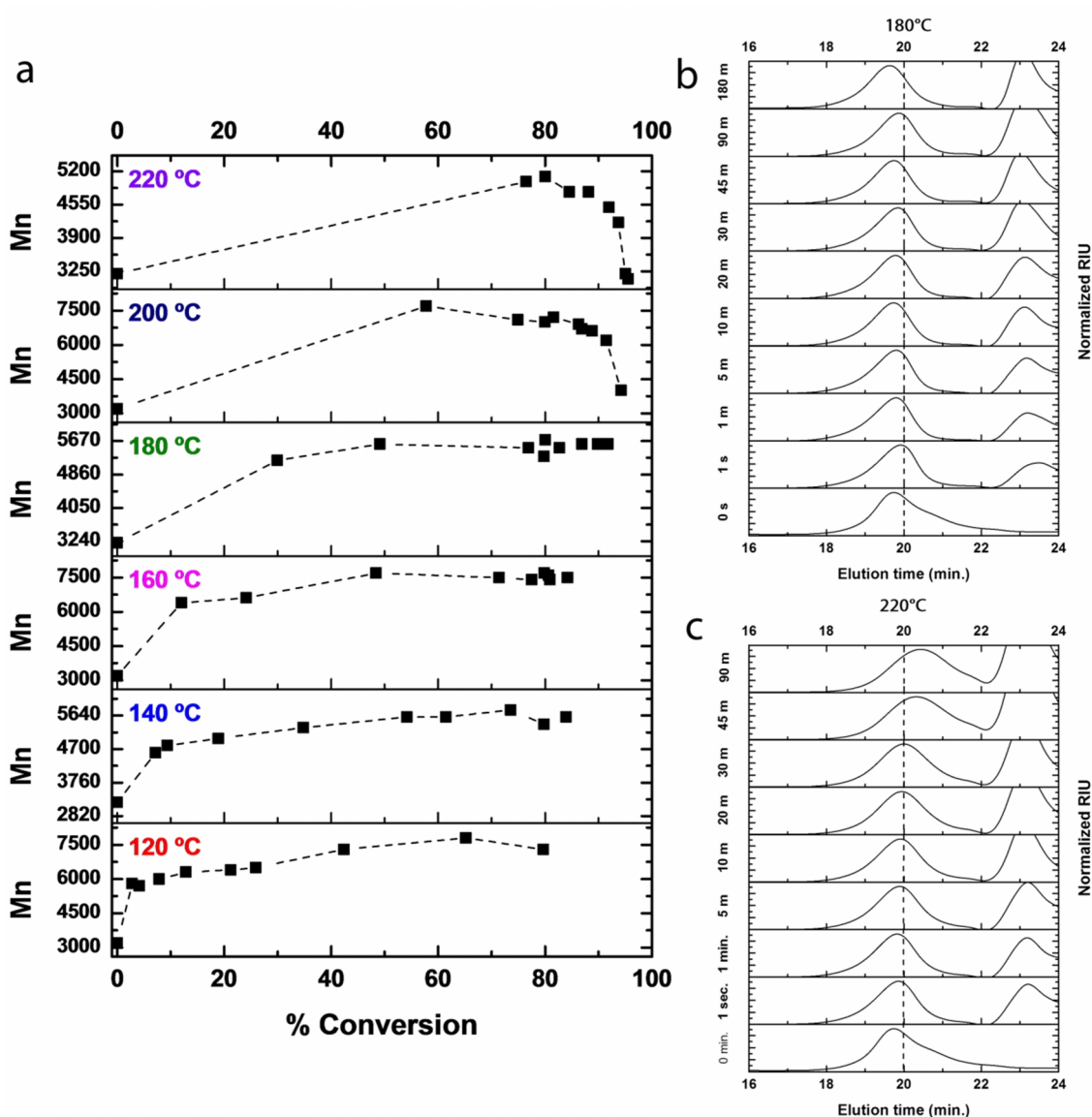


Figure 2.2.7. HFIP-SEC analysis of partially hydrolyzed PEtOx polymers at different temperatures ($[HCl] = 1.0 M$). a) Number average molecular weight (M_n) of the obtained PEtOx-co-PEI copolymers plotted against the degree of hydrolysis. Dashed lines are included to guide the eye: the M_n increases with the conversion, as EI units result in an increase on the hydrodynamic volume of the copolymer in HFIP.

However, at temperatures higher than 180 °C, a sharp decrease in the M_n values is observed, indicating degradation of the polymer backbone into oligomers. b) Chromatograms corresponding to the hydrolysis of PEtOx at 180 °C. A steady decrease in elution time is observed, as the EI content in the PEtOx-co-PEIcopolymer increases, resulting in an increase in the copolymer hydrodynamic volume. c) Chromatograms corresponding to the hydrolysis of PEtOx at 220 °C. A decrease in the hydrodynamic volume and the appearance of oligomers is observed beyond 10 min. reaction time, due to polymer degradation. Dashed line is included to guide the eye.

Nonetheless, at all temperatures the expected trend towards higher M_n values with increasing conversion is observed; however, at temperatures of 200 °C and higher, the M_n values abruptly drop as a consequence of polymer backbone degradation (see SEC traces in Figure 2.2.7.c). At these temperatures and pressures (close to 30 bar), the energy applied to the polymer appears to be sufficiently high for the degradation of its main chain $(-\text{CH}_2-\text{CH}_2-\text{NH}-)_n$ bonds. These results clearly indicate that 180 °C is the maximum temperature at which the hydrolysis can be performed using 1.0 M concentration HCl_{aq} without affecting the polymer integrity. By consequence, PEtOx hydrolysis cannot be further accelerated under these conditions.

To understand the influence of acid on polymer degradation, and to elucidate whether the hydrolysis could be performed under acid-free conditions, the hydrolysis of PEtOx was also investigated in near-critical water using a multimode microwave reactor.^[44, 45] The polymer was dissolved in an aqueous 0.03 M NaCl solution, and the vial was heated to 270 °C (IR sensor) for 60 minutes, with the pressure reaching 80 bar. The addition of NaCl as electrolyte is necessary, as the drop in dielectric constant of near-critical water turns it nearly transparent to microwave radiation. Under these acid-free conditions, PEtOx was readily hydrolyzed but it also degraded over time, obtaining nearly complete decomposition of the polymer after 1h of reaction, and thus demonstrating that acid-free hydrolysis of PEtOx is impossible.

As indicated earlier, to study the influence of PEtOx molecular weight, analogous hydrolysis experiments were also performed using commercial PEtOx with a M_n of 50 kDa and $\text{Đ} \approx 4$ (Aquazol 50). Hydrolysis experiments of this larger PEtOx yielded comparable results as obtained for PEtOx 3 kDa, which was expected from previous research.^[34]

2.2.4. Controlling PEtOx hydrolysis by variation of acid concentration

Once the optimal PEtOx hydrolysis temperature was found to be 180 °C, we focused our attention on gathering precise control over the degree of hydrolysis. Assuming that the aforementioned hydronium depletion upon hydrolysis accounts for the flattening of the first order kinetic plots, it was hypothesized that sub-stoichiometric amounts of HCl_{aq} would prevent hydrolysis to proceed beyond a specific degree of conversion.

To explore this hypothesis, a range of HCl concentrations ranging from 0.1 M to 1.0 M were used to partially hydrolyze PEtOx at 180 °C. A fast hydrolysis was found in all cases, up to a plateau that correlates with the acid concentration used (see Figure 2.2.8.a).

After an initial fast hydrolysis, the degree of hydrolysis stabilized after 30 minutes, only slowly increasing thereafter. The robustness of this acid-concentration controlled hydrolysis is demonstrated in Figure 2.2.8.b: when the hydrolysis is performed for 90 minutes, a variation of ± 30 minutes in reaction time only has a minor impact on the hydrolysis conversion, demonstrating accurate control over the degree of hydrolysis in a reproducible manner. The hydrolysis was also repeated in conventionally heated pressure tubes, giving the same results (✱ in Figure 2.2.8b) to demonstrate the applicability of the method beyond microwave chemistry.

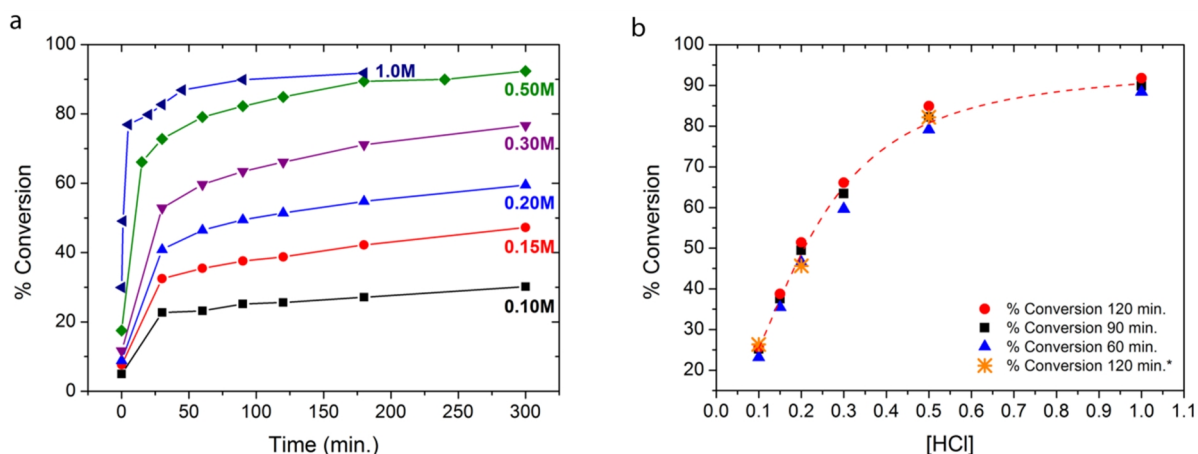
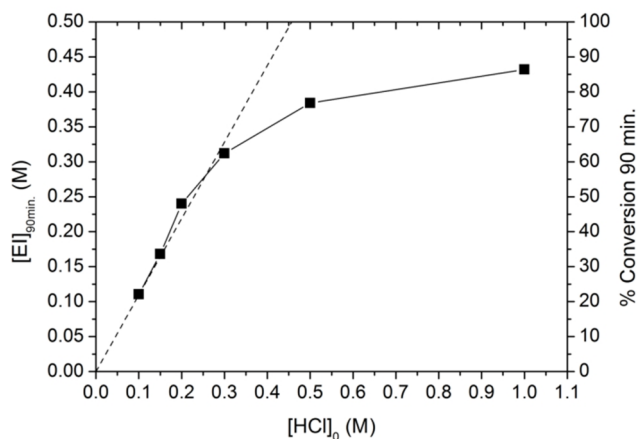


Figure 2.2.8. a) Conversion versus time plot for the hydrolysis of PEOx 3 kDa ($[A] = \text{amide concentration} = 0.48 \text{ M}$) at 180°C under various HCl concentrations ranging from 0.10 M to 1.0 M . The degree of hydrolysis levels off at defined values at each acid concentration, therefore allowing good control over the degree of hydrolysis. b) Conversion plotted against HCl concentration. * Reactions performed in pressure tubes and conventional heating instead of in the microwave reactor. The robustness of the partial hydrolysis is demonstrated by the small impact that variations of 30 minutes reaction time have on the degree of hydrolysis.

During the PEOx hydrolysis, the produced ethylene imine (EI) units will be protonated, since the pH of the reaction medium is below the pK_a of L-PEI ($\text{pK}_a \approx 7.2\text{--}7.9$).^[46] Consequently, every newly formed EI unit drains a hydronium ion from the acidic solution. This translates to a pH neutralization of the solution at the point where the concentration of EI groups equals the initial acid concentration, preventing further hydrolysis. The released propionic acid units will only have a minor influence as they are insufficiently acidic to hydrolyze PEOx. Figure 2.2.9. shows the relationship between EI concentration present after 90 min. reaction time and the initial HCl concentration used. A direct relationship between $[\text{HCl}]_0$ and $[\text{EI}]_{90\text{min}}$ is observed under sub-stoichiometric HCl concentrations ($[\text{HCl}]_0 < [A] = 0.48 \text{ M}$), demonstrating that controlling the initial HCl concentration constitutes an effective method to tailor and accurately control the degree of hydrolysis of the resulting PEOx-co-PEI copolymer.

Figure 2.2.9. Concentration of ethyleneimine units ($[\text{EI}]_{90\text{min}}$) formed upon hydrolysis versus HCl concentration, showing a close direct relationship between both. The right axis indicates the corresponding % conversion of amide side-chains into EI. The dotted line guides the eye through the linear region of the curve, where sub-stoichiometric amounts of HCl are used. Data from the hydrolysis of PEOx 3 kDa, $[A] = \text{amide concentration} = 0.48 \text{ M}$, $T = 180^\circ\text{C}$.



2.2.5. Conclusions

The hydrolysis kinetics of PEOx 3 kDa and 50 kDa in the presence of 1.0 M HCl at different temperatures are reported. Increasing the reaction temperature is demonstrated to be an effective way to accelerate the hydrolysis rate, even when comparatively low acid concentrations were used. The maximum acceleration can be achieved at 180°C , as the polymer degrades into

oligomers at higher temperatures. Acid-free, near-critical water conditions (275 °C, 80 bar) also led to polymer decomposition into oligomers after only 60 min., indicating the inability to perform PEtOx hydrolysis in pure water.

In addition, the evolution of the hydrolysis conversion over time was found to abruptly level off at defined values dependent on the acid concentration. When using sub-stoichiometric concentrations of HCl, the ethylenimine units generated upon hydrolysis are protonated, capturing hydronium ions from the reaction medium and consequently halting the hydrolysis reaction. The proposed method provides accurate control on the final PEtOx-*co*-PEI composition by judiciously selecting and controlling the acid concentration, while reducing reaction times and rationalizing the use of acid. This method can alternatively be applied to pressure reactors, therefore finding applicability beyond microwave chemistry.

2.3 Enhanced selectivity for the hydrolysis of block copoly(2-oxazoline)s in ethanol-water resulting in linear poly(ethyleneimine) copolymers

2.3.1. Introduction

In the second part of our research on the hydrolysis of PAOx,^{*} we aimed to gain control over the selective partial hydrolysis of PAOx block-copolymers by studying the influence of the solvent on the amide hydrolysis process. Particularly, ethanol-water solvent mixtures have long attracted a great deal of attention due to the non-ideal mixing behavior that arise from incomplete mixing at the molecular level.^{22,23} Ethanol molecules represent very short amphiphiles that interact with each other and with water molecules in a defined non-ideal manner dependent on the ratio of the two solvents.²⁴ Furthermore, ethanol molecules establish hydrogen bonds and hydrophobic interactions with solutes present in the mixture, enabling control on different chemical reactions, including hydrolysis of different molecules.²⁵⁻²⁸ Specifically, ethanol-water solvent mixtures were found²⁹ to selectively lower the rate of acidic hydrolysis of alkyl substituted amides, which becomes more pronounced with increasing the alkyl chain length from methyl to ethyl and propyl. Consequently, the acidic hydrolysis of PAOx in ethanol-water mixtures constitutes a promising approach to increase selectivity and could open the path towards the selective hydrolysis of double hydrophilic block copoly(2-oxazoline)s.

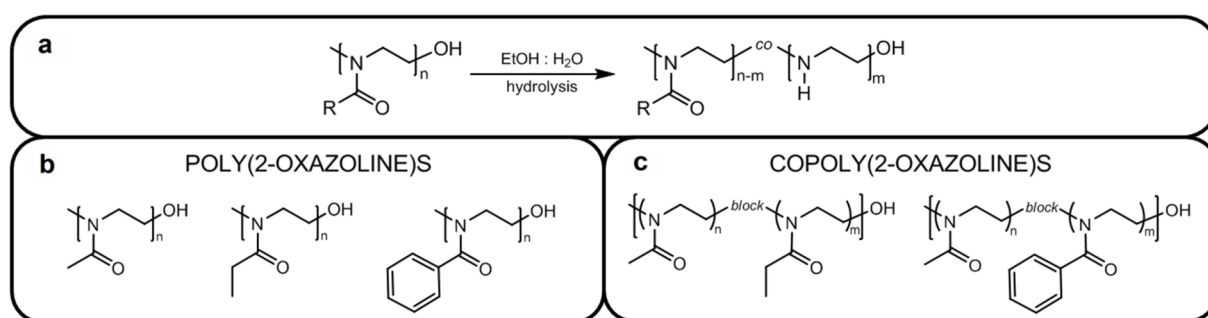


Figure 2.3.1. (a) General scheme for the partial hydrolysis of poly(2-oxazoline)s in a ethanol-water 80:20 (v/v) binary solvent mixture with 3 M HCl_{aq}. Poly(2-oxazoline)-co-poly(ethylene imine) copolymers were obtained starting from various poly(2-oxazoline) homopolymers (b), and block copolymers (c).

In the current study, we report the hydrolysis of poly(2-methyl-2-oxazoline) (PMeOx), poly(2-ethyl-2-oxazoline) (PEtOx), and poly(2-phenyl-2-oxazoline) (PPhOx) homopolymers in an ethanol-water 80:20 (v/v) solvent mixture, which was previously found to homogeneously dissolve all three polymers (see Figure 2.3.1).^{30,31} Subsequently, the hydrolysis of PMeOx-*b*-PPhOx and PMeOx-*b*-PEtOx block copolymers will be discussed in the same solvent mixture providing unexpected selectivity for the hydrolysis of the PMeOx-*b*-PEtOx. To further understand this observation, the effect of ethanol-water solvent composition on the selective hydrolysis will be addressed.

2.3.2. Synthesis of PAOx homopolymers and block-copolymers

To study the influence of binary ethanol-water solvent mixtures on the hydrolysis of different PAOx, we synthesized three PAOx homopolymers ranging from highly hydrophilic to highly hydrophobic. PMeOx and PEtOx have been extensively studied in the biomedical field, as they are

* Note that chronologically, this research was performed previously than the one described in the first part of the chapter. Therefore, the optimized hydrolysis conditions with regard to temperature and acid concentration were not applied in this part.

biocompatible polymers that exhibit stealth behavior and hydrophilicity close to that of PEG.^[1, 7] Therefore, PMeOx and PEtOx were selected as hydrophilic polymers for the hydrolysis studies. On the other hand, the water-insoluble PPhOx that, due to its water insolubility, cannot be hydrolyzed in aqueous acid solutions, was chosen as hydrophobic polymer. In addition, a block copolymer containing PMeOx and PPhOx was synthesized to assess the effect of the ethanol-water binary solvent mixture on the selectivity of the hydrolysis, by comparison with the previously reported selective hydrolysis of a PMeOx-*b*-PPhOx block copolymer micelles in aqueous medium.^[23] Finally, to evaluate the possibility of obtaining a double-hydrophilic PAOx-PEI block copolymer by selective hydrolysis, a PMeOx-*b*-PEtOx block copolymer was synthesized. The characterization details of all polymers are summarized in Table 2.3.1.

Polymer composition	DP	SEC	
		M _n	Đ
PMeOx-OH	100	11 400 ^{a)}	1.40
PEtOx-OH	100	12 600 ^{a)}	1.18
PPhOx-OH	100	12 500 ^{a)}	1.29
PMeOx ₆₀ - <i>b</i> -PPhOx ₁₅ -OH	75	11 700 ^{b)}	1.20
PMeOx ₅₀ - <i>b</i> -PEtOx ₅₀ -OH	100	11 500 ^{b)}	1.30

Table 2.3.1. Size exclusion chromatography (SEC) data for the synthesized PAOx (co)polymers. SEC eluent: ^{a)}*N,N*-dimethylacetamide, calibrated against poly(methyl methacrylate) standards. ^{b)}Hexafluoroisopropanol, calibrated against polystyrene standards. DP was based on monomer to initiator ratio.

2.3.3. Hydrolysis kinetics of homo poly(2-oxazoline)s

The hydrolysis of PMeOx, PEtOx and PPhOx with a DP of 100 in the ethanol-water 80:20 solvent mixture containing 3 M HCl was evaluated at 100 °C under microwave irradiation. Temperature, acid concentration, and amide concentration are important parameters that influence the hydrolysis rate and thus were kept constant for all reactions. After reacting separate samples at various times, the samples were basified and the conversion from PAOx to PEI was determined by ¹H NMR spectroscopy. The addition of NaOH_{aq} during work-up assures the quantitative formation of the acids sodium salts, that would otherwise be partially lost as in the protonated form during the sample freeze-drying process.

For the hydrolysis of homopolymers, the calculation method used for determining the composition is based on the integral values of the PAOx and PEI backbone signals, in analogy with the method described earlier in part 2.2.3. For the block copolymers, however, due to overlapping of signals corresponding to the different PAOx side chains, the calculations include the integral values (*I*) of the signals corresponding to the released carboxylates. In the case of the PMeOx₆₀-*b*-PPhOx₁₅ copolymer, the degree of hydrolysis conversion of PAOx into PEI was calculated as follows:

$$\% \text{ Conversion PMeOx} = \frac{I[\text{Acetic Acid CH}_3]}{I[\text{MeOx CH}_3] + I[\text{Acetic Acid CH}_3]} \times 100 \quad \text{Equation 2.3.1.}$$

$$I[\text{PhOx Ar, 5H}] = \text{Integral}(8.5 \text{ ppm}-6.5 \text{ ppm}) - \frac{5}{2} \times I[\text{Benzoic Acid Ar, 2H}] \quad \text{Equation 2.3.2.}$$

$$\% \text{ Conversion PPhOx} = \frac{\frac{5}{2} I[\text{Benzoic Acid Ar, 2H}]}{I[\text{PhOx Ar, 5H}] + \frac{5}{2} I[\text{Benzoic Acid Ar, 2H}]} \times 100 \quad \text{Equation 2.3.3.}$$

$$\text{Conversion Ratio } \text{MeOx}/\text{PhOx} = \frac{\% \text{ Conversion PMeOx}}{\% \text{ Conversion PPhOx}} \quad \text{Equation 2.3.4.}$$

The composition of the partially hydrolyzed $\text{PMeOx}_{50}\text{-}b\text{-PEtOx}_{50}$ copolymers was calculated as described in the following equations:

$$\% \text{ Conversion PEtOx} = \frac{I[\text{EtOx CH}_3 + \text{Propionic Acid CH}_3] - 1.5 \times I[\text{EtOx CH}_2]}{I[\text{EtOx CH}_3 + \text{Propionic Acid CH}_3]} \times 100 \quad \text{Equation 2.3.5.}$$

$$\text{Conversion Ratio } \text{MeOx}/\text{EtOx} = \frac{I[\text{Acetic Acid CH}_3]}{I[\text{EtOx CH}_3 + \text{Propionic Acid CH}_3] - 1.5 \times I[\text{EtOx CH}_2]} \quad \text{Equation 2.3.6.}$$

$$\% \text{ Conversion PMeOx} = \text{Conversion Ratio } \text{MeOx}/\text{EtOx} \times \% \text{ Conv. PEtOx} \quad \text{Equation 2.3.7.}$$

The results of the hydrolysis investigations for the three homopoly(2-oxazoline)s are displayed in Figure 2.3.2., and show an unexpectedly pronounced difference in hydrolysis rate for PMeOx in comparison with PEtOx and PPhOx, being the lowest for PPhOx. After 180 minutes, PMeOx is almost fully hydrolyzed while the conversion of PEtOx and PPhOx is only 22% and 13%, respectively, as can be seen in the conversion plot (Figure 2.3.2., left). The hydrolysis kinetics are, in principle, dependent on both the poly(2-oxazoline) amide concentration and the acid concentration. However, due to the large acid excess of hydrochloric acid, its concentration will remain nearly constant during the hydrolysis yielding pseudo-first order kinetics, as demonstrated by the linearity obtained in the $\ln[A]_0/[A]_t$ kinetic plot (see Figure 2.3.2, right). Nonetheless, the pseudo-first order kinetic plot for PMeOx deviates from linearity at low conversion, only following the ideal linear behavior above *ca.* 10% hydrolysis. The increased hydrolysis rate above this threshold may be ascribed to the presence of protonated ethylene imine units randomly distributed throughout the PMeOx backbone enhancing the hydration of the polymer and, thus, the hydrolysis rate. In addition, the protonated ethyleneimine groups are proposed to establish strong intermolecular hydrogen bonds with the carbonyl oxygen of neighboring amide groups, exacerbating the partial positive charge on the carbonyl carbon, further accelerating the hydrolysis. Similar acceleration in hydrolysis rate through auto-catalysis was also observed in previously reported acidic hydrolysis of PAOx in water.^[34]

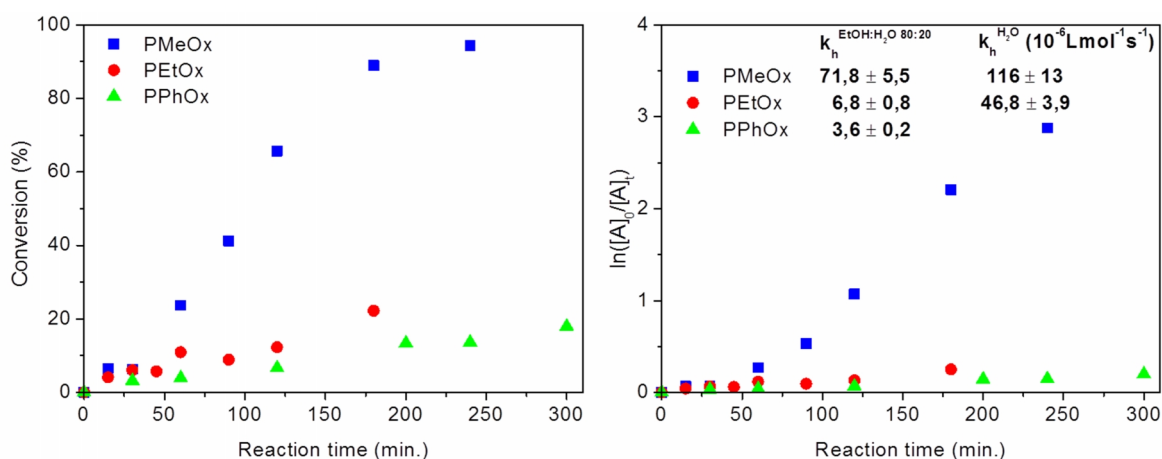


Figure 2.3.2. Left: Conversion versus time plot for the hydrolysis of PMeOx, PEtOx and PPhOx homopolymers in an ethanol-water 80:20 (v/v) solvent mixture, $[Amide] = 0.48M$, $[H^+] \approx 3M$ (12 wt.%) at 100 °C. Right: Corresponding pseudo-first order kinetic plot. The calculated hydrolysis rate constants in ethanol-water ($k_h^{\text{EtOH:H}_2\text{O } 80:20}$) are shown in the inset together with previously reported hydrolysis rate constants in aqueous HCl ($k_h^{\text{H}_2\text{O}}$; $[H^+] = 5.67M$) for comparison.^[34]

The differential hydrolysis rate among diverse poly(2-oxazoline)s is determined by the characteristics of the amide substituent at the polymer backbone wherein hydrophilicity should play a minor role compared to sterical and electronic effects, due to the selected ethanol-water solvent mixture. The low PPhOx hydrolysis rate reflects its bulkiness and the positive mesomeric effect provided by the phenyl ring, which stabilizes the carbocation intermediate formed upon protonation of the amide carbonyl group. However, the notorious difference in hydrolysis rate observed between PMeOx and PEtOx was not expected, considering the relatively small steric and electronic differences between both methyl and ethyl groups. The hydrolysis rate constants calculated based on previously reported data for PMeOx in pure water^[34] is in accordance with the one obtained in the present research. In stark contrast, the hydrolysis rate constant obtained for PEtOx is found to be ca. 8 times slower in the ethanol-water 80:20 solvent mixture compared to pure water, leading to ten times faster hydrolysis of PMeOx in ethanol-water compared to PEtOx and even 20 times faster compared to PPhOx. The hydrolysis rate constants in both water and the ethanol-water 80:20 mixture are listed in Figure 2.3.2, right, for comparison.

It is proposed that this observed, unexpected behavior in ethanol-water 80-20 can be ascribed to hydrophobic interactions established between the pendant groups of the poly(2-oxazoline) and the ethanol molecules. In fact, efficient amide hydration is critical for the hydrolysis reaction, as the cooperative interaction of three water molecules with each amide group has been demonstrated, by molecular modeling, to be required for its acidic hydrolysis.^[47] In the current system, solvating ethanol molecules are believed to preferentially shield the hydrophobic PEtOx side chains obstructing the access of water molecules to the amide carbonyl group (Figure 2.3.3), thereby suppressing the hydrolysis rate. This effect does not occur for PMeOx, where the arrangement of water molecules around the amides is not hindered, due to the much weaker hydrophobic solvation of the methyl groups by ethanol compared to ethyl groups. As a result, the ethanol-water solvent mixture provides significantly enhanced control and selectivity in the hydrolysis process of PAOx compared to water.

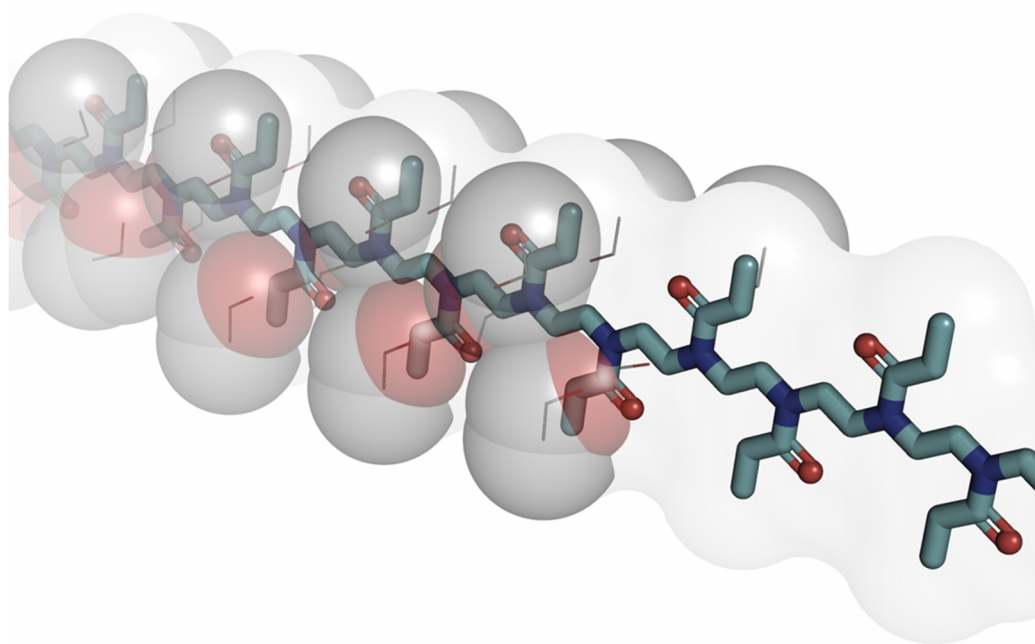


Figure 2.3.3. *Schematic representation of the proposed mechanism for the increased stability of PEtOx towards hydrolysis in ethanol-water 80:20 (v/v). The specific solvation of the PEtOx ethyl side chains by ethanol molecules is proposed to hinder the access of water molecules, thereby shielding the amide groups from hydrolysis.*

2.3.4. Hydrolysis kinetics of block copoly(2-oxazoline)s

The observed disparity in hydrolysis rate for the homopoly(2-oxazoline)s suggested the possibility of selectively hydrolyzing the corresponding block copolymers. Consequently, the selective hydrolysis of two block copolymers, namely P([MeOx]₆₀-*b*-[PhOx]₁₅) and P([MeOx]₅₀-*b*-[EtOx]₅₀) was investigated following the aforementioned protocol (see part 2.3.3).

The hydrolysis of the P([MeOx]₆₀-*b*-[PhOx]₁₅) block copolymer was achieved with a high level of selectivity, whereby the hydrolysis degrees of both PMeOx and PPhOx blocks were comparable to those observed in the hydrolysis of the homopolymers. As displayed in Figure 2.3.4., 95 % of the PMeOx block was hydrolyzed after 240 minutes while preserving most of the PPhOx block, with a hydrolysis degree of only 10%. This results represents a strongly enhanced selectivity compared to acidic hydrolysis in water, despite that PPhOx does not dissolve in water indicating that the hydrophobic solvation by ethanol molecules also plays a major role for the hydrolysis of PPhOx. It is also noteworthy that the block copolymer hydrolysis kinetic plot does not show an inhibition time for the hydrolysis of PMeOx, which is speculatively ascribed to the disruption of the ethanol solvation sheath at the interface of both PMeOx and PPhOx blocks, providing a region where access to water molecules might not be hindered by ethanol molecules.

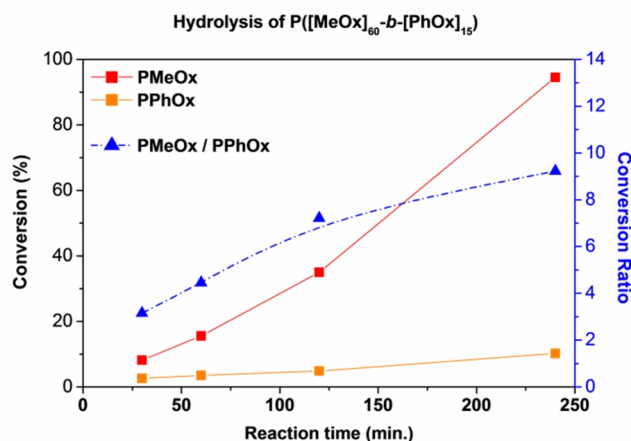


Figure 2.3.4. Left: Conversion versus time plot for the hydrolysis of the P([MeOx]₆₀-*b*-[PhOx]₁₅) block copolymer in an ethanol-water 80:20 (v/v) solvent mixture revealing a high level of selectivity by the PMeOx/PPhOx conversion ratio. ([Amide] = 0.48M, [H⁺] ≈ 3M at 100 °C).

The hydrolysis kinetics for P([MeOx]₅₀-*b*-[EtOx]₅₀) revealed very high selectivity at low conversion with PMeOx/PEtOx conversion ratio of ~10 with 30% PMeOx conversion (repetition of this data point confirmed the high selectivity). On the other hand, the hydrolysis kinetics of P([MeOx]₅₀-*b*-[EtOx]₅₀) showed a marked lower level of selectivity at higher conversions than expected from the homopolymer hydrolysis, as can be seen by the drop in conversion ratio for the ethanol-water 80:20 solvent mixture in Figure 2.3.5a. It is also evident by the flattening of the PMeOx block conversion plot, while the hydrolysis rate of the PEtOx block shows a slight acceleration in time.

This drop in selectivity with increasing PMeOx conversion again can be ascribed to two factors: 1) better hydration of the PEtOx block due to the presence of EI units along the adjacent partially hydrolyzed PMeOx block, especially close to the block junction; 2) the presence of protonated EI units triggers an intramolecular auto-catalytic hydrolysis process, whereby the EI units in the PMeOx part also catalyze the PEtOx hydrolysis. In fact, this observation indirectly supports the proposed hydrophobic shielding of PEtOx leading to slow hydrolysis. Nevertheless, even though

the selectivity drops with increasing PMeOx conversion, it is noteworthy that 70% of the PMeOx block could be hydrolyzed while only 25% of the PEtOx block was hydrolyzed after 240 minutes.

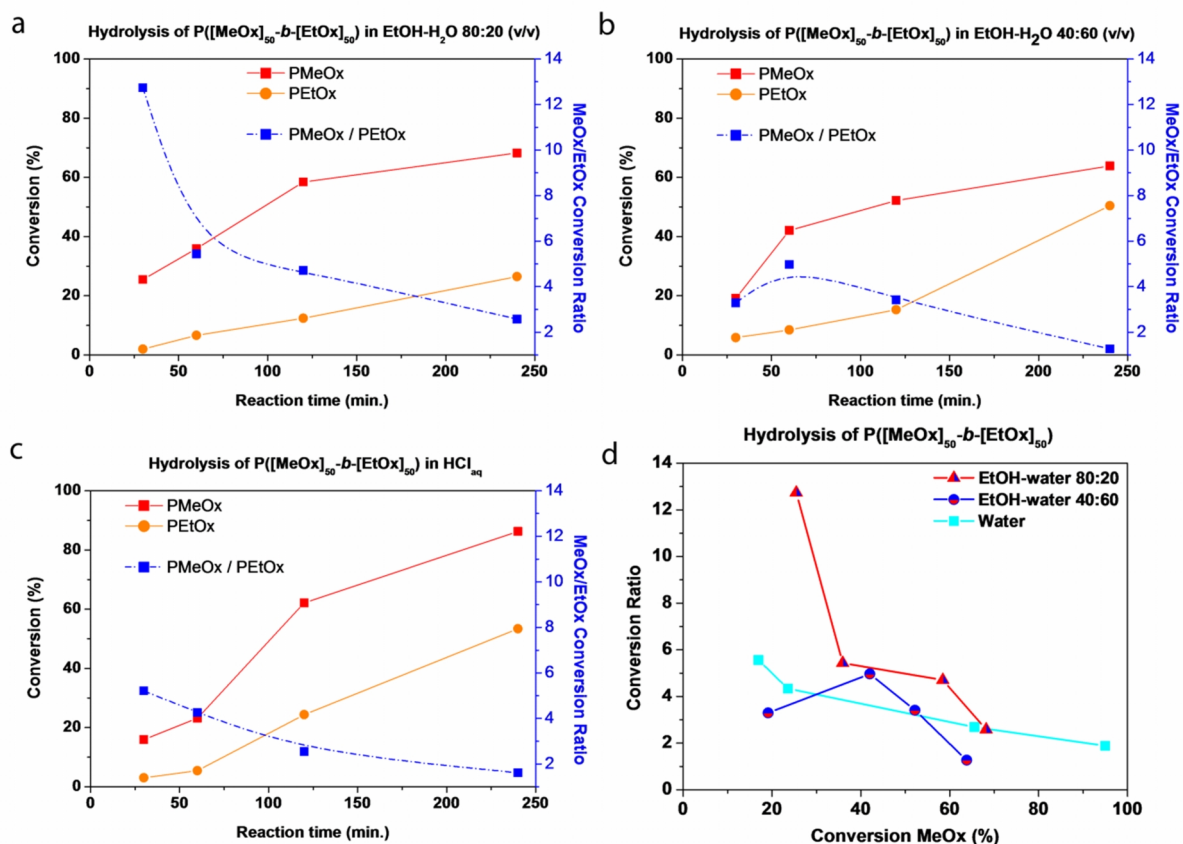


Figure 2.3.5. Conversion versus time plot for the hydrolysis of the $P([MeOx]_{50}\text{-}b\text{-}[EtOx]_{50})$ block copolymer investigated in aqueous HCl and ethanol-water solvent mixtures. a) Conversion ratios of PMeOx/PEtOx versus PMeOx conversion plot for the hydrolysis of the $P([MeOx]_{50}\text{-}b\text{-}[EtOx]_{50})$ block copolymer in two different ethanol-water solvent mixtures and in aqueous HCl. b) Ethanol-water 80:20 (v/v) solvent mixture, whereby the selectivity strongly decreases in time. The experiments (emphasizing the first) were repeated yielding consistent results. c) Ethanol-water 40:60 (v/v) solvent mixture. The notoriously low selectivity at low conversion can be ascribed to the presence of $H_2O\text{-}EtOH$ 3:1 complexes, that are able to solvate more efficiently the PEtOx side groups. d) Aqueous HCl. A low level of selectivity is observed at low conversion due to the higher hydrophilicity of the PMeOx block. An acceleration of the hydrolysis rate is observed due to the presence of protonated EI units that trigger an auto-catalytic hydrolysis process. $[Amide] = 0.48M$, $[H^+] \approx 3M$ at $100^\circ C$.

To further understand the effect of solvent mixture on the $P([MeOx]_{50}\text{-}b\text{-}[EtOx]_{50})$ block copolymer hydrolysis, the hydrolysis was also performed in an ethanol-water 40:60 binary solvent mixture and pure water, with similar acid and amide concentrations. As expected from the hydrolysis rate constants in water, the selectivity for the hydrolysis in pure water is relatively low and vanishes at higher levels of conversion (see Figure 2.3.5c), when protonated EI units in both blocks increase the hydration. The auto-catalytic hydrolysis process triggered by the presence of protonated EI units is also observed for both blocks. The importance of the ethanol-water 80:20 solvent mixture for selective hydrolysis is evidenced by the observed low selectivity in ethanol-water 40:60, which is rather similar to the result obtained in water (Figure 2.3.5d).

The main difference between these ethanol-water solvent mixtures is that the 40:60 mixture comprises $H_2O\text{-}EtOH$ 3:1 complexes while the 80:20 mixture comprises mainly individual ethanol

molecules and H₂O-EtOH 1:1 complexes²⁴ (which can be seen as individual water molecules). Therefore, the ethanol molecules in the 40:60 mixture are shielded in water clusters suppressing their hydrophobic hydration ability. In contrast, the individual ethanol molecules in the 80:20 solvent mixture can effectively form a hydrophobic solvation layer around the ethyl side chains of PEtOx. As such, the non-ideal mixing behavior of the ethanol-water solvent mixtures directly accounts for the observed enhanced selectivity of the hydrolysis.

Considering the strong similarity of PEtOx and PMeOx, these results highlight the importance of the ethanol-water 80:20 (v/v) binary solvent mixture on the hydrolysis kinetics of PAOx when compared with pure water, leading to enhanced selectivity for block copolymer hydrolysis even for very similar PAOx blocks.

2.3.5. Conclusions

In the present research, a novel methodology for the controlled and selective hydrolysis of copoly(2-oxazoline)s is developed, opening the path towards a wide range of poly(2-oxazoline-*co*-ethylene imine) copolymers with tunable degree of hydrolysis and properties. The utilized ethanol-water mixture enabled good control over the hydrolysis process, and high conversions could be achieved following first order kinetics. Specifically, a high level of selectivity was achieved for the hydrolysis of P([MeOx]₆₀-*b*-[PhOx]₁₅), resulting in 95% hydrolysis of the available methyl side chains while preserving the integrity of 90% of the PhOx block. The hydrolysis of P([MeOx]₅₀-*b*-[EtOx]₅₀) was found to be less selective than expected from the homopolymers hydrolysis kinetics, but still unexpectedly high considering the analogy between methyl and ethyl groups, which was ascribed to hydrophobic shielding of the amide groups by solvation with ethanol. It is noteworthy that 70% of the PMeOx block could be hydrolyzed while only 25% of the PEtOx block was hydrolyzed after 240 minutes.

The ability of merging the properties of poly(2-oxazoline)s and poly(ethylene imine) is of high interest for developing new applications and improving existing ones, such as gene delivery, especially in the biomedical field. This fact, together with the diverse end group functionality attainable in the CROP of 2-oxazolines, highly extends the application potential of this polymer class. In addition, the here reported improved hydrolysis selectivity towards different poly(2-oxazoline)s in ethanol-water will be the basis for future investigations to further improve the selectivity of the hydrolysis of poly(2-oxazoline) copolymers.

2.4 Experimental Section

Materials

Solvents and reagents were purchased from Sigma Aldrich and used as received, unless otherwise specified. Methyl tosylate (MeOTs) was distilled prior to use. 2-Methyl-2-oxazoline (MeOx), 2-ethyl-2-oxazoline (EtOx) and 2-phenyl-2-oxazoline (PhOx) were distilled over barium oxide (BaO). Acetonitrile (CH₃CN, Acros) was dried over molecular sieves (3Å). Poly(2-ethyl-2-oxazoline) 50 kDa and 200 kDa (Aquazol[®] 50 and 200, respectively) and HCl (37 (w/w) %) were purchased from Aldrich. NaOH (>97%) was purchased from Acros Organics. CD₃OD (99.8% D) was obtained from Eurisotop, France.

Deionized water was obtained from a Sartorius Arium 611 with a Sartopore 2 150 (0.45 + 0.2 μm pore size) cartridge filter (resistivity less than 18.2 MΩ cm).

Instrumentation

Microwave chemistry

Polymerizations were performed in capped vials in a single mode microwave reactor CEM Discovery (IR sensor) (part 2.3), or in a Monowave 300 microwave synthesizer (part 2.2. and all hydrolysis experiments), from Anton Paar GmbH, equipped with a MAS 24 auto sampler. Temperature was monitored with the built-in IR sensor. For the polymer synthesis, commercial caps were used. For the hydrolysis experiments, to ensure integrity of the microwave vials' septa at high temperatures and pressures under acidic conditions, custom septa were used. They comprised one 22 mm Ø, 2mm thick PTFE disk, and a 22 mm Ø, 1mm thick silicon/PTFE septum placed underneath (Bartelt GmbH).

For the polymerizations, the microwave vials were heated to 130°C for at least two hours, and cooled down under argon before usage.

The near critical water experiments were carried out in a Multiwave 3000 multimode microwave reactor from Anton Paar GmbH. The instrument was fitted with two magnetrons, with continuous microwave output power from 0 to 1400 W. The cavity was fitted with an eight-vessel rotor, with 80 mL quartz glass vessels dedicated for reactions at high pressure (80 bar controlled pressure) and temperatures (300 °C). Accurate temperature measurement was achieved by inserting a thermometer into one reference vessel. Additionally, the surface temperatures of all vessels could be monitored by IR. Pressure was monitored by a load-cell-type simultaneous hydraulic pressure sensing system for all vessels, with monitoring of the highest pressure level and pressure increase. The reactor's built-in electronics allowed reaction control in a temperature vs. time mode. After irradiation, the rotor was cooled to approximately 40 °C within 20 minutes.

General Procedure for the MW-NCW Experiments: A quartz vessel (80 ml) fitted with a Teflon-coated stirring bar was loaded with a PEtOx 200 kDa solution (0.48 M amide concentration) containing NaCl (0.03 M), for a total volume of 15 ml. The vessel was sealed and inserted into the 8-position rotor at position 1. Another 80 mL quartz vessel was fitted with an identical stirring bar and filled with NaCl solution (0.03 M, 15 mL). After sealing, this vessel was placed at position 5. Additionally, two sealed vessels containing only 0.03M NaCl solution (15 mL) were placed at positions 3 and 7 (as the rotor top plate contains the hydraulic system for simultaneous pressure sensing it is important to charge the rotor symmetrically; four fitted positions are necessary to achieve a flat position of the plate to guarantee accurate pressure measurement). After the vessels had been fixed by tightening the screws of the rotor top plate, the temperature probe was inserted into vessel 1. Finally, the rotor was closed with the protection hood and placed inside the cavity of the microwave reactor.

Characterization

Size exclusion chromatography (SEC) measurements in DMA as eluent were performed on an Agilent 1260-series equipped with a 1260 ISO-pump, a 1260 Diode Array Detector (DAD), a 1260 Refractive Index Detector (RID), and a PSS Gram30 column in series with a PSS Gram1000 column inside a 1260 Thermostated Column Compartment (TCC) at 50 °C using DMA containing 50 mM of LiCl (flow rate of 0.6 mL min⁻¹) as solvent. Molar masses and dispersities were calculated against poly(methyl methacrylate) standards.

SEC measurements in HFIP as eluent were performed in two different systems: for part 2.2., in an Agilent 1260-series system, equipped with two PL HFIP gel columns (250 x 4.6 mm) in series. The eluent used was HFIP (Apollo Scientific limited) containing 22 mM of sodium trifluoroacetate

(NaTFAc) at a flow rate of 0.3 ml min⁻¹. Molar masses and \bar{D} values were calculated against PMMA standards from Polymer Labs. The samples corresponding to the PEtOx 3 kDa hydrolysis experiments with various HCl concentrations in part 2.2., and all the samples in part 2.3., were measured in a system equipped with a Shimadzu LC-10AD pump, a waters 2414 refractive index detector (35 °C), a Spark Holland MIDAS injector, a PSS PFG guard column followed by two PFG-linear-XL (7 μ m, 8 x 300 mm) columns in series at 40 °C. Hexafluoroisopropanol (HFIP, Apollo Scientific Limited) with potassium trifluoroacetate (3 g L⁻¹) was used as eluent (flow rate of 0.8 mL min⁻¹), and the molar masses were calculated against polystyrene standards.

The samples were dried in a freeze-drier (Thermo-electron Corporation) equipped with a vacuum pump (Pfeiffer) and a Heto drywinner cooling system.

¹H-NMR spectra were recorded in CDCl₃ on a Bruker Avance 300 MHz spectrometer. Spectra were processed using TOPSPIN 3.0.

PAOx synthesis

PEtOx with a DP_n of 30 was synthesized via cationic ring-opening polymerization of EtOx. A 4 M solution of the monomer was prepared in acetonitrile together with methyl tosylate, resulting in a monomer to initiator ratio of 30. The solution was heated for 40 min. at 100 °C under microwave irradiation, calculated to reach $\ln([M]_0/[M]_t) = 4$ (98% conversion),³¹ cooled down to 40 °C, and quenched by the addition of NaOH/H₂O. The synthesized polymer was analyzed by SEC to determine the molar mass distribution and dispersity (\bar{D}), and by ¹H NMR spectroscopy in CDCl₃ to ascertain near quantitative monomer conversion. The resulting homopolymer was dried under reduced pressure, redissolved in dichloromethane and purified by precipitation in cold diethyl ether.

PEtOx₃₀: M_{n, ¹H-NMR} = 2900 Da. M_{n, DMA-SEC} = 6000 Da; $\bar{D}_{DMA-SEC}$ = 1.07. M_{n, HFIP-SEC} = 3300 Da; $\bar{D}_{HFIP-SEC}$ = 1.55. ¹H NMR (300 MHz, CDCl₃, δ): 3.80 – 3.28 (4H, -CH₂-CH₂-N-), 3.1 – 2.8 (3Hⁱⁿⁱ, CH₃-NCOCH₂CH₃), 2.45 – 2.13 (2H; -NCOCH₂), 1.15 – 0.95 (3H; -NCOCH₂CH₃).

PMeOx, PEtOx and PPhOx with a DP of 100 were synthesized via a cationic ring-opening polymerization mechanism. A 4 M solution of the monomer was prepared in dry acetonitrile together with methyl tosylate, resulting in a monomer to initiator ratio of 100. The solution was heated for different times at 140 °C under microwave irradiation, calculated to reach $\ln([M]_0/[M]_t) = 4$,³¹ cooled down to 40 °C, and quenched by the addition of H₂O. The synthesized polymers were analyzed by SEC to determine the molar mass distribution and dispersity (\bar{D}), and by ¹H NMR spectroscopy in CDCl₃ to ascertain near quantitative monomer conversion. The resulting homopolymers were dried under reduced pressure, redissolved in dichloromethane and purified by precipitation in cold diethyl ether.

PMeOx₁₀₀: M_{n, DMA-SEC} = 11 400 Da; PDI_{DMA-SEC} = 1.40. ¹H NMR (300 MHz, CDCl₃, δ): 3.37 – 3.18 (4H, -CH₂-CH₂-N-), 1.97 – 1.87 (3H; -NCOCH₃).

PEtOx₁₀₀: M_{n, DMA-SEC} = 12 600 Da; PDI_{DMA-SEC} = 1.18. ¹H NMR (300 MHz, CDCl₃, δ): 3.53 – 3.28 (4H, -CH₂-CH₂-N-), 2.45 – 2.13 (2H; -NCOCH₂), 1.15 – 0.95 (3H; -NCOCH₂CH₃).

PPhOx₁₀₀: M_{n, DMA-SEC} = 12 500 Da; PDI_{DMA-SEC} = 1.29. ¹H NMR (300 MHz, CDCl₃, δ): 7.44 – 6.95 (5H, Ar), 3.90 – 2.52 (4H; -CH₂-CH₂-N-).

The synthesis of poly(2-methyl-2-oxazoline)-block-poly(2-ethyl-2-oxazoline) with a ratio of 50:50 was previously reported.^[34] Poly(2-methyl-2-oxazoline)-block-(2-phenyl-2-oxazoline) with a ratio of 60:15 was prepared in a similar manner.

PMeOx₅₀-*b*-PEtOx₅₀: $M_{n, \text{HFIP-SEC}} = 11\,500$ Da; $\text{PDI}_{\text{HFIP-SEC}} = 1.30$. ¹H NMR (300 MHz, CDCl₃, δ): 3.66 – 3.40 (4H, -CH₂-CH₂-N-, PMeOx, PMeOx), 2.58 – 2.22 (2H; -NCOCH₂, PEtOx), 2.22 – 2.01 (3H, -NCOCH₃, PMeOx), 1.20 – 0.85 (3H; -NCOCH₂CH₃).

PMeOx₆₀-*b*-PPhOx₁₅: $M_{n, \text{HFIP-SEC}} = 11\,700$ Da; $\text{PDI}_{\text{HFIP-SEC}} = 1.20$. ¹H NMR (300 MHz, CDCl₃, δ): 7.52 – 7.00 (5H, Ar, PPhOx), 3.85 – 3.34 (4H; -CH₂-CH₂-N-, PMeOx, PPhOx), 2.22 – 1.95 (3H, NCOCH₃, PMeOx).

Kinetics investigations for the hydrolysis of PEtOx 3 kDa (described in part 2.2)

The hydrolysis kinetics were performed either in 4 mL pressure tubes (Ace glass Inc.) in an oil bath, or in a monomode microwave synthesizer. The desired total volume in each vial (2-5 ml microwave vial) was 3 mL with a concentration of 1.0 M HCl_(aq). Therefore 0.25 mL of a 36 wt.% (11.96 M HCl_(aq)) solution was mixed with 2.75 ml of PEtOx 3 kDa stock solution (amide concentration = [A] = 0.48 M). The vials were heated for different times at temperatures ranging from 120 °C to 220 °C. Upon completion of the desired reaction time, the obtained reaction mixture was cooled down by passing compressed air and made basic with 1 mL of a 4 M NaOH_(aq) solution to reach a pH of 8-9. Subsequently, the samples were freeze-dried for HFIP-SEC and ¹H-NMR spectroscopy in deuterated methanol.

To determine the hydrolysis kinetics at 180 °C with different HCl concentrations a stock solution of PEtOx 3kDa (0.53 M amide concentration) was prepared. A 18 mL portion was taken and the necessary amounts of 36 wt.% HCl_(aq) were added, completing the volume to 20 mL with milli-Q water to obtain the desired HCl_(aq) concentration and 0.48 M amide concentration. The work up and analysis were performed analogously as for the hydrolysis with 1.0 M HCl concentration (*vide supra*).

Kinetics investigations for the Hydrolysis of (co)poly(2-oxazoline)s (described in part 2.3)

For the kinetic screening of the PAOx hydrolysis, the different (co)poly(2-oxazoline)s were dissolved in pure ethanol (4.16 mL) and subsequently 35 wt.% HCl (1.60 mL) was added yielding an homogeneous ethanol-water 80:20 (v/v) solvent mixture, containing 12 wt.% HCl. The amide concentration was kept constant at 0.48 M for the different PAOx. For the hydrolysis in ethanol-water 40:60 (v/v), 0.150 grams of the PMeOx-*b*-PEtOx copolymer were dissolved in a mixture of 1.14 mL of water and 1.26 mL of ethanol. When the solution was complete, 1.00 mL of HCl 35 wt.% was added yielding a solution with [A] = amide concentration = 0.48 M containing 12 wt.% HCl. The PMeOx-*b*-PEtOx copolymer was also hydrolyzed in an aqueous medium, by dissolving the copolymer (0.1553 g.) in water (2.53 mL) and subsequently adding 35 wt. % HCl (0.97 mL). Each hydrolysis reaction was performed separately in the microwave synthesizer at various temperatures and times, yielding (co)poly(2-oxazoline)s with different hydrolysis degrees. Upon completion of the desired reaction time, the obtained reaction mixture was cooled down by passing compressed air and neutralized with a 1M NaOH solution to reach a pH of 8-9. Thereafter, the solvent was removed under reduced pressure and the product was dissolved in deuterated methanol. The conversion and composition of the resulting copolymers was assessed by ¹H-NMR spectroscopy.

The conversion is calculated from the ¹H-NMR spectra using the signals of the hydrolysis products. All the signals described in the previous section for both copolyoxazolines are present, together with the signals correspondent to their respective hydrolysis products.

PMeOx_{50-x}-*co*-PEI_x-*b*-PEtOx_{50-y}-*co*-PEI_y: ¹H NMR (300 MHz, CDCl₃, δ): PMeOx₅₀-*b*-PEtOx₅₀, + hydrolysis products: 3.00 – 2.65 (2H, -NH-CH₂), 2.20 – 2.00 (3H, -NCOCH₃, PMeOx, 2H, CH₃CH₂COOH), 1.99 (s, 3H, CH₃COOH), 1.20 – 0.85 (3H, -NCOCH₂CH₃, 3H, CH₃CH₂COOH).

PMeOx_{60-x}-CO-PEI_x-b-PPhOx_{15-y}-CO-PEI_y: ¹H NMR (300 MHz, CDCl₃, δ): PMeOx₆₀-b-PPhOx₁₅ + hydrolysis products: 8.1 (dd, 2H, Ar, benzoic acid), 7.62 – 7.00 (5H, Ar, PPhOx, 3H, Ar, benzoic acid), 3.00 – 2.65 (2H, -NH-CH₂), 1.99 (s, 3H, CH₃COOH).

2.5. References

- [1] T. X. Viegas, M. D. Bentley, J. M. Harris, Z. Fang, K. Yoon, B. Dizman, R. Weimer, A. Mero, G. Pasut, F. M. Veronese, *Bioconjugate Chem.* **2011**, *22*, 976.
- [2] R. Hoogenboom, *Angew. Chem. Int. Ed.* **2009**, *48*, 7978.
- [3] E. Altuntaş, C. Weber, K. Kempe, U. S. Schubert, *Eur. Polym. J.* **2013**, *49*, 2172.
- [4] B. Guillermin, S. Monge, V. Lapinte, J.-J. Robin, *Macromol. Rapid Commun.* **2012**, *33*, 1600.
- [5] R. Hoogenboom, F. Wiesbrock, M. A. M. Leenen, M. A. R. Meier, U. S. Schubert, *J. Comb. Chem.* **2004**, *7*, 10.
- [6] F. Wiesbrock, R. Hoogenboom, M. A. M. Leenen, M. A. R. Meier, U. S. Schubert, *Macromolecules* **2005**, *38*, 5025.
- [7] R. Luxenhofer, Y. Han, A. Schulz, J. Tong, Z. He, A. V. Kabanov, R. Jordan, *Macromol. Rapid Commun.* **2012**, *33*, 1613.
- [8] E. Rossegger, V. Schenk, F. Wiesbrock, *Polymers* **2013**, *5*, 956.
- [9] J. Kronek, E. Paulovičová, L. Paulovičová, Z. Kroneková, J. Luston, *Biocompatibility and Immunocompatibility Assessment of Poly(2-Oxazolines), Practical Applications in Biomedical Engineering*, InTech., available from www.intechopen.com/books, **2013**.
- [10] V. de la Rosa, *J Mater Sci: Mater Med* **2013**, *1*.
- [11] M. Barz, R. Luxenhofer, R. Zentel, M. J. Vicent, *Polym. Chem.* **2011**, *2*, 1900.
- [12] K. Knop, R. Hoogenboom, D. Fischer, U. S. Schubert, *Angew. Chem. Int. Ed.* **2010**, *49*, 6288.
- [13] T. Saegusa, H. Ikeda, H. Fujii, *Macromolecules* **1972**, *5*, 108.
- [14] J. H. Jeong, S. H. Song, D. W. Lim, H. Lee, T. G. Park, *J. Control. Release* **2001**, *73*, 391.
- [15] L. Tauhardt, K. Kempe, K. Knop, E. Altuntaş, M. Jäger, S. Schubert, D. Fischer, U. S. Schubert, *Macromol. Chem. Phys.* **2011**, *212*, 1918.
- [16] H. M. L. Lambermont-Thijs, L. Bonami, F. E. Du Prez, R. Hoogenboom, *Polym. Chem.* **2010**, *1*, 747.
- [17] J.-H. Jeon, S.-H. Lee, J.-H. Lim, K.-M. Kim, *J. Appl. Polym. Sci.* **2010**, *116*, 2937.
- [18] C. Tsitsilianis, G. Gotzamanis, Z. Iatridi, *Eur. Polym. J.* **2011**, *47*, 497.
- [19] M. Jager, S. Schubert, S. Ochrimenko, D. Fischer, U. S. Schubert, *Chem. Soc. Rev.* **2012**, *41*, 4755.
- [20] S. Halacheva, G. J. Price, V. M. Garamus, *Macromolecules* **2011**, *44*, 7394.
- [21] C. Legros, M.-C. De Pauw-Gillet, K. C. Tam, S. Lecommandoux, D. Taton, *Polym. Chem.* **2013**, *4*, 4801.
- [22] K. M. Kem, *J. Polym. Sci. Polym. Chem. Ed.* **1979**, *17*, 1977.
- [23] H. M. L. Lambermont-Thijs, J. P. A. Heuts, S. Hoepfener, R. Hoogenboom, U. S. Schubert, *Polym. Chem.* **2011**, *2*, 313.
- [24] H. P. C. Van Kuringen, J. Lenoir, E. Adriaens, J. Bender, B. G. De Geest, R. Hoogenboom, *Macromol. Biosci.* **2012**, *12*, 1114.
- [25] M. Neu, D. Fischer, T. Kissel, *J. Gene Med.* **2005**, *7*, 992.
- [26] M. Breunig, U. Lungwitz, R. Liebl, C. Fontanari, J. Klar, A. Kurtz, T. Blunk, A. Goepferich, *J. Gene Med.* **2005**, *7*, 1287.
- [27] M. A. Mintzer, E. E. Simanek, *Chem. Rev.* **2008**, *109*, 259.
- [28] L. Wightman, R. Kircheis, V. Rössler, S. Carotta, R. Ruzicka, M. Kursá, E. Wagner, *J. Gene Med.* **2001**, *3*, 362.
- [29] M. H. Louis, S. Dutoit, Y. Denoux, P. Erbacher, E. Deslandes, J. P. Behr, P. Gauduchon, L. Poulain, *Cancer Gene Ther* **2005**, *13*, 367.
- [30] A. Adib, F. Stock, P. Erbacher, *Method for manufacturing linear polyethylenimine (pei) for transfection purpose and linear pei obtained with such method*, Polyplus Transfection, **2009**.
- [31] C. Englert, L. Tauhardt, M. Hartlieb, K. Kempe, M. Gottschaldt, U. S. Schubert, *Biomacromolecules* **2014**, *15*, 1124.
- [32] P. D. J. M. Klee, Maximilian; Fik, Christoph P.; Ritter, Prof. Dr. Helmut, *Dental composition* E. P. Office, EP2662067 (A1), Dentsply Detrey GmbH, Germany, **2013**.
- [33] E. R. Tóke, O. Lőrincz, E. Somogyi, J. Lisziewicz, *Int. J. Pharm.* **2010**, *392*, 261.
- [34] H. M. L. Lambermont-Thijs, F. S. van der Woerd, A. Baumgaertel, L. Bonami, F. E. Du Prez, U. S. Schubert, R. Hoogenboom, *Macromolecules* **2009**, *43*, 927.
- [35] J. C. Q. Fernandes, Xingping; Winnik, Françoise M.; Benderdour, Mohamed; Zhang, Xiaoling; Dai, Kerong; Shi, Qin *Int. J. Nanomedicine* **2013**, *8*, 4091
- [36] A. Beyerle, A. Braun, O. Merkel, F. Koch, T. Kissel, T. Stoeger, *J. Control. Release* **2011**, *151*, 51.

- [37] S. Bauhuber, R. Liebl, L. Tomasetti, R. Rachel, A. Goepferich, M. Breunig, *J. Control. Release* **2012**, *162*, 446.
- [38] G.-H. Hsiue, H.-Z. Chiang, C.-H. Wang, T.-M. Juang, *Bioconjugate Chem.* **2006**, *17*, 781.
- [39] C. Chandrashekar, B. Pons, C. D. Muller, N. Tounsi, R. Mulherkar, G. Zuber, *Acta Biomaterialia* **2013**, *9*, 4985.
- [40] Y.-Y. Won, H. Lee, *J. Control. Release* **2013**, *170*, 396.
- [41] B. Liang, M.-L. He, C.-y. Chan, Y.-c. Chen, X.-P. Li, Y. Li, D. Zheng, M. C. Lin, H.-F. Kung, X.-T. Shuai, Y. Peng, *Biomaterials* **2009**, *30*, 4014.
- [42] D. Zahn, *J. Phys. Chem. B* **2003**, *107*, 12303.
- [43] C. Comminges, S. Frasca, M. Sutterlin, E. Wischerhoff, A. Laschewsky, U. Wollenberger, *RSC Advances* **2014**, *4*, 43092.
- [44] D. Dallinger, C. O. Kappe, *Chem. Rev.* **2007**, *107*, 2563.
- [45] J. M. Kremsner, C. O. Kappe, *Eur. J. Org. Chem.* **2005**, *2005*, 3672.
- [46] B. Brissault, A. Kichler, C. Guis, C. Leborgne, O. Danos, H. Cheradame, *Bioconjugate Chem.* **2003**, *14*, 581.
- [47] K. Hori, Y. Ikenaga, K. Arata, T. Takahashi, K. Kasai, Y. Noguchi, M. Sumimoto, H. Yamamoto, *Tetrahedron* **2007**, *63*, 1264.

Synthesis and micellization behavior of poly(2-oxazoline)-polycarbonate block copolymers

The polymerization of 2-ethyl-2-oxazoline (EtOx) yielding PEOx-OH polymers was studied in detail, and the reaction conditions optimized to minimize undesired chain-transfer and side-reactions and to maximize polymer end-group fidelity. The obtained hydroxyl-terminated PEOx polymers were utilized as macroinitiators for the polymerization of a range of different cyclic carbonates yielding PEOx-*b*-PC block copolymers with low dispersities. These amphiphilic block copolymers underwent self-assembly in water, and their micellization behavior was studied. Variation of the PEOx hydrophilic block length and, specially, the composition of the hydrophobic PC block, resulted in the formation of a wide-range of well-defined structures, from crew-cut and star-micelles to polymersomes. The results obtained represent a promising opportunity for the use of PEOx-*b*-PC amphiphilic block copolymers as drug/gene nanocarriers or in other biomedical applications such as imaging.

3.1 Introduction

Polymeric micelles have been extensively explored as drug carriers, as an alternative to polymer-drug conjugates, and increasingly complex constructs can be found in literature.^[1, 2] Micellar systems are advantageous since they have the capability of transporting high loadings of poorly soluble drugs, a challenge especially in cancer treatment; moreover, micelles can feature both passive and active targeting, since they accumulate in the tumor site by the enhanced permeability and retention (EPR) effect and can also serve as a platform for the incorporation of targeting groups.^[3-5]

The use of these nanocarrier systems thus increases blood circulation times and the overall efficacy of drugs, significantly lowering their side effects and the required administered quantities.^[6, 7] In addition, the cargo is not chemically bonded to the polymeric system, and multiple drug or protein formulations can be loaded in a straightforward manner, facilitating combination therapy, personalized treatments, and simplifying regulatory approval matters since the cargo is not chemically modified. Moreover, the distribution of drug-loaded polymeric micelles in the body can be controlled by its size and surface properties, being largely independent from the nature of the cargo encapsulated into the micellar inner core. This allows facile optimization of the nanocarrier and its applicability to a wide range of therapeutics, from anti-cancer drugs, photosensitizers, contrast agents or anti-oxidants, to biomolecules such as peptides, proteins or genes.^[2, 8-11]

Polymeric micelles are composed of two separated functional segments: an inner core and an outer shell. The outer shell controls the *in vivo* pharmacokinetic behavior, while the inner core is responsible for drug loading capacity, stability and drug release behavior. To fulfill their mission of transporting and efficiently delivering their cargo in a specific tissue or cellular organelle, these

nanocarriers need to overcome a series of obstacles, including stability and long circulation time in the bloodstream, accumulation in the desired tissue, and cellular uptake. Once inside the cell, endo/lysosome escape of the nanocarrier is necessary to achieve effective intracellular drug or gene release.^[12, 13] To overcome these intracellular obstacles, the focus has been put on the hydrophobic polymer block, and a wide range of biodegradable polymers has been studied, including poly(*L*-amino acid)s and polyesters such as poly(glycolic acid) (PGA), poly(lactic acid) (PLA), poly(ϵ -caprolactone) (PCL), and side chain-modified analogs.^[14]

On the other hand, albeit several different polymers have been studied as candidates to constitute the hydrophilic polymer block, including poly(ethylene glycol) (PEG), poly(*N*-vinyl pyrrolidone) (PVP), poly(*N*-isopropyl acrylamide) (PNIPAM), or poly(hydroxypropyl methacrylamide) (PHPMA),^[15, 16] the vast majority of micellar systems reported are currently based on PEG.^[14, 17, 18] This is due to PEG's stealth behavior properties and its regulatory status, being several PEG-based micellar nanocarriers currently involved in clinical trials^[19] and one already in clinical use for the treatment of breast cancer (Genexol-PM).^[20] Nevertheless, the importance of the outer micellar corona, in contact with the environment, should not be overlooked, as it directly interacts with biological factors such as proteins and antibodies, governing the biodistribution of the micelles *in vivo*.^[11] Despite its popularity, PEG also has its drawbacks and limitations.^[21, 22] The development of anti-PEG antibodies has been repeatedly observed in patients, as well as in 25% of human population never treated with PEGylated APIs before (due to its ubiquity in cosmetics and food-additives), and is suggested to be responsible for the accelerated blood clearance of PEG conjugates after multiple injections.^[23-25]

Poly(2-alkyl-2-oxazoline)s (PAOx) are attracting increasing attention in the biomedical field, owing to their highly defined structure, tuneable properties, and excellent biocompatibility arising from its structural analogy with poly(peptide)s.^[26-29] In particular, the hydrophilic poly(2-methyl-2-oxazoline) (PMeOx) and poly(2-ethyl-2-oxazoline) (PEtOx) exhibit stealth behavior, excellent protein antifouling properties,^[30-32] and beneficial physico-chemical characteristics such as low viscosity and high stability. Furthermore, PAOx physical properties can be accurately tuned by selection of the 2-oxazoline monomer, allowing straightforward analysis of structure-property relationships.^[33] Consequently, PAOx have been extensively studied as the optimal polymer platform for biomedical applications.^[21, 22, 34] In addition, the accurate control on polymer molecular weight distribution, stimuli-responsiveness, and functionalization versatility make PAOx ideal for the development of (responsive) micellar systems for biomedical applications.^[33, 35, 36] As such, PAOx appears to be an optimal polymer for the constitution of the external corona of polymeric micelles and vesicles. However, their *in vivo* stability might constitute a drawback for effective cargo release once the nanocarrier has entered the cell.

Therefore, the preparation of PAOx-based amphiphilic copolymers in conjunction with biodegradable polymers is of high interest for the development of optimal polymeric nanocarriers. In this context, the synthesis and micellar characteristics of diblock copolymers based on PEtOx as hydrophilic block and aliphatic polyesters such as PLA and PCL, or polycarbonates such as poly(1,3-trimethylene carbonate) (PTMC) as hydrophobic block have been reported.^[37-40] The PAOx-polycarbonate block copolymer (PAOx-*b*-PC) synthesis has been previously reported *via* a two-stage process by using hydroxyl-terminated PEtOx as macro-initiator for the polymerization of the carbonate cyclic monomer in the presence of tin(II) 2-ethylhexanoate as a catalyst.^[37, 40] Although this method has yielded PAOx-*b*-PC copolymers with good self-assembly properties, the use of a toxic metal catalyst, albeit FDA-approved as trace impurity, is undesired for prospective biomedical applications of the resulting polymeric micelles. Hereby, we report a novel efficient

method for the preparation of highly-defined PAOx-*b*-PC amphiphilic copolymers including a detailed study of the often overlooked synthesis of the PAOx block, with special emphasis on the end-group fidelity assessment. Finally, the self-assembly behavior in aqueous medium of the obtained amphiphilic block copolymers will be discussed.

3.2 Poly(2-ethyl-2-oxazoline) synthesis optimization

A high level of control on the terminal functionalities of the PAOx macroinitiator is required to obtain the intended PAOx-*b*-PC architectures. To this end, a study of the influence of the polymerization temperature and terminating agent on the end-group fidelity of the final polymer composition was performed. To understand the obtained data, we will first describe the main side reactions affecting the polymerization and termination of 2-oxazolines that may have a negative impact on the polymer end-group functionality.

The main side reaction affecting the end-group functionality of poly(2-oxazoline)s is chain-transfer to monomer, generally ascribed to β -elimination.^[41] Chain transfer results in the formation of two species: a chain transferred polymer with an enamine functionality at the chain end, and a protonated oxazolinium cation. The obtained reactive enamine end-group is able to re-polymerize, mostly at the end of the polymerization process, resulting in chain coupling whereas a new chain is initiated by the oxazolinium cation. As seen in Figure 3.2.1, β -elimination produces one chain bearing the intended alpha-functionality in both ends, and one proton-initiated chain bearing a secondary amide in the alpha terminus.

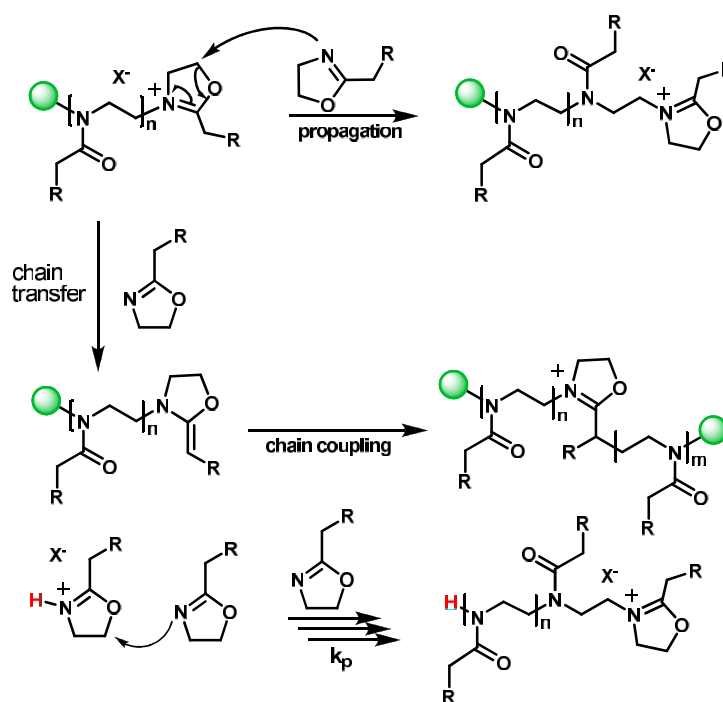


Figure 3.2.1. Mechanism of the intrinsic chain-transfer β -elimination side-reaction during polymerization of 2-oxazolines

Proton initiated chains can also be formed if water is present in the polymerization mixture. Water molecules can terminate living chains liberating a proton, able to initiate a new chain.

During the termination step, water molecules may add to the polymer living chain either in position 2 or in position 5 of the oxazolinium ring, producing two different end-group functionalities.^[42] The addition to the 2 position is reversible and kinetically controlled, resulting in an easily hydrolysable amine ester functionality. The amine ester is formed as kinetic product, which could be explained by a stereoelectronic theory of the intermediate structures while the amide alcohol is the thermodynamic product.^[43, 44] Water termination leads to significant occurrence of the kinetically favored H₂O addition to the 2-position of the oxazolinium species and subsequent formation of the amine ester end-group, therefore the presence of water along with the terminating agent must be avoided to assure quantitative termination in the 5 position of the oxazolinium ring (see Figure 3.2.2).

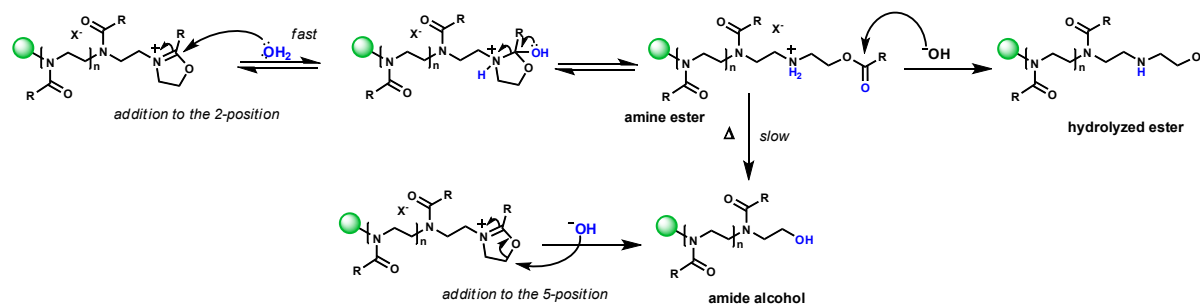


Figure 3.2.2. *The ambident character of oxazolinium ions results in two possible nucleophilic additions: in the 2-position (kinetically controlled and reversible) and in the 5-position (thermodynamically controlled, irreversible).*

The amine ester terminated polymer can be identified by ¹H-NMR spectroscopy, due to the characteristic signals of the protons from the methylene group next to the ester oxygen (see Figure 3.2.3).

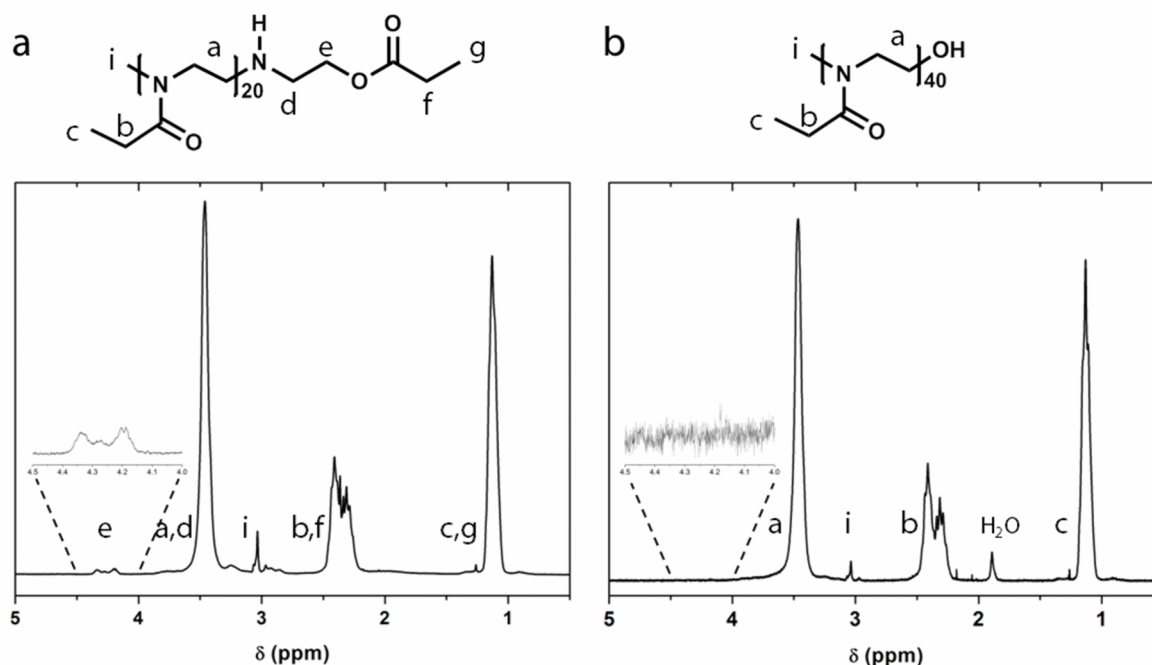


Figure 3.2.3. *¹H-NMR spectra of two different hydroxyl-terminated poly(2-ethyl-2-oxazoline)s (PEtOx_n,OH) showing the presence (a) or absence (b) of amine ester end-groups.*

Termination with methanolic KOH has been reported to proceed through efficient OH⁻ nucleophilic attack to the 5 position, and as such has been often used for PEtOx termination yielding hydroxyl end-groups quantitatively.^[39, 42, 45] Nevertheless, in our hands, PEtOx termination following this protocol sometimes, and mostly for short polymers, resulted in the appearance of an extra distribution attributed to the hydrolyzed amine ester product, as observed by matrix-assisted laser desorption/ionization time-of-flight mass spectrometry (MALDI-TOF MS, see Figure 3.2.4.a, distribution C). Possibly, the presence of trace amounts of water in the highly alkaline methanolic solution resulted in the fast formation of the amine ester product that was subsequently hydrolyzed.

Nevertheless, it should be kept in consideration that MALDI-TOF MS is not a quantitative technique and the relative intensities observed do not necessarily relate to the relative ratios of the different species in the final polymer. This was highlighted by the relative increase in signal intensity for the hydrolyzed amine ester product (C) when low laser intensities were applied (Figure 3.2.4.a), as the hydrolyzed species seem to be much easier ionized than the target amide alcohol-terminated polymer. This is possibly a consequence of the basicity of the terminal secondary amine, more prone to form adducts with charged metal ions than the amide alcohol.

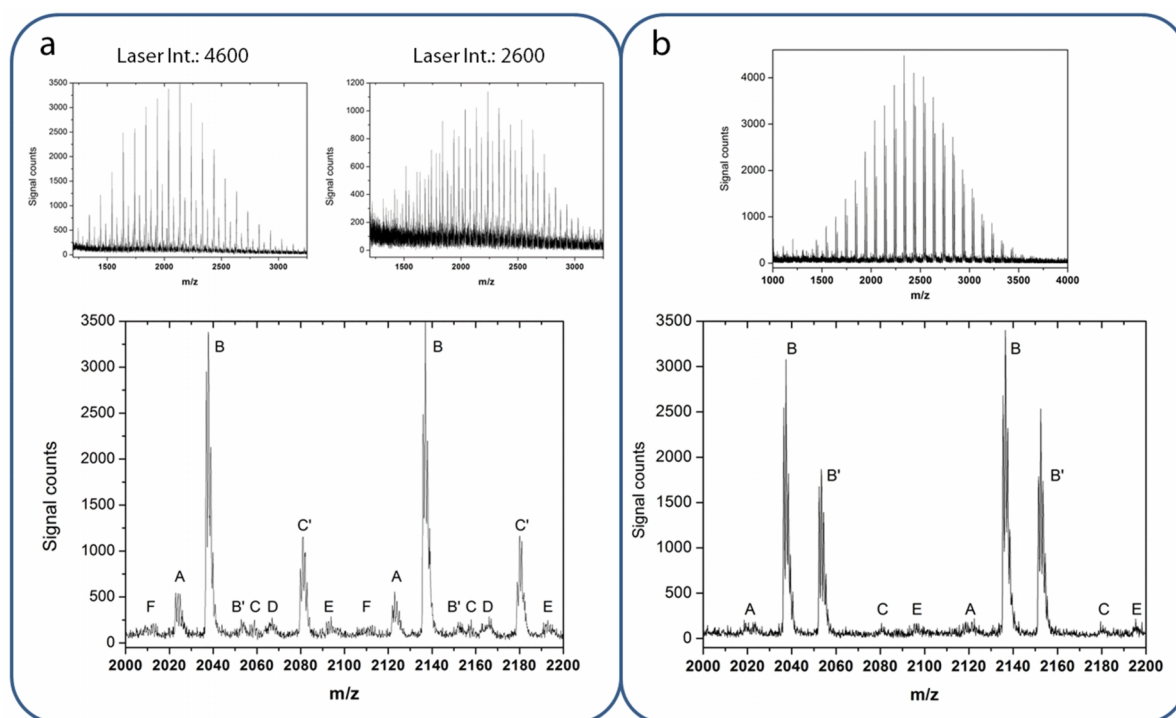
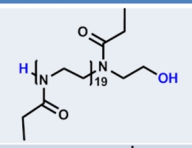
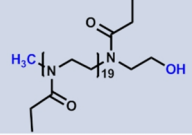
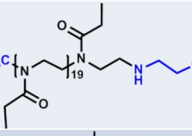
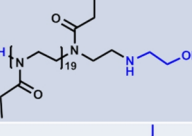
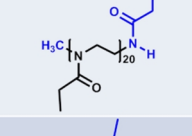
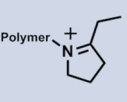
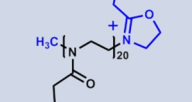


Figure 3.2.4. MALDI-TOF MS analysis of two different PEtOx₂₀OH obtained upon polymerization in acetonitrile at 80 °C for 120 minutes. Initiator: methyl tosylate. [EtOx] = 4 M. [M] / [I] = 20. a) MALDI-TOF mass spectra corresponding to PEtOx₂₀OH terminated with a KOH solution in methanol. Spectra measured with different laser intensities are shown above. b) MALDI-TOF mass spectra corresponding to PEtOx₂₀OH terminated with a 25 wt. % solution of N(CH₃)₄OH in methanol wherein the signals corresponding to the target polymer structure (B) are predominant.

In addition, the increased signal for distribution F at low laser intensities confirmed the assignment to living polymer chains (charged species) and ruled out the assignment to neutral coupled species that have the same mass. Distribution E was assigned to end group degradation, as has been previously reported.^[46] However, we could not identify the mechanism of formation of these degradation species. The detailed assignment of the MALDI-TOF mass spectra is provided in Table 3.2.1.

To enhance end-group fidelity and aiming to develop a better termination agent for –OH functionalization, stoichiometric amounts of tetramethylammonium hydroxide in methanol (25 wt. %) were used. This terminating agent yielded reproducible hydroxyl addition to the 5 position, proving efficient to obtain the intended terminal amide alcohol functionality, also for low molar mass polymers. The effectiveness of this terminating agent is ascribed to the lower basicity of the $N(CH_3)_4OH$ solution in comparison to the KOH solution, permitting the irreversible conversion of any ester functionality into the intended thermodynamic product before irreversible hydrolysis of the ester group. Figure 3.2.4. illustrates the impact of the terminating agent on the end-group fidelity of the final polymer, wherein $N(CH_3)_4OH$ termination promotes the formation of the desired polymer structure. In all cases, termination was performed with stoichiometric amounts of terminating agent at 0 °C while stirring the living polymerization mixture, and the solution was allowed to warm to room temperature overnight while stirring.

Table 3.2.1. Detailed peak assignment of the MALDI-TOF spectra of $PEtOx_nOH$.

Label	Polymer Species			Structure	m/z	
	Description	Alpha terminus	Omega terminus		Theoretical	MALDI-TOF
A	Side product 1: Proton initiated polymer due to chain transfer and water present in the polymerization mixture	H-	-OH		2022.378 (Na ⁺)	2022.838 (Na ⁺)
B	Target polymer	CH ₃ -	-OH		2036.394 (Na ⁺) 2052.492 (K ⁺)	2036.867 (Na ⁺) 2052.849 (K ⁺)
C	Side product 2: Hydrolyzed amine ester. Water-termination in highly basic medium	CH ₃ -	-NHCH ₂ CH ₂ OH		2057.436 (H ⁺) 2079.425 (Na ⁺)	2057.773 (H ⁺) 2079.911 (Na ⁺)
D	Side product 3: H-initiated, hydrolyzed amine ester. Water-termination in highly basic medium	H-	-NHCH ₂ CH ₂ OH		2065.421 (Na ⁺)	2065.793 (Na ⁺)
E	Ethene elimination (end-group cleavage)	CH ₃ -	-NHCOCH ₂ CH ₃		2091.436 (Na ⁺)	2091.837 (Na ⁺)
F	Living polymer	CH ₃ -			2110.484	2110.681

Once the occurrence of amide ester functionality was suppressed, the attention was focused on optimizing the polymerization temperature. A stock solution of EtOx and MeOTs ($[M] / [I] = 30$) was prepared, and a series of polymerizations at different temperatures were carried out under microwave irradiation. The livingness of the polymerization of 2-oxazolines allows accurate calculation of the required polymerization times, as the polymerization follows linear first-order kinetics (Equations 3.2.1 and 3.2.2). The polymerization rate constants for EtOx at different temperatures were calculated based on the reported frequency factor (A) and activation energy (E_a) parameters in the Arrhenius equation (Equation 3.2.3).^[47] The polymerization time at each temperature was calculated to reach 95 % monomer conversion in each polymerization,^[48] and was verified by gas chromatography.^[49]

$$-\frac{d[M]}{dt} = k_p[P^*][M] \quad \text{Equation 3.2.1}$$

$$\ln \frac{[M_0]}{[M_t]} = k_p[I_0]t \quad \text{Equation 3.2.2}$$

$$k_p = Ae^{-E_A/RT} \quad \text{Equation 3.2.3}$$

wherein, for EtOx in acetonitrile and tosylate counter – ion,
 $A = 1.99 \pm 0.85 \cdot 10^8 \text{ L mol}^{-1} \text{ s}^{-1}$ and $E_A = 73.4 \pm 0.5 \text{ kJ mol}^{-1}$

The polymerization of EtOx was performed at temperatures ranging from 80 to 140 °C under microwave irradiation, and the obtained polymers were terminated with stoichiometric amounts of $\text{N}(\text{CH}_3)_4\text{OH}$ in methanol. The polymerization mixtures were analyzed by size exclusion chromatography (SEC) to assess the impact of temperature on the polymer molecular weight distribution (see Table 3.2.2.).

Table 3.2.2. Overview of the synthesized PEtOx₃₀OH polymers. Higher polymerization temperatures only slightly increase the extent of chain-transfer. Right: SEC traces wherein a minor increase of the high molecular weight distribution is observed at high temperatures. Eluent: N,N-dimethylacetamide. Calibrated against PMMA standards.

Polymerization parameters		% Conv. (GC)	SEC		MALDI-TOF	
Temperature (°C)	Time (s)		M _n	Đ	M _n	Đ
140	235	99.6	4850	1.13	2960	1.08
120	660	95.2	4650	1.11	2850	1.07
100	2220	94.0	4800	1.10	2770	1.05
80	8220	94.5	4800	1.08	2730	1.05

Higher temperatures consistently resulted in slightly higher dispersities, due to the rise in the high molecular weight distribution ascribed to chain coupling, albeit this effect was minor. Furthermore, although at 140 °C the dispersity was 0.05 units higher than at 80 °C, it should be noted that the conversion was also 5% higher, due to the polymerization that already starts during the heating ramp. Therefore, increasing temperature in the investigated range can reduce polymerization times by a factor of 35 while increasing dispersity by less than 5%.

Once the effect of increasing temperatures on the polymer molecular weight distribution was assessed, its impact on the end-group fidelity was investigated by MALDI-TOF MS. As seen in Figure 3.2.5., the overall isotope pattern was not affected by the polymerization temperature. End-group analysis also showed no differences among the different investigated polymerization temperatures, all exhibiting the main expected distribution and proton-initiated species (A), together with amine ester hydrolysis product (D) with relative intensities of *ca.* 5%, compared to the main distribution.

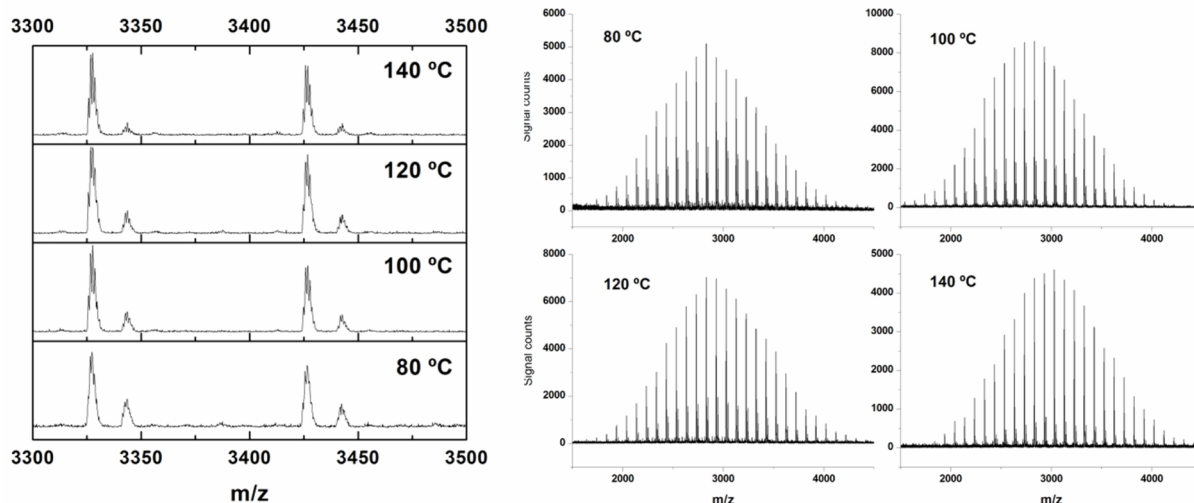


Figure 3.2.5. MALDI-TOF mass spectra of PEOx₃₀OH produced at different temperatures. The overall signal pattern is independent from the polymerization temperature, as is the occurrence of side-products.

It can be thus concluded that increasing the temperature from 80 °C to 140 °C only exerts a minor negative effect on the final PEOx molecular weight distribution, while not affecting the end-group fidelity of the final polymer.

The optimized protocol for the synthesis of hydroxyl-terminated PAOx was applied to the polymerization of EtOx to obtain PEOx-OH macro-initiators for the preparation of PEOx-*b*-PC copolymers. Two polymers were synthesized, bearing 24 and 43 EtOx repeating units. Full characterization is shown in Figure 3.2.6., confirming the intended polymer composition.

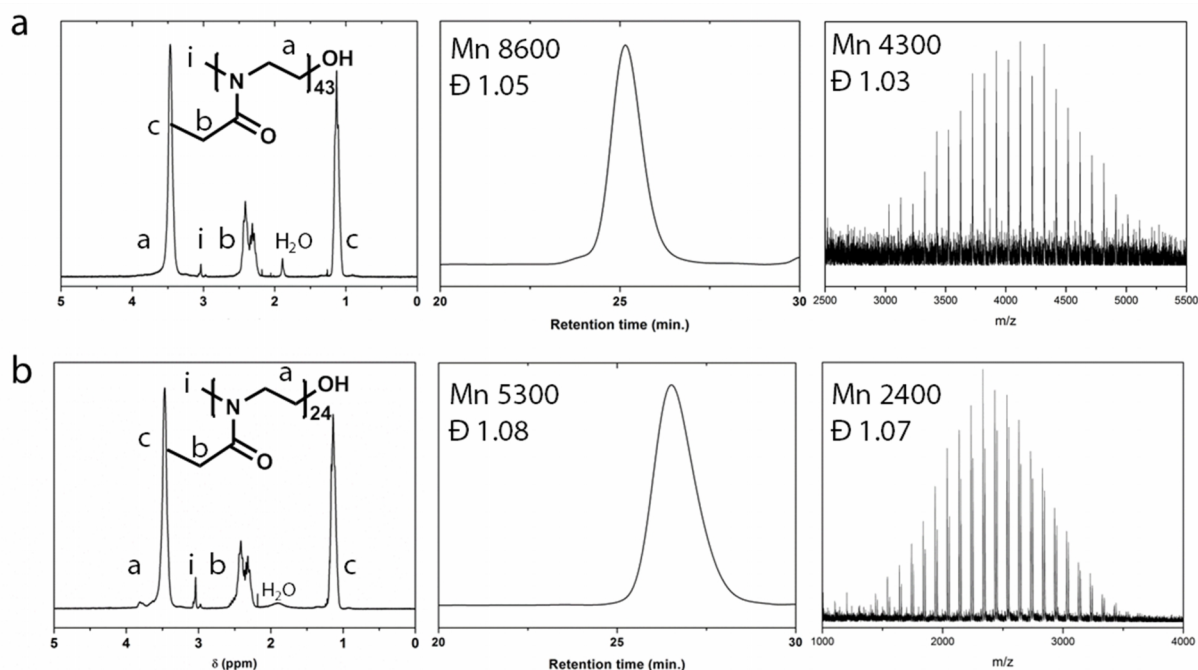


Figure 3.2.6. Characterization data of the two PEOx_{*n*}OH homopolymers to be used as macroinitiators for the polymerization of cyclic carbonates. ¹H-NMR spectra (left) confirm the absence of amine ester terminal functionality, whereas MALDI-TOF MS (right) shows quantitative hydroxyl polymer termination. For PEOx₄₃OH, Na⁺ adduct is observed, whereas for PEOx₂₄OH, Na⁺ and K⁺ adducts of the

target polymer are observed. SEC traces (center) show monomodal narrow distributions for both polymers, with absence of chain coupling species.

3.3 Synthesis of poly(2-ethyl-2-oxazoline)-*b*-poly(carbonate) copolymers

Block-copolymer synthesis performed by Dr. Sarah Tempelaar and Prof. Laetitia Mespouille, at the Laboratory of Polymeric and Composite Materials (LPCM), Center of Innovation and Research in Materials and Polymers (CIRMAP), University of Mons (UMONS). Belgium.

Size Exclusion Chromatography characterization performed by Victor R. de la Rosa at the Supramolecular Chemistry Group, Ghent University (UGent). Belgium.

The synthesis of poly(2-ethyl-2-oxazoline)-*b*-poly(carbonate) block copolymers was achieved using PEOx_nOH polymers as macroinitiators for cyclic carbonate ring-opening polymerization (ROP), whereby the hydroxyl group at the PEOx ω-chain end acts as the initiating group. Keeping the potential biomedical applications of the block copolymers in mind, polymerizations were performed using a bifunctional organic catalyst system based on DBU and 1-(3,5-bis(trifluoromethyl)phenyl)-3-cyclohexylthiourea (TU).^[50] Polymerizations were performed in CHCl₃ or CDCl₃ as solvent at ambient temperature, using 5 mol% TU and 1 mol% DBU ([M] = 0.5 M) and the appropriate amounts of poly(2-ethyl-2-oxazoline) macroinitiator.

Initially, the simple non-functional monomer trimethylene carbonate (TMC) was used to investigate the suitability of the PEOx macroinitiators for cyclic carbonate ROP. The successful polymerization of TMC was further extended to a variety of functional cyclic carbonate monomers, with equally successful results. Chain extension of PEOX₂₄ and PEOX₄₃ could be carried out with six membered cyclic carbonate monomers with benzyl (5-methyl-5-benzoxycarbonyl-propylene carbonate, MBC), allyl (5-methyl-5-allyloxy carbonyl-trimethylenecarbonate, MAC), propargyl (poly(5-methyl-5-propargyloxycarbonyl-1,3-dioxan-2-one, MPC), and morpholino (MTC-MORPH) functionalities (Figure 3.3.1). The use of these monomers was previously reported in the synthesis of a biodegradable hydrogels and drug delivery vehicles often in combination with poly(ethylene)oxides.^[50-53] All block copolymers were analyzed by ¹H NMR spectroscopy and size exclusion chromatography (SEC).

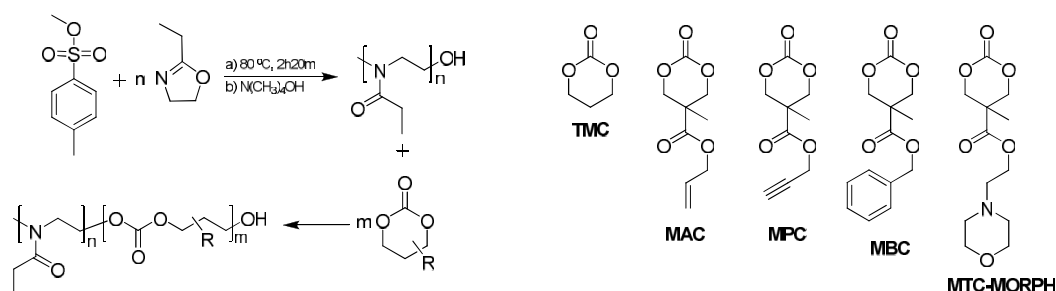


Figure 3.3.1. Left: Schematic representation of the synthetic method in the preparation of block copolymers of PEOx_nOH and (functional) 6-membered cyclic carbonates. Right: selected (functional) six-membered cyclic carbonate monomers.

SEC analysis of the block copolymers revealed that the narrow dispersities of the macroinitiators were retained with dispersities (\bar{D}) ranging 1.1 to 1.3. A shift of the molecular weight distribution to lower retention time for each block copolymer further indicated that successful chain extension had taken place (see Figures 3.3.2. and 3.3.3).

ID	Polymer composition	Polymer structure	SEC data	
			M_n	\bar{D}
	PEtOx ₂₄		5 300	1.08
SD1	PEtOx ₂₄ - <i>b</i> -PTMC ₂₄		10 100	1.09
SD2	PEtOx ₂₄ - <i>b</i> -PMPC ₃₀		14 500	1.20
SD3	PEtOx ₂₄ - <i>b</i> -PMAC ₃₀		5 780	1.08
SD4	PEtOx ₂₄ - <i>b</i> -PMBC ₂₇		14 200	1.10
ST1	PEtOx ₂₄ - <i>b</i> -PMAC _{5.5} - <i>b</i> -P(MTC-MORPH) ₂₆		13 500	1.09

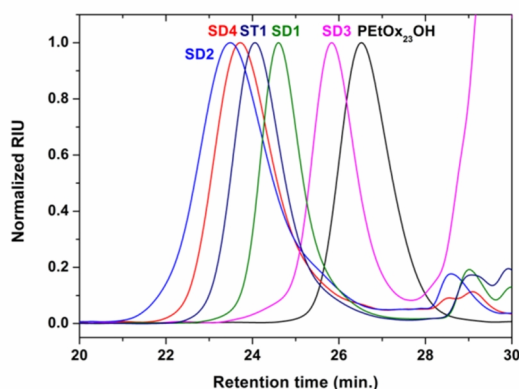


Figure 3.3.2. Structures and size exclusion chromatography (SEC) traces recorded in *N,N*-dimethylacetamide data of the synthesized PEtOx₂₄-*b*-PC block copolymers. Well-defined polymers were obtained in all cases, according to size exclusion chromatography, with dispersity values below 1.20 and generally close to 1.10. Polymer composition was calculated by ¹H NMR spectroscopy analysis. Polymer ID legend: S = short PEtOx₂₄OH, D = di-block, T = tri-block.

¹H-NMR spectroscopy analysis of the prepared block copolymers showed in each case the presence of both the poly(2-ethyl-2-oxazoline) block as well as the poly(carbonate) block allowing the determination of the final block copolymer composition. Signals corresponding to PEtOx were observed at 3.45 ppm, 2.23-2.45 ppm and 1.12 ppm, while those corresponding to the poly(carbonate) backbone appeared at ca. 4.3 ppm for the functional blocks and at 4.23 ppm and 2.05 ppm in case of PTMC. The chemical shifts of the signals corresponding to the PC pendant groups were observed at 4.73 ppm and 2.54 ppm (propargyl), 5.88 ppm, 5.22-5.32 ppm, 4.62 ppm (allyl), 3.67 ppm, and 2.61 ppm and 2.48 ppm (morpholino).

The living nature of the ROP allows for the addition of a third monomer and subsequent formation of a triblock copolymer. This was applied for the synthesis of triblock copolymers with a middle PMAC block containing pendant allyl functionalities and a final block with pendant morpholino functionalities (MTC-MORPH) using PEtOx_nOH as the macroinitiator.

Unimodal SEC traces were obtained for all the copolymers based on PEtOx₂₄OH, indicating full initiator efficiency. In contrast, SEC analysis of the copolymers initiated by the longer PEtOx₄₃OH macroinitiator revealed the presence of remaining PEtOx₄₃OH homopolymer (Figure 3.3.3. right). Since the presence of an undesired end-group functionality on the ω-terminus of the polymer was not observed, this lack of initiating efficiency was ascribed to steric hindrance, as the access to the -OH end-group might be impaired by the increased length of the polymer. Nevertheless, the presence of remaining homopolymer did not prevent the formation of well-defined self-assembled structures, as we shall see further in this chapter.

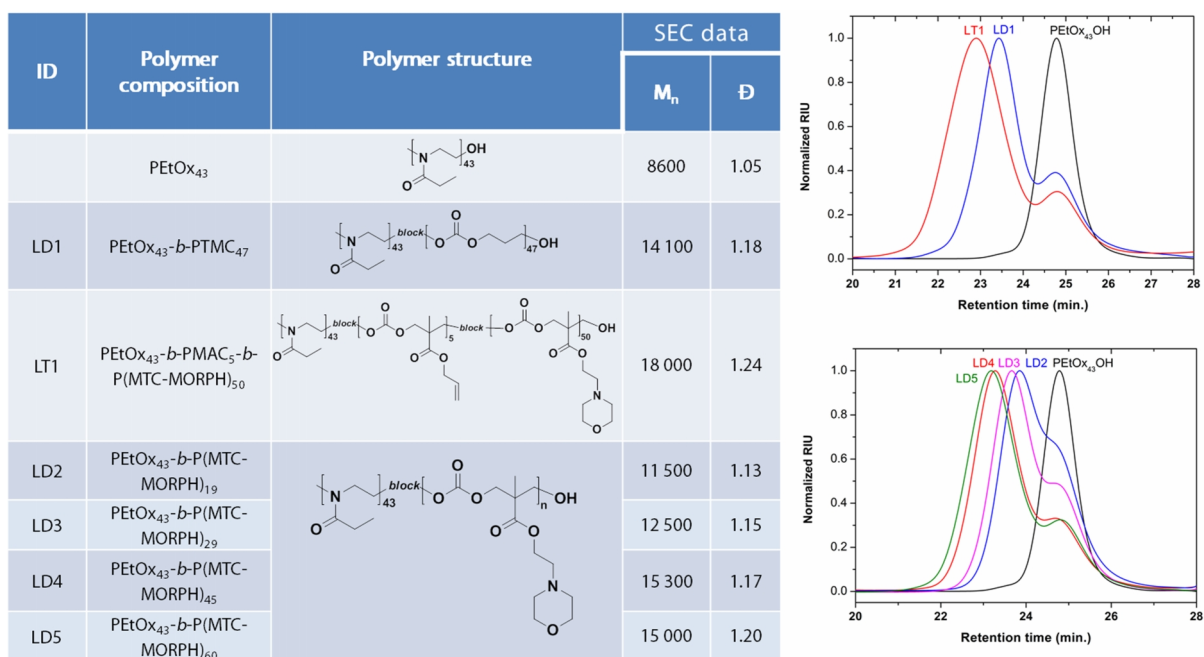


Figure 3.3.3. Structures and size exclusion chromatography (SEC) data of the synthesized PEtOx₄₃-*b*-PC block copolymers. As seen in the size exclusion chromatography traces (right), remaining PEtOx homopolymer can be found in all copolymers. Nevertheless, the overall dispersity values are kept below 1.20. Polymer composition was calculated by ¹H-NMR analysis. Polymer ID legend: L = long PEtOx₄₃OH, D = di-block, T = tri-block.

3.4 Poly(2-ethyl-2-oxazoline)-*b*-poly(carbonate) self-assembly

Self-assembly of amphiphilic block copolymers can be performed by applying different techniques, mainly based on polymer rehydration or on solvent-switching. Polymer rehydration techniques are based on the dissolution of the polymer in an organic solvent and subsequent evaporation in a flask leading to the formation of a polymer thin-layer. The polymer is then suspended in water that penetrates through the defects in the polymer layers yielding polydisperse vesicular structures.^[54, 55] On the other hand, the solvent-switch or phase inversion technique is based on dissolving the block copolymer in a good organic solvent for both blocks, followed by hydration of the solution. Hydration can be achieved by slow addition of water to the organic phase or *vice versa*. In the present research, the polymer solution was slowly injected in water under stirring, rendering the hydrophobic block insoluble and thus inducing the copolymer self-assembly into micellar structures as a result of increasing interfacial tension between the hydrophobic blocks and the environmental water molecules.^[56, 57]

PEtOx-*b*-PCs, as amphiphilic block copolymers, have the ability to self-assemble in solution giving rise to multiple different morphologies including spheres, cylinders and vesicles. These are governed in the equilibrium by the hydrophilic block thermodynamic area.^[58, 59] In the classical (dynamic equilibrium) description, the curvature of the hydrophobic-hydrophilic interface that describes the morphology of the self-assembled structures is governed by the packing parameter p , determined by the volume/length ratio of the hydrophobic block (V_o/l_o) and the equilibrium area per molecule at the aggregate interface (a_e).^[58] The packing parameter is thus defined as $p = V_o/(a_e l_o)$ and its value usually corresponds to different shapes of self-assembled structures in solution: sphere ($p \leq 1/3$), cylinder ($1/3 \leq p \leq 1/2$), and bilayers ($1/2 \leq p \leq 1$). As we shall see, the importance of the hydrophobic block composition and weight will have a strong impact on the micellization properties of the synthesized amphiphilic block-copolymers, as the hydrophobic suppresses dynamic equilibration of the self-assembled polymer ensembles leading to kinetically-trapped structures.^[60]

Additional factors that control the morphology of the self-assembled nanostructures include the chemical structure of the copolymer, the hydrophilic/hydrophobic ratio, concentration, presence of salts, pH, or the organic solvent used and method to prepare the copolymer solution.^[61, 62] Therefore, in the present research, a consistent approach was followed for the preparation of copolymer solutions, maintaining solvent, temperature and concentration constant to minimize the impact of such external factors on the micellization behavior of the different block copolymers studied.

3.4.1 PEtOx₂₄-*b*-PC block copolymers

Initially, we studied the micellization behavior of a series of PEtOx-*b*-PCs based on the short PEtOx₂₄OH as the hydrophilic block. To produce the micelles, a 10 mg mL⁻¹ solution in acetone of each copolymer was prepared and subsequently added to milli-Q water at a 5 μ L min⁻¹ rate under gentle stirring (see Experimental Section for details). Upon complete addition of the polymer, the solution was heated to 55 °C for 24h under stirring, to promote the formation of thermodynamically stable micelles and to remove the residual acetone, obtaining a 1 mg mL⁻¹ aqueous solution of copolymer. This concentration is well above the critical micelle concentration that is typically in the range of 2 – 20 μ g mL⁻¹ for amphiphilic block copolymers.^[37, 63] Subsequently, the obtained self-assembled structures were investigated by dynamic light scattering (DLS). As seen in Table 3.4.1., all the studied PEtOx-*b*-PC blocks underwent self-assembly when dispersed in water, wherein the composition and length of the hydrophobic poly(carbonate) block had a large influence on the supramolecular structures formed.

Table 3.4.1. Characterization of the self-assembled PEtOx₂₄OH-*b*-PC amphiphilic block copolymers. f_{EtOx} represents the PEtOx weight fraction on the copolymer calculated by ¹H NMR analysis. The average particle diameter (Z_{ave}) and corresponding polydispersity index were measured by dynamic light scattering in milli-Q water, at 1 mg mL⁻¹ polymer concentration. Polymer ID legend: S = short PEtOx₂₄OH, D = di-block, T = tri-block.

ID	Polymer composition	SEC		f_{EtOx} (%)	DLS	
		M_n	\bar{D}		Z_{ave} [nm]	PDI
	PEtOx ₂₄	5 300	1.08	100	-	-
SD1	PEtOx ₂₄ - <i>b</i> -PTMC ₂₄	10 100	1.09	48	25.2 ± 0.7	0.202 ± 0.008
SD2	PEtOx ₂₄ - <i>b</i> -PMPC ₃₀	14 500	1.20	28	48.5 ± 0.1	0.281 ± 0.002
SD3	PEtOx ₂₄ - <i>b</i> -PMAC ₃₀	5 780	1.08	28	79.8 ± 0.4	0.092 ± 0.002
SD4	PEtOx ₂₄ - <i>b</i> -PMBC ₂₇	14 200	1.10	25	54.9 ± 0.4	0.223 ± 0.004
ST1	PEtOx ₂₄ - <i>b</i> -PMAC _{5,5} - <i>b</i> -P(MTC-MORPH) ₂₆	13 500	1.09	22	32.3 ± 0.4	0.070 ± 0.002

The obtained aggregates can be separated in two groups based on the definition in their size distribution. The blocks containing PTMC, PMPC and PMBC exhibited a PDI in the range from 0.2 to 0.3, presenting a narrow distribution corresponding to individual micelles and an extra distribution corresponding to larger aggregates. Micelle aggregation is a consequence of the inability of the short PEtOx block to efficiently isolate the hydrophobic micellar core from the environment, and has been previously found for amphiphilic block copolymers containing a relatively short PEG corona. This phenomenon is ascribed to hydrophobic-hydrophobic interactions and van der Waals interactions between the exposed cores of the individual micelles (see Figure 3.4.1.).^[64-66]

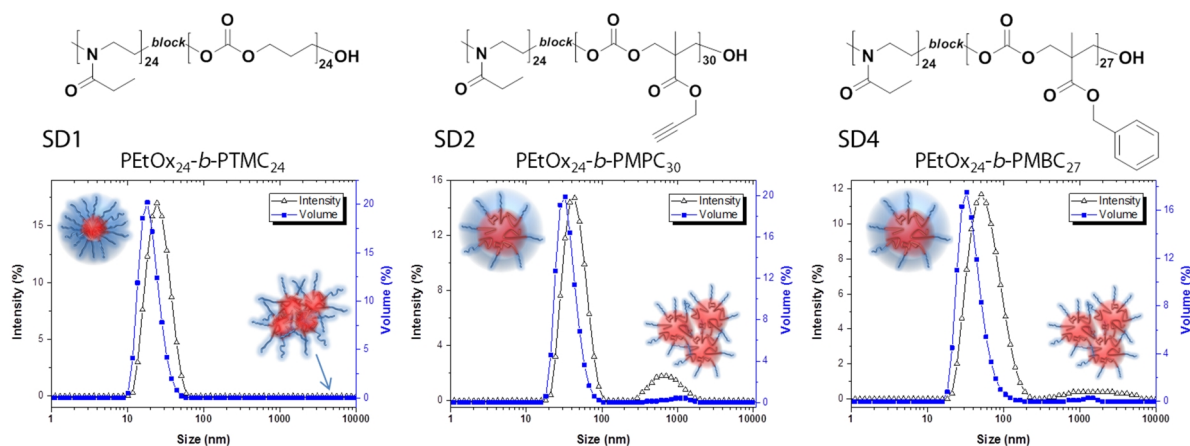


Figure 3.4.1. Particle size distribution for aqueous solutions containing 1 mg mL^{-1} of $\text{PEtOx}_{24}\text{-b-PC}$ copolymers, measured by dynamic light scattering (DLS). Each copolymer exhibited one narrow distribution corresponding to individual micelles of increasing size with increasing weight of the PC block and an additional broad distribution as a result of micelle aggregation. (The drawings are artistic representations of the formed structures, rather than accurate descriptions of the actual particle morphologies, that cannot be determined by DLS).

The $\text{PEtOx}_{24}\text{-b-PTMC}_{24}$ block copolymer, with almost a 1:1 weight ratio of both blocks, self-assembles into compact star micelles with a size of $\approx 26 \text{ nm}$. This is a result of the compact molecular architecture of the PTMC block, that does not feature side chains, allowing efficient packing of the hydrophobic chains in the micelle hydrophobic core. On the other hand, PMPC and PMBC include side chains that need to pack in the micelle core, resulting in larger micelles with a size following the increasing molecular weight of the polycarbonate block. The increasing volume of the hydrophobic PC block and its inefficient packing, together with the relatively small PEtOx corona, accounts for the occurrence of inter-micellar interactions and aggregation.

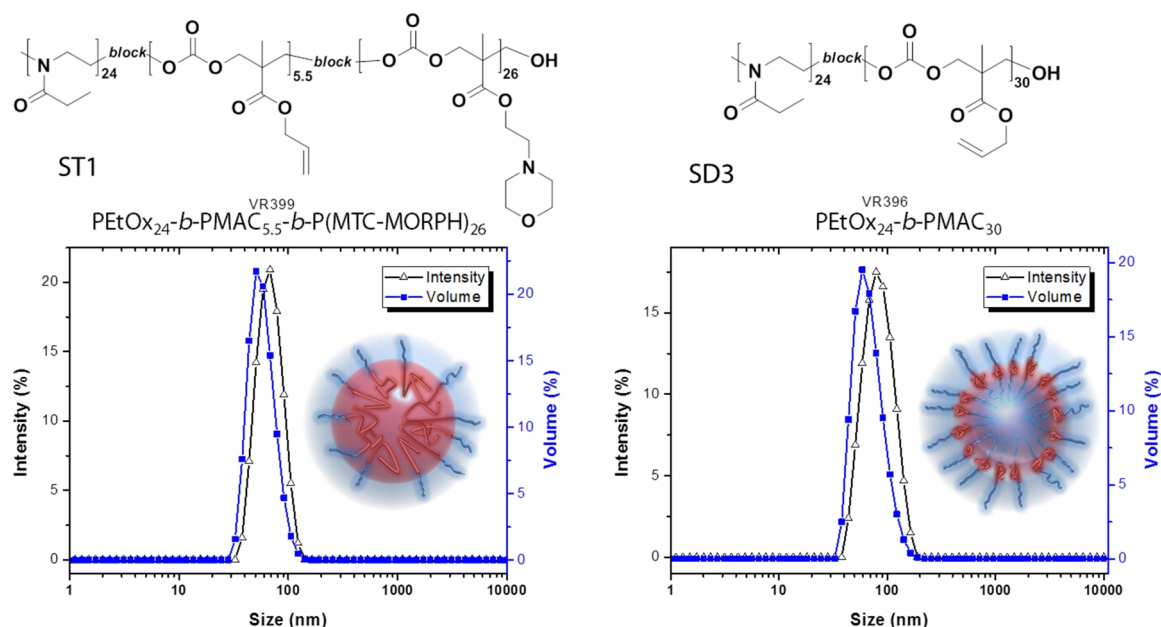


Figure 3.4.2. Particle size distributions corresponding to aqueous solutions containing 1 mg mL^{-1} of $\text{PEtOx}_{24}\text{-b-PC}$ copolymers, measured by dynamic light scattering. Both copolymers exhibited a single narrow distribution corresponding to crew-cut micelles, in the case of the $\text{PEtOx}_{24}\text{-b-PMAC}_{5.5}\text{-b-P(MTC-MORPH)}_{26}$ tri-block copolymer and to vesicles in the case of the $\text{PEtOx}_{24}\text{-b-PMAC}_{30}$ di-block copolymer. (The drawings are artistic representations of the formed structures).

In contrast with these three described block copolymers, aqueous dispersion of the remaining block copolymers resulted in well-defined particle size distributions with the absence of large aggregates (see Figure 3.4.2).

Interestingly, the $\text{PEtOx}_{24}\text{-}b\text{-PMAC}_{5.5}\text{-}b\text{-P(MTC-MORPH)}_{26}$ tri-block copolymer, with the largest hydrophobic domain, formed compact crew-cut micelles. The efficient packing of the MTC-MORPH units is believed to account for the formation of these compact well-defined micelles (PDI = 0.070). The important role of the PMAC block, acting as a spacer to facilitate the packing of the PMTC-MORPH domain, will be further highlighted in the micellization of the block copolymers comprising a longer PEtOx chain (*vide infra*).

Surprisingly, instead of resulting in the formation of compact micelles, the dispersion of $\text{PEtOx}_{24}\text{-}b\text{-PMAC}_{30}$ in water affords large monodisperse (PDI = 0.092) structures with a size of *ca.* 80 nm. Considering the length of the block copolymer and the PMAC hydrophobic block contribution to the copolymer mass (*ca.* 72 %), it is reasonable to ascribe the observed particle size distribution to vesicle formation.^[67] It seems that the PMAC block suffers a high entropic penalty related to core-chain stretching, rendering the formation of simple micelles unfavorable as low-energy morphology. The loose packing of the PMAC blocks in the hydrophobic core of the aggregate thus promotes the transition towards vesicular structures that allocate more space for the packing of the hydrophobic block chains.

3.4.2 $\text{PEtOx}_{43}\text{-}b\text{-PC}$ block copolymers

Next, a series of different poly(carbonate) block-copolymers containing *ca.* 50% to 20% wt. ratio of a longer PEtOx_{43} -hydrophilic was suspended in water following the same protocol as for the $\text{PEtOx}_{24}\text{-}b\text{-PC}$ copolymers. It was hypothesized that the longer PEtOx_{43} hydrophilic block would provide better stabilization of the micellar structures. Indeed, as seen in Table 3.4.2., all the $\text{PEtOx}_{43}\text{-}b\text{-PC}$ copolymers self-assembled into well-defined micellar structures. However, unexpectedly, a sufficiently long hydrophobic block was required for the micellization of $\text{PEtOx}_{43}\text{-}b\text{-P(MTC-MORPH)}_n$ copolymers, as will be discussed later (*vide infra*).

Table 3.4.2. Characterization of the self-assembled structures of $\text{PEtOx}_{43}\text{OH-}b\text{-PC}$ amphiphilic block copolymers. f_{EtOx} represents the PEtOx weight fraction on the copolymer calculated by ^1H NMR analysis. The average particle diameter (Z_{ave}) and corresponding polydispersity index were measured by dynamic light scattering in milli-Q water, at 1 mg mL^{-1} polymer concentration. Polymer ID legend: L = long $\text{PEtOx}_{43}\text{OH}$, D = di-block, T = tri-block.

ID	Polymer composition	SEC		f_{EtOx} (%)	DLS	
		M_n	\bar{D}		Z_{ave} [nm]	PDI
	PEtOx_{43}	8600	1.05	100	-	-
LD1	$\text{PEtOx}_{43}\text{-}b\text{-PTMC}_{47}$	14 100	1.18	47	48.7 ± 0.2	0.109 ± 0.005
LT1	$\text{PEtOx}_{43}\text{-}b\text{-PMAC}_5\text{-}b\text{-P(MTC-MORPH)}_{50}$	18 000	1.24	22	65.2 ± 0.4	0.066 ± 0.002
LD2	$\text{PEtOx}_{43}\text{-}b\text{-P(MTC-MORPH)}_{19}$	11 500	1.13	45	210 ± 4	0.165 ± 0.004
LD3	$\text{PEtOx}_{43}\text{-}b\text{-P(MTC-MORPH)}_{29}$	12 500	1.15	35	236 ± 3	0.149 ± 0.002
LD4	$\text{PEtOx}_{43}\text{-}b\text{-P(MTC-MORPH)}_{45}$	15 300	1.17	26	165 ± 2	0.017 ± 0.006
LD5	$\text{PEtOx}_{43}\text{-}b\text{-P(MTC-MORPH)}_{60}$	15 000	1.20	20	133 ± 1	0.029 ± 0.001

Importantly, albeit the presence of remaining $\text{PEtOx}_{43}\text{OH}$ macroinitiator was observed in all $\text{PEtOx}_{43}\text{-}b\text{-PC}$ copolymers by SEC analyses (Figure 3.3.3), no free polymer chains were detected by DLS in aqueous solutions of the copolymers. This indicates that the $\text{PEtOx}_{43}\text{OH}$ homopolymers

were incorporated into the micellar structures. As a result of its slight amphiphilicity, PEtOx tendency to self-assemble in solution below its T_{CP} has been previously observed.^[68]

In agreement with the results obtained for the analogous PEtOx₂₄ copolymer (SD1), the PEtOx₄₃-*b*-PTMC₄₇ copolymer, with a weight ratio of both blocks close to 1:1, formed compact star micelles with a size matching that of the fully stretched block-copolymer chain (≈ 50 nm). The larger hydrophilic corona provided by the PEtOx₄₃ blocked proved sufficient to suppress any micelle-micelle interaction and aggregation.

The PEtOx₄₃-*b*-PMAC₅-*b*-P(MTC-MORPH)₅₀ tri-block copolymer, with a much larger hydrophobic domain, also formed compact micelles with a size close to that of the copolymer chain (≈ 58 nm). As described earlier for the analogous PEtOx₂₄ copolymer, the intermediate short PMAC block seems to promote efficient packing of the P(MTC-MORPH) block and the formation of well-defined (PDI = 0.07) crew-cut micelles (see Figure 3.4.3). The role of the PMAC spacer was subsequently evaluated upon analysis of the micellization behaviour of PEtOx₄₃-*b*-P(MTC-MORPH)_n di-block copolymers that do not contain PMAC.

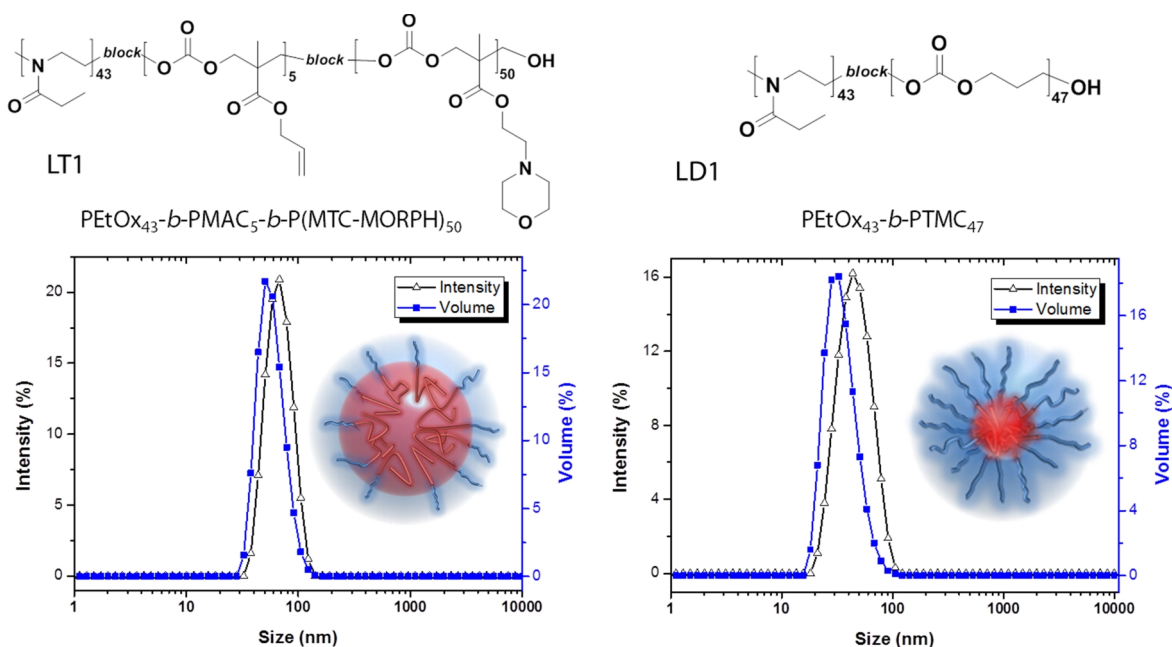


Figure 3.4.3. Particle size distributions corresponding to aqueous solutions containing 1 mg mL⁻¹ of PEtOx₄₃-*b*-PC copolymers, measured by dynamic light scattering. Both copolymers exhibited a single narrow distribution corresponding to crew-cut micelles, in the case of the PEtOx₄₃-*b*-PMAC₅-*b*-P(MTC-MORPH)₅₀ tri-block and to star micelles in the case of the PEtOx₄₃-*b*-PMAC₄₇ di-block copolymer. (The drawings are artistic representations of the formed structures).

Unexpectedly, instead of compact micelles, all copolymers from the analyzed series of PEtOx₄₃-*b*-P(MTC-MORPH)_n copolymers, with P(MTC-MORPH) lengths ranging from 19 (f_{EtOx} (weight) = 0.45) to 60 (f_{EtOx} (weight) = 0.20) yielded much larger micelles, possibly indicating the formation of multi compartmented micelles or vesicles. Although the introduction of a small intermediate polycarbonate block has been reported to favor polymer self-assembly and increase thermodynamic stability of the formed micelles, modification of the micelle size or structure was not observed.^[63, 69]

As seen in Figure 3.4.4., all $\text{PEtOx}_{43}\text{-}b\text{-P(MTC-MORPH)}_n$ di-block copolymers yielded highly defined micellar structures with sizes ranging from *ca.* 140 to 230 nm and polydispersities between 0.16 to 0.02. However, it should be noted that the results corresponding to copolymers LD2 and LD3 are not representative, since a large amount of macroscopic aggregates were obtained upon addition of the $\text{PEtOx}_{43}\text{-}b\text{-P(MTC-MORPH)}_n$ copolymer solution to water. In contrast to copolymers LD4 and LD5, that readily formed well-defined micellar solutions, LD2 and LD3 solutions had to be repeatedly annealed by heating to 50 °C and cooling back to room temperature. This heating-cooling process is thought to favor the formation of kinetically-trapped structures. After several cycles, micellar solutions were obtained, as seen by the slightly blue coloration of the solution, and the partial dissolution of the macroscopic copolymer aggregates.

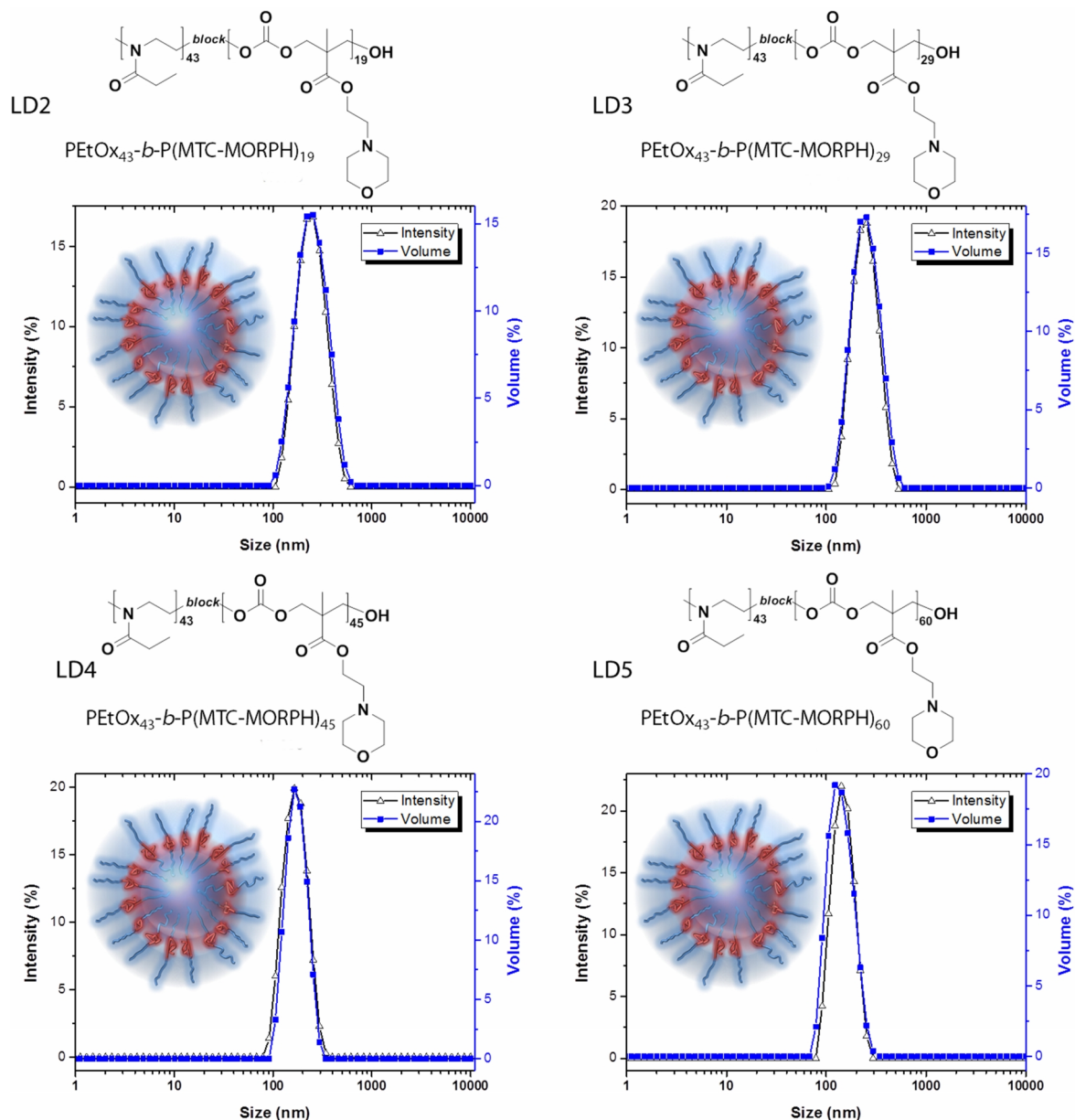


Figure 3.4.4. Particle size distribution for aqueous solutions containing 1 mg mL^{-1} of $\text{PEtOx}_{43}\text{-}b\text{-PC}$ copolymers, measured by dynamic light scattering (DLS). Results corresponding to copolymers LD2 and LD3 are not representative, as their concentration in solution is lower due to partial formation of macroscopic aggregates. In contrast, LD4 and LD5 exhibited narrow distributions corresponding to vesicular structures. The drawings are artistic representations of the formed structures, rather than accurate descriptions of the actual particle morphologies, that cannot be determined by DLS.

Nevertheless, the samples had to be filtered to remove the aggregates still present and therefore the copolymer concentration in solution was estimated to be well below the intended 1 mg mL^{-1} . It thus seems that the relatively short length of the hydrophobic $P(\text{MTC-MORPH})_n$ blocks (19 and 29 MTC-MORPH units) was insufficiently hydrophobic to induce the formation of core-shell micellar structures in which the hydrophobic part is efficiently shielded from water, as the copolymers containing longer $P(\text{MTC-MORPH})_n$ blocks (45 and 60 MTC-MORPH units) resulted in well-defined self-assembled structures.

Interestingly, as the hydrophobic core volume increases to 45 and 60 MTC-MORPH units, the core-block stretching term dictates a further transition towards vesicular structures with an apparent hydrodynamic diameter that decreases from 165 to 133 nm with increasing length of the $P(\text{MTC-MORPH})$ block (see Table 3.4.2).

To further confirm the formation of vesicles, a mixture of calcein disodium salt (2 mg) and the $\text{PEtOx}_{43}\text{-}b\text{-}P(\text{MTC-MORPH})_{45}$ copolymer (2.5 mg) was dispersed in 2.5 mL milli-Q water, yielding vesicles loaded with the calcein fluorescent probe in the aqueous core. Subsequently, the solution was purified by preparative size-exclusion chromatography to remove excess of free dye in solution. Figure 3.4.5 shows a picture taken under UV radiation (366 nm) of the different fractions collected by preparative SEC, where the first fraction contains calcein-loaded polymer vesicles and the following fractions increasing concentrations of free dye in solution. As can be seen, the first fraction exhibits a very low level of fluorescence due to the calcein self-quenching in the constricted intravesicular environment.^[70]

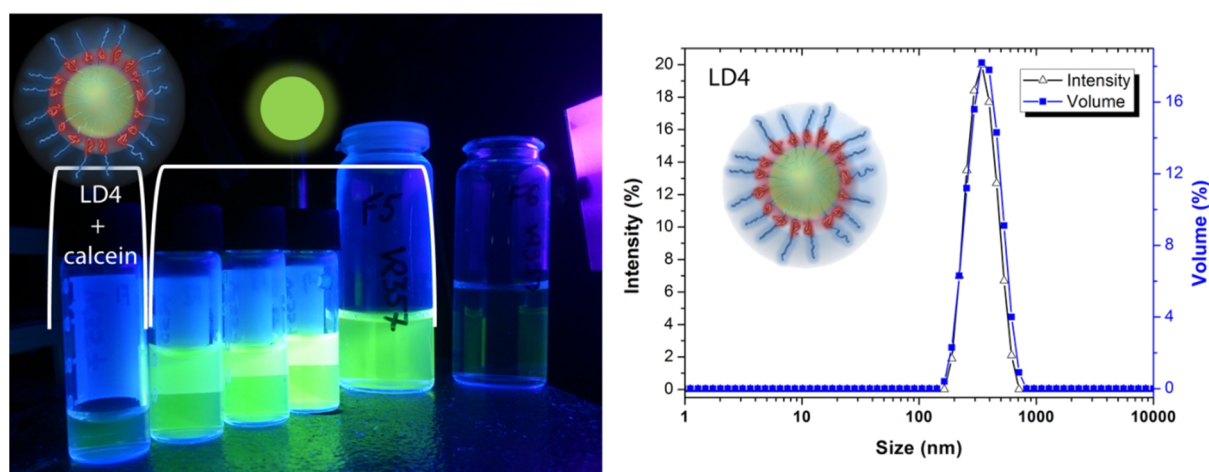


Figure 3.4.5. Left: Preparative size-exclusion chromatography fractions of calcein-loaded $\text{PEtOx}_{43}\text{-}b\text{-}P(\text{MTC-MORPH})_{45}$ vesicles under 366 nm UV light. The first fraction exhibits very low fluorescence properties, as a result of calcein self-quenching inside the vesicle core. Right: particle size distribution of calcein-loaded $\text{PEtOx}_{43}\text{-}b\text{-}P(\text{MTC-MORPH})_{45}$ vesicles (1 mg mL^{-1}) measured by dynamic light scattering.

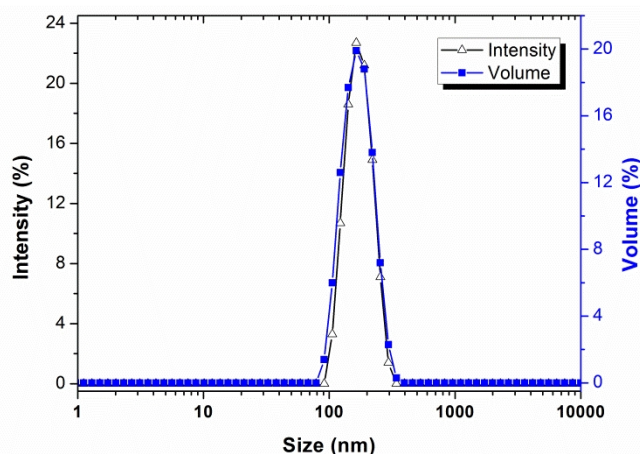
DLS measurements of the collected fraction demonstrated the integrity of the vesicles upon purification. In addition, the average size remained mainly unaffected by the inclusion of calcein.

To further proof the formation of vesicles, a sample of calcein-loaded vesicle solution was dialyzed against milli-Q water. In parallel, a solution containing free calcein was also dialyzed against milli-Q water. After 72 hours, fluorescence was observed upon UV-irradiation of the dialysis water corresponding to free calcein, indicating diffusion of the molecule through the dialysis membrane (Mwt cut-off = 1000 Da). On the other hand, no fluorescence was observed in the dialysis water

corresponding to calcein-loaded vesicles, indicating the entrapment of the fluorescent molecules inside the vesicle core, and the impermeability of the polymer membrane.

To assess the stability of the vesicles, a 1 mg mL^{-1} $\text{PEtOx}_{43}\text{-}b\text{-P(MTC-MORPH)}_{45}$ solution was acidified to pH 2 with HCl_{aq} and incubated for 72 hours after which the solution was analyzed by DLS. Since no apparent change was observed, the solution was basified with NaOH_{aq} to pH = 12 for 24h, as the carbonate groups are less stable in basic conditions, and subjected to DLS analysis. Unexpectedly, as seen in Figure 3.4.6., the particle size distribution remained mainly unvaried, indicating a tight packing of the PEtOx chains that conform the vesicle hydrophilic corona, efficiently shielding the micellar polycarbonate core from the aqueous environment.

Figure 3.4.6. Particle size distribution measured by dynamic light scattering of $\text{PEtOx}_{43}\text{-}b\text{-P(MTC-MORPH)}_{45}$ vesicles (1 mg mL^{-1}) after being exposed to an environmental pH of 2 for 72 hours and of 12 for 24 hours. No apparent change is visible, indicating high stability of the vesicles ascribed to efficient shielding of the vesicle hydrolysable core by the compactly-packed PEtOx corona.



3.5. Conclusions

The polymerization of 2-ethyl-2-oxazoline (EtOx) yielding PEtOx-OH polymers was studied in detail by $^1\text{H-NMR}$ spectroscopy, SEC and MALDI-TOF MS, and the reaction conditions were optimized to minimize undesired chain-transfer and side-reactions and maximize polymer end-group fidelity. The obtained hydroxyl-terminated PEtOx polymers were utilized as macroinitiators for the polymerization of a range of different cyclic carbonates obtaining PEtOx-*b*-PC block copolymers with low dispersities, typically below $\text{Đ} = 1.20$. These amphiphilic block copolymers underwent self-assembly in water, and their micellization behavior was studied. The block copolymers containing a short PEtOx_{24} block formed micelles and micellar aggregates due to the inability of the small hydrophilic corona to efficiently isolate the micellar hydrophobic core from the environment, resulting in micelle-micelle interactions and aggregation. The composition of the hydrophobic block, however was found to be key to control nanoparticle size and stability, and both compact star or hairy and crew-cut micelles were obtained with sizes close to that of the fully stretched copolymer chain. These micelles were stable towards aggregation and exhibited polydispersity indexes below 0.1 as determined by dynamic light scattering.

On the other hand, copolymers containing a longer PEtOx_{43} hydrophilic block, formed well-defined ($\text{PDI} < 0.15$) nanostructures stable against aggregation. Comparison of the results obtained for the shorter PEtOx_{24} copolymers showed that PMAC promotes the formation of stable star-like micelles, possibly due to its efficient inter-chain packing. In addition, the presence of a short PMAC block at the interface between both hydrophilic and hydrophobic domains demonstrated to promote the formation of well-defined compact crew-cut micelles, as it seems to assist on the packing of the contiguous hydrophobic P(MTC-MORPH) block. Interestingly, in the absence of this PMAC spacer, the formation of vesicles is observed for PEtOx-*b*-P(MTC-MORPH). In this case, a sufficiently large hydrophobic block (>70 wt.%) was found to be necessary to obtain well-defined structures. The formation of PEtOx-*b*-P(MTC-MORPH)-based vesicles was further proven by calcein encapsulation,

where a clear fluorescence quenching of the calcein fluorescent probe was observed. Finally, the stability of the obtained vesicles was assessed by suspending the micelles in a highly acidic (pH = 2) and basic (pH = 12) solutions for a period of 72 and 24 hours, respectively. No macroscopic precipitation or apparent change in the particle size distribution was observed by DLS, indicating a tight packing of the PEO_{x43} chains that conform a protective corona efficiently shielding the vesicular core from the environment. These results represent a promising opportunity for the use of PEO_x-*b*-PC amphiphilic block copolymers as drug/gene nanocarriers or in other biomedical applications such as imaging. Preliminary studies to determine their cell-uptake and *in vivo* toxicity have yielded highly promising results, and research is ongoing to valorize these nanocarriers as useful tools in biomedicine.

3.6. Experimental Section

Materials

Solvents and reagents were purchased from Sigma Aldrich, and used as received unless otherwise specified. Methyl tosylate (MeOTs) was distilled twice under vacuum prior to use. 2-Ethyl-2-oxazoline (EtOx, Aldrich) was distilled over barium oxide (BaO). Acetonitrile (CH₃CN, Acros Organics) was dried over molecular sieves (3Å). All reagents were stored and handled under a dry argon or nitrogen atmosphere. KOH, and tetramethylammonium hydroxide in methanol (25 wt.%) were used as received.

Deionized (Milli-Q) water was obtained from a Sartorius Arium 611 with a Sartopore 2 150 (0.45 + 0.2 μm pore size) cartridge filter (resistivity ≥ 18.2 MΩ cm).

Instrumentation

Polymerizations were performed in a Biotage initiator sixty microwave synthesizer utilizing capped microwave vials. The vials were heated to 120 °C for 24 hours and cooled down to room temperature under vacuum prior to use. All polymerizations were performed with temperature control (IR sensor).

¹H-NMR spectra were recorded in CDCl₃ on a Bruker Avance 300 MHz spectrometer. Spectra were all processed using TOPSPIN 3.0.

Gas chromatography was performed on a 7890A from Agilent Technologies with an Agilent J&W Advanced Capillary GC column (30 m, 0.320 mm, and 0.25 μm) equipped with a flame ionization detector (FID) and hydrogen as carrier gas. Injections were performed with an Agilent Technologies 7693 auto sampler.

Size exclusion chromatography (SEC) measurements were performed on an Agilent 1260-series equipped with a 1260 ISO-pump, a 1260 Diode Array Detector (DAD), a 1260 Refractive Index Detector (RID), and a PSS Gram30 column in series with a PSS Gram1000 column inside a 1260 Thermostated Column Compartment (TCC) at 50°C using dimethylacetamide containing 50 mM of LiCl (flow rate of 0.6 mL min⁻¹) as solvent. Molar masses and dispersities were calculated against poly(methyl methacrylate) standards.

MALDI-TOF (Matrix-Assisted Laser Desorption and Ionization Time of Flight) mass spectrometry analysis was performed on an Applied Biosystems Voyager-DE STR instrument equipped with nitrogen laser operating at 337 nm, pulsed ion extraction source and reflectron detector. The laser pulse width is 3 ns with a maximum power of 20 Hz. Spectra were recorded in reflector mode with

an acceleration voltage of 19 kV and delay of 400 ns. 100 single shot acquisitions were summed to give the spectra and the data were analyzed using Data Explorer software. Samples were prepared by dissolving the matrix 2-(4-hydroxyphenylazo) benzoic acid HABA in the solvent (acetone, 20 mg/mL⁻¹), mixing with the polymer (1 mg/mL⁻¹) and sodium iodide in acetone (15 mg/mL⁻¹) that was used as cationizing agent.

Dynamic light scattering (DLS) was performed on a Zetasizer Nano-ZS Malvern apparatus (Malvern Instruments Ltd) using disposable PMMA cuvettes. The excitation light source was a He–Ne laser at 633 nm, and the intensity of the scattered light was measured at 173°. This method measures the rate of the intensity fluctuation and the size of the particles is determined through the Stokes–Einstein equation ($d(H) = \sqrt{kT/3\pi\eta D}$) where $d(H)$ is the mean hydrodynamic diameter, k is the Boltzmann constant, T is the absolute temperature, η is the viscosity of the dispersing medium, and D is the apparent diffusion coefficient. Before starting the measurements, samples were equilibrated at the specific temperature for at least 300 s. The samples were analysed four times, allowing the calculation of the corresponding Z_{ave} and PDI uncertainties. Samples were filtered through Millipore membranes with a pore size of 0.2 μm prior to measurement.

Poly(2-ethyl-2-oxazoline) synthesis optimization

A stock solution of 2-ethyl-2-oxazoline (5.65 mL, 5.55 g, 56 mmol) was prepared in acetonitrile (8.35 mL) in the presence of methyl tosylate (283 μL , 0.347 g, 1.87 mmol), yielding a 4 M monomer concentration and a M/I ratio of 30. A sample of the stock solution was taken for GC analysis to calculate the monomer conversion. Aliquots of 2 mL were taken to different microwave reaction vials (10 mL nominal volume) equipped with a stirring bar, and capped. All the process was performed in a glove-box under a dry nitrogen atmosphere. The vials were heated in a microwave synthesizer at different temperatures and times, calculated via the following equation:

$$t = \frac{\ln[M]_0}{[M]_t} (k_p [I]_0)$$

where, for a monomer conversion of 95%, $\ln[M]_0/[M]_t = 3$. For $[M] / [I] = 30$, $[I]_0 = 4/30 \text{ mol l}^{-1}$. The polymerization rate constants (k_p) at different temperatures were calculated via the Arrhenius equation using the thermodynamical parameters reported by Wiesbrock, Schubert *et al.*^[47]

Upon reaction time completion, a sample was taken under inert atmosphere and dispersed in dichloromethane for GC analysis to calculate monomer conversion. Finally, 108 μL (1 equivalent) of methanolic tetramethylammonium hydroxide (25 wt.%) was injected into the polymerization mixture, that was let stirring overnight at room temperature. The obtained polymers were analyzed without purification by ¹H-NMR spectroscopy, SEC and MALDI-TOF MS.

The synthesis of PEtOx-OH to be used as macroinitiators for the polymerization of carbonates was performed in an analogous manner as described. After end-capping of the living polymer (18 hours r.t.), the solvent was evaporated under reduced pressure and the polymer re-dissolved in dichloromethane. The polymer was then purified by precipitation in cold diethyl ether. This process was repeated 3 times to assure complete removal of unreacted EtOx monomer. Polymer purity and structure were evaluated by ¹H-NMR spectroscopy, SEC and MALDI-TOF MS.

Micelle preparation

Self-assembled nanostructures were prepared by the solvent-switch or phase inversion technique. A 10 mg mL⁻¹ stock solution in acetone of each copolymer was prepared. Subsequently, 200 μL of this solution were injected into a vial containing 2 mL milli-Q water at a 5 $\mu\text{L min}^{-1}$ rate under

gentle stirring. The slow addition was performed with an automatic syringe pump (Harvard Apparatus, keeping the solution at 25 °C. Upon completion of the polymer addition, the vial was opened and temperature was increased to 55 °C for 24h, to assure total removal of the acetone and to promote the formation of thermodynamically stable nanostructures, obtaining a 1 mg mL⁻¹ aqueous solution of copolymer.

To load vesicles with calcein, 2.5 mg of polymer were first dissolved in 200 µL of a 10 mg mL⁻¹ calcein solution. The mixture was then added to milli-Q water following the same protocol as described above.

Calcein-loaded vesicle purification

The vesicles were purified by preparative size exclusion chromatography using a PD10 desalting column (GE Healthcare). Dialysis leakage experiments were performed using 1 mL of calcein-loaded vesicles (1mg mL⁻¹) and free calcein (0.5 mg mL⁻¹) in 50 mL milli-Q water.

3.7. References and notes

- [1] Z. L. Tyrrell, Y. Shen, M. Radosz, *Prog. Polym. Sci.* **2010**, *35*, 1128.
- [2] H. Wei, R.-X. Zhuo, X.-Z. Zhang, *Prog. Polym. Sci.* **2013**, *38*, 503.
- [3] G. S. Kwon, K. Kataoka, *Adv. Drug Delivery Rev.* **1995**, *16*, 295.
- [4] G. S. Kwon, T. Okano, *Adv. Drug Delivery Rev.* **1996**, *21*, 107.
- [5] Y. Kawashima, *Adv. Drug Delivery Rev.* **2001**, *47*, 1.
- [6] O. Onaca, R. Enea, D. W. Hughes, W. Meier, *Macromol. Biosci.* **2009**, *9*, 129.
- [7] Y. Matsumura, K. Kataoka, *Cancer Sci.* **2009**, *100*, 572.
- [8] K. Kataoka, A. Harada, Y. Nagasaki, *Adv. Drug Delivery Rev.* **2012**, *64*, Supplement, 37.
- [9] P. L. Anelli, L. Lattuada, V. Lorusso, M. Schneider, H. Tournier, F. Uggeri, *Magn. Reson. Mater. Phys., Biol. Med.* **2001**, *12*, 114.
- [10] K. S. Kim, W. Park, J. Hu, Y. H. Bae, K. Na, *Biomaterials* **2014**, *35*, 337.
- [11] J. Gong, M. Chen, Y. Zheng, S. Wang, Y. Wang, *J. Control. Release* **2012**, *159*, 312.
- [12] D. W. Pack, A. S. Hoffman, S. Pun, P. S. Stayton, *Nat. Rev. Drug Discov.* **2005**, *4*, 581.
- [13] R. Cheng, F. Feng, F. Meng, C. Deng, J. Feijen, Z. Zhong, *J. Control. Release* **2011**, *152*, 2.
- [14] U. Kedar, P. Phutane, S. Shidhaye, V. Kadam, *Nanomedicine: NBM* **2010**, *6*, 714.
- [15] B. S. Lele, J. C. Leroux, *Macromolecules* **2002**, *35*, 6714.
- [16] F. Xu, S.-Z. Zheng, Y.-L. Luo, *J. Polym. Sci., Part A: Polym. Chem.* **2013**, *51*, 4429.
- [17] K. Miyata, R. J. Christie, K. Kataoka, *React. Funct. Polym.* **2011**, *71*, 227.
- [18] A. Kowalczyk, R. Trzcinska, B. Trzebicka, A. H. E. Müller, A. Dworak, C. B. Tsvetanov, *Prog. Polym. Sci.* **2014**, *39*, 43.
- [19] S. N. S. Alconcel, A. S. Baas, H. D. Maynard, *Polym. Chem.* **2011**, *2*, 1442.
- [20] C. Oerlemans, W. Bult, M. Bos, G. Storm, J. F. Nijsen, W. Hennink, *Pharm. Res.* **2010**, *27*, 2569.
- [21] K. Knop, R. Hoogenboom, D. Fischer, U. S. Schubert, *Angew. Chem. Int. Ed.* **2010**, *49*, 6288.
- [22] M. Barz, R. Luxenhofer, R. Zentel, M. J. Vicent, *Polym. Chem.* **2011**, *2*, 1900.
- [23] Y. Zhao, C. Wang, L. Wang, Q. Yang, W. Tang, Z. She, Y. Deng, *Eur. J. Pharm. Biopharm.* **2012**, *81*, 506.
- [24] T. Tagami, K. Nakamura, T. Shimizu, N. Yamazaki, T. Ishida, H. Kiwada, *J. Control. Release* **2010**, *142*, 160.
- [25] Y. Ma, Q. Yang, L. Wang, X. Zhou, Y. Zhao, Y. Deng, *Eur. J. Pharm. Sci.* **2012**, *45*, 539.
- [26] R. Hoogenboom, *Angew. Chem. Int. Ed.* **2009**, *48*, 7978.
- [27] R. Luxenhofer, Y. Han, A. Schulz, J. Tong, Z. He, A. V. Kabanov, R. Jordan, *Macromol. Rapid Commun.* **2012**, *33*, 1613.

- [28] V. R. de la Rosa, *J. Mater. Sci.: Mater. Med.* **2014**, *25*, 1211.
- [29] T. X. Viegas, M. D. Bentley, J. M. Harris, Z. Fang, K. Yoon, B. Dizman, R. Weimer, A. Mero, G. Pasut, F. M. Veronese, *Bioconjugate Chem.* **2011**, *22*, 976.
- [30] S. Zalipsky, C. B. Hansen, J. M. Oaks, T. M. Allen, *J. Pharm. Sci.* **1996**, *85*, 133.
- [31] R. Konradi, C. Acikgoz, M. Textor, *Macromol. Rapid Commun.* **2012**, *33*, 1663.
- [32] F. C. Gaertner, R. Luxenhofer, B. Blechert, R. Jordan, M. Essler, *J. Control. Release* **2007**, *119*, 291.
- [33] R. Luxenhofer, G. Sahay, A. Schulz, D. Alakhova, T. K. Bronich, R. Jordan, A. V. Kabanov, *J. Control. Release* **2011**, *153*, 73.
- [34] O. Sedlacek, B. D. Monnery, S. K. Filippov, R. Hoogenboom, M. Hruby, *Macromol. Rapid Commun.* **2012**, *33*, 1648.
- [35] R. Luxenhofer, A. Schulz, C. Roques, S. Li, T. K. Bronich, E. V. Batrakova, R. Jordan, A. V. Kabanov, *Biomaterials* **2010**, *31*, 4972.
- [36] M. Hruby, S. K. Filippov, J. Panek, M. Novakova, H. Mackova, J. Kucka, D. Vetvicka, K. Ulbrich, *Macromol. Biosci.* **2010**, *10*, 916.
- [37] C. Kim, S. C. Lee, J. H. Shin, J.-S. Yoon, I. C. Kwon, S. Y. Jeong, *Macromolecules* **2000**, *33*, 7448.
- [38] G.-H. Hsiue, C.-H. Wang, C.-L. Lo, C.-H. Wang, J.-P. Li, J.-L. Yang, *Int. J. Pharm.* **2006**, *317*, 69.
- [39] S. C. Lee, Y. Chang, J.-S. Yoon, C. Kim, I. C. Kwon, Y.-H. Kim, S. Y. Jeong, *Macromolecules* **1999**, *32*, 1847.
- [40] K.-Y. Peng, S.-W. Wang, R.-S. Lee, *J. Polym. Sci., Part A: Polym. Chem.* **2013**, *51*, 2769.
- [41] M. Litt, A. Levy, J. Herz, *J. Macromol. Sci.-Chem.* **1975**, *9*, 703.
- [42] O. Nuyken, G. Maier, A. Groß, H. Fischer, *Macromol. Chem. Phys.* **1996**, *197*, 83.
- [43] R. Hoogenboom, in *Handbook of Ring-Opening Polymerization* (Eds.: D. P., C. O., R. J.-M.), Wiley-VCH Verlag GmbH & Co. KGaA, Weinheim, Germany, **2009**, pp. 141.
- [44] S. Kobayashi, E. Masuda, S. Shoda, Y. Shimano, *Macromolecules* **1989**, *22*, 2878.
- [45] G. H. Hsiue, A. X. Swamikannu, M. H. Litt, *J. Polym. Sci., Part A: Polym. Chem.* **1988**, *26*, 3043.
- [46] E. Altuntaş, C. Weber, K. Kempe, U. S. Schubert, *Eur. Polym. J.* **2013**, *49*, 2172.
- [47] F. Wiesbrock, R. Hoogenboom, M. A. M. Leenen, M. A. R. Meier, U. S. Schubert, *Macromolecules* **2005**, *38*, 5025.
- [48] The polymerization time was calculated with the following equation: $t = (\ln[M]_0/[M]_t) / (kp [I]_0)$ where, for a monomer conversion of 95%, $\ln[M]_0/[M]_t = 3$. For $[M] / [I] = 30$, $[I]_0 = 4/30 \text{ mol l}^{-1}$.
- [49] Conversion was calculated from the difference between the t_0 and t_{final} GC samples, whereby acetonitrile was taken as internal standard.
- [50] F. Suriano, O. Coulembier, J. L. Hedrick, P. Dubois, *Polym. Chem.* **2011**, *2*, 528.
- [51] C. Bartolini, L. Mespouille, I. Verbruggen, R. Willem, P. Dubois, *Soft Matter* **2011**, *7*, 9628.
- [52] A. L. Z. Lee, V. W. L. Ng, S. Gao, J. L. Hedrick, Y. Y. Yang, *Adv. Funct. Mater.* **2014**, *24*, 1538.
- [53] J. Xu, T. M. Fillion, F. Prifti, J. Song, *Chemistry – An Asian Journal* **2011**, *6*, 2730.
- [54] K. Kita-Tokarczyk, J. Grumelard, T. Haeefele, W. Meier, *Polymer* **2005**, *46*, 3540.
- [55] C. LoPresti, H. Lomas, M. Massignani, T. Smart, G. Battaglia, *J. Mater. Chem.* **2009**, *19*, 3576.
- [56] L. Zhang, A. Eisenberg, *Science* **1995**, *268*, 1728.
- [57] L. Luo, A. Eisenberg, *Langmuir* **2001**, *17*, 6804.
- [58] J. N. Israelachvili, D. J. Mitchell, B. W. Ninham, *J. Chem. Soc., Faraday Trans. 2* **1976**, *72*, 1525.
- [59] C. Tanford, *The Hydrophobic Effect: Formation of Micelles and Biological Membranes*, 2nd Edition ed., John Wiley & Sons, Somerset. NJ., **1980**.
- [60] R. Nagarajan, *Langmuir* **2001**, *18*, 31.
- [61] P. Lim Soo, A. Eisenberg, *J. Polym. Sci., Part B: Polym. Phys.* **2004**, *42*, 923.
- [62] J. Du, R. K. O'Reilly, *Soft Matter* **2009**, *5*, 3544.
- [63] M. Danquah, T. Fujiwara, R. I. Mahato, *J. Polym. Sci., Part A: Polym. Chem.* **2013**, *51*, 347.
- [64] R. Xu, M. A. Winnik, F. R. Hallett, G. Riess, M. D. Croucher, *Macromolecules* **1991**, *24*, 87.

- [65] A. Harada, K. Kataoka, *Macromolecules* **1995**, *28*, 5294.
- [66] C. Allen, Y. Yu, D. Maysinger, A. Eisenberg, *Bioconjugate Chem.* **1998**, *9*, 564.
- [67] S. Jain, F. S. Bates, *Science* **2003**, *300*, 460.
- [68] L. T. T. Trinh, H. M. L. Lambermont-Thijs, U. S. Schubert, R. Hoogenboom, A.-L. Kjøniksen, *Macromolecules* **2012**, *45*, 4337.
- [69] M. Danquah, T. Fujiwara, R. I. Mahato, *Biomaterials* **2010**, *31*, 2358.
- [70] M. Nallani, M. Andreasson-Ochsner, C.-W. Tan, E.-K. Sinner, Y. Wisantoso, S. Geifman-Shochat, W. Hunziker, *Biointerphases* **2011**, *6*, 153.

Chapter 4

Colorimetric logic gates based on novel poly(2-alkyl-2-oxazoline) coated gold nanoparticles

A new end-capping strategy is devised to synthesize xanthate-functional poly(2-alkyl-2-oxazoline)s (PAOx) that enable gold nanoparticle functionalization by a direct “grafting to” approach with citrate-stabilized gold nanoparticles (AuNPs). Presumably due to the presence of remaining citrate groups, the obtained PAOx@AuNPs exhibit dual stabilization by repulsive electrostatic and steric interactions giving access to water soluble molecular AND logic gates wherein environmental temperature and ionic strength constitute the input signals, and the solution color the output signal. The temperature input value could be tuned by variation of the PAOx polymer composition, from 22 °C for poly(2-*n*-propyl-2-oxazoline)@AuNPs to 85 °C for poly(2-ethyl-2-oxazoline)@AuNPs. Besides advancing the fascinating field of molecular logic gates, the present research offers a facile strategy for the synthesis of PAOx@AuNPs of interest in fields spanning nanotechnology and biomedical sciences. In addition, the reported functionalization of PAOx with a xanthate end-group offers straightforward access to thiol-functional PAOx of high interest in polymer science.

4.1 Introduction

Gold nanoparticles (AuNPs) constitute a rapidly growing research area, which has led to applications spanning across nanotechnology,^[1] biotechnology,^[2, 3] catalysis and sensing,^[4] due to their distinctive properties with respect to those of the bulk metal solid. AuNPs exhibit a strong localized surface plasmon resonance (SPR) due to the collective coherent oscillation of conduction band electrons across the nanoparticle upon interaction with light at a specific resonant wavelength. The shape and frequency of the SPR band depends on the size and shape of the particle, as well as on the dielectric properties of the medium surrounding the nanoparticle. The shifts in the SPR band, or the corresponding color variation associated to a change in the microenvironment have been exploited as an analytical output signal to develop ultrasensitive bioanalyte detection and diagnostics.^[5-7] As a result, AuNPs represent an ideal platform to translate molecular events into logic systems with a large impact on the color properties of the solution, therefore allowing to replicate Boolean logic gates on a molecular scale. These colorimetric systems are particularly attractive for point-of-use detection and diagnostics applications, and to construct memory elements of sequential logic operations with the ability to store information.^[7-9]

Chemical tuning of the AuNP surface is necessary to impart stability, water-solubility, biological compatibility and specificity to the nanoparticles. Stabilization of AuNPs with polymers has been widely investigated to confer the polymer properties to the final polymer@AuNP constructs.^[10, 11] In this context, antifouling AuNPs have been produced by functionalization with polyethylene glycol (PEG) for the development of drug/gene delivery vectors and as contrast agents,^[2, 12] although some concerns about their applicability *in vivo* are arising.^[13, 14] Similarly, stimuli-responsive AuNPs

have been produced through functionalization with thermoresponsive polymers such as PNIPAm^[15, 16] or poly(oligoethylene glycol) methacrylates.^[17] These temperature responsive systems are of high interest in colorimetry due to the high sensitivity derived from the large absorption extinction coefficient of AuNPs that usually stands *ca.* 3 orders of magnitude beyond that of organic dyes. Poly(2-alkyl-2-oxazoline)s (PAOx) have been proposed as suitable alternatives to PEG and, moreover, their thermo-responsiveness can be easily tuned by variation of the alkyl substituent in the 2-oxazoline monomer.^[18-21] However, despite the potential of PAOx for the preparation of stimuli-responsive nanoparticles, the research on PAOx-coated AuNPs has remained on hold after the pioneering work of Jordan *et al.*,^[22] who developed a grafting-from methodology. In the present work, a new facile strategy is developed for the synthesis of PAOx@AuNPs *via* a grafting-to approach. As recently found for PNIPAm@AuNPs,^[23] these PAOx@AuNPs exhibit dual stabilization by both repulsive electrostatic and steric interactions (see Figure 4.1.1).^[24] The PAOx@AuNPs remained insensitive to temperature changes in the absence of an electrolyte to screen the nanoparticle's negative charges, whereas aggregation was observed in the presence of an electrolyte only beyond the PAOx transition temperature. This dual stabilization mechanism is exploited in this contribution for the utilization of the PAOx@AuNPs as supramolecular "AND" Boolean logic gates, by controlling temperature and electrolyte concentration as logic inputs and the color of the solution as output. In addition, variation of the alkyl-substituent of the polymer enabled control over the temperature input value, further advancing on the promising field of AuNP-based logic gates.^[8, 25]

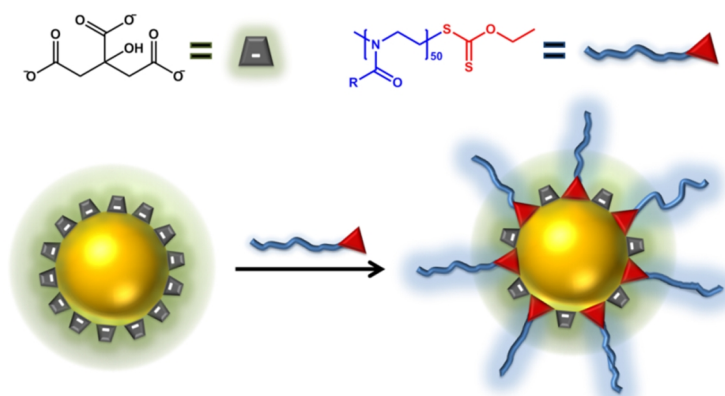


Figure 4.1.1. Schematic representation for the ligand exchange of citrate-stabilized AuNPs with xanthate-functional poly(2-alkyl-2-oxazoline)s. The resulting poly(2-alkyl-2-oxazoline)-grafted gold nanoparticles exhibit dual stabilization by repulsive electrostatic and steric interactions.

4.2 Synthesis and characterization of xanthate-functionalized poly(2-alkyl-2-oxazoline)s

Poly(2-alkyl-2-oxazoline)s (PAOx) are readily obtained via the living cationic ring-opening polymerization (CROP) of 2-alkyl-2-oxazolines. Telechelic functional polymers are accessible by selection of the initiator and terminating agent (a nucleophile) in a one pot fashion.^[26] Unlike other biocompatible polymers such as poly(ethyleneglycol) PEG, or temperature-responsive polymers such as PNIPAm, PAOx permit the variation of the polymer side chain hydrophobicity by gradually tuning the length of the alkyl chain in the 2-alkyl-2-oxazoline monomer (*e.g.* methyl, ethyl, propyl). Thereby, structure-property relationships can be evaluated by systematic variation of one single parameter (polymer side-chain hydrophobicity)^[27] thus turning PAOx into an ideal polymer platform for the stabilization of AuNPs and the tuning of the nanoparticle stimuli-responsiveness.

The hereby developed method for the preparation of PAOx-AuNP constructs is based on xanthate-terminated PAOx that are subsequently used to functionalize citrate-stabilized AuNPs through ligand exchange. Xanthate groups inherently adsorb to gold in a similar fashion as trithiocarbonates, which have been applied for the direct functionalization of AuNPs with polymers synthesized *via* RAFT polymerization.^[28-30] Furthermore, xanthates can be easily transformed into thiols by aminolysis, making them interesting for further polymer modification and coupling. The preparation of xanthate functionalized PAOx was envisioned by direct end-capping of the living polymer chains with the commercially available potassium ethyl xanthogenate as terminating nucleophile (see Figure 4.2.1, top).

To study the influence of the polymer hydrophilicity on the thermo-responsiveness of the resulting PAOx@AuNPs, poly(2-methyl-2-oxazoline) (PMeOx), poly(2-ethyl-2-oxazoline) (PEtOx) and poly(2-*n*-propyl-2-oxazoline) (P^{*n*}PrOx) with a length of 50 repeating units were synthesized and end-capped with potassium ethyl xanthogenate, resulting in well-defined xanthate-functionalized polymers (Figure 4.2.2). The presence of the xanthate groups at the polymer terminus was confirmed by ¹H-NMR spectroscopy and MALDI-TOF mass spectrometry, both showing quantitative functionalization (see Figure 4.2.1).

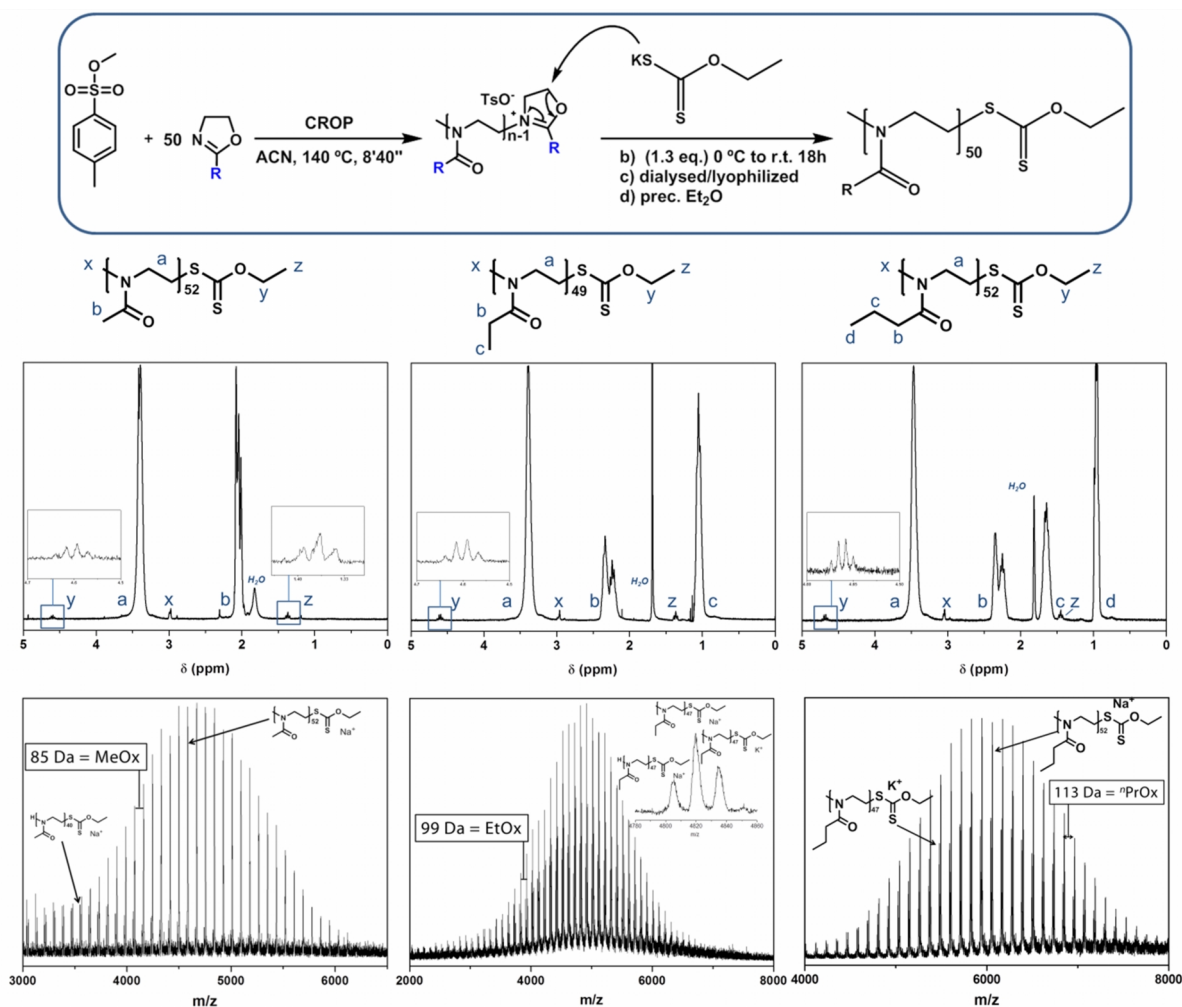


Figure 4.2.1. Top: Synthesis of xanthate-functionalized poly(2-alkyl-2-oxazoline)s. *R* = CH₃- (MeOx), CH₃CH₂- (EtOx), or CH₃CH₂CH₂- (^{*n*}PrOx). Bottom: ¹H-NMR spectra of PAOx₅₀-xanthate polymers in CDCl₃ (300 MHz) and corresponding MALDI-TOF mass spectrum confirming the intended polymer structure. Major distribution: Na⁺ adduct. Secondary distribution: K⁺ adduct.

While PMeOx exhibits a hydrophilicity somewhat larger than that of PEG and is not thermoresponsive,^[31] PEtOx and PⁿPrOx exhibit a lower critical solution temperature (LCST) behavior due to their negative entropy of solvation. Turbidimetry studies were performed on 5 mg mL⁻¹ polymer solutions in deionized water to quantify the phase transition temperature or cloud point temperature (T_{CP}) of the three synthesized PAOx-xanthate (see Figure 4.2.2). As expected, PMeOx₅₀-xanthate did not exhibit temperature responsiveness, whereas PEtOx₅₀-xanthate showed a cloud point of *ca.* 90 °C. PⁿPrOx₅₀-xanthate, the polymer with the largest hydrophobicity, exhibited a $T_{CP} = 20$ °C, below the reported T_{CP} of 25 °C, ascribed to the presence of the xanthate hydrophobic end-group. The turbidimetry measurements were also performed in the presence of 50 mM NaCl_{aq}, yielding comparable results due to the low concentration of NaCl used.^[32] Nevertheless, we will later observe a clear-cut impact of 50 mM NaCl_{aq} on the temperature responsiveness of PAOx-coated AuNPs (*vide infra*).

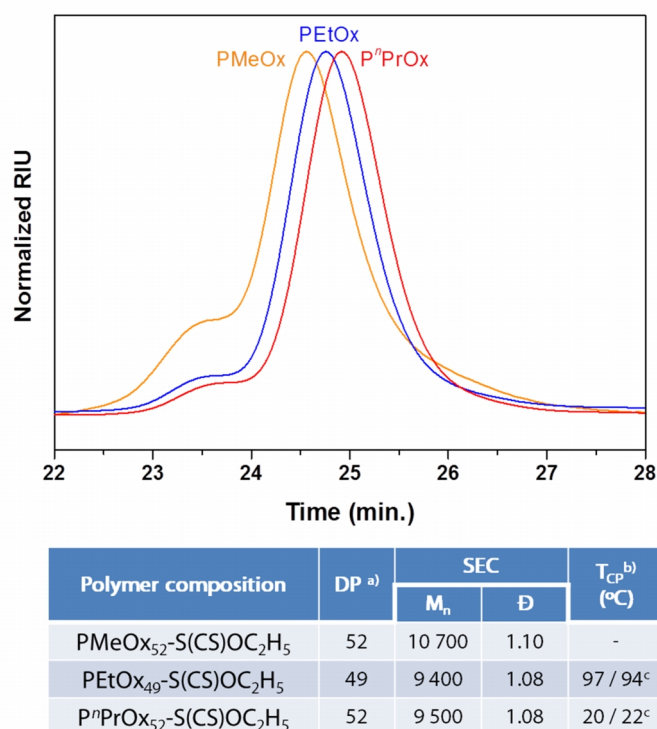


Figure 4.2.2. Composition and size exclusion chromatography (SEC) data of the synthesized PAOx-xanthate polymers. The elution time is related to the polymer hydrophilicity (PMeOx > PETOx > PⁿPrOx), as the hydrodynamic volume of the polymer increases with its hydrophilicity. However a high molecular weight shoulder is observed in all SEC traces, ascribed to chain coupling, well-defined polymers were obtained with dispersity values below 1.10. SEC eluent: *N,N*-dimethylacetamide, calibrated against PMMA standards. ^{a)}Degree of polymerization, calculated based on MALDI-TOF mass spectrometry. ^{b)} Measured by turbidimetry in milli-Q water or in a ^{c)} 50 mM NaCl_{aq} solution.

4.3 Synthesis and characterization of poly(2-alkyl-2-oxazoline) coated AuNPs

AuNPs were synthesized based on the aqueous method of Turkevitch and Frens, wherein citrate was used as both a reducing agent for HAuCl₄ and a stabilizer for the generated AuNPs, yielding citrate-stabilized AuNPs. Upon reflux in aqueous medium, a deep-purple solution was obtained, containing citrate@AuNPs with an estimated mean diameter of 25 nm as measured by TEM. Citrate ligands, weakly bound to the nanoparticle, were subsequently displaced by addition of the xanthate-functional PAOx in aqueous medium, followed by three centrifugation-redispersion

steps to remove all unbound PAOx. In analogy to dithioesters and trithiocarbonates, xanthate group coordination to gold surfaces leads to the formation of stable monolayers, thereby not requiring the previous aminolysis of the xanthate group.^[17, 23, 28, 33-36] TEM measurements undoubtedly showed the presence of the PAOx coating on the surface of the AuNPs after the exchange (see Figure 4.3.1).

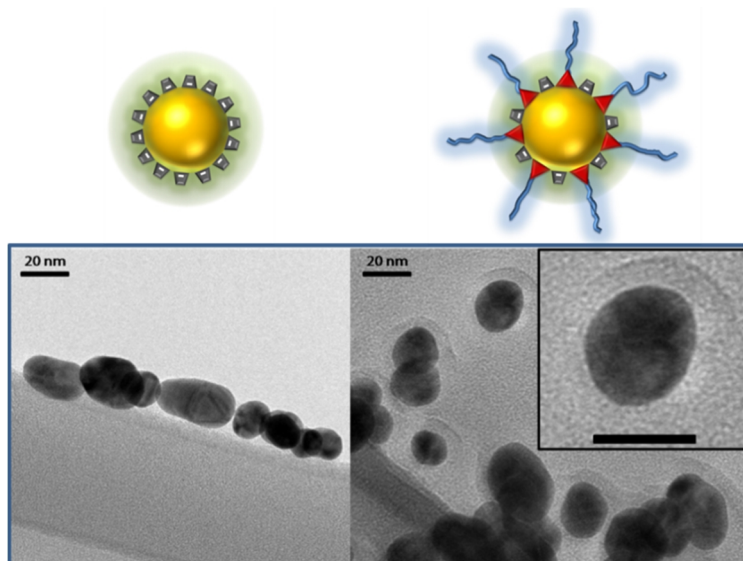


Figure 4.3.1. Transmission electron microscopy (TEM) pictures of citrate-stabilized AuNPs (left) and PETox-coated AuNPs (right). The inset displays one of the nanoparticles where the PETox corona is clearly visible (scale bar = 20 nm).

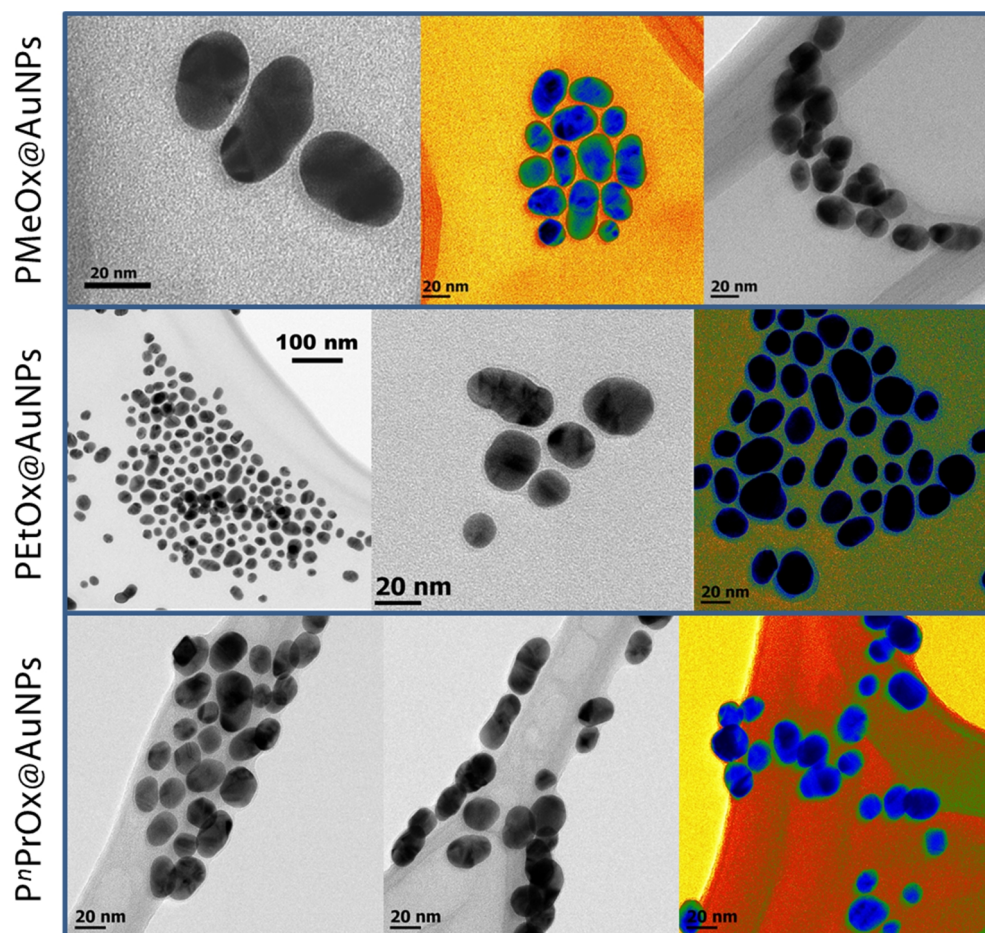


Figure 4.3.2. Bright field transmission electron microscopy (TEM) pictures of PAOx-coated AuNPs. Some of the pictures have been colored to highlight the polymer corona around the gold nanoparticle.

Depending on the composition of the PAOx polymer, the observed thickness of the PAOx corona ranged from 6 to 1.5 nm as measured by TEM, being the smallest for PⁿPrOx-coated AuNPs,

indicating a lower surface coverage of the polymer. This polymer has a larger footprint due to the n -propyl side chains, thus resulting in lower coverage of the nanoparticle. In addition, their less hydrated structure in aqueous solution during displacement of citrate leads to a less dense packing (see Figure 4.3.2).

The AuNPs were subsequently evaluated by dynamic light scattering (DLS), observing an increase in particle average diameter from 40 nm for citrate@AuNPs to 70 nm for PEtOx@AuNPs (see Figure 4.3.3). The observed increase in particle diameter is slightly smaller than the length of a fully stretched PAOx₅₀ chain, of *ca.* 18 nm. PMeOx-coated AuNPs showed a 4 nm larger mean size, possibly due to the high hydrophilicity of PMeOx that results in better-hydrated, more stretched PMeOx chains. In contrast, the more hydrophobic PⁿPrOx-coated AuNPs exhibited a lower average diameter of 57 nm, as a consequence of chain-chain hydrophobic interactions that result in a more compact packing of the polymer brush. An additional distribution was observed in all DLS measurements, with a size below 10 nm, which was demonstrated to be an artifact due to rotational diffusion of the nanoparticles.

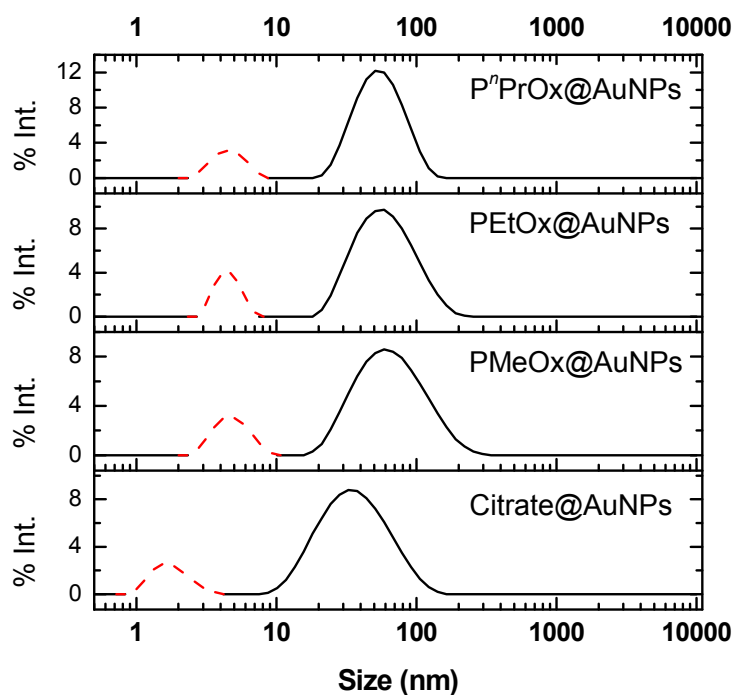


Figure 4.3.3. Dynamic light scattering data for the citrate@AuNPs and the PAOx@AuNPs. A clear shift in particle size is observed for all the PAOx-coated AuNPs compared to citrate@AuNPs, with a size following the order of oxazoline hydrophilicity: PMeOx > PEtOx > PⁿPrOx. The minor distribution observed below 10 nm was proven to be an artifact due to rotational diffusion of the AuNPs. Conditions: AuNPs concentration = 0.09 mg mL⁻¹ in deionized (milli-Q) water. Temperature = 25 °C. Angle = 173 ° (backscattering mode).

Although rotational diffusion is usually not observed in DLS measurements, it can manifest itself when measuring non-spherical or birefringent gold particles, as has been previously reported.^[37] Let us first analyze the theoretical basis behind particle size determination by DLS to better understand the rationale of our demonstration.

DLS measurements determine the size of a particle, *i.e.* its hydrodynamic volume H , from the translational diffusion coefficient (D) by using the Stokes-Einstein equation.^[38]

$$d(H) = \frac{kT}{3\mu\eta D} \quad \text{Equation 4.3.1}$$

Where k is the Boltzmann constant, T the absolute temperature, and η the solution viscosity.

The diameter obtained by this technique is the diameter of a sphere that has the same translational diffusion coefficient as the particle. To calculate the translational diffusion coefficient, DLS determines the speed at which the sample diffuses in solution due to Brownian motion.

To this end, the sample is irradiated with a light beam (in the present case, with $\lambda = 633$ nm) and the intensity of the scattered light is measured over short time intervals. The intensity measured at a particular time t is compared with the intensity of the scattered light at time $t+\delta$ (where the lag time δ is usually nanoseconds or microseconds) resulting in a correlation coefficient. Perfect correlation between the two signals is indicated by unity (1.0) whereas no correlation is indicated by zero (0.0). Indeed, a random process such as Brownian motion can be correlated if sufficiently short time-scales apply. As such, the correlation will be perfect after a short time interval, and will decay with increasing times, reaching zero after a sufficiently long time. A correlogram is then built representing the correlation function versus the time delay τ . The obtained exponential decay can be fitted to a correlation function G . For monodisperse particles in Brownian motion, as in the present case, the correlation function G follows an exponential decay in function of the correlator time delay τ .

$$G(\tau) = A[1 + B e^{-2\Gamma\tau}] \quad \text{Equation 4.3.2}$$

A and B are respectively the baseline and intercept of the correlation function, and the decay rate or relaxation time Γ is given by:

$$\Gamma = Dq^2 \quad \text{Equation 4.3.3}$$

Here we can already see the translational diffusion D that is required to obtain the hydrodynamic volume of the particle. q is the scattering vector, defined as:

$$q = \frac{4\pi n}{\lambda_0} \sin(\theta/2) \quad \text{Equation 4.3.4}$$

Where n is the refractive index of the dispersant (in this case water), λ_0 the wavelength of the laser (633 nm), and θ the scattering angle.

As can be seen, for translational diffusion, the relaxation time Γ is dependent on the scattering angle θ . Therefore, a measured signal that originates from particle translational diffusion will shift when measured at different angles. On the other hand, the relaxation time of rotational diffusion is not angular dependent, *i.e.* a signal originating from rotational diffusion will remain unaffected upon changes in the measurement angle.^[37, 39]

To ascertain whether the second observed distribution observed originates from a real distribution of particles, or had its origin on the rotational diffusion of the AuNPs, DLS measurements were performed at two different scattering angles (90° and 173°). The obtained intensity is represented against the relaxation time in Figure 4.3.4 and, as expected, the main signal corresponding to translational diffusion of the AuNPs displaced upon changing the measurement angle. In contrast, the second small size distribution remained unvaried, confirming its origin in rotational diffusion. Once proven that this size distribution was an artefact, it was excluded for determination of the nanoparticles mean size.

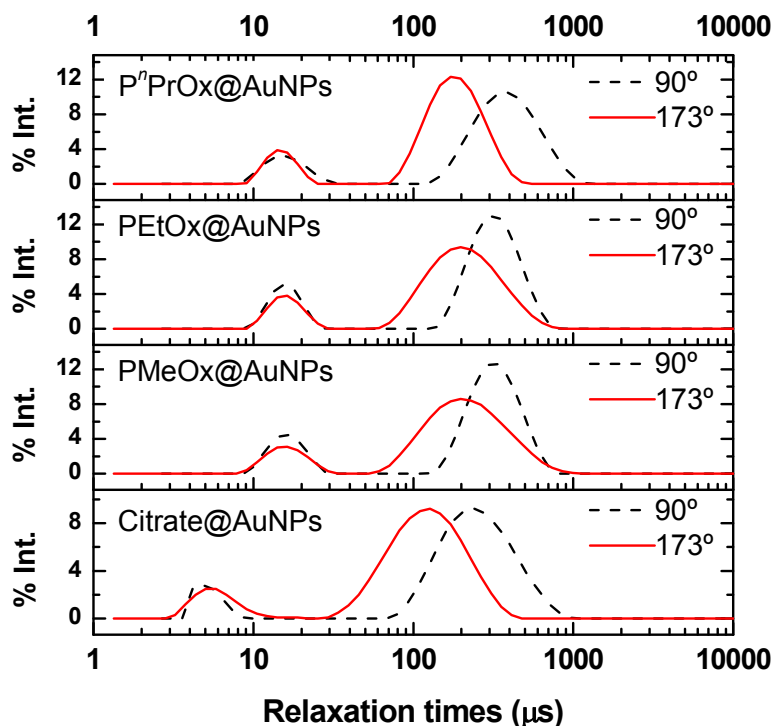


Figure 4.3.4. *Relaxation time versus intensity plot for citrate@AuNPs, measured at 90 and 173 degree scattering angles. The main peak shows angular dependence, as it is related to the translational diffusion. On the other hand, the small peak does not depend on the scattering angle, thus revealing that it is originating from rotational diffusion of the large particles.*

Next, the PAOx grafting on the AuNPs was investigated by UV-Vis spectroscopy. The citrate-stabilized AuNPs showed a broad absorption with a maximum at 524 nm, corresponding to the surface plasmon resonance (SPR). SPR of noble metal nanoparticles is a consequence of the polarized oscillations of the electron cloud, induced by the oscillating electric field of the incident electromagnetic wave, according to Mie's theory. This phenomenon is highly sensitive to the dielectric constant of the microenvironment around the nanoparticle and therefore AuNP coverage by a polymer corona can be manifested as alterations in the SPR band.^[40]

Upon grafting with PAOx, the SPR band of the AuNPs is slightly broadened and red shifted, indicating the change in the dielectric constant of the microenvironment around the gold nanocore, as seen in Figure 4.3.5. This reflects the variation in chemical composition at the gold-water interface, and explains the observed trend in SPR band displacement, that follows the hydrophobicity order of the PAOx: PⁿPrOx- > PEtOx- > PMeOx-grafted AuNPs. An estimation of the PAOx grafting density was made through calculation of the AuNPs molecular weight via UV-Vis spectroscopy,^[41, 42] resulting in 2 to 4 chains/nm², in line with previous reports on adsorption of RAFT polymers to Au surfaces^[36] (see Experimental Section). Aqueous solutions of the PAOx-coated AuNPs remained stable when kept at room temperature without showing any color change or macroscopic precipitation when kept for several days at room temperature.

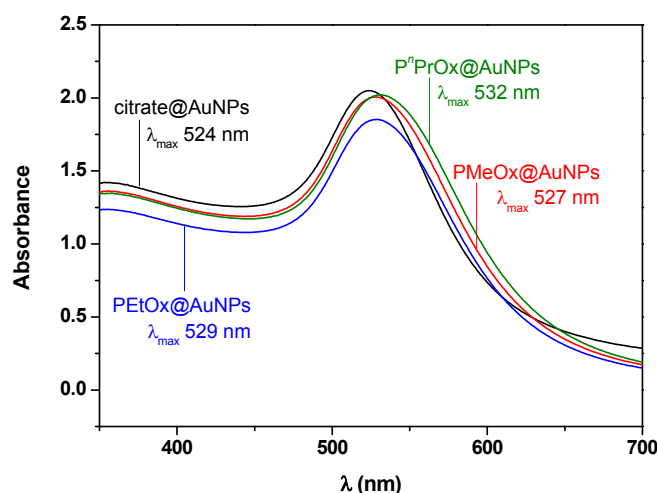


Figure 4.3.5. UV-Vis spectra of the synthesized AuNPs. Upon PAOx grafting onto the AuNPs, the spectra appear broadened and slightly red shifted, following the order of polymer hydrophobicity: $\lambda_{\max}(\text{citrate@AuNPs}) < \lambda_{\max}(\text{PMeOx@AuNPs}) < \lambda_{\max}(\text{PEtOx@AuNPs}) < \lambda_{\max}(\text{P}^n\text{PrOx@AuNPs})$. Concentration: 0.1 mg mL^{-1} . Temperature = $25 \text{ }^\circ\text{C}$.

4.4 Evaluation of the temperature responsiveness of poly(2-alkyl-2-oxazoline) coated AuNPs

The thermoresponsive behavior of the PAOx-coated AuNPs was assessed by variable-temperature UV-Vis spectroscopy. Interestingly, unlike the individual PAOx-xanthate polymers, PAOx-grafted AuNP solutions in demineralized water were found to be insensitive to temperature variations, even at temperatures far above the T_{CP} of the independent PAOx. As seen in Figure 4.4.1 a-c, no change in the SPR band maximum wavelength can be observed upon heating any of the PAOx@AuNPs solutions. The slight decrease in signal intensity observed with increasing temperatures, of about 0.10 a.u., can be ascribed to solvent thermal expansion that results in a slightly lower concentration of nanoparticles. In contrast to the high stability shown by PAOx@AuNPs, citrate-stabilized AuNPs subjected to the same heating ramp exhibited a decrease in signal intensity larger than 0.7 a.u., due to partial macroscopic precipitation of the AuNPs (see Figure 4.4.2).

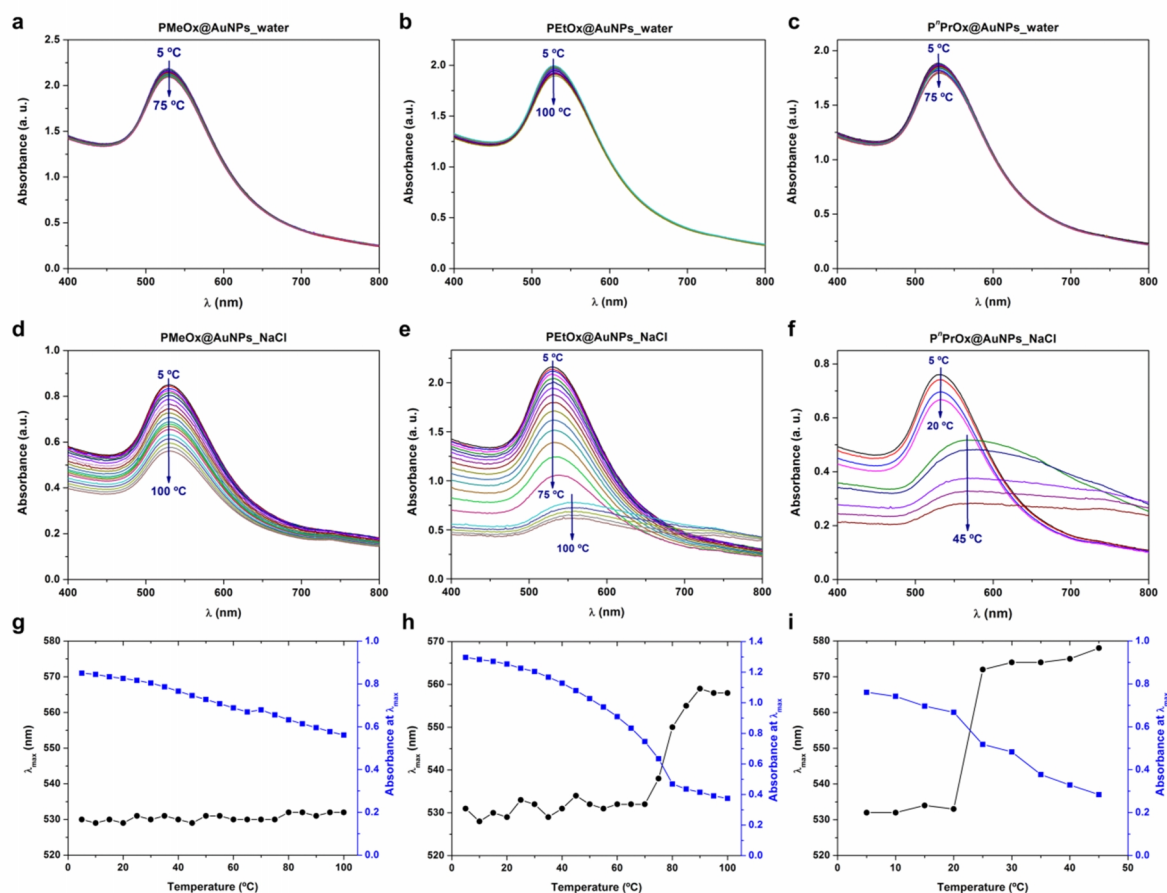


Figure 4.4.1. UV-Vis spectra of the synthesized PAOx@AuNPs. a-c) UV-Vis spectra upon heating the PAOx@AuNPs solutions in demineralized water (milli-Q), wherein no SPR band shift is observed. d-f) UV-Vis spectra upon heating the PAOx@AuNPs solutions in the presence of 50 mM NaCl_{aq}; PMeOx@AuNPs show a decrease in absorption intensity partially due to macroscopic particle precipitation, however no SPR band shift is observed, indicating no nanoparticle aggregation. PEtOx- and PⁿPrOx-coated AuNPs exhibit a temperature-triggered nanoparticle aggregation, causing a shift in the SPR band of 33 nm for PEtOx@AuNPs and of 37 nm for PⁿPrOx@AuNPs at 75–80 °C and 20–25 °C, respectively. g-i) Evolution of the SPR band maximum wavelength (λ_{max}) and the associated absorbance with increasing temperatures. The temperature-triggered shift of λ_{max} is especially sharp for PⁿPrOx@AuNPs, coinciding with the T_{CP} of the free PⁿPrOx₅₀-xanthate polymer at 22 °C.

It was speculated that the absence of a temperature-induced aggregation of the thermoresponsive PAOx@AuNPs was caused by electrostatic stabilization of the nanoparticles due to the remaining presence of citrate units on the surface of the AuNPs, as it was recently reported for PNIPAm-stabilized AuNPs.^[23] Therefore, the variable-temperature UV-Vis spectroscopy experiments were reproduced in a 50 mM NaCl_{aq} solution to screen the citrate negative charges and suppress nanoparticle stabilization due to repulsive Coulombic interactions (Figure 4.4.1. d-i). PMeOx@AuNPs showed no SPR band shift upon heating, as expected from the lack of thermoresponsiveness of PMeOx. A progressive decrease of absorption intensity was nevertheless observed for PMeOx@AuNPs, due to solvent thermal expansion and a minor AuNPs macroscopic precipitation, although no appreciable difference by eye was found between the solution before and after heating.

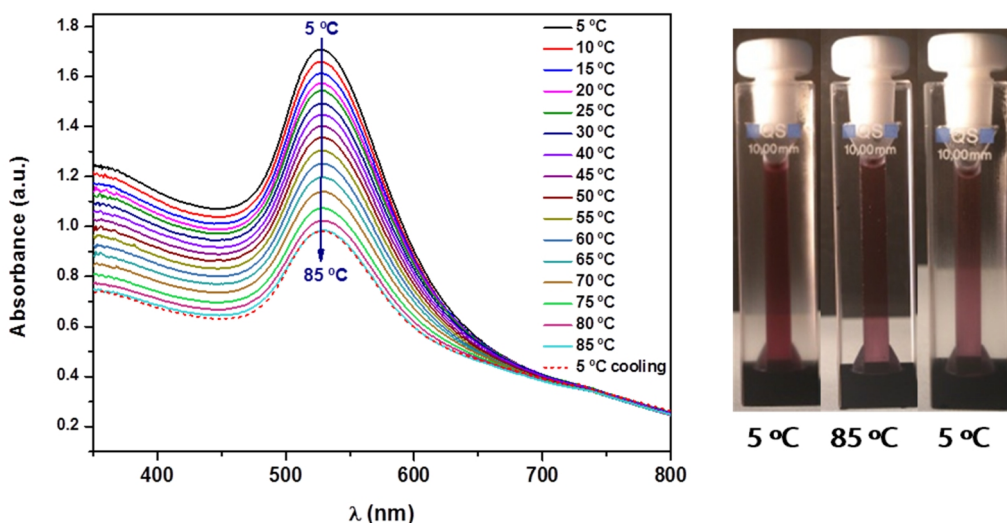


Figure 4.4.2. UV-Vis spectra upon heating a citrate@AuNPs solution in demineralized water (milli-Q). No SPR band shift is observed, although a decrease of 0.7 a.u. indicates the loss of AuNPs as a macroscopic precipitate. The pictures show the solution at 5 °C, 85 °C and cooled back to 5 °C, where the irreversibility of the precipitation is observed. $\lambda_{max} = 528$ nm. Concentration = 0.1 mg mL⁻¹. Heating rate: 1 K min⁻¹.

In contrast to PMeOx@AuNPs, PEtOx- and PⁿPrOx-coated AuNPs did exhibit a temperature-triggered aggregation, as indicated by the sharp red shift in the SPR band produced by interparticle surface plasmon coupling^[43] at temperatures close to the T_{CP} of the individual PAOx. The transition temperature of PEtOx@AuNPs is lowered by about 15 °C, which is ascribed to the increased local concentration of the polymer in combination with the high concentration dependence of the T_{CP} of PEtOx.^[44] In the presence of a strong electrolyte such as NaCl, the electrostatic stabilization is suppressed and the nanoparticles were solely stabilized by the steric hindrance exerted by the PAOx brush and thus their aggregation became governed by the LCST transition of the grafted PAOx.

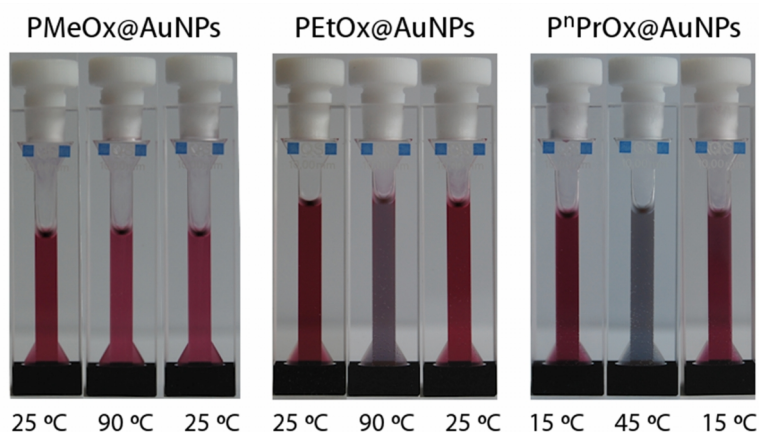


Figure 4.4.3. Photographs of PAOx-grafted AuNPs solutions in the presence of 50 mM NaCl_{aq} at temperatures below the corresponding polymer phase-transition temperatures, above, and back to the initial temperature. A clear color change is observed for the thermoresponsive PEtOx@AuNPs and PⁿPrOx@AuNPs, whereas the solution containing PMeOx@AuNPs remains unchanged. The samples were kept at high temperature for 5 minutes. Concentration: 0.1 mg mL⁻¹.

The temperature-induced aggregation of the PAOx@AuNPs and the subsequent shift in the SPR band resulted in a color change from violet to blue clearly visible by eye. As seen in Figure 4.4.3, the PAOx@AuNPs recovered their original appearance when brought back to a temperature below the polymer T_{CP} , thus demonstrating the reversibility of the transition.

The dual stabilization of the PAOx@AuNPs by both steric stabilization resulting from the PAOx brush and repulsive Coulombic interactions due to remaining citrate units was assessed by zeta potential measurements. As seen in Table 4.4.1, citrate@AuNPs showed a zeta potential of *ca.* -40 mV, while PAOx@AuNPs $\zeta_{pot.}$ values were in the range of -25 mV, indicating the presence of sufficient remaining citrate groups on the nanoparticle surface to render effective stabilization via repulsive electrostatic interactions. Upon PAOx@AuNPs dispersion in a 50 mM NaCl_{aq} solution, the citrate negative charges became screened by the Na⁺ ions of the electrolyte, and the zeta potential values dropped to *ca.* -5 mV, which is insufficient for electrostatic stabilization. While citrate@AuNPs immediately aggregated in 50 mM NaCl_{aq} resulting in macroscopic precipitation, PAOx@AuNPs remained stable and, in the case of PEtOx- and PⁿPrOx-grafted AuNPs, became susceptible to changes in the environmental temperature.

Table 4.4.1. Characterization of PAOx-functionalized gold nanoparticles ^{a)} Mean particle size, calculated by dynamic light scattering (0.1 mg mL⁻¹ in water); ^{b)} Zeta potential measurements performed on 0.1 mg mL⁻¹ AuNPs solutions in milli-Q water or in 50 mM NaCl aqueous solution; ^{c)} Transition temperature (AuNP aggregation) measured by temperature-dependent UV-Vis spectroscopy in 50 mM NaCl aqueous solution. The AuNP transition temperature can be selected by tuning PAOx composition. ^{d)} λ_{max} calculated by UV-Vis spectroscopy (0.1 mg mL⁻¹ in 50 mM NaCl_{aq}) below the T_{CP} and above (e).

AuNP	Size ^{a)} (nm)	Zeta potential		T_{CP} ^{b)} (°C)	λ_{max} ^{d)} (nm)
		$\zeta_{pot.}$ (water) ^{b)} (mV)	$\zeta_{pot.}$ (water) ^{b)} (mV)		
Citrate@AuNP	40.2 ± 20.6	-42.3	-	-	524
PMeOx@AuNP	73.4 ± 34.2	-26.5	-5.7	-	527
PEtOx@AuNP	69.7 ± 35.7	-25.2	-8.6	80 ^{d)}	529 – 562 ^{e)}
P ⁿ PrOx@AuNP	57.3 ± 21.2	-23.9	-4.6	22 ^{d)}	532 – 569 ^{e)}

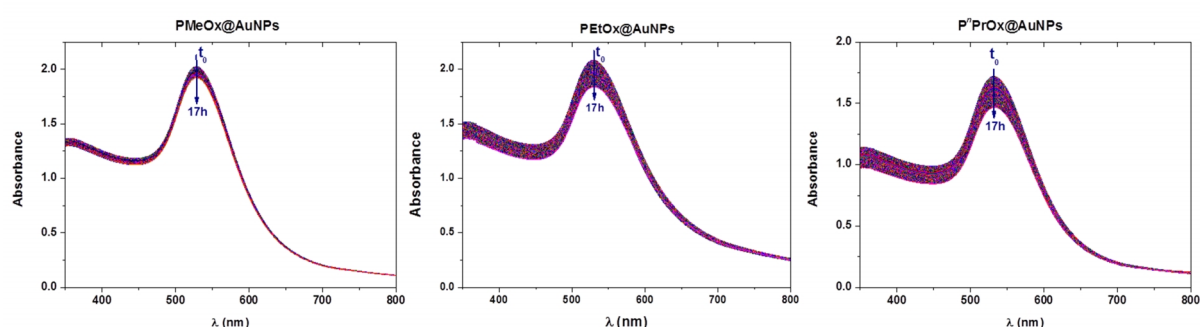


Figure 4.4.4. UV-Vis spectra at isothermal conditions of PAOx@AuNPs solutions (0.1 mg mL⁻¹) monitored during 17 hours. The solutions were maintained at 25 °C for PMeOx- and PEtOx-coated AuNPs and at 15 °C (below the T_{CP}) for PⁿPrOx@AuNPs. A small decrease in absorbance is observed due to nanoparticle macroscopic precipitation. λ_{max} (PMeOx) = 527 nm, λ_{max} (PEtOx) = 529 nm, λ_{max} (PⁿPrOx) = 532 nm.

The stability of the PAOx-stabilized AuNPs in the presence of NaCl was assessed by monitoring the evolution of the PAOx UV-Vis spectrum isothermally below their transition temperature. A progressive decrease in overall intensity was observed as a consequence of nanoparticle

precipitation. This decay was nevertheless very slow, constituting a maximum of 10 % decrease in nanoparticle concentration after 17 hours (see Figure 4.4.4) and, importantly, did not lead to a shift in the SPR band and in the associated solution color. P_{MeOx}@AuNPs exhibited the highest stability, due to the high hydrophilicity of P_{MeOx}.

4.5 Colimetric logic gates based on poly(2-alkyl-2-oxazoline) coated AuNPs

The dual stabilization of PAOx@AuNPs by steric and electrostatic interactions was further exploited to use temperature and solution ionic strength as inputs for a molecular logic gate.

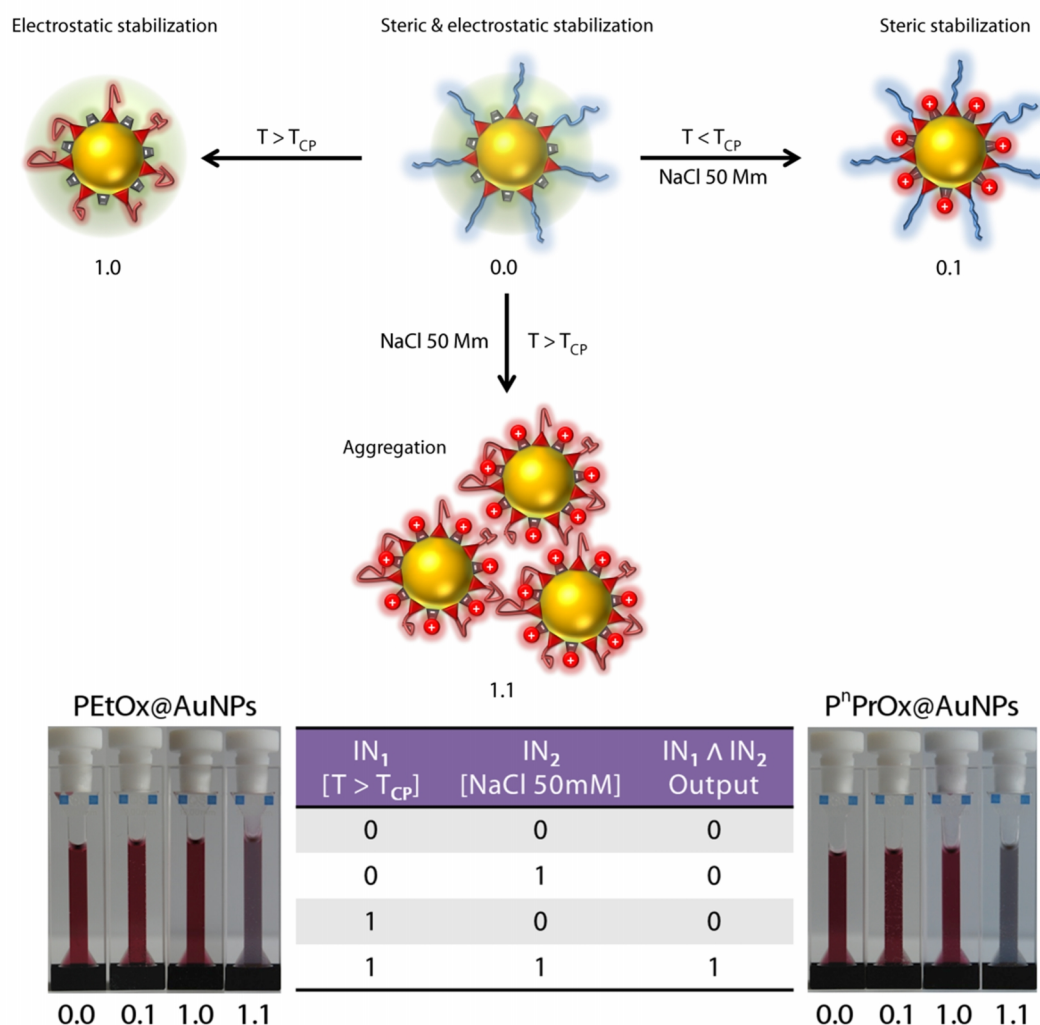


Figure 4.5.1. *Top: Schematic representation of the working mechanism of the PAOx@AuNP – based AND gate. Bottom: Logic table of the AND gate. Input 1: Temperature above PAOx transition temperature. Input 2: 50 mM NaCl_{aq}. The shift in the surface plasmon resonance band occurs only if both inputs are true, with the consequent color change observed. The pictures show PⁿEtOx@AuNPs and PⁿPrOx@AuNPs solutions corresponding to the four possible input combinations. T_{CP}(PⁿEtOx@AuNPs) = 80 °C. T_{CP}(PⁿPrOx@AuNPs) = 22 °C. Concentration = 0.10 mg mL⁻¹.*

As schematically depicted in Figure 4.5.1. (top), increasing the temperature beyond the PAOx T_{CP} (input 1) results in a collapse of the polymer by virtue of its LCST behavior. However, PAOx@AuNP aggregation is impeded by the remaining electrostatic repulsive forces, leading to invariability of

the solution appearance. Similarly, the addition of NaCl (input 2) produces the screening of the citrate negative charges on the surface of the AuNP, suppressing Coulombic stabilization, but aggregation is now impaired by the PAOx brush repulsive steric interactions. Therefore, both inputs need to be simultaneously applied to obtain an output solution color change, corresponding to a logical conjunction or AND gate (see logic table in Figure 4.5.1). Interestingly, selection of the PAOx composition granted control over the value of the temperature input, from 22 °C for PⁿPrOx@AuNPs to 80 °C for PEtOx@AuNPs.

4.6 Conclusions

A new end-capping strategy was devised to synthesize xanthate-functional PAOx that allowed direct grafting to citrate-stabilized AuNPs. The obtained PAOx@AuNPs exhibited dual stabilization by repulsive electrostatic and steric interactions giving access to water soluble molecular AND logic gates wherein environmental temperature and ionic strength constitute the input signals, and the solution color the output (see Figure 4.5.1). Furthermore, the temperature input value could be tuned by variation of the PAOx polymer composition, from 22 °C to 80 °C for PⁿPrOx@AuNPs and PEtOx@AuNPs, respectively. Besides advancing in the fascinating field of molecular logic gates, the present research offers a facile strategy for the synthesis of PAOx@AuNPs of interest in fields spanning nanotechnology and biomedical sciences. Moreover, functional initiators and monomers may be used in future work to render multifunctional PAOx@AuNPs with high potential in biotechnology. In addition, the reported xanthate-functionalized PAOx can be easily converted into thiol-functional PAOx with many post-modification possibilities being of high interest in polymer science.

4.7 Experimental Section

Materials

Solvents and reagents were purchased from Sigma Aldrich, and used as received unless otherwise specified. Methyl tosylate (MeOTs, Aldrich) was distilled prior to use. 2-Methyl-2-oxazoline, 2-ethyl-2-oxazoline (EtOx, Aldrich) and 2-ⁿ-propyl-2-oxazoline (ⁿPrOx, synthesized as previously reported^[45]) were distilled over barium oxide (BaO, Aldrich). Acetonitrile (CH₃CN, Acros) was dried over molecular sieves (3Å).

Deionized (Milli-Q) water was obtained from a Sartorius Arium 611 with a Sartopore 2 150 (0.45 + 0.2 µm pore size) cartridge filter (resistivity ≥ 18.2 MΩ cm).

Instrumentation

Polymerizations were performed in a Biotage initiator sixty microwave synthesizer utilizing capped microwave vials. The vials were heated to 120 °C for 24 hours and cooled down to room temperature under vacuum prior to use. All polymerizations were performed with temperature control (IR sensor).

¹H-NMR spectra were recorded in CDCl₃ on a Bruker Avance 300 MHz spectrometer. Spectra were processed using TOPSPIN 3.0.

Size exclusion chromatography (SEC) measurements were performed on an Agilent 1260-series equipped with a 1260 ISO-pump, a 1260 Diode Array Detector (DAD), a 1260 Refractive Index Detector (RID), and a PSS Gram30 column in series with a PSS Gram1000 column inside a 1260 Thermostated Column Compartment (TCC) at 50°C using dimethylacetamide containing 50 mM of

LiCl (flow rate of 0.6 mL min⁻¹) as solvent. Molar masses and dispersities were calculated against poly(methyl methacrylate) standards.

MALDI-TOF (Matrix-Assisted Laser Desorption and Ionization Time of Flight) mass spectrometry analysis was performed on an Applied Biosystems Voyager-DE STR instrument equipped with nitrogen laser operating at 337 nm, pulsed ion extraction source and reflectron detector. The laser pulse width is 3 ns with a maximum power of 20 Hz. Spectra were recorded in reflector mode with an acceleration voltage of 19 kV and delay of 400 ns. 100 single shot acquisitions were summed to give the spectra and the data were analyzed using Data Explorer software. Samples were prepared by dissolving the matrix 2-(4-hydroxyphenylazo) benzoic acid HABA in the solvent (acetone, 20 mg/mL⁻¹), mixing with the polymer (1 mg/mL⁻¹) and sodium iodide in acetone (15 mg/mL⁻¹) that was used as cationizing agent.

Dynamic light scattering (DLS) was performed on a Zetasizer Nano-ZS Malvern apparatus (Malvern Instruments Ltd.) using disposable cuvettes. The excitation light source was a He-Ne laser at 633 nm, and the intensity of the scattered light was measured at a 173 degree angle (backscattering mode). Measurements at a 90 degree scattering angle were performed in a Zetasizer Nano S90 (backscattering mode). Both methods measure the rate of the intensity fluctuation and the size of the particles is determined through the Stokes-Einstein equation ($d(H) = \sqrt{kT/3\pi\eta D}$) where $d(H)$ is the mean hydrodynamic diameter, k is the Boltzmann constant, T is the absolute temperature, η is the viscosity of the dispersing medium, and D is the apparent diffusion coefficient. Before starting the measurements, samples were incubated at the specific temperature for at least 300s to reach equilibrium.

Synthesis of Poly(2-alkyl-2-oxazoline)-xanthate

All reagents were stored and handled under dried nitrogen in a glove-box (Vigor gas purification technologies, Inc.). A 4M solution of the 2-alkyl-2-oxazoline monomer was prepared in acetonitrile in the presence of 1/50 equivalents of methyl tosylate. The polymerization mixture was heated to 140 °C in the microwave synthesizer for 8 min. 40 sec., calculated according to the previously reported kinetics,^[46] cooled to 0 °C and the living polymer chains were terminated by addition of 1.3 equivalents potassium ethyl xanthogenate (Aldrich) under a dry nitrogen atmosphere. The polymerization mixture was kept stirring for 18 hours at room temperature after which the solvent was evaporated under reduced pressure. PEtOx-xanthate and PⁿPrOx-xanthate were re-dissolved in dichloromethane and washed three times with water and brine to remove the excess of potassium ethyl xanthogenate. The organic phase was dried over anhydrous magnesium sulphate, filtered and the polymer precipitated in cold diethyl ether, obtaining a white powder that was filtered and dried in a vacuum oven at 30 °C for 24h. The PMeOx-xanthate polymerization mixture was purified by dialysis against demineralized water (Spectra Por dialysis tubing, Mwt. cut-off 1000 Da), freeze-dried and subsequently precipitated in cold diethyl ether from dichloromethane.

The polymers were characterized by ¹H-NMR spectroscopy, MALDI-TOF mass spectrometry and size exclusion chromatography.

Synthesis of citrate-stabilized gold nanoparticles

Citrate stabilized gold nanoparticles were synthesized according to the reported literature procedures.^[47] All glassware was first washed with aqua regia and then rinsed with milli-Q water several times prior to synthesis. Briefly, 20 mL of 1 mM HAuCl₃ was refluxed for 30 min. Then 2 mL of 1 wt % sodium citrate was quickly added and the color of solution changed from yellow to wine red within 5 min. After cooling, the reaction solution was stored at 4 °C.

Synthesis and characterization of Poly(2-alkyl-2-oxazoline)-grafted gold nanoparticles

A total of 9 mL of a citrate stabilized gold nanoparticles solution was mixed with 200 μL of an aqueous solution containing 8 mg of PAOx-xanthate and stirred overnight at low temperature. The resulting conjugates were three times purified by centrifugation at 4 $^{\circ}\text{C}$ and 10 000 g for 30 min followed by re-dispersion in pure water.

The PAOx@AuNPs were characterized by Transmission Electron Microscopy (TEM). A drop of gold nanoparticle solution was allowed to air-dry onto a Formvar-carbon-coated 200 mesh copper grid and visualized using 80 keV TEM (Jeol 1010, Japan). TEM images of the AuNPs were processed via ImageJ to determine the number average size distribution in the dry state.

UV-Vis spectroscopy

UV-Vis spectra were acquired in a CARY Bio 100 UV-VIS spectrophotometer equipped with a temperature controller. Gold nanoparticle solutions were placed in quartz cuvettes (concentration 0.1 mg mL⁻¹) and scanned in the 300 – 800 nm range at different temperatures. Temperatures were changed in 5 $^{\circ}\text{C}$ intervals and incubated 2 min. to assure thermal equilibration.

Turbidimetry studies

Turbidimetry measurements were performed in a CARY Bio 100 UV-VIS spectrophotometer equipped with a temperature controller, at a wavelength of 600 nm. The temperature sensor was placed in a cuvette containing the same volume of milli-Q water as the polymer solutions. Solutions of the polymers were prepared in milli-Q water or 50 mM NaCl_{aq} at 5 mg mL⁻¹. Three full heating cycles were applied with a heating/cooling rate of 1K min⁻¹ with hold steps of 10 min. at the extreme temperatures. The cloud points are given as the 50% transmittance point during the second heating ramp.

Estimation of the PAOx-brush grafting density

The grafting density of the PAOx coating onto the AuNPs was calculated by UV-Vis spectrometry.^[37,38] The extinction coefficient of citrate@AuNPs with a mean diameter of 25 nm was calculated with the following equation:

$$\ln \varepsilon = k \ln D + a$$

Where the coefficients are defined as: $k = 3.33211$ and $a = 10.80505$, yielding: $\varepsilon = 2.934 \cdot 10^9 \text{ L mol}^{-1} \text{ cm}^{-1}$.

From the absorbance at λ_{max} (524 nm) of a solution containing 0.113 mg mL⁻¹ citrate@AuNPs and the calculated extinction coefficient for citrate@AuNPs, the molarity of the solution was found to be of $6.57 \cdot 10^{-10} \text{ mol L}^{-1}$, and consequently the molecular weight of the citrate@AuNPs could be estimated to be $1.72 \cdot 10^8 \text{ g mol}^{-1}$.

UV-Vis absorbance spectra were recorded for a series of solutions containing 0.10 mg mL⁻¹ PAOx@AuNPs and, assuming the extinction coefficient of the PAOx@AuNPs remained the same as calculated for citrate@AuNPs, the molarity for each solution was calculated with the following equation:

$$c (\text{mol L}^{-1}) = \frac{A}{\varepsilon l}$$

Where $\varepsilon = 2.934 \cdot 10^9 \text{ L mol}^{-1} \text{ cm}^{-1}$ and $l = 1 \text{ cm}$. And, likewise for the citrate@AuNPs, the molecular weight was calculated by the equation:

$$M_{wt} = \frac{c \text{ (g L}^{-1}\text{)}}{c \text{ (mol L}^{-1}\text{)}}$$

The number of polymer chains per nanoparticle was then calculated by subtracting the M_{wt} of the citrate@AuNPs from the M_{wt} of the PAOx@AuNPs,¹ and dividing from the M_{wt} of the individual PAOx chain. This number was divided over the nanoparticle's surface, yielding the grafting density, as described in the following equation:

$$\text{Grafting density (chains/nm}^2\text{)} = \frac{M_{wt}(\text{PAOx@AuNPs}) - M_{wt}(\text{citrate@AuNPs})}{M_{wt}(\text{PAOx}) S(\text{AuNP})}$$

Where $\text{Surface AuNP} = S = 4\pi r^2 = 1963 \text{ nm}^2$

The results obtained are summarized in the table below:

AuNP	Mwt (g mol ⁻¹)	Grafting density (chains nm ⁻²)
Citrate@AuNP	1.72 10 ⁸	-
PMeOx@AuNP	1.98 10 ⁸	3.0
PEtOx@AuNP	2.15 10 ⁸	4.3
P ⁿ PrOx@AuNP	1.98 10 ⁸	2.4

4.8. References

- [1] M.-C. Daniel, D. Astruc, *Chem. Rev.* **2003**, *104*, 293.
- [2] E. C. Dreaden, A. M. Alkilany, X. Huang, C. J. Murphy, M. A. El-Sayed, *Chem. Soc. Rev.* **2012**, *41*, 2740.
- [3] J. Conde, A. Ambrosone, V. Sanz, Y. Hernandez, V. Marchesano, F. Tian, H. Child, C. C. Berry, M. R. Ibarra, P. V. Baptista, C. Tortiglione, J. M. de la Fuente, *ACS Nano* **2012**, *6*, 8316.
- [4] K. Saha, S. S. Agasti, C. Kim, X. Li, V. M. Rotello, *Chem. Rev.* **2012**, *112*, 2739.
- [5] R. Elghanian, J. J. Storhoff, R. C. Mucic, R. L. Letsinger, C. A. Mirkin, *Science* **1997**, *277*, 1078.
- [6] W. Zhao, M. A. Brook, Y. Li, *ChemBioChem* **2008**, *9*, 2363.
- [7] J. Sun, Y. Xianyu, X. Jiang, *Chem. Soc. Rev.* **2014**, *43*, 6239.
- [8] D. Liu, W. Chen, K. Sun, K. Deng, W. Zhang, Z. Wang, X. Jiang, *Angew. Chem. Int. Ed.* **2011**, *50*, 4103.
- [9] Y. Xianyu, Z. Wang, J. Sun, X. Wang, X. Jiang, *Small* **2014**, n/a.
- [10] J. Pyun, T. Emrick, in *Macromolecular Engineering*, Wiley-VCH Verlag GmbH & Co. KGaA, **2007**, pp. 2409.
- [11] I. Lilge, H. Schönherr, *Eur. Polym. J.* **2013**, *49*, 1943.
- [12] Y. Cheng, A. C. Samia, J. D. Meyers, I. Panagopoulos, B. Fei, C. Burda, *J. Am. Chem. Soc.* **2008**, *130*, 10643.
- [13] N. B. Shah, G. M. Vercellotti, J. G. White, A. Fegan, C. R. Wagner, J. C. Bischof, *Mol. Pharm.* **2012**, *9*, 2146.
- [14] Z. He, J. Liu, L. Du, *Nanoscale* **2014**, *6*, 9017.
- [15] J. Shan, M. Nuopponen, H. Jiang, E. Kauppinen, H. Tenhu, *Macromolecules* **2003**, *36*, 4526.
- [16] K. Kusolkamabot, P. Sae-ung, N. Niamnont, K. Wongravee, M. Sukwattanasinitt, V. P. Hoven, *Langmuir* **2013**, *29*, 12317.
- [17] C. Boyer, M. R. Whittaker, M. Luzon, T. P. Davis, *Macromolecules* **2009**, *42*, 6917.
- [18] F. C. Gaertner, R. Luxenhofer, B. Blechert, R. Jordan, M. Essler, *J. Control. Release* **2007**, *119*, 291.
- [19] V. R. de la Rosa, *J. Mater. Sci.: Mater. Med.* **2014**, *25*, 1211.

¹ Since the number of citrate groups released upon PAOx grafting onto the citrate@AuNPs was not known, no mass was withdrawn from the citrate@AuNPs in the calculation. Considering that a fraction of citrate groups is likely released upon PAOx grafting on the AuNP, the calculated values of PAOx grafting density are possibly underestimated.

- [20] K. Knop, R. Hoogenboom, D. Fischer, U. S. Schubert, *Angew. Chem. Int. Ed.* **2010**, *49*, 6288.
- [21] O. Sedlacek, B. D. Monnery, S. K. Filippov, R. Hoogenboom, M. Hruby, *Macromol. Rapid Commun.* **2012**, *33*, 1648.
- [22] R. Jordan, N. West, A. Ulman, Y.-M. Chou, O. Nuyken, *Macromolecules* **2001**, *34*, 1606.
- [23] Z. Zhang, S. Maji, A. B. d. F. Antunes, R. De Rycke, Q. Zhang, R. Hoogenboom, B. G. De Geest, *Chem. Mater.* **2013**, *25*, 4297.
- [24] G. Gyulai, C. B. Péntzes, M. Mohai, F. Csempesz, É. Kiss, *Eur. Polym. J.* **2013**, *49*, 2495.
- [25] J. Du, S. Yin, L. Jiang, B. Ma, X. Chen, *Chem. Commun.* **2013**, *49*, 4196.
- [26] M. A. Tasdelen, M. U. Kahveci, Y. Yagci, *Prog. Polym. Sci.* **2011**, *36*, 455.
- [27] A. Sundaramurthy, M. Vergaelen, S. Maji, R. Auzély-Velty, Z. Zhang, B. G. De Geest, R. Hoogenboom, *Adv. Healthcare Mater.* **2014**, 10.1002/adhm.201400377.
- [28] O. Tzhayik, P. Sawant, S. Efrima, E. Kovalev, J. T. Klug, *Langmuir* **2002**, *18*, 3364.
- [29] A. B. Lowe, B. S. Sumerlin, M. S. Donovan, C. L. McCormick, *J. Am. Chem. Soc.* **2002**, *124*, 11562.
- [30] A. E. Smith, X. Xu, T. U. Abell, S. E. Kirkland, R. M. Hensarling, C. L. McCormick, *Macromolecules* **2009**, *42*, 2958.
- [31] T. X. Viegas, M. D. Bentley, J. M. Harris, Z. Fang, K. Yoon, B. Dizman, R. Weimer, A. Mero, G. Pasut, F. M. Veronese, *Bioconjugate Chem.* **2011**, *22*, 976.
- [32] M. M. Bloksma, D. J. Bakker, C. Weber, R. Hoogenboom, U. S. Schubert, *Macromol. Rapid Commun.* **2010**, *31*, 724.
- [33] A. Ihs, K. Uvdal, B. Liedberg, *Langmuir* **1993**, *9*, 733.
- [34] C.-A. Fustin, C. Colard, M. Filali, P. Guillet, A.-S. Duwez, M. A. R. Meier, U. S. Schubert, J.-F. Gohy, *Langmuir* **2006**, *22*, 6690.
- [35] J. W. Hotchkiss, A. B. Lowe, S. G. Boyes, *Chem. Mater.* **2006**, *19*, 6.
- [36] S. Slavin, A. H. Soeriyadi, L. Voorhaar, M. R. Whittaker, C. R. Becer, C. Boyer, T. P. Davis, D. M. Haddleton, *Soft Matter* **2012**, *8*, 118.
- [37] B. N. Khlebtsov, N. G. Khlebtsov, *Colloid J.* **2011**, *73*, 118.
- [38] B. J. Berne, R. Pecora, *Dynamic Light Scattering: With Applications to Chemistry, Biology, and Physics*, Courier Dover Publications, Mineola, NY, **2000**.
- [39] S. W. Provencher, P. Štěpánek, *Particle & Particle Systems Characterization* **1996**, *13*, 291.
- [40] P. I. V. T. Pradeep, A. Ashokreddy, *A Textbook of Nanoscience and Nanotechnology*, Tata McGraw-Hill Education, **2012**.
- [41] D. J. Lewis, T. M. Day, J. V. MacPherson, Z. Pikramenou, *Chem. Commun.* **2006**, 1433.
- [42] X. Liu, M. Atwater, J. Wang, Q. Huo, *Colloids Surf. B. Biointerfaces* **2007**, *58*, 3.
- [43] S. Srivastava, B. L. Frankamp, V. M. Rotello, *Chem. Mater.* **2005**, *17*, 487.
- [44] R. Hoogenboom, H. M. L. Thijs, M. J. H. C. Jochems, B. M. van Lankvelt, M. W. M. Fijten, U. S. Schubert, *Chem. Commun.* **2008**, 5758.
- [45] M. M. Bloksma, C. Weber, I. Y. Perevyazko, A. Kuse, A. Baumgärtel, A. Vollrath, R. Hoogenboom, U. S. Schubert, *Macromolecules* **2011**, *44*, 4057.
- [46] F. Wiesbrock, R. Hoogenboom, M. A. M. Leenen, M. A. R. Meier, U. S. Schubert, *Macromolecules* **2005**, *38*, 5025.
- [47] J. Turkevich, P. C. Stevenson, J. Hillier, *Farad. Discuss.* **1951**, *11*, 55.

Chapter 5

Tuning temperature responsive polymers by supramolecular interactions

Within this work, the interplay between different supramolecular host molecules on the thermoresponsive properties of a range of relatively simple copolymers with hydrophobic alkyl side chains has resulted in the formation of a variety of different supramolecular nanostructures. Besides allowing the control over the copolymer phase transition temperature, modification of polymer composition and supramolecular host resulted in sharp or progressive responses towards temperature, and even in sensors able to account for the thermal history of the solution.

5.1 Introduction

Temperature constitutes a fundamental parameter of utmost importance for all scientific disciplines, ranging from physical to biological sciences, and is at the core of thermodynamic properties. The prevalent position of temperature in science and technology has triggered the development of an extensive range of different thermoresponsive materials for their use as smart materials and sensors.^[1, 2] Polymers provide an ample synthetic versatility to obtain thermometers with physical properties tailored to the final application, such as the development of temperature-responsive polymeric hydrogels, micro- and nanoparticles, or printable films.^[3-11] Solution nanosensors are of great interest for the temperature monitoring in cellular research, imaging and microscopy, fields where polymeric sensors have already shown their effectiveness.^[3-10]

The use of a well-defined polymer in the design of a polymeric temperature sensor is crucial to ensure correct interpretation of the experimental observations of the sensor behavior. Moreover, any prospective application of the sensor for in vivo thermography of living matter or biomedicine requires the use of biocompatible building blocks.

As has been seen in Chapter 1, poly(2-alkyl-2-oxazoline)s (PAOx) reemerged at the dawn of the new millennium due to their narrow molecular weight distribution, tunable properties, and excellent biocompatibility.^[12, 13] In addition, PAOx exhibit the so-called Lower Critical Solution Temperature (LCST) behavior,^[14-17] and thermoresponsive PAOx have been developed for their use as sensors, and in a variety of biomedical applications including drug and gene delivery, or tissue engineering.^[17, 18] Importantly, the LCST of PAOx can be tuned by varying the hydrophilicity of the polymer side chains (see Figure 1.2.2, and section 1.4 in Chapter 1).^[19]

The temperature at which this transition takes place for a specific polymer composition and concentration in solution is regarded as cloud-point temperature (T_{CP}). The T_{CP} of random copoly(2-oxazoline)s based on 2-ethyl-2-oxazoline (EtOx) (hydrophilic) and 2-nonyl-2-oxazoline (NonOx) (hydrophobic) can therefore be modified by changing the ratio of both monomers in the

final copolymer.^[16, 19-21] In addition, the polymer hydrophilicity can be tuned through specific supramolecular interactions with host macromolecules, as has been previously shown for end-group modified PAOx and in other polymer platforms.^[22-25]

Cyclodextrins are torus shaped cyclic oligosaccharides containing several glucose units bound by $\alpha(1-4)$ glycosidic bonds. These biocompatible cavitands feature a hydrophobic cavity and a hydrophilic outer shell decorated by primary and secondary hydroxyl groups. Cyclodextrins have received considerable attention, especially from the pharmaceutical industry, for their ability to form inclusion complexes with hydrophobic drugs, highly increasing their water solubility.^[26, 27] The combination of cyclodextrins with polymers has resulted in the development of novel smart materials^[28-35] such as molecular tubes, insulated molecular wires,^[36] drug delivery vehicles and for biomedicine,^[37-40] responsive hydrogels^[41-43] and supramolecular nanoparticles.^[44-46]

Modification of cyclodextrins alters their physicochemical properties and their ability to form host-guest inclusion complexes. The exchange of the hydroxyl groups present in cyclodextrins by hydroxypropyl groups highly enhances their water solubility and thus their capacity to solubilize hydrophobic guests. In addition, these hydroxypropyl groups disrupt the ordered intermolecular hydrogen-bonding network between cyclodextrins, suppressing their self-aggregation and enhancing their aqueous solubility.^[47-51]

In this work we report our results on the fascinating behavior of relatively simple thermoresponsive poly(2-oxazoline) copolymers with pendent ethyl and nonyl side chains and their complex formation with a variety of cyclodextrins and curcubit[7]uril as supramolecular host molecules.

To be able to establish structure-property relationships and to obtain insights on the interplay between the polymer and supramolecular hosts, we first assessed the impact of different supramolecular hosts on the thermoresponsive properties of the copolymer (Figure 5.1.1).

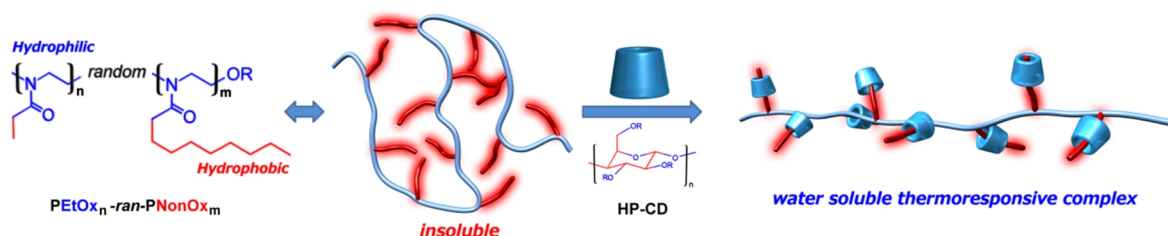


Figure 5.1.1. A series of amphiphilic PEtOx-ran-PNonOx random copolymers were synthesized and their solubility properties studied in the presence of a range of different supramolecular host molecules. The picture describes the supramolecular complexation of a PEtOx-ran-PNonOx random copolymer with cyclodextrins resulting in the formation of thermoresponsive supramolecular complexes.

For this purpose, a PEtOx-ran-PNonOx random copolymer containing 12 % nonyl side chains was initially employed. Subsequently, the influence of polymer composition, *i.e.* number of nonyl side chains, and length was analyzed. For this purpose, a series of PEtOx-ran-PNonOx random copolymers with increasing NonOx content and varying degree of polymerization was synthesized.

5.2 Poly(2-ethyl-2-oxazoline)-*ran*-poly(2-nonyl-2-oxazoline) synthesis

The copolymerizations were performed following a previously reported protocol^[20] by preparing solutions of EtOx and NonOx with the desired stoichiometry in dry acetonitrile, and a total monomer concentration of 4 M. The initiator used was methyl tosylate (MeOTs) and the monomer to initiator ratio was selected to obtain copolymers with the desired length (details are given in the Experimental Section). All polymerizations were performed to up to full conversion in capped vials in a microwave synthesizer at 140 °C and terminated with methanolic KOH, resulting in hydroxyl-terminated polymers (see Figure 5.2.1).*

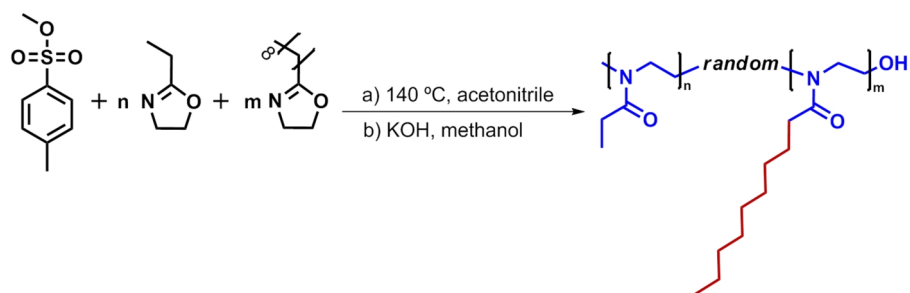


Figure 5.2.1. Schematic representation of the living cationic ring-opening copolymerization of 2-ethyl-2-oxazoline (EtOx) and 2-nonyl-2-oxazoline (NonOx) initiated by methyl tosylate resulting in P*EtOx-ran*-P*NonOx* random copolymers.

Interestingly, the EtOx-NonOx statistical copolymerization results in random copolymer structures, since the reactivity ratios of both monomers are close to unity, as has been previously reported.^[20, 52] The obtained P[(EtOx)_n-*ran*-(NonOx)_m] copolymer compositions were determined by ¹H-NMR spectroscopy (see Figure 5.2.2).

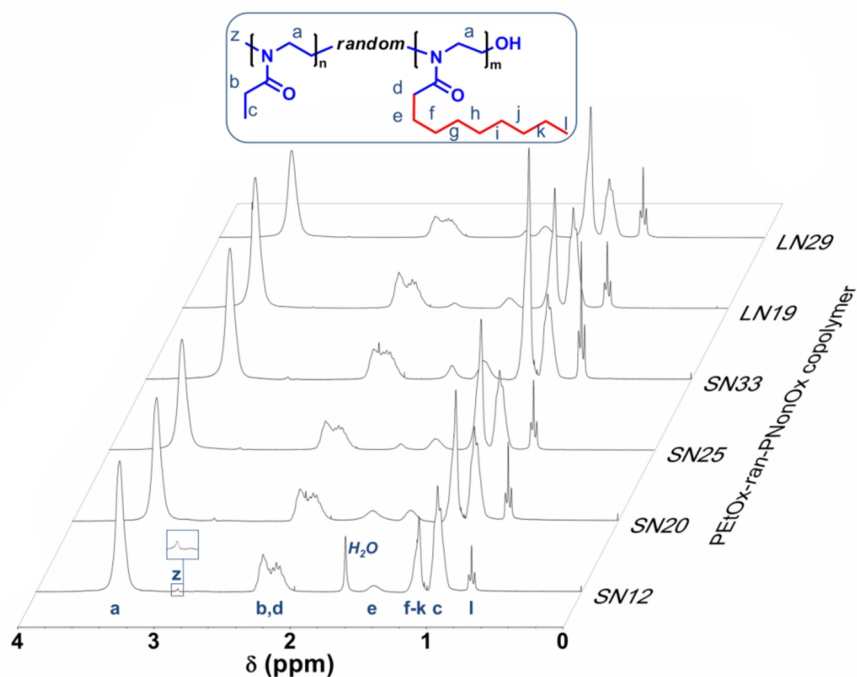


Figure 5.2.2. ¹H-NMR spectra of the investigated P*EtOx-ran*-P*NonOx* random copolymers in CDCl₃. Legend: S = Short polymer, DP \approx 100, L = Long polymer DP \approx 200. N = % Nonyl side chains in number.

* This research was performed earlier in time than the research described in Chapter 3, therefore methanolic KOH, instead of N(CH₃)₄OH was used as terminating agent to obtain hydroxyl-terminated polymers.

All the synthesized copolymers exhibited dispersities below 1.15, as determined by size exclusion chromatography, indicating good control over the polymerizations (see Figure 5.2.3).

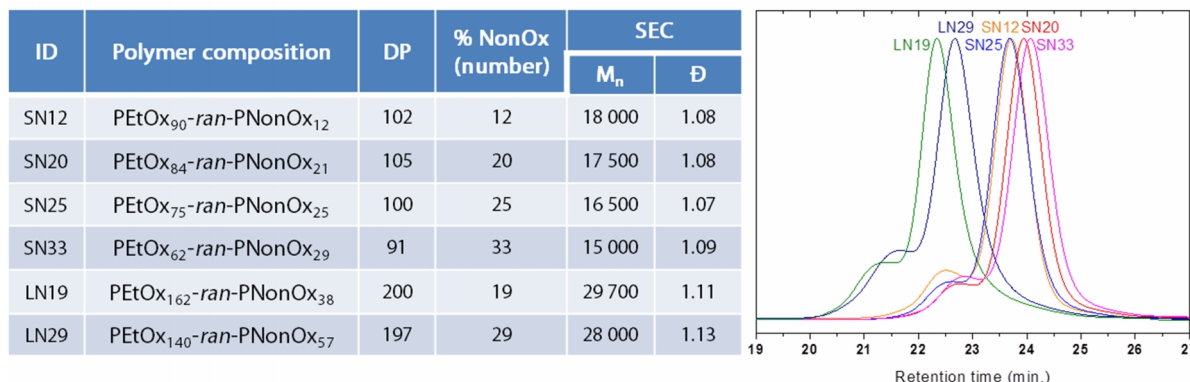


Figure 5.2.3. *Composition and size exclusion chromatography (SEC) data of the synthesized PEtOx_n-*ran*-PNonOx_m random copolymers. Albeit a high molecular weight distribution is observed in all cases, ascribed to chain coupling, well-defined polymers were obtained. Dispersity values were below 1.15 and generally below to 1.10. Polymer composition was calculated by ¹H NMR analysis. Polymer ID legend: S = Short polymer, DP ≈ 100, L = Long polymer DP ≈ 200. SEC eluent: N,N-dimethylacetamide. Calibrated against PMMA standards.*

Nevertheless, as commonly observed, a high molecular weight shoulder was present in all copolymers, presumably due to chain-transfer reactions, as has been described in Chapter 3. The observed differences in retention time are not only ascribed to different number average molecular weight, but also to the different copolymer hydrophobicity. As the content of NonOx in the copolymer increases, so does its hydrophobicity, resulting in a less efficient solvation by the polar *N,N*-dimethylacetamide eluent, producing a smaller hydrodynamic volume. Consequently, prolonged retention times are observed for the most hydrophobic copolymers. This effect is especially noticeable for the LN19 and LN29 copolymers, both with a degree of polymerization (DP) close to 200 repeating units; albeit LN29 has a higher molecular weight, its retention time is higher than that of LN19, indicating a distinctly larger hydrophobicity. Later on, these preliminary observations will translate into marked differences in the copolymer solubility properties.

5.3 Influence of different supramolecular hosts on the solubility properties of poly(2-ethyl-2-oxazoline)-*ran*-poly(2-nonyl-2-oxazoline)s

5.3.1. Cyclodextrins as supramolecular host molecules

Cyclodextrins are cyclic oligosaccharides consisting on six to eight D(+)-glucopyranose units connected through α -1,4 glycosidic bonds.^[53] They exhibit a truncated cone shape, with a hollow cavity of 7.9 Å depth. The diameters of the cyclodextrin rims are 4.7 and 5.3 Å for α CD, 6.0 and 6.5 Å for β CD and 7.5 and 8.3 Å for γ CD,^[54] as summarized in Figure 5.3.2. The interior is constituted by C-H groups and glycosidic oxygen bonds, making it apolar in relation to the highly hydrophilic exterior, which is decorated by primary and secondary hydroxyl groups. Cyclodextrins' combination of a hydrophilic outer shell and a hydrophobic cavity makes them suitable for the inclusion of a wide range of organic molecules in aqueous solution. Therefore, cyclodextrins constitute one of the first receptor molecules whose ability to complexate organic molecules in water and take part in complex supramolecular structures^[55, 56] have been extensively studied.^[57-59]

The formation of host-guest complexes with organic molecules, such as the PAOx pendant nonyl chains in the present research, involves the insertion of the hydrophobic guest into the cyclodextrin cavity. The inclusion complex formation results in the release of water molecules initially solvating the hydrophobic guest and the hydrophobic interior of the cyclodextrin to the bulk aqueous medium. Two important factors are involved in the binding process from the cyclodextrin host standpoint. First, the entropically-favored release of water molecules originally forming a network in the cyclodextrin rims, and those included inside the host cavity, to the bulk water.^[60-62] Crystallography experiments have shown five to six water molecules residing within the native α CD cavity, two of them hydrogen-bonded to peripheral hydroxyl groups.^[63] For the larger β CD, one extra water molecule is included,^[64] although up to eleven have been found to be hydrogen-bonded to the macromolecule.^[65] The release of water molecules upon complexation appears to produce a profound effect on the cyclodextrin host-guest complex formation. The binding of adamantane with β CD, for instance, has been reported to involve the total release of 15 to 25 water molecules upon association (see Figure 5.3.1).^[66]

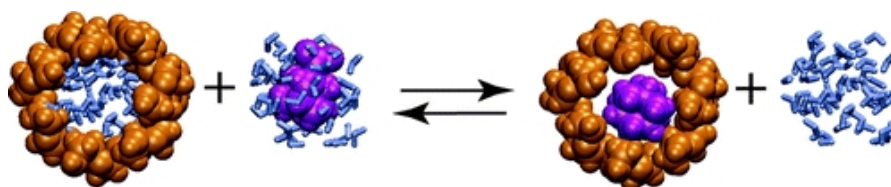


Figure 5.3.1. Schematic representation of the release of water molecules associated to host-guest complex formation between β CD and adamantane carboxylic acid in aqueous medium.^[66]

In addition to the entropic gain from the release of water molecules, the factors involved in the binding are primarily van der Waals and hydrophobic interactions. The transfer of the nonyl side-chains from water to the highly hydrophobic cyclodextrin cavity is similar to a typical hydrophobic interaction process, such as the partitioning of an organic molecule from an aqueous to an organic phase. The nature of the guest molecule dictates the energy balance of these interactions, as the establishment of hydrogen-bonding or π - π interactions^[67] are able to further increase the stability of the inclusion complex.^[68] Furthermore, the enthalpy-entropy compensation often found in cyclodextrin host-guest complexation calorimetric studies, can be explained by the dehydration of both guest and cyclodextrin host molecules upon complexation, together with conformational changes on the cyclodextrin molecule.^[69] In this regard, it has been reported that intramolecular hydrogen-bonding promotes a rigid conformation of the cyclodextrin molecule that undergoes substantial conformational changes upon complexation.^[70-72] The strain release associated to these conformational changes constitutes the second factor to consider in host-guest complex formation. This factor is sharply manifested in chemically modified cyclodextrins. For instance, partial methylation of the cyclodextrin hydroxyl groups distorts the intramolecular hydrogen-bonding network resulting in the extension of the hydrophobic cavity. The increased flexibility of the free cyclodextrin minimizes the strain release upon complexation and therefore host-guest hydrophobic interactions acquire a preeminent role. High degrees of methylation of the hydroxyl groups eventually result in a loss of the cyclodextrin rigid structure and in the destabilization of host-guest complexes due to highly unfavorable conformational entropies.^[73] Similar observations have been made for hydroxypropyl-substituted cyclodextrins.^[74-76]

The strong intramolecular hydrogen-bond network also accounts for the abnormal solubility behavior of native cyclodextrins, especially acute in the case of β CD. The disruption of this intramolecular network may explain the large impact that chemical modification of the

cyclodextrin hydroxyl groups by hydroxypropyl units has on its solubility,^[50] increasing from 18.5 mg mL⁻¹ for β CD to over 500 mg mL⁻¹ for HP β CD (see Figure 5.3.2).

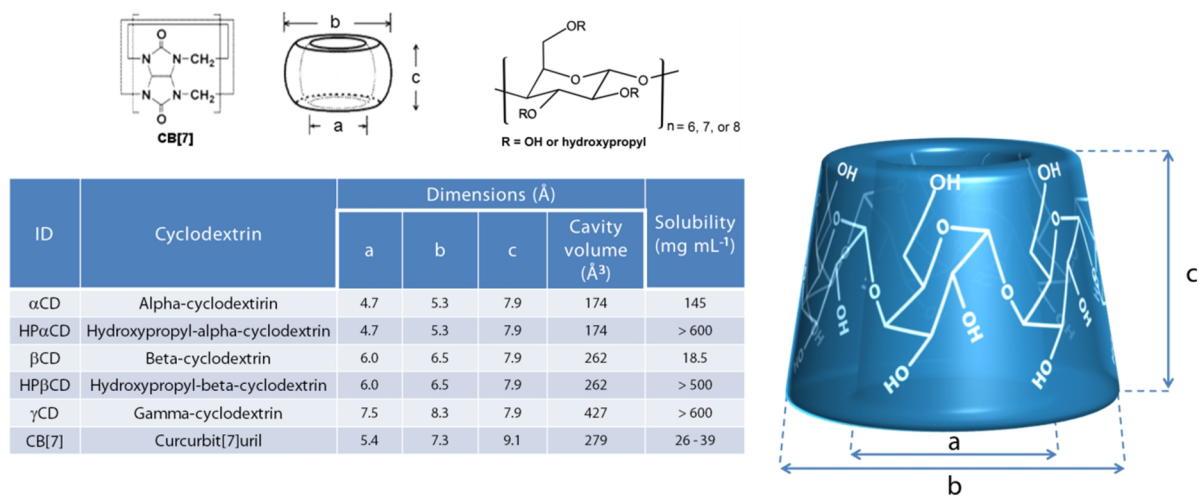


Figure 5.3.2. Dimensions and water solubility values (25 °C) of the three natural cyclodextrins: α , β and γ , made of 6, 7, and 8 D(+)-glucopyranose units, respectively. Hydroxypropylated cyclodextrins are cyclodextrins in which some of the hydroxyl groups (0.6 per glucopyranose unit, in the current study) have been exchanged by hydroxypropyl groups.^[77, 78]

5.3.2. Turbidimetry Experiments

The temperature-responsiveness of the PEO_n-*ran*-PNO_x_m random copolymers and their ensembles with supramolecular hosts was studied by turbidimetry. In this method, a light beam is passed through a cuvette containing a solution of the polymer in milli-Q water. The light is collected in a photoelectric cell, allowing the monitoring of the amount of light absorbed by the solution.^[79] The ratio between the transmitted radiant intensity (I) to that incident on the sample (I_0) defines the transmittance (T), that can also be defined as % T , as described in Figure 5.3.3.

$$T = \frac{I}{I_0}; \quad \%T = 100 \times T$$

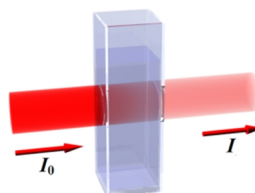


Figure 5.3.3. Expression describing the transmittance and representation of a cuvette containing a polymer solution being irradiated with light of intensity I_0 . The intensity of the transmitted light (I) is detected, and monitored while applying a temperature heating/cooling ramp.

The wavelength of the incident radiation in the reported turbidimetry measurements was fixed at 700 nm. The experiments were performed in a UV-Vis spectrophotometer equipped with a temperature-controlled block. In a typical experiment, a 5 mg mL⁻¹ polymer solution was prepared, cooled to 0 °C under argon, and heated at 1 K min⁻¹ to a temperature at least 10 K beyond the polymer T_{CP} . Temperature was brought back to 0 °C at the same rate, allowing the measurement of both the cloud point temperature upon heating and the clearance point temperature upon cooling. The cycles were repeated at least twice and the second cycle is reported.

Initially, we assessed the impact of different cyclodextrin supramolecular hosts on the thermoresponsive properties of the PEO_n-*ran*-PNO_x random copolymer. For this purpose, the

PEtOx₉₀-*ran*-PNonOx₁₂ random copolymer containing 12 % nonyl side chains (SN12) was employed as a model polymer.

5.3.3. Alpha-cyclodextrin (α CD)

Due to its high water solubility and ability to form host-guest complexes with linear aliphatic chains,^[57, 72] we first studied the self-assembly behavior of native alpha-cyclodextrin (α CD) with the copolymer, to determine the influence it exerts on the thermoresponsive properties.

A 5 mg mL⁻¹ solution of the PEtOx₉₀-*ran*-PNonOx₁₂ random copolymer was prepared in an ice bath, becoming opaque when brought to room temperature. Different aliquots of this solution were titrated with a 120 mg mL⁻¹ solution of α CD. The polymer solution became transparent upon addition of 1.0 equivalent of the cyclodextrin host (Figure 5.3.4, top picture). The PEtOx₉₀-*ran*-PNonOx₁₂ random copolymer exhibited a cloud-point solubility phase transition at *ca.* 10 °C, passing from a clear transparent solution to a white opaque solution when heated beyond this temperature. This translated into a sharp drop in the % transmittance, from *ca.* 100 % to *ca.* 0 %, as measured by temperature-dependent turbidimetry. As seen in Figure 5.3.4., the addition of increasing amounts of α CD to the copolymer solution resulted in a progressive increase of the T_{CP}.

The T_{CP} increased from 10 °C for the free copolymer to *ca.* 40 °C in the presence of 2 equivalents of α CD in relation to the nonyl chains. The T_{CP} did not linearly increase with the concentration of cyclodextrin added but, instead, it followed a logarithmic trend towards higher temperatures. This is in agreement with the evolution of any observable shift due to a supramolecular association, leading to a plateau value at full complexation.^[80, 81] It thus seems that the fully complexed copolymer- α CD ensemble exhibits a phase transition in the ballpark of 40 °C. To assess the binding constant associated to the complex formation and its stoichiometry, isothermal titration calorimetry (ITC) measurements were performed on the copolymer- α CD couple; however, due to the need for cooling to temperatures close to 0 °C to ensure complete copolymer dissolution, the measurements were affected by large environmental thermal variations and, as a result, the titration process yielded unclear results. Nevertheless, considering the length of a fully stretched nonyl alkylic chain, of *ca.* 1.1 nm, and the longitudinal size of the cyclodextrin cavity (0.79 nm), a 1:1 stoichiometry is proposed. Later on, this statement will be supported by non-linear fitting of the T_{CP} values against the corresponding cyclodextrin/nonyl ratios (*vide infra*), that yielded a good fitting when applying a 1:1 binding stoichiometry model.

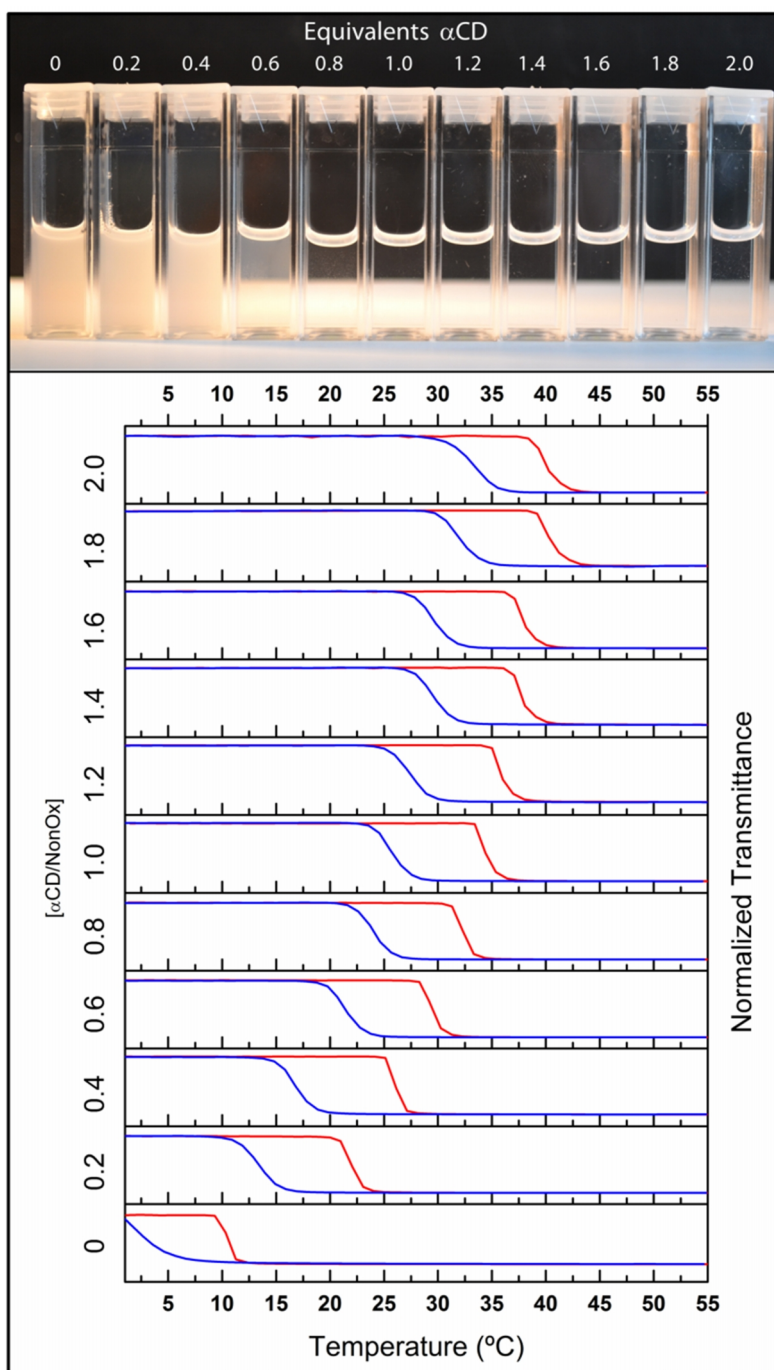


Figure 5.3.4. Turbidimetry studies of 5 mg mL^{-1} solutions of $\text{P}[(\text{EtOx})_{90}\text{-ran-}(\text{NonOx})_{12}]$ with increasing $\alpha\text{CD}/\text{NonOx}$ molar ratios. The heating and cooling ramps are represented by the top (red) and bottom (blue) curves, respectively. Rate: 1 K min^{-1} , $\lambda = 700 \text{ nm}$. The top picture displays the corresponding samples after being cooled to $0 \text{ }^{\circ}\text{C}$ and then let to warm to room temperature. At least 1.0 equivalent of αCD is necessary to keep the solution transparent at room temperature.

All the solutions exhibited a marked solubility hysteresis behavior of *ca.* 10 K. This hysteresis is ascribed to kinetic reasons, due to the relatively fast heating/cooling rate applied (1 K min^{-1}), that does not allow sufficient time for the copolymer-cavitand inclusion complexes to break/re-form. This is also applicable to the free copolymer, whose aggregates require a certain amount of time to re-hydrate from the collapsed globular conformation. To prove this hypothesis, and rule out the possibility of a thermodynamically stable hysteresis, isothermal turbidimetry experiments were performed on the sample containing 1.0 equivalent αCD . The solution was heated at 1 K min^{-1} to

30 °C, that lays in central part of the hysteresis window. Temperature was then maintained stable and the evolution of the solution transmittance was followed during 2 hours. In analogy, the solution was heated to 55 °C, provoking the collapse of the copolymer and the appearance of a white opaque solution, and subsequently cooled at 1 K min⁻¹ to 30 °C, where the transmittance was monitored in time. As seen in Figure 5.3.5, the previously heated solution (blue curve) remained mostly opaque. On the other hand, the previously cooled transparent solution became turbid, quickly losing 50 % transmittance during 20 minutes, as a result of the breakage of copolymer- α CD inclusion complexes and the consequent collapse of the copolymer chains.

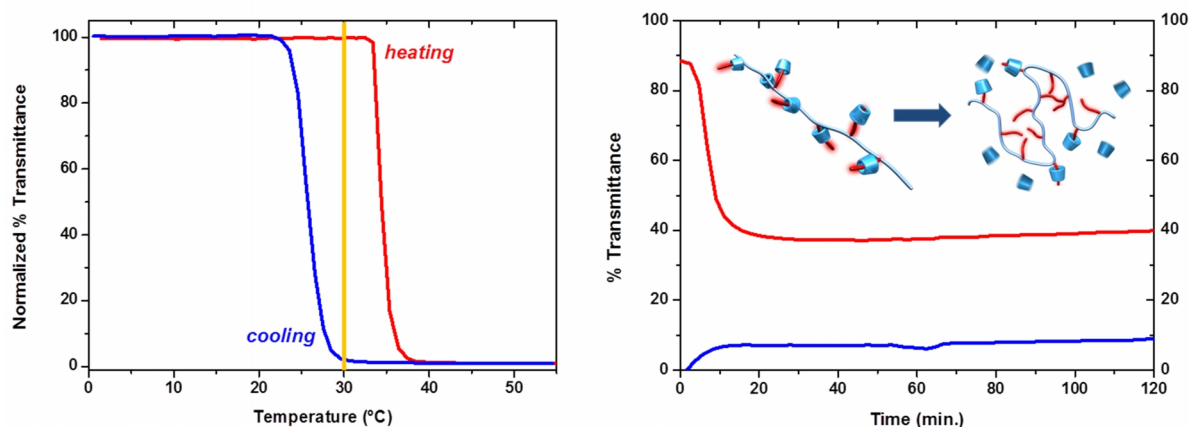


Figure 5.3.5. *Left: Temperature-dependent turbidimetry studies of a 5 mg mL⁻¹ solution of P[(EtOx)₉₀-ran-(NonOx)₁₂] in the presence of 1.0 equivalent of α CD (relative to nonyl chains), were a hysteresis of ca. 10 K can be observed. Right: Evolution of the transmittance in time of the same solution at isothermal conditions (30 °C) during 120 minutes. The sample was cooled to ca. 0 °C (top curve) or heated to 55 °C (bottom curve) and brought to 30 °C at 1K min⁻¹ before starting the measurements. As can be seen, the copolymer- α CD inclusion complexes partially disassemble during the first 20 min., resulting in a 50% decrease in transmittance. $\lambda = 700$ nm.*

Although the decay in transmittance occurred rapidly, it stabilized at ca. 40 % transmittance, indicating partial but not total breakage of the copolymer- α CD inclusion complexes. Therefore, it can be concluded that the hysteresis observed arises from the experimental conditions, due to the relatively fast heating/cooling rate of 1 K min⁻¹ applied, and partially from thermodynamic reasons, *i.e.* the need of applying a different temperature to fully break the inclusion complexes (higher) than to re-form them (lower).

Temperature dependent dynamic light scattering (DLS) studies were also performed to investigate the nature of the formed aggregates and their evolution with temperature after long equilibration times (heating/cooling rate of approximately 0.01 K min⁻¹). Therefore, a solution of the P[EtOx₉₀-ran-PNonOx₁₂] copolymer in the presence of 1.0 equivalent of α CD was prepared, and its particle size distribution monitored while temperature was varied from 15 to 50 °C (red curve) and back to 15 °C (blue curve).

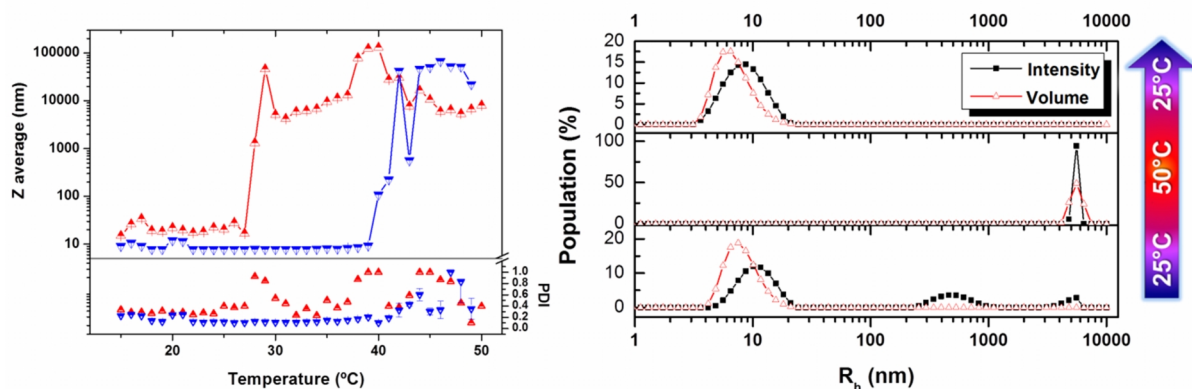


Figure 5.3.6. Temperature-dependent Dynamic Light Scattering (DLS) data for a 5 mg mL⁻¹ solution of P[(EtOx)₉₀-ran-(NonOx)₁₂] and 1.0 equivalent of αCD (relative to nonyl side chains). Left: Z average and PDI evolution with temperature. ▲ heating; ▼ cooling. Random coil copolymer-cyclodextrin ensembles are formed at low temperature and are stable up to ≈33 °C (transparent solution); above this temperature, large aggregates are formed (opaque solution), that eventually precipitate (Note the logarithmic scale of the Z_{ave} axis). Four measurements are averaged at every temperature. Approximate heating/cooling rate: ≈ 0.01 K min⁻¹. Right: Particle size distribution of the sample at 25 °C, 50 °C and back to 25 °C. At 25 °C random coil copolymers, together with a small fraction of aggregates are observed. Heating to 50 °C leads to the abrupt appearance of large aggregates. Back to 25 °C, the large aggregates have re-dissolved and only free polymer chains are observed.

As seen in Figure 5.3.6, at 25 °C, soluble copolymer-αCD ensembles (≈ 11 nm, PDI = 0.30) constitute the majority of the solution, that also contains a small fraction of large aggregates (≈ 850 and 4300 nm, as seen in the size distribution). Upon heating the solution, a sharp transition towards large aggregates of *ca.* 10 μm in size arises. The transition temperature, of *ca.* 28 °C, is lower than the T_{CP} of 34 °C measured in turbidimetry experiments, laying in between the cloud and the clearance point temperatures (red and blue curves in Figure 5.3.4). The difference between the T_{CP} measured by temperature-dependent turbidimetry and by DLS arises from the different heating rates used in both experiments, of 1 K min⁻¹ and ≈ 0.01 K min⁻¹, respectively. The slow heating/cooling rate in DLS experiments allows sufficient time for the most thermodynamically stable aggregate structures to form whereas, in turbidimetry measurements, a faster heating rate is applied allowing the presence of metastable soluble copolymer-αCD structures.

Following the cooling curve in the T-dependent DLS plot, an apparent hysteresis behavior is observed. However, the disappearance of the large aggregates is actually originated from their collapse into large macroscopic particles that precipitate to the bottom of the cuvette, and thus become undetectable as confirmed by visual inspection. This is a result of the long exposure to high temperatures of the solution containing large 10 μm particles. These large aggregates re-dissolved when the solution was cooled back to 25 °C, resulting in an aggregate-free, colorless transparent solution consisting of random coil copolymer-αCD ensembles (Z_{ave} = 8 nm, PDI = 0.12).

To understand the dynamics of the cyclodextrin-PEtOx-*ran*-PNonOx host guest complexation, and answer the question of whether the nonyl-cyclodextrin inclusion complexes are fixed or involved in a constant exchange, a competitive guest test was performed. Cyclohexanol was selected as a competitive guest, as it is known that it has similar but somewhat lower affinity for αCD (K_a ≈ 10¹ M⁻¹) and can effectively compete with the alkyl chain hosts (K_a ≈ 10² M⁻¹).^[57] A solution of PEtOx₉₀-*ran*-PNonOx₁₂ was therefore prepared in the presence of 2 equivalents of αCD. The T_{CP} of this solution was *ca.* 38 °C. Four equivalents of cyclohexanol were then added to this solution as

a competitive guest for binding to α CD, lowering the T_{CP} to *ca.* 32 °C as a result of their complexation with part of the α CD in solution (see Figure 5.3.7).

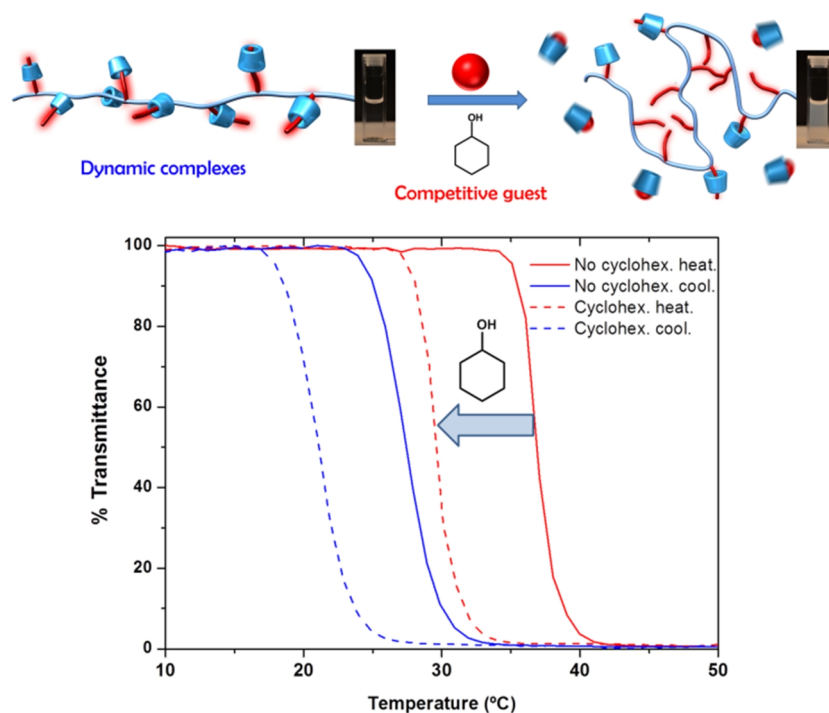


Figure 5.3.7. Cyclodextrins form dynamic complexes with the PEtOx-*ran*-PNonOx copolymer, as proven through the addition of cyclohexanol to a solution containing copolymer-CD ensembles. Turbidimetry shows a decrease of the T_{CP} from \approx 38 °C to \approx 32 °C upon addition of the cyclohexanol competitive guest.

To summarize, α CD formed dynamic inclusion complexes with the nonyl side chains borne by the PEtOx₉₀-*ran*-PNonOx₁₂ copolymer, rendering them hydrophilic and consequently producing a shift in its T_{CP} towards higher temperatures. The extent of the temperature shift was correlated with the ratio of α CD to nonyl chains present in solution (see Figure 5.3.8)

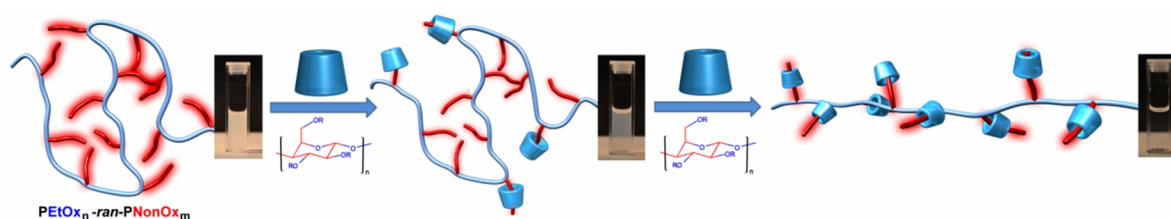


Figure 5.3.8. Schematic representation of the progressive solubilization observed for the amphiphilic PEtOx-*ran*-PNonOx copolymer in the presence of increasing concentrations of cyclodextrin hosts. Cyclodextrins render the aliphatic nonyl chains hydrophilic by inclusion complex formation.

Once this good understanding of the host-guest complexation between the PEtOx₉₀-*ran*-PNonOx₁₂ nonyl side chains and the α CD host molecule was achieved, the attention was focused on evaluating the influence of different hosts on the supramolecular association and its consequences on the copolymer thermoresponsive properties.

5.3.4. Effect of the Supramolecular Host: Hydroxypropyl- α -cyclodextrin (HP α CD), Hydroxypropyl- β -cyclodextrin (HP β CD) and Curcubit[7]uril (CB[7])

In this part of the study, we investigated the effect of partial substitution of the cyclodextrin hydroxyl groups by hydroxypropyl units on the host-guest complex formation, by using hydroxypropyl- α -cyclodextrin (HP α CD). The average degree of hydroxypropyl substitution per glucose unit was of 0.6 (average of 3.6 HP groups per α CD molecule) as determined by $^1\text{H-NMR}$ spectroscopy. Subsequently, the effect of an extended cavity size of the host was assessed by employing HP β CD, which features one extra glycopyranose unit, with the same hydroxypropyl degree of substitution. Finally, a different host, curcubit[7]uril (CB[7]), provided by Prof. Werner Nau from Jacobs University, Bremen, Germany, a relatively rigid host known to establish strong inclusion complexes with hydrophobic molecules, was tested.^[77] Unlike cyclodextrins, that exhibit a tapered cylinder shape with one opening wider than the other, CB[7] is symmetrical with both portals having the same size. CB[7] is slightly more voluminous than β CD, being also larger in the longitudinal axis (9.1 Å instead of 7.9 Å for cyclodextrins) and exhibits a relatively low solubility, similar to that of β CD. In contrast with the slightly positively polarized cyclodextrins, CB[7] shows a negative electrostatic potential around the portals, increasing its tendency to bind with cationic guests and enabling the formation of strong charge-dipole interactions with the guest (Figure 5.3.9). CB[7] has been found to exhibit a remarkably high binding affinity towards a variety of hydrophobic guests, including linear aliphatic chains,^[82, 83] therefore becoming a promising candidate to establish strong host-guest complexes with the PEtOx-*ran*-PNonOx copolymer nonyl chains.

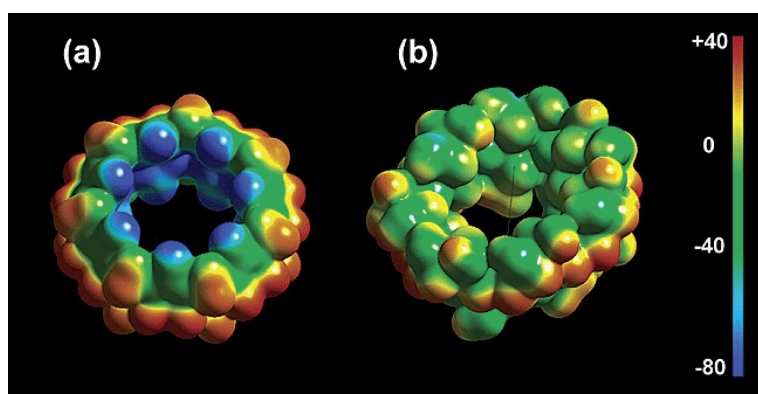


Figure 5.3.9. *Electrostatic potential maps for a) CB[7] and b) β CD. The structure of CB[7] exhibits a higher degree of symmetry than that of β CD. The electrostatic potential at the portals and within the cavity of CB[7] is significantly more negative than for β CD. Scale bar: +40 kcal mol⁻¹ to -80 kcal mol⁻¹.*^[84]

In analogy to the protocol performed earlier for α CD, a 5 mg mL⁻¹ solution of the PEtOx₉₀-*ran*-PNonOx₁₂ random copolymer was prepared in an ice bath, and different aliquots of this solution were titrated with a stock solution of each cavitaand. Temperature-dependent turbidimetry experiments were subsequently performed. As seen in Figure 5.3.10, all the tested supramolecular hosts produced an increase in the solubility phase-transition temperature of the PEtOx₉₀-*ran*-PNonOx₁₂ copolymer, indicating the formation of host-guest complexes.

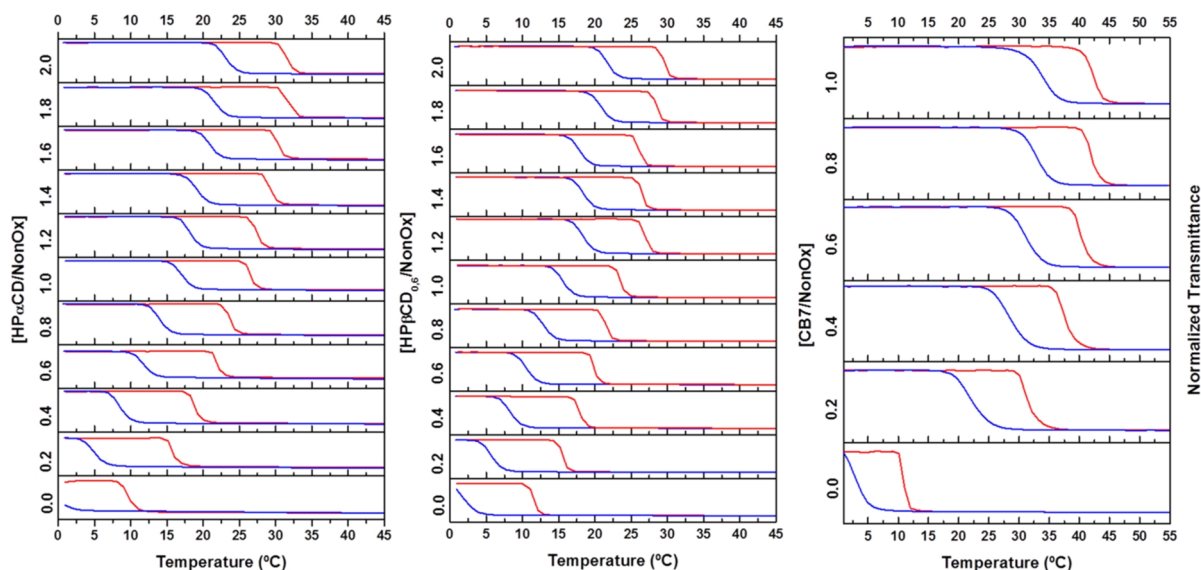


Figure 5.3.10. Turbidimetry studies of 5 mg mL^{-1} solutions of $PI(EtOx)_{90}\text{-ran-}(NonOx)_{12}$ with increasing cavitand/NonOx molar ratios. The heating and cooling ramps are represented by the top (red) and bottom (blue) curves, respectively. Rate: 1 K min^{-1} , $\lambda = 700 \text{ nm}$. At least 1.2 equivalents of $HP\alpha CD$ or $HP\beta CD$ are necessary to keep the solution transparent at room temperature, in contrast to less than 0.2 equivalents of $CB[7]$.

Several studies have explored the impact of chemical modification on the cyclodextrin binding abilities. In particular, partial substitution of the cyclodextrin hydroxyl groups by hydroxypropyl is thought to affect complexation in two opposite ways.^[50, 85-87] First, a negative effect has been ascribed to the steric blockage of the cyclodextrin cavity entrance by hydroxypropyl groups, sterically hindering inclusion complex formation. Secondly, as previously described, chemical modification disrupts the cyclodextrin intramolecular hydrogen-bond network resulting in the extension of the hydrophobic cavity. The larger hydrophobic surface can then lead to increased interactions with the hydrophobic guest, leading to stronger host-guest complexation.^[51, 73, 75, 88, 89]

Analysis of the results indicates that, even though the hydrophilicity of $HP\alpha CD$ is much higher than that of native αCD , host-guest complexation with the copolymer had a lower impact on its T_{CP} . This is illustrated by the variation on T_{CP} obtained upon addition of 1.0 equivalent of the cavitand, which increased by 24 K with αCD and only by 17 K with $HP\alpha CD$. The lower impact of $HP\alpha CD$ on the T_{CP} is ascribed to a lower association constant between $HP\alpha CD$ and nonyl chains. This is possibly related to the steric hindrance exerted by the hydroxypropyl groups that partially block the cyclodextrin cavity entrance, sterically hindering inclusion complex formation.^[75, 85, 87] Considering the tight fit between alkyl chains and αCD , in combination with the large polymer structure, it is reasonable to assume a relatively large impact of steric effects on the inclusion complex formation.

On the other hand, the negative contribution of the hydroxypropylation due to steric reasons should have a minor effect on the larger cavity of $HP\beta CD$. This is demonstrated by the turbidimetry results, showing a displacement of the copolymer T_{CP} comparable to that produced by $HP\alpha CD$. Therefore, in the case of $HP\beta CD$, the positive contribution of the extended hydrophobic cavity seems to positively affect its binding affinity bringing it close to $HP\alpha CD$, even though it is known that βCD undergoes rather weak binding with small alkyl chains due to loose host-guest fitting.^[72]

Both modified cyclodextrins seem, therefore, to form weaker host-guest complexes with the PEOx-*ran*-PNonOx copolymer nonyl side chains than the native α CD. On the other hand, addition of curcubit[7]uril (CB[7]) to the copolymer solution exerted a remarkable displacement of its T_{CP} . Whereas at least 1.2 equivalents of hydroxypropylated cyclodextrins were necessary to maintain the copolymer in solution at 25 °C, the same result was achieved with less than 0.2 equivalents of CB[7]. Considering the relatively low hydrophilicity of CB[7], these observations indicate that the stability of host-guest complexes between the copolymer pendant nonyl chains and CB[7] largely surpasses that of those formed with any of the cyclodextrins tested. The symmetry of the CB[7] molecule, that features the same size in both cavity entrances, may relate to a higher tendency to thread along the nonyl chains forming pseudorotaxanes. In addition, CB[7]'s higher rigidity in comparison to cyclodextrins is expected to translate into a higher binding stability constant, as has been reported for a variety of hydrophobic guests.^[77] The titration of the PEOx-*ran*-PNonOx solution could not be continued beyond 1.0 equivalent due to the relatively low water solubility of CB[7], of ≈ 20 mM at 25 °C. Figure 5.3.11 displays an overview of the titrations performed with all cavitands, where CB[7] and α CD stand out over the hydroxypropylated cyclodextrins with regard to increase of the T_{CP} upon host-guest complexation.

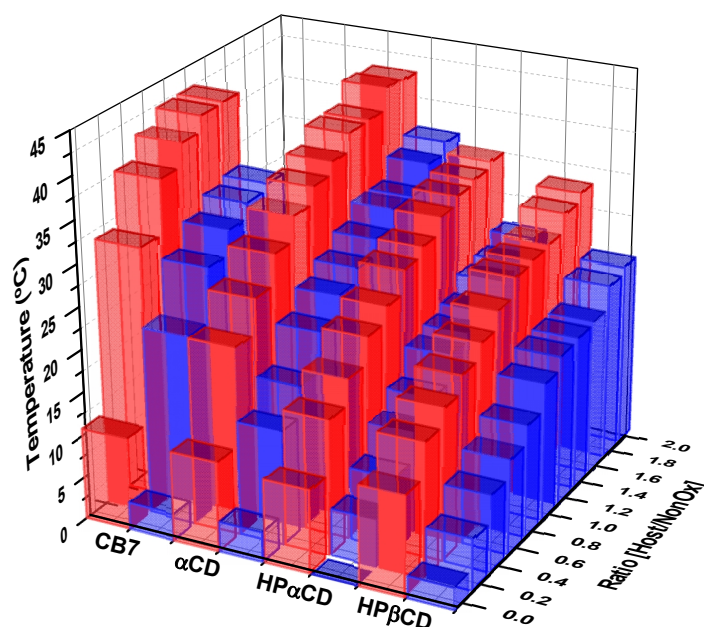


Figure 5.3.11. Overview of the temperature-dependent turbidimetry titrations performed with CB[7], α CD, HP α CD, and HP β CD. The red bars represent the T_{CP} upon heating, and the blue ones upon cooling. CB[7] clearly produces the steepest increase in T_{CP} , followed by α CD. HP α CD and HP β CD provided the lowest increase in T_{CP} . The T_{CP} values plateau at different temperatures for each cavitand in an order unrelated with its hydrophilicity, therefore indicating that T_{CP} is mostly controlled by the cavitand binding constant to nonyl chains.

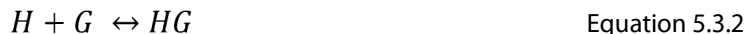
Importantly, at high cavitand concentrations, the T_{CP} of the copolymer-cavitand solution was found to be highest for CB[7] and α CD that are, especially in the case of CB[7], the least hydrophilic supramolecules of the series. This indicates that the temperature-triggered phase transition occurs as a result of host-guest complex breakage. If the T_{CP} of the copolymer-cavitand ensemble would be responsible for the observed phase separation, the observed order of T_{CP} increase should be reversed, being the highest for hydroxypropylated-cyclodextrins, which truly constitute the most hydrophilic molecules of the series.

As noted earlier, isothermal titration calorimetry was explored as a method to determine the thermodynamic parameters associated with the host-guest complexation. However, the low temperatures needed to keep the free copolymer in solution complicated the measurements and led to inconclusive results. Therefore, since T_{CP} increase was found to be directly correlated to host-guest complex stability, we evaluated the possibility of using the variation of T_{CP} as a measure to calculate the binding constant of the investigated supramolecular host molecules with the PEOx-*ran*-PNonOx nonyl chains. T_{CP} , as a property proportional to the concentration of nonyl-cavitand inclusion complexes, seemed to be suitable to perform these calculations.^[90] It should be noted, however, that the association constant is temperature-dependent, as it is related to the molar Gibbs free energy of the process (ΔG).

$$K_a = e^{-\frac{\Delta G}{RT}} \quad \text{Equation 5.3.1}$$

Nevertheless, considering that the temperature range at which the T_{CP} variations occur is restricted to $\approx 20 - 30$ K, a minor effect of temperature over the association constant values may be assumed. Being aware of the limitations of this method, and the approximations made, the calculated values should be taken for comparative reasons and as an indication of the order of magnitude for the actual binding constants.

Once the method constraints have been stated, let us consider the equilibrium between the copolymer nonyl chains and the supramolecular host molecule. For simplicity, the copolymer solution will be modelled as a solution containing individual nonyl chains. Considering, as has been discussed earlier, a 1 : 1 equilibrium between nonyl chain guest (G) and supramolecular host (H) species,



the equilibrium constant is described by the following expression

$$K_a = \frac{[HG]}{[H][G]} \quad \text{Equation 5.3.3}$$

where K_a is the binding constant, $[HG]$ the molar concentration of cavitand-nonyl host-guest complexes, and $[H]$ and $[G]$ the molar concentrations of cavitand host and nonyl chain guest, respectively.

In the equilibrium, the fraction of nonyl chains complexed with a host molecule is defined as p , according to the expression

$$p = \frac{[HG]}{[G]_t} \quad \text{Equation 5.3.4}$$

where $[G]_t$ represents the total concentration of nonyl chains.

Denoting the T_{CP} property as X , and considering that the observed T_{CP} (X_{obs}) corresponds to the T_{CP} inherent to the copolymer (uncomplexed nonyl chains) and a contribution from the copolymer-host ensemble (complexed nonyl chains), the observed T_{CP} can be described as

$$X_{obs} = X_0 + pX_{HG} \quad \text{Equation 5.3.5}$$

Where X_0 corresponds to the T_{CP} inherent to the copolymer, p is the fraction of complexed nonyl chains, and X_{HG} is the T_{CP} of the copolymer where all the nonyl chains are complexed.

Considering that

$$[G]_t = [G] + [HG] \quad \text{Equation 5.3.6}$$

and introducing Equation 5.3.3, p can be rewritten as

$$p = \frac{[HG]}{[G]_t} = \frac{[HG]}{[G] + [HG]} = \frac{K_a[H]}{1 + K_a[H]} \quad \text{Equation 5.3.7}$$

that can be introduced in Equation 5.3.5, finally yielding

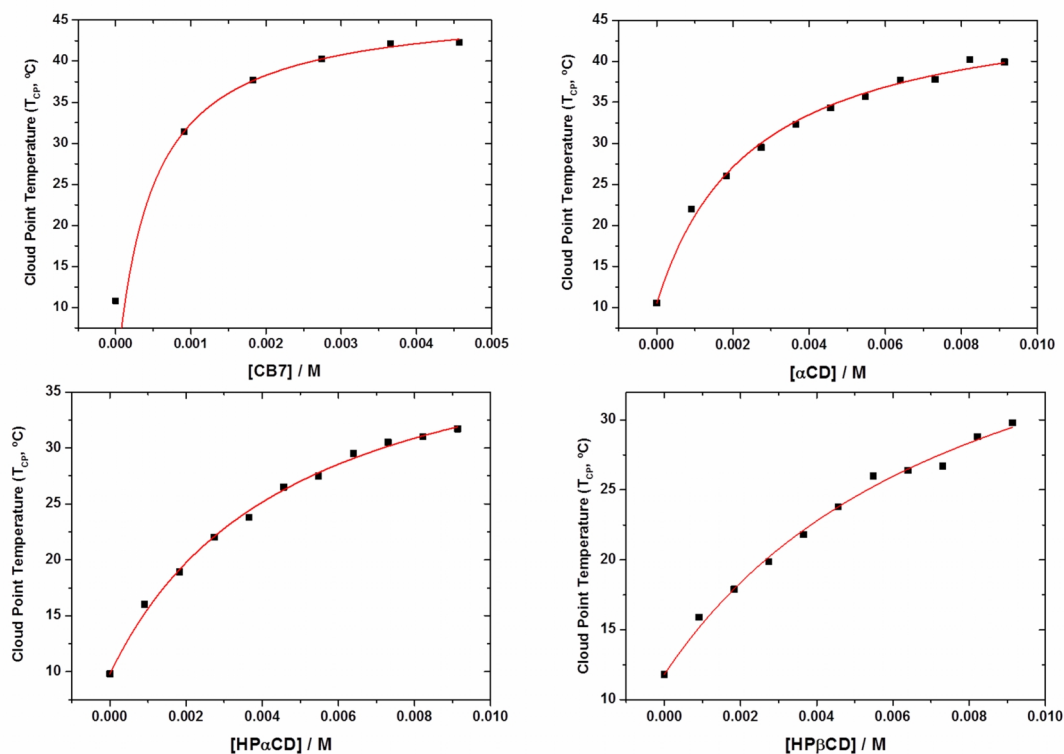
$$X_{obs} = X_0 + X_{HG} \frac{K_a[H]}{1 + K_a[H]} \quad \text{Equation 5.3.8}$$

This equation describes the titration curve in function of the variable $[H]$. Therefore, the T_{CP} values found for each turbidimetry titration were represented against the corresponding host concentration. Non-linear curve fitting of the data using Equation 5.3.8 allowed to calculate the binding constant (K_a) for each supramolecular host investigated and also estimate the T_{CP} value for complete copolymer complexation (X_{HG}) (see Figure 5.3.12)

The calculated binding constant for α CD-nonyl complexation is $K_a \approx 401 \pm 35 \text{ M}^{-1}$, twice the value found for HP α CD which in turn exhibits a value 70 % higher than that of HP β CD. CB[7] clearly forms the strongest host-guest complexes, with a $K_a \approx 2100 \pm 1600 \text{ M}^{-1}$. It should be noted that all the calculated K_a values for cyclodextrin hosts have an associated standard deviation of *ca.* 10 %, whereas CB[7] suffers a larger uncertainty. This is a result of the lower number of titration steps performed (6 instead of 11), especially in the concentration range that provides intermediate complexation ($0 \leq [CB[7]] \leq 1 \text{ mM}$).

In conclusion, a wide range of supramolecular hosts has been shown to form host-guest complexes with the aliphatic nonyl chains present in a thermoresponsive PEtOx₉₀-*ran*-PNonOx₁₂ copolymer. These inclusion complexes are dynamic and maintain the copolymer in solution as a random coil. The temperature-induced breakage of the inclusion complexes constitutes the driving force for the copolymer phase transition, which is thus tuned by the stability of the host-guest complexes. Titration of a copolymer solution with the supramolecular host, followed by temperature dependent turbidimetry allowed the estimation of the average binding constant of the nonyl chains with each cavitand. The order in affinity between nonyl chains and the investigated cavitands was found to be: CB[7] \gg α CD > HP α CD > HP β CD.

The large association constant of nonyl chains with CB[7] was ascribed to its rigidity and cylindrical shape, that is thought to facilitate threading through the alkylic chain pseudo-rotaxane formation. α CD forms relatively strong host-guest complexes with alkyl chains, due to its tight fit with the nonyl alkyl chains, as has been previously reported. On the other hand, HP α CD binding is possibly penalized by the steric hindrance associated to the introduction of hydroxypropyl groups at the cavity entrances. HP β CD is less affected due to its larger cavity diameter, and advantages from an extended hydrophobic surface, which partially compensate its worse fit with the small nonyl alkyl chains.



ID	Cyclodextrin	Non-linear fitting		
		R ²	K _a [M ⁻¹]	T _{CP} (HG) [°C]
αCD	Alpha-cyclodextrin	0.994	401 ± 35	47 ± 1
HPαCD	Hydroxypropyl-alpha-cyclodextrin	0.997	210 ± 16	43 ± 1
HPβCD	Hydroxypropyl-beta-cyclodextrin	0.992	121 ± 17	45 ± 3
CB7	Curcubit[7]uril	0.84	2166 ± 1620	47 ± 6

Figure 5.3.12. Turbidimetry titration curves corresponding to 5 mg mL⁻¹ solutions of PEtOx₉₀-*ran*-PNonOx₁₂ and non-linear curve fitting based on Equation 5.3.8. Below: Overview of the obtained data. The average stability constants between the copolymer nonyl chains and cavitands follow the order: CB[7] >> αCD > HPαCD > HPβCD.

5.4 Influence of nonyl side chain content: poly(2-ethyl-2-oxazoline)-*ran*-poly(2-nonyl-2-oxazoline) containing 20% nonyl chains

Once the effect of the supramolecular hosts was evaluated, the focus was set on varying the content of nonyl side chains in the copolymer and studying its influence on the solubility phase transition of the supramolecular system.

To this purpose, a PEtOx-*ran*-PNonOx with the same length as the previously evaluated copolymer, but a higher content of nonyl side chains was synthesized. The obtained PEtOx₈₄-*ran*-PNonOx₂₁ copolymer contained 20 % nonyl chains in number, therefore roughly doubling the NonOx content of the previously discussed PEtOx₉₀-*ran*-PNonOx₁₂ copolymer. The additional NonOx content made this copolymer insoluble in water, and therefore the addition of host molecules to the solution, followed by freezing and thawing under sonication in an ice-bath was necessary to

bring the copolymer in solution. This protocol seemed to favor the formation of inclusion complexes with the nonyl chains affording the solubilization of the copolymer.

In analogy to the previously described study, a 5 mg mL^{-1} solution of the $\text{PEtOx}_{84}\text{-}ran\text{-PNonOx}_{21}$ random copolymer was prepared and titrated with different cavitands, while monitoring the evolution of the copolymer T_{CP} . However, since this copolymer was insoluble in water, the solubilization had to be performed in the presence of hosts. The cavitands that exhibited a stronger binding constant with nonyl chains in part 5.3 were selected to perform these studies, namely CB[7], αCD , and $\text{HP}\alpha\text{CD}$. To be able to titrate CB[7], due to its relatively low solubility, a 2 mg mL^{-1} solution of the copolymer was used. As seen in the previous study, the temperature-triggered phase transition of all solutions could be tuned by the addition of the cavitands (see Figure 5.4.1).

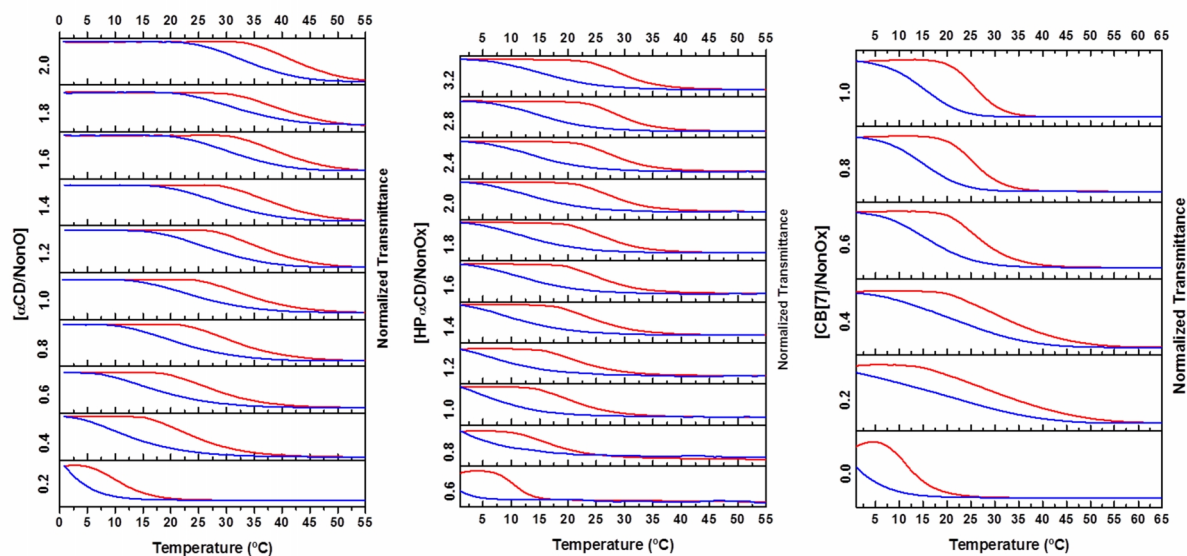


Figure 5.4.1. Turbidimetry studies of $P[(\text{EtOx})_{84}\text{-}ran\text{-}(\text{NonOx})_{21}]$ with increasing cavitand/NonOx molar ratios. 5 mg mL^{-1} solutions of copolymer were titrated with αCD and $\text{HP}\alpha\text{CD}$, whereas a 2 mg mL^{-1} solution of copolymer was titrated with CB[7]. The heating and cooling ramps are represented by the top (red) and bottom (blue) curves, respectively. Rate: 1 K min^{-1} , $\lambda = 700 \text{ nm}$.

However, instead of a sharp shift in transmittance, the transition was now much more progressive. Since the solubility phase-transition is produced by the disassembly of the host-guest complexes, the progressive transition observed here indicates slow kinetics in the breakage/formation of the cavitand-nonyl host-guest complexes. This can be explained by the larger hydrophobicity of the copolymer that forms kinetically-trapped nanoparticles entrapping the cavitands and partially isolating them from the surrounding aqueous solution. This hypothesis was evaluated by temperature-dependent DLS measurements, that showed the formation of well-defined nanoparticles beyond *ca.* $20 \text{ }^\circ\text{C}$. As seen in Figure 5.4.2, at low temperatures a single particle distribution of *ca.* 10 nm in size ($\text{PDI} = 0.15$) is observed. This is ascribed to the formation of well hydrated random-coil copolymer-cavitand ensembles, and is analogous to the behavior observed for the previously studied copolymer containing 12% NonOx. However, upon heating beyond the T_{CP} , at *ca.* $22 \text{ }^\circ\text{C}$, instead of large $>1000 \text{ nm}$ aggregates, the formation of moderate size well-defined nanoparticles is observed ($\approx 250 \text{ nm}$, $\text{PDI} < 0.15$). The slow heating/cooling rate applied in the DLS experiments ($\approx 0.01 \text{ K min}^{-1}$) grants the copolymer-cavitand ensembles with the sufficient time to change their conformation and adapt to the progressive temperature-induced breakage of

nonyl-cavitand inclusion complexes. The nanoparticles slowly increased in size with temperature, possibly due to the incorporation of extra copolymer chains during heating or due to further agglomeration of the initially formed nanoparticles.

The lower binding constant of HP α CD with nonyl chains produces in this case a marked impact on the cloud point temperatures, that increase much less than when α CD is added. In fact, 0.6 equivalents of HP α CD were necessary to solubilize the copolymer at near-zero degrees, in contrast to only 0.2 equivalents of α CD. On the other hand, the similar progressive decay in transmittance in the presence of HP α CD suggests the formation of kinetically-trapped structures as in the case of α CD.

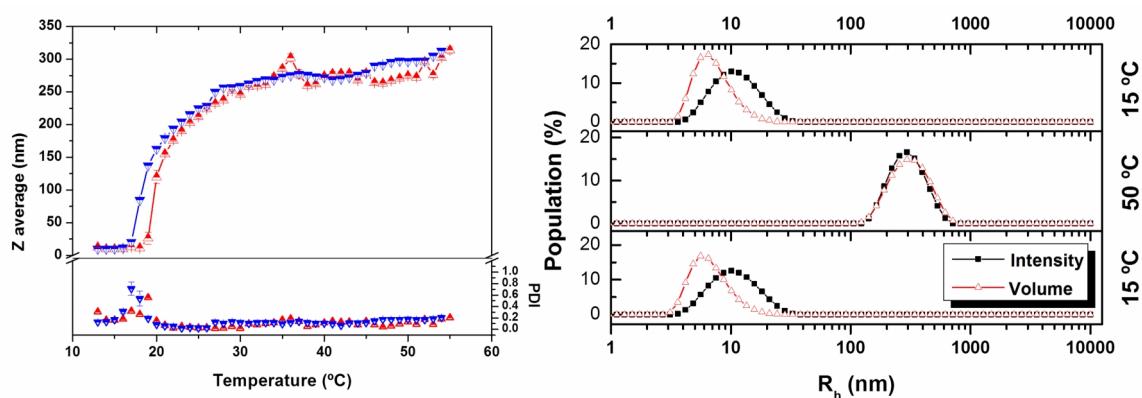


Figure 5.4.2. Temperature-dependent Dynamic Light Scattering (DLS) data for a 5 mg mL⁻¹ solution of P[(EtOx)₈₄-ran-(NonOx)₂₁] and 1.0 equivalent of α CD (relative to nonyl side chains). Left: Z average and PDI evolution with temperature. \blacktriangle heating; \blacktriangledown cooling. Random coil copolymer-cavitand ensembles are formed at low temperature and are stable up to ≈ 20 °C (transparent solution); above this temperature, the copolymer-cavitand ensembles re-arrange of into well-defined nanoparticles (279 nm, PDI = 0.090 at 50 °C). Four measurements are averaged at every temperature. Approximate heating/cooling rate: ≈ 0.01 K min⁻¹. Right: Particle size distribution of the sample at 15 °C, 50 °C and back to 15 °C. At 15 °C copolymer-cavitand ensembles are observed. Heating beyond 20 °C leads to the formation of well-defined nanoparticles that slowly grow with temperature (279 nm, PDI 0.090 at 50 °C). Back to 15 °C, the host-guest complexes re-form and random coil copolymer ensembles are observed (10 nm, PDI = 0.136).

On the other hand, CB[7] produced an apparent large impact on the T_{CP} initially but, overall, did not have a large effect on the copolymer T_{CP}. Temperature dependent DLS studies were performed in samples containing 0.2 and 1.0 equivalent of CB[7] to investigate the reasons behind this behavior. The sample containing 0.2 equivalents of CB[7] showed the absence of nanoparticle formation and the presence of large aggregates, even at low temperatures. This is manifested by the high PDI values observed below 20 °C in the DLS data (Figure 5.4.3). Possibly, the lower hydrophilicity of the macromolecule constitutes an obstacle to disrupt the compact copolymer globules, which are stabilized by hydrophobic interactions between the nonyl side chains. One equivalent of the cavitand was sufficient to form random coil copolymer ensembles of ≈ 9 nm in size, but these coexisted with aggregates with a variety of sizes (PDI ≈ 0.8). Temperatures above 20 °C produced the collapse of the small aggregates (40 – 100 nm) into large particles in the micrometer range.

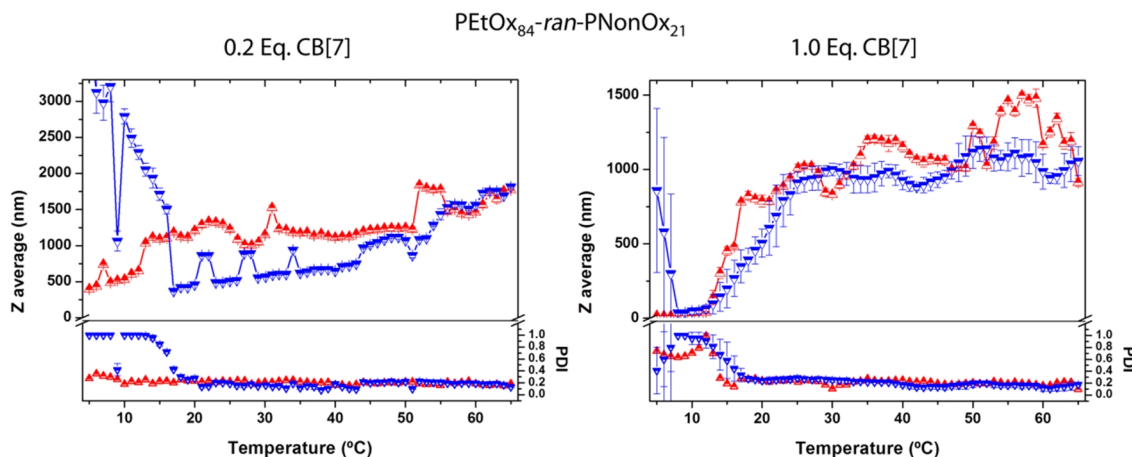


Figure 5.4.3. Temperature-dependent Dynamic Light Scattering (DLS) data for a 2 mg mL^{-1} solution of $P[(\text{EtOx})_{84}\text{-ran-(NonOx)}_{21}]$ in the presence of 0.2 or 1.0 equivalent of CB[7] (relative to nonyl side chains). Z average and PDI evolution with temperature: \blacktriangle heating; \blacktriangledown cooling. 0.2 Eq. CB[7]: At low temperatures, ill-defined aggregates are formed. Upon heating, macromolecular precipitates appear, that partially re-dissolve upon cooling below 20°C , resulting in an increase in the Z_{ave} . 1.0 Eq. CB[7]: At low temperature, random coil ensembles ($\approx 9 \text{ nm}$) coexist with aggregates of sizes from 40 to 300 nm. Beyond 20°C , large aggregates are formed. Four measurements are averaged at every temperature. Approximate heating/cooling rate: $\approx 0.01 \text{ K min}^{-1}$.

To summarize, the increment in NonOx content in the copolymer to 20% had a strong impact on its solubility properties. The copolymer was water insoluble and could only be brought in solution in the presence of cavitands. The increased number of nonyl groups per copolymer chain induced the formation of kinetically-trapped nanoparticles in solution when sufficiently hydrophilic cavitands, *i.e.* αCD and $\text{HP}\alpha\text{CD}$ were present. In this case, the optimal balance of binding affinity to nonyl chains and hydrophilicity was found with native αCD .

5.5 Highly hydrophobic copolymers: poly(2-ethyl-2-oxazoline)-*ran*-poly(2-nonyl-2-oxazoline) containing 25% and 30% nonyl chains

In part 5.4 we have seen that a 20% content of NonOx in the copolymer began to induce its self-assembly behavior in solution giving rise to kinetically-trapped nanoparticles. To evaluate the possibility to enhance this behavior, two copolymers with the same chain length (≈ 100 repeating units) and higher NonOx contents of 25% and 33% were synthesized (SN25 and SN33, respectively). The copolymers were dissolved in the presence of αCD following the same protocol as described for the previous copolymer with 20% NonOx. Due to the higher hydrophobicity of the newly synthesized copolymers, a higher concentration of αCD was necessary to solubilize the copolymers. One equivalent of αCD was required to solubilize SN25, whereas the more hydrophobic SN33 could only be solubilized in a near-saturated solution of the cavitand. Therefore, the more hydrophilic $\text{HP}\alpha\text{CD}$, with a solubility of over 600 mg mL^{-1} was utilized, whereby more than 1.7 equivalents of the cavitand were employed to solubilize the copolymer. Strong hydrophobic interactions established among the nonyl chains are proposed to hinder the access of the host molecules, that disrupt the hydrophobic copolymer association and progressively extend the polymer chain, opening up new nonyl chains for complexation. Thus,

repeated cycles of freezing and thawing the solution under sonication at 0 °C were found to be required to solubilize the copolymer.

Figure 5.5.1 shows the results of the titration of both copolymers with the cavitands. In both cases, addition of more cavitand to the solution had a minor effect on the T_{CP} . This atypical behavior is ascribed to the formation of kinetically-trapped nanoparticles (see Chapter 6) that contain most of the nonyl chains in the core, isolated from the solution and inaccessible for further host-guest complexation. The formation of these kinetically-trapped nanoparticles results, in the case of SN33, in the development of a hysteresis behavior of unprecedented magnitude (≈ 40 K). Once the copolymer-HP α CD ensemble was dissolved at low temperatures, the solution remained transparent up to *ca.* 50 °C, when the solution became white opaque due to aggregation of copolymer-HP α CD nanoparticles. The solution then remained opaque in the whole temperature range, and it was necessary to lower the temperature to *ca.* 0 °C to break the aggregates and recover a transparent solution containing individual nanoparticles. The copolymer-HP α CD ensemble was thus able to remember the thermal history of the solution, resulting in a temperature sensor with memory function. An in-depth study was performed to understand the reasons behind the highly unusual solution behavior of this copolymer-cavitand ensemble, constituting the central focus of Chapter 6.

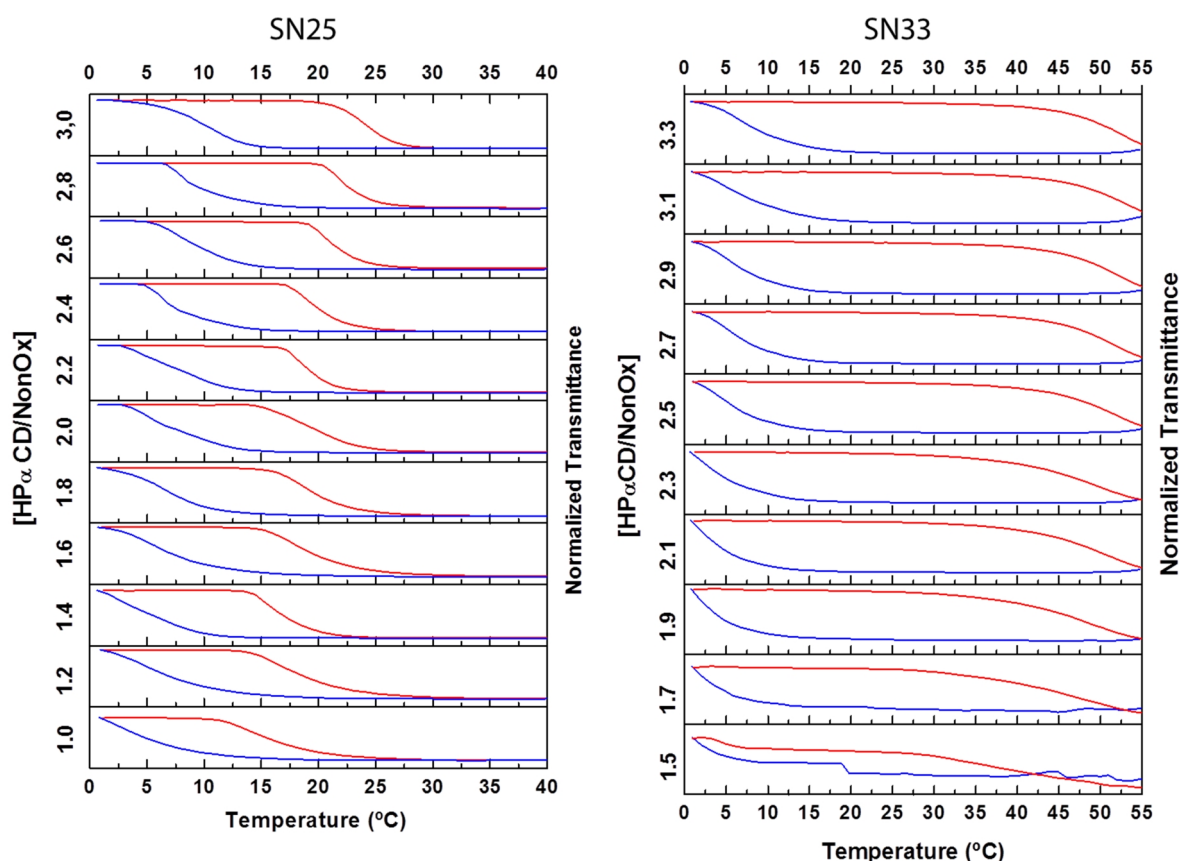


Figure 5.5.1. Turbidimetry studies of of 5 mg mL⁻¹ solutions of P[(EtOx)₇₅-ran-(NonOx)₂₅] (SN25) and P[(EtOx)₆₂-ran-(NonOx)₂₉] (SN33) with increasing HP α CD/NonOx molar ratios. Both copolymers exhibited minor variations of the T_{CP} upon addition of increasing amounts of cavitand, which is ascribed to nanoparticle formation where the nonyl chains are isolated from the aqueous environment. In the case of SN33, an unprecedented large hysteresis of 40 °C was found. The heating and cooling ramps are represented by the top (red) and bottom (blue) curves, respectively. Rate: 1 K min⁻¹, $\lambda = 700$ nm.

5.6 Poly(2-ethyl-2-oxazoline)-ran-poly(2-nonyl-2-oxazoline): influence of polymer length

Finally, the effect of polymer chain length on the solubility behavior of the PEtOx-*ran*-PNonOx copolymers was investigated. To this end, two copolymers were synthesized bearing *ca.* 200 repeating units, thus double the length of the copolymers studied previously. The copolymers had a NonOx content of 19% (LN19) or 29% (LN29) and were, as expected, insoluble in the absence of cavitands. In fact, the increase in polymer chain length rendered both copolymers more difficult to dissolve, requiring 2 and 4 equivalents of HP α CD to solubilize LN19 and LN29, respectively.

Figure 5.6.1 shows the temperature dependent turbidimetry results, that yielded a sharp LCST transition in both copolymers. In contrast with the shorter copolymers containing 25% and 33% NonOx, the hysteresis was similar to the one observed previously for the polymer containing 12 % NonOx, of *ca.* 10 K. The higher number of nonyl groups present in a single polymer chain seems to enhance the intramolecular nonyl-nonyl hydrophobic interactions further stabilizing the insoluble globular morphology of the copolymer. This results in the need to add a large excess of HP α CD to disrupt the nonyl-nonyl hydrophobic interactions.

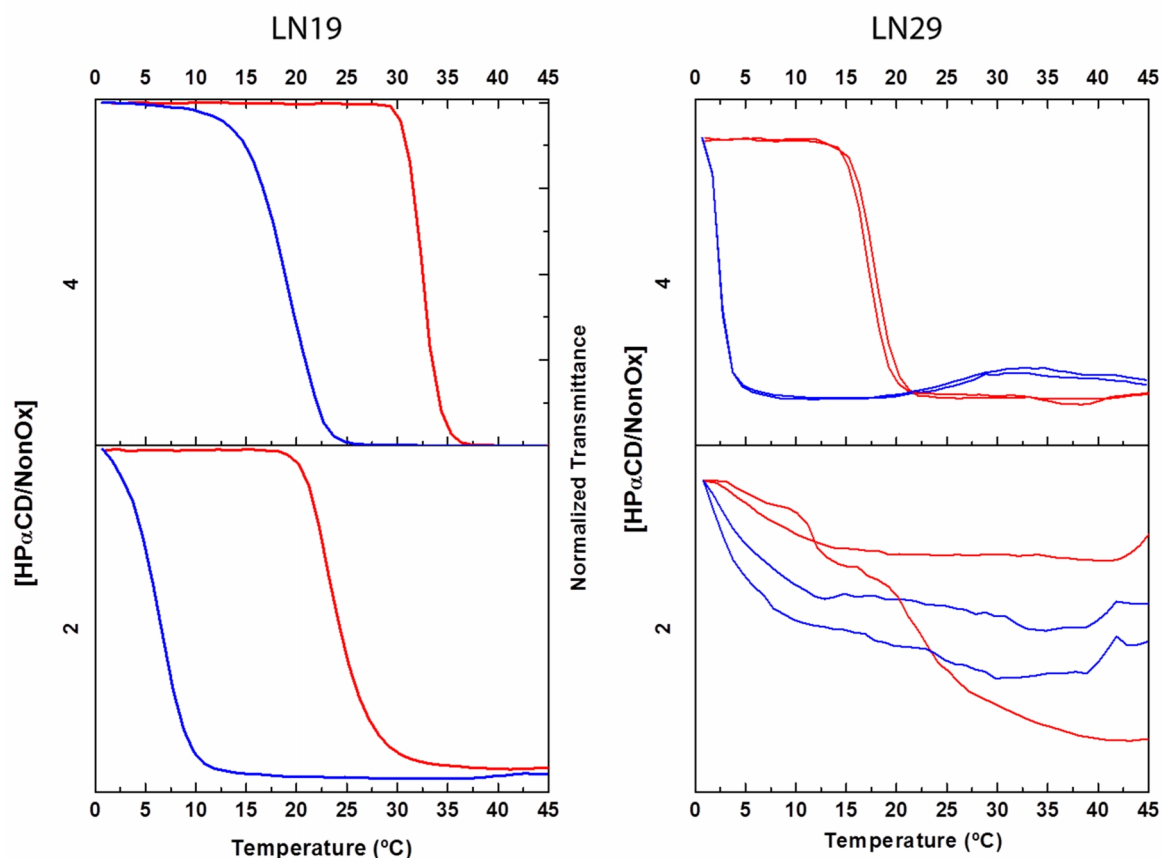


Figure 5.6.1. Turbidimetry studies of of 5 mg mL⁻¹ solutions of P[(EtOx)₁₆₂-*ran*-(NonOx)₃₈] (LN19) and P[(EtOx)₁₄₀-*ran*-(NonOx)₅₇] (LN29) with increasing HP α CD/NonOx molar ratios. Large HP α CD excesses are required to solubilize both copolymers, especially in the case of LN29. The heating and cooling ramps are represented by the top (red) and bottom (blue) curves, respectively. Rate: 1 K min⁻¹, λ = 700 nm.

5.7 Conclusions

A range of supramolecular hosts has been shown to form host-guest complexes with the aliphatic nonyl chains present in amphiphilic PEOx-*ran*-PNonOx copolymers. These inclusion complexes are dynamic and allow tuning of the copolymer phase transition temperature.

The temperature-induced breakage of the inclusion complexes constitutes the driving force for the copolymer phase transition, which is tuned by the strength of the nonyl-cavitand association. Analysis of the T_{CP} variation upon addition of different cavitands allowed to estimate the binding constant for each supramolecular host, resulting in the following order of binding affinity towards nonyl chains: CB[7] \gg α CD $>$ HP α CD $>$ HP β CD.

The least hydrophilic of the cavitands tested (CB[7]) resulted in the strongest association while, unexpectedly, partial substitution of the native α CD hydroxyl groups by hydroxypropyl units decreased by a factor of 2 the association constant with nonyl chains.

Interestingly, the copolymer composition was found to exert a tremendous impact on its host-guest complexation capabilities and on the structures formed at the nanoscale upon complexation with supramolecular hosts. For a copolymer containing 12 % NonOx, cavitand-nonyl complexation resulted in the extension of the polymer chain and the formation of random-coil polymer-cavitand ensembles. Unexpectedly, the copolymer containing the lowest number of nonyl chains was the one whose T_{CP} could be tuned across a wider temperature range by addition of cavitands. Increasing the nonyl content to 20 - 25 % promoted the formation of kinetically-trapped nanoparticles, in whose core nonyl chains are shielded from the aqueous environment. Macroscopically, this translated into a progressive temperature-induced phase transition. When the NonOx content was further increased to 33 % kinetically-trapped nanoparticle formation promoted the appearance of a large hysteresis, that resulted in temperature sensors with the potential to exhibit a memory function, which will be further discussed in Chapter 6.

Finally, increase of copolymer chain length to 200 repeating units seemed to favor intramolecular nonyl-nonyl hydrophobic interactions, promoting a polymer globular structure and hindering host-guest complex formation. Thus, large excesses of cavitand were required to solubilize these longer copolymers.

Overall, the results obtained demonstrate that, when coupled to a polymer structure, simple and relatively weak supramolecular interactions in water can trigger the formation of a variety of complex architectures at the nanoscale. These supramolecular architectures are determined by subtle changes in molecular structure and dictate the macroscopic behavior of the solution.

5.8 Experimental Section

Materials

Solvents and reagents were purchased from Sigma Aldrich, and used as received unless otherwise specified. Methyl tosylate (MeOTs) was distilled twice under vacuum prior to use. 2-Ethyl-2-oxazoline (EtOx, Aldrich) was distilled over barium oxide (BaO). Acetonitrile (CH₃CN, Acros Organics) was dried over molecular sieves (3Å). All reagents were stored and handled under a dry argon or nitrogen atmosphere.

Deionized (Milli-Q) water was obtained from a Sartorius Arium 611 with a Sartopore 2 150 (0.45 + 0.2 μ m pore size) cartridge filter (resistivity \geq 18.2 M Ω cm).

Instrumentation

Polymerizations were performed in a Biotage initiator sixty microwave synthesizer utilizing capped microwave vials. The vials were heated to 120 °C for 24 hours and cooled down to room temperature under vacuum prior to use. All polymerizations were performed with temperature control (IR sensor).

¹H-NMR spectra were recorded in CDCl₃ on a Bruker Avance 300 MHz spectrometer. Spectra were processed using TOPSPIN 3.0.

Size exclusion chromatography (SEC) measurements were performed on an Agilent 1260-series equipped with a 1260 ISO-pump, a 1260 Diode Array Detector (DAD), a 1260 Refractive Index Detector (RID), and a PSS Gram30 column in series with a PSS Gram1000 column inside a 1260 Thermostated Column Compartment (TCC) at 50°C using dimethylacetamide containing 50 mM of LiCl (flow rate of 0.6 mL min⁻¹) as solvent. Molar masses and dispersities were calculated against poly(methyl methacrylate) standards.

Turbidimetry and dynamic light scattering studies

Turbidimetry measurements were performed in a CARY Bio 100 UV-VIS spectrophotometer equipped with a temperature controller, at a wavelength of 700 nm. Heating/cooling cycles were performed at a rate of 1K min⁻¹ with stirring. The polymer concentration was kept at 5 mg mL⁻¹ in deionized water. The equivalents of cyclodextrin added were calculated in relation to the equivalents of nonyl side chains.

Dynamic light scattering (DLS) was performed on a Zetasizer Nano-ZS Malvern apparatus (Malvern Instruments Ltd) using disposable PMMA cuvettes. The excitation light source was a He-Ne laser at 633 nm, and the intensity of the scattered light was measured at 173°. This method measures the rate of the intensity fluctuation and the size of the particles is determined through the Stokes-Einstein equation ($d(H) = \sqrt{kT/3\pi\eta D}$) where $d(H)$ is the mean hydrodynamic diameter, k is the Boltzmann constant, T is the absolute temperature, η is the viscosity of the dispersing medium, and D is the apparent diffusion coefficient. Before starting the measurements, samples were equilibrated at the specific temperature for at least 300 s. The samples were analysed four times, allowing the calculation of the corresponding Z_{ave} and PDI uncertainties. Samples were filtered through Millipore membranes with a pore size of 0.2 µm prior to measurement.

Poly[(2-ethyl-2-oxazoline)-*ran*-(2-nonyl-2-oxazoline)] synthesis

The polymerization was performed as previously reported.^[20] The microwave vials were loaded in a glove box (Vigor Gas Purification Technologies Inc.) with EtOx and NonOx copolymers in the desired molar ratio, maintaining a total monomer concentration of 4 M in acetonitrile. Polymer length was tuned by the ratio of MeOTs initiator to monomer. The following table summarizes the amounts of initiator, monomers, and solvent that were used to produce each copolymer:

ID	Target Polymer composition	Obtained Polymer composition ^a	DP (target/obtained)	MeOTs (g)	EtOx (g)	NonOx (g)	MeCN (mL)
SN12	PEtOx ₉₀ - <i>ran</i> -PNonOx ₁₀	PEtOx ₉₀ - <i>ran</i> -PNonOx ₁₂	100/102	0.0335	1.606	0.355	2.491
SN20	PEtOx ₈₀ - <i>ran</i> -PNonOx ₂₀	PEtOx ₈₄ - <i>ran</i> -PNonOx ₂₁	100/105	0.0272	1.454	0.747	2.299
SN25	PEtOx ₇₅ - <i>ran</i> -PNonOx ₂₅	PEtOx ₇₅ - <i>ran</i> -PNonOx ₂₅	100/100	0.0223	0.892	0.592	1.155
SN33	PEtOx ₇₀ - <i>ran</i> -PNonOx ₃₀	PEtOx ₆₂ - <i>ran</i> -PNonOx ₂₉	100/91	0.0272	1.272	1.120	2.108
LN19	PEtOx ₁₆₀ - <i>ran</i> -PNonOx ₄₀	PEtOx ₁₆₂ - <i>ran</i> -PNonOx ₃₈	200/200	0.0109	0.933	0.464	1.502
LN29	PEtOx ₁₄₀ - <i>ran</i> -PNonOx ₆₀	PEtOx ₁₄₀ - <i>ran</i> -PNonOx ₅₇	200/197	0.0112	0.833	0.710	1.104

^a*Determined by ¹H-NMR spectroscopy.*

The polymerizations were run for 15 minutes at 140 °C (DP 100) or 30 minutes (DP 200). The polymers were terminated with KOH in methanol, yielding hydroxyl-terminated polymers. The solvent was evaporated under reduced pressure, and each polymer was subsequently precipitated in diethyl ether from dichloromethane. The pure polymer was then dried in a vacuum oven at 50 °C for 24h.

Preparation of Poly[(2-ethyl-2-oxazoline)-*ran*-(2-nonyl-2-oxazoline)] solutions and titration

General protocol followed for the copolymer titrations with cavitands

For all the titrations with a cavitand stock solution, PMMA cuvettes for Vis-spectroscopy (Karl-Roth), each equipped with a stirring bar, were filled with 2mL of copolymer solution. To calculate the amount of cavitand stock solution necessary to add to each cuvette, the following calculations were performed.

First, the weight fraction of NonOx (f_{NonOx}) in each copolymer was calculated, according to the following equation:

$$Wt. \text{ fraction NonOx } (f_{NonOx}) = \frac{DP (NonOx) M_{wt}(NonOx)}{DP (EtOx) M_{wt}(EtOx) + DP (NonOx) M_{wt}(NonOx)}$$

Where DP is the degree of polymerization *i.e.* the number of repeating units of each monomer in the copolymer.

Then, the mass of cavitand necessary to equal the number of NonOx groups contained in 2 mL (cuvette) of 5 mg mL⁻¹ copolymer solution is calculated.

$$m \text{ cavitand (grams)} = \frac{f_{NonOx} \times 5 \text{ mg mL}^{-1} \times 2 \text{ mL}}{M_{wt}(NonOx)} \times M_{wt}(cavitand)$$

Finally, the volume of cavitand stock solution required to add to each copolymer solution is calculated:

$$V \text{ cavitand } (\mu\text{L}) = 1000 \times \frac{m \text{ cavitand (g)}}{\text{concentration cavitand } \left(\frac{\text{g}}{\text{mL}}\right)} \times \text{Number of equivalents}$$

In the present study, the number of equivalents typically ranged from 0.2 to 2.0. The aliquots were measured and dispensed with a micropipette.

PEtOx₉₀-ranPNonOx₁₂ SN12

Since this copolymer was water soluble at low temperatures, a 5 mg mL⁻¹ stock solution was prepared. PMMA cuvettes were filled with 2 mL of the copolymer solution. Subsequently, increasing amounts of a cavitand stock solution were added to each cuvette, obtaining the desired cavitand concentration. Cavitand stock solution concentrations ranged from 120 mg mL⁻¹ for α CD to 150 mg mL⁻¹ for HP α CD and HP β CD. The dilution of the copolymer by addition of cavitand was always kept below 10%.

Due to the relatively low solubility of CB[7], a 4 mM solution of the cavitand was prepared (4.83 mg mL⁻¹). To avoid high dilution effects upon titration, the copolymer was directly weighted in the cuvette, and the necessary amounts of water and CB[7] stock solution added to obtain a 5 mg mL⁻¹ concentration of copolymer.

Other copolymers

For the other copolymers investigated, the protocol followed was analogous as for SN12. The main difference is related to the water insolubility of these polymers, that required the preparation of copolymer stock solutions in the presence of cavitand (*e.g.* 0.2 equivalents HP α CD for SN20, or 1.7 equivalents HP α CD for SN33).

In all cases, the cavitand-copolymer mixture was frozen and thawed under sonication in an ice bath. This protocol was repeated until all macroscopic polymer particles disappeared.

5.9. References

- [1] X.-d. Wang, O. S. Wolfbeis, R. J. Meier, *Chem. Soc. Rev.* **2013**, *42*, 7834.
- [2] P. R. N. Childs, J. R. Greenwood, C. A. Long, *Rev. Sci. Instrum.* **2000**, *71*, 2959.
- [3] T. Tsuji, S. Yoshida, A. Yoshida, S. Uchiyama, *Anal. Chem.* **2013**, *85*, 9815.
- [4] C.-Y. Chen, C.-T. Chen, *Chem. Commun.* **2011**, *47*, 994.
- [5] C. Gota, K. Okabe, T. Funatsu, Y. Harada, S. Uchiyama, *J. Am. Chem. Soc.* **2009**, *131*, 2766.
- [6] X. Guan, X. Liu, Z. Su, P. Liu, *React. Funct. Polym.* **2006**, *66*, 1227.
- [7] F. Ye, C. Wu, Y. Jin, Y.-H. Chan, X. Zhang, D. T. Chiu, *J. Am. Chem. Soc.* **2011**, *133*, 8146.
- [8] R. J. Meier, L. H. Fischer, O. S. Wolfbeis, M. Schäferling, *Sens. Actuators, B* **2013**, *177*, 500.
- [9] K. Okabe, N. Inada, C. Gota, Y. Harada, T. Funatsu, S. Uchiyama, *Nat. Commun.* **2012**, *3*, 705.
- [10] E. M. Graham, K. Iwai, S. Uchiyama, A. Prasanna de Silva, S. W. Magennis, A. C. Jones, *Lab on a Chip* **2010**, *10*, 1267.
- [11] C. Pietsch, U. S. Schubert, R. Hoogenboom, *Chem. Commun.* **2011**, *47*, 8750.
- [12] R. Hoogenboom, *Angew. Chem. Int. Ed.* **2009**, *48*, 7978.
- [13] V. R. de la Rosa, *J. Mater. Sci.: Mater. Med.* **2013**, *1*.
- [14] P. I. Freeman, J. S. Rowlinson, *Polymer* **1960**, *1*, 20.
- [15] F. Wang, S. Saeki, T. Yamaguchi, *Polymer* **1999**, *40*, 2779.
- [16] M. M. Bloksma, R. M. Paulus, H. P. C. van Kuringen, F. van der Woerd, H. M. L. Lambermont-Thijs, U. S. Schubert, R. Hoogenboom, *Macromol. Rapid Commun.* **2011**, *33*, 92.
- [17] R. Hoogenboom, in *Complex Macromolecular Architectures*, John Wiley & Sons (Asia) Pte Ltd, **2011**, pp. 685.
- [18] R. Luxenhofer, Y. Han, A. Schulz, J. Tong, Z. He, A. V. Kabanov, R. Jordan, *Macromol. Rapid Commun.* **2012**, *33*, 1613.
- [19] R. Hoogenboom, H. M. L. Thijs, M. J. H. C. Jochems, B. M. van Lankvelt, M. W. M. Fijten, U. S. Schubert, *Chem. Commun.* **2008**, 5758.
- [20] M. W. M. Fijten, J. M. Kranenburg, H. M. L. Thijs, R. M. Paulus, B. M. van Lankvelt, J. de Hullu, M. Springintveld, D. J. G. Thielen, C. A. Tweedie, R. Hoogenboom, K. J. Van Vliet, U. S. Schubert, *Macromolecules* **2007**, *40*, 5879.
- [21] H. M. L. Lambermont-Thijs, R. Hoogenboom, C.-A. Fustin, C. Bomal-D'Haese, J.-F. Gohy, U. S. Schubert, *J. Polym. Sci., Part A: Polym. Chem.* **2009**, *47*, 515.
- [22] G. Volet, V. Chanthavong, V. Wintgens, C. Amiel, *Macromolecules* **2005**, *38*, 5190.
- [23] G. Volet, L. Auvray, C. Amiel, *J. Phys. Chem. B* **2009**, *113*, 13536.
- [24] G. Volet, A.-C. L. Deschamps, C. Amiel, *J. Polym. Sci., Part A: Polym. Chem.* **2010**, *48*, 2477.

- [25] H. Ritter, O. Sadowski, E. Tepper, *Angew. Chem. Int. Ed.* **2003**, *42*, 3171.
- [26] M. E. Brewster, T. Loftsson, *Adv. Drug Delivery Rev.* **2007**, *59*, 645.
- [27] T. R. Thatiparti, A. J. Shoffstall, H. A. von Recum, *Biomaterials* **2010**, *31*, 2335.
- [28] B. V. K. J. Schmidt, M. Hetzer, H. Ritter, C. Barner-Kowollik, *Macromol. Rapid Commun.* **2013**, *34*, 1306.
- [29] B. V. K. J. Schmidt, M. Hetzer, H. Ritter, C. Barner-Kowollik, *Prog. Polym. Sci.* **2014**, *39*, 235.
- [30] J. Willenbacher, B. V. K. J. Schmidt, D. Schulze-Suenninghausen, O. Altintas, B. Luy, G. Delaittre, C. Barner-Kowollik, *Chem. Commun.* **2014**, *50*, 7056.
- [31] J. Li, X. Ni, Z. Zhou, K. W. Leong, *J. Am. Chem. Soc.* **2003**, *125*, 1788.
- [32] G. V. Dubacheva, T. Curk, B. M. Mognetti, R. Auzély-Velty, D. Frenkel, R. P. Richter, *J. Am. Chem. Soc.* **2014**, *136*, 1722.
- [33] A. Hashidzume, A. Harada, *Polym. Chem.* **2011**, *2*, 2146.
- [34] I. Willerich, T. Schindler, H. Ritter, F. Grohn, *Soft Matter* **2011**, *7*, 5444.
- [35] S. Tan, K. Ladewig, Q. Fu, A. Blencowe, G. G. Qiao, *Macromol. Rapid Commun.* **2014**, *35*, 1166.
- [36] J. Terao, *Polym. Chem.* **2011**, *2*, 2444.
- [37] Y. Lan, X. J. Loh, J. Geng, Z. Walsh, O. A. Scherman, *Chem. Commun.* **2012**, *48*, 8757.
- [38] F. Yhaya, J. Lim, Y. Kim, M. Liang, A. M. Gregory, M. H. Stenzel, *Macromolecules* **2011**, *44*, 8433.
- [39] J.-H. Seo, S. Kakinoki, Y. Inoue, T. Yamaoka, K. Ishihara, N. Yui, *J. Am. Chem. Soc.* **2013**, *135*, 5513.
- [40] J. Li, X. J. Loh, *Adv. Drug Delivery Rev.* **2008**, *60*, 1000.
- [41] T. Kataoka, M. Kidowaki, C. Zhao, H. Minamikawa, T. Shimizu, K. Ito, *J. Phys. Chem. B* **2006**, *110*, 24377.
- [42] J. Li, in *Inclusion Polymers, Vol. 222* (Ed.: G. Wenz), Springer Berlin Heidelberg, **2009**, pp. 175.
- [43] L. Zhou, J. Li, Q. Luo, J. Zhu, H. Zou, Y. Gao, L. Wang, J. Xu, Z. Dong, J. Liu, *Soft Matter* **2013**, *9*, 4635.
- [44] H. Liu, Y. Zhang, J. Hu, C. Li, S. Liu, *Macromol. Chem. Phys.* **2009**, *210*, 2125.
- [45] J. Wang, M. Jiang, *J. Am. Chem. Soc.* **2006**, *128*, 3703.
- [46] H. Wang, S. Wang, H. Su, K.-J. Chen, A. L. Armijo, W.-Y. Lin, Y. Wang, J. Sun, K.-i. Kamei, J. Czernin, C. G. Radu, H.-R. Tseng, *Angew. Chem. Int. Ed.* **2009**, *48*, 4344.
- [47] B. G. Mathapa, V. N. Paunov, *J. Mater. Chem. A* **2013**, *1*, 10836.
- [48] M. Bonini, S. Rossi, G. Karlsson, M. Almgren, P. Lo Nostro, P. Baglioni, *Langmuir* **2006**, *22*, 1478.
- [49] I. Puskás, M. Schrott, M. Malanga, L. Szenté, *J. Inclusion Phenom. Macrocyclic Chem.* **2013**, *75*, 269.
- [50] C. Yong, C. Washington, W. Smith, *Pharm. Res.* **2008**, *25*, 1092.
- [51] S. Concha-Santos, S. Pérez-Casas, P. Brocos, Á. Piñeiro, *J. Chem. Thermodyn.* **2013**, *67*, 112.
- [52] R. Hoogenboom, M. W. M. Fijten, S. Wijnans, A. M. J. van den Berg, H. M. L. Thijs, U. S. Schubert, *J. Comb. Chem.* **2006**, *8*, 145.
- [53] V. T. D'Souza, K. B. Lipkowitz, *Chem. Rev.* **1998**, *98*, 1741.
- [54] S. Li, W. C. Purdy, *Chem. Rev.* **1992**, *92*, 1457.
- [55] Y. Takashima, S. Hatanaka, M. Otsubo, M. Nakahata, T. Kakuta, A. Hashidzume, H. Yamaguchi, A. Harada, *Nat. Commun.* **2012**, *3*, 1270.
- [56] H.-X. Zhao, D.-S. Guo, L.-H. Wang, H. Qian, Y. Liu, *Chem. Commun.* **2012**, *48*, 11319.
- [57] M. V. Rekharsky, Y. Inoue, *Chem. Rev.* **1998**, *98*, 1875.
- [58] S. A. Nepogodiev, J. F. Stoddart, *Chem. Rev.* **1998**, *98*, 1959.
- [59] G. Chen, M. Jiang, *Chem. Soc. Rev.* **2011**, *40*, 2254.
- [60] G. Barone, G. Castronuovo, P. Del Vecchio, V. Elia, M. Muscetta, *J. Chem. Soc., Faraday Trans. 1* **1986**, *82*, 2089.
- [61] D. Hallen, A. Schon, I. Shehatta, I. Wadso, *J. Chem. Soc., Faraday Trans.* **1992**, *88*, 2859.
- [62] C. Saudan, F. A. Dunand, A. Abou-Hamdan, P. Bugnon, P. G. Lye, S. F. Lincoln, A. E. Merbach, *J. Am. Chem. Soc.* **2001**, *123*, 10290.
- [63] P. C. Manor, W. Saenger, *J. Am. Chem. Soc.* **1974**, *96*, 3630.
- [64] K. Lindner, W. Saenger, *Angew. Chem. Int. Ed. Engl.* **1978**, *17*, 694.
- [65] T. Steiner, W. Saenger, R. E. Lechner, *Mol. Phys.* **1991**, *72*, 1211.
- [66] D. Harries, D. C. Rau, V. A. Parsegian, *J. Am. Chem. Soc.* **2005**, *127*, 2184.
- [67] C. R. Martinez, B. L. Iverson, *Chem. Sci.* **2012**, *3*, 2191.
- [68] R. Onnainty, E. M. Schenfeld, M. A. Quevedo, M. A. Fernández, M. R. Longhi, G. E. Granero, *J. Phys. Chem. B* **2012**, *117*, 206.
- [69] Y. Inoue, T. Hakushi, Y. Liu, L. Tong, B. Shen, D. Jin, *J. Am. Chem. Soc.* **1993**, *115*, 475.
- [70] W. Saenger, *Angew. Chem. Int. Ed. Engl.* **1980**, *19*, 344.
- [71] M. L. Bender, M. Komiyama, *Cyclodextrin Chemistry, Vol. 6*, Springer Berlin Heidelberg, **1978**.
- [72] P. Brocos, X. Banquy, N. Díaz-Vergara, S. Pérez-Casas, Á. Piñeiro, M. Costas, *J. Phys. Chem. B* **2011**, *115*, 14381.
- [73] C. Schönbeck, P. Westh, J. C. Madsen, K. L. Larsen, L. W. Ståde, R. Holm, *Langmuir* **2011**, *27*, 5832.
- [74] J. Szejtli, *Cyclodextrin Technology, Vol. 1*, Springer, Dordrecht, **1988**.

- [75] C. Schönbeck, P. Westh, J. C. Madsen, K. L. Larsen, L. W. Städe, R. Holm, *Langmuir* **2010**, *26*, 17949.
- [76] L. Szente, J. Szejtli, *Adv. Drug Delivery Rev.* **1999**, *36*, 17.
- [77] J. Lagona, P. Mukhopadhyay, S. Chakrabarti, L. Isaacs, *Angew. Chem. Int. Ed.* **2005**, *44*, 4844.
- [78] J. Szejtli, *Chem. Rev.* **1998**, *98*, 1743.
- [79] Laboratory Instrumentation
- [80] C. Dethlefs, J. Eckelmann, H. Kobarg, T. Weyrich, S. Brammer, C. Näther, U. Lüning, *Eur. J. Org. Chem.* **2011**, *2011*, 2066.
- [81] L. Fielding, S. C. McKellar, A. J. Florence, *Magn. Reson. Chem.* **2011**, *49*, 405.
- [82] J. Mohanty, W. M. Nau, *Angew. Chem. Int. Ed.* **2005**, *44*, 3750.
- [83] D. M. Bailey, A. Hennig, V. D. Uzunova, W. M. Nau, *Chem. Eur. J.* **2008**, *14*, 6069.
- [84] J. W. Lee, S. Samal, N. Selvapalam, H.-J. Kim, K. Kim, *Acc. Chem. Res.* **2003**, *36*, 621.
- [85] C. Yuan, Z. Jin, X. Li, *Food Chem.* **2008**, *106*, 50.
- [86] C. Trinadha Rao, J. Pitha, B. Lindberg, J. Lindberg, *Carbohydr. Res.* **1992**, *223*, 99.
- [87] Á. Buvári-Barcza, L. Barcza, *Talanta* **1999**, *49*, 577.
- [88] C. Tang, A. Inomata, Y. Sakai, H. Yokoyama, T. Miyoshi, K. Ito, *Macromolecules* **2013**, *46*, 6898.
- [89] H. Chen, H. Ji, *Supramol. Chem.* **2014**, 1.
- [90] H.-J. Schneider, A. Yatsimirsky, *Principles and Methods in Supramolecular Chemistry*, John Wiley and Sons Ltd, Chichester, **1999**.

Chapter 6

Solution polymeric temperature sensors with long-term memory function

A poly[(2-ethyl-2-oxazoline)-*ran*-(2-nonyl-2-oxazoline)] copolymer in combination with hydroxypropylated-cyclodextrins is demonstrated to lead to a supramolecular self-assembly process resulting in the formation of kinetically-trapped thermoresponsive nanoparticles. Selection of the type of cyclodextrin provides control over the nanoparticle phase-transition thermodynamics, affording temperature sensors with an unprecedented, long-term thermal memory function, either reversible or irreversible. Finally, the general applicability of the developed supramolecular temperature sensor approach is applied to a different supramolecular polymer system based on dialkoxynaphthalene-functionalized poly(*N*-isopropylacrylamide) (PNIPAAm) and cyclobis(paraquat-*p*-phenylene) tetrachloride (CBPQT⁴⁺), also enabling a memory function. This research also sheds light onto kinetic and dynamic supramolecular assemblies, providing important insights as similar supramolecular processes are at the foundation of living matter.

6.1 Introduction

In Chapter 5 we found that polymer composition had a profound impact on the solubility and self-assembly in solution of amphiphilic PEtOx-*ran*-PNonOx copolymers. In particular, increasing the content of nonyl side chains to 33 % (in number) led to water insoluble copolymers that could only be dissolved upon repeated freeze/thaw cycles under sonication in the presence of excess of HP α CD cavitands. This protocol was required to promote the formation of HP α CD-nonyl host-guest complexes, and the progressive unfolding and hydration of the copolymer. The copolymer-HP α CD ensembles were found to form kinetically-trapped nanoparticles in solution at low temperature. These nanoparticles aggregated upon increasing temperature to *ca.* 50 °C, and remained stable even after lowering the temperature far below the ensemble T_{CP} , thereby recording thermal information from the solution. It thus appeared possible to exploit this system as memory function for a temperature sensor in solution.

Polymeric temperature sensors are interesting as their intrinsic phase transitions, such as glass, melting, liquid crystalline and solubility transitions may be exploited for the development of temperature sensors that not only respond but also record temperature changes, *i.e.* exhibit a memory function.^[1-6] However, the few recently reported examples of polymeric temperature sensors with memory function exhibit a thermal memory based on glass and melting transitions in solid, shape-memory, or liquid-crystalline polymeric materials. We are not aware of any previous

Parts of this chapter have been published in: de la Rosa, V. R.; Hoogenboom, R. *Chem. Eur. J.* **2014**, DOI: 10.1002/chem.201405161.

examples of soluble polymeric sensors with a memory function based on a solubility phase transition, which have great potential for *in vivo* thermography of living matter as has already been demonstrated for polymeric thermometers without memory (see section 1.4.2.2, in Chapter 1).^[7-9]

This chapter is devoted to studying the mechanism behind nanoparticle formation and the long term stability of these kinetically trapped structures, which are key to the thermal memory. In addition, different hydroxypropylated cyclodextrins have been investigated as hosts for the aliphatic nonyl chains present in the EtOx-NonOx copolymer, to control the copolymer phase-transition temperature. Moreover, the choice of cyclodextrin provided control over the copolymer phase/transition kinetics and thermodynamics, leading to the first reported reversible and irreversible temperature sensors with long-term memory effect, driven by specific supramolecular host-guest interactions.

6.2 Poly(2-ethyl-2-oxazoline)₆₂-*ran*-poly(2-nonyl-2-oxazoline)₂₉ synthesis

A P[(EtOx)₆₂-*ran*-(NonOx)₂₉] copolymer with a random distribution of ethyl and nonyl side chains along the polymer backbone was prepared by living cationic ring-opening polymerization of the two monomers, in analogy to the synthesis reported in Chapter 5.

Statistical copolymerization of EtOx and NonOx yields random copolymers, as the reactivity ratios of both monomers are close to unity.^[10] The obtained P[(EtOx)₆₂-*ran*-(NonOx)₂₉] copolymer composition was determined by ¹H-NMR spectroscopy, whereas size exclusion chromatography revealed a defined copolymer with a dispersity of 1.09 (see Figure 6.2.1). The minor molecular weight distribution observed in the SEC trace corresponds to double molecular weight species formed due to chain-coupling as a result of performing the polymerization at high temperature (140 °C) and full monomer conversion (see discussion in Chapter 3, section 3.2).

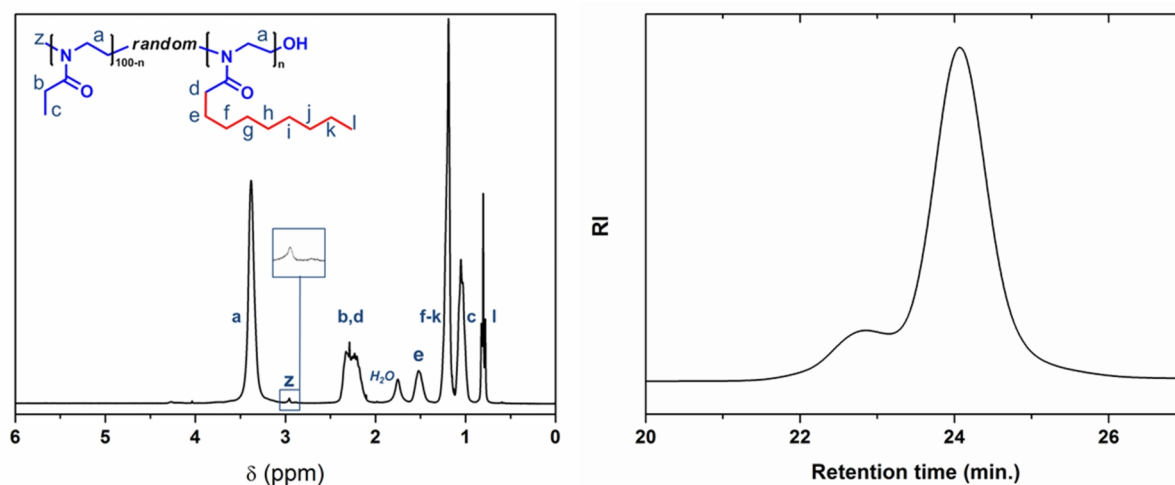


Figure 6.2.1. ¹H NMR spectrum of P[(EtOx)₆₂-*ran*-(NonOx)₂₉] (300 MHz, CDCl₃, 298K) and corresponding size exclusion chromatogram of P[(EtOx)₆₂-*ran*-(NonOx)₂₉]. Eluent: *N,N*-Dimethylacetamide with 50 mM LiCl. $M_n = 15000$, $M_m = 16400$, $\bar{D} = 1.09$. The molar masses were calculated against PMMA standards.

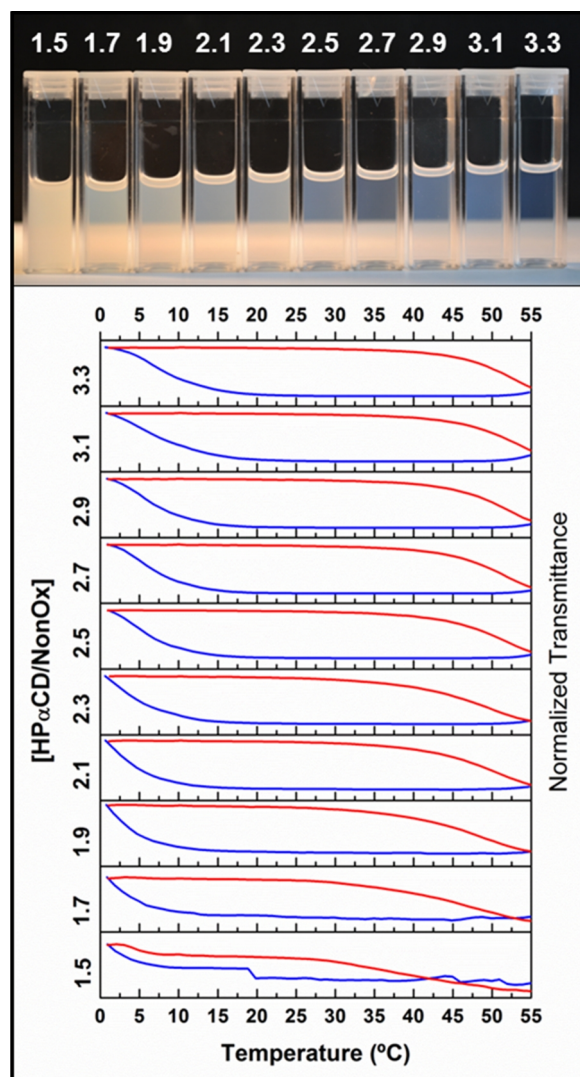
6.3 Poly(2-ethyl-2-oxazoline)₆₂-*ran*-poly(2-nonyl-2-oxazoline)₂₉ host-guest complexation with HP α CD

The copolymer is water insoluble due to its relatively high content of nonyl groups (49 wt.%), and it could be initially speculated that addition of hydroxypropyl- α -cyclodextrin (HP α CD) would render these aliphatic chains hydrophilic through the formation of inclusion complexes, bringing the polymer in solution, as observed earlier (Chapter 5) for analogous PEtOx-*ran*-PNonOx copolymers with a lower NonOx content (see Figure 5.1.1 in page 105).^[11-13]

However, addition of a HP α CD solution (0.6 average degree of hydroxypropyl substitution per glucose unit, *i.e.* DS = 0.6) to the solid copolymer followed by sonication, was ineffective to solubilize the copolymer, most likely due to too strong hydrophobic association of the nonyl side chains. Then, the sample was frozen and thawed under sonication in an ice bath, in the presence of at least 1.7 equivalents -relative to nonyl side chains- of HP α CD, to enhance the solubility of the copolymer by lowering the entropic penalty of hydration. When utilizing this procedure, the solid copolymer swelled and slowly dissolved after two repeated freeze-thaw cycles under sonication. Unexpectedly, the copolymer-HP α CD solutions exhibited a T_{CP} that remained virtually unvaried with increasing concentrations of HP α CD.

The measured T_{CP} was *ca.* 50 °C and a remarkably large hysteresis of 40 °C was found, as the solution only became clear again below 10 °C during cooling (see Figure 6.3.1.). Upon heating to 55 °C, the solutions became white opaque due to the temperature-driven aggregation of the copolymer, presumably due to breakage of the cyclodextrin-nonyl inclusion complexes in the hydrophobically associated polymer globules (see Chapter 5), and when the solutions were brought back to room temperature they remained cloudy. The solutions only recovered their initial transparency upon cooling to the clearance point temperature of the copolymer, at *ca.* 5 °C, and their transparency remained upon heating to room temperature. The existence of such a large 40 °C hysteresis indicates the formation of metastable soluble polymer structures during the freeze-thaw dissolution procedure, and is the basis for the thermal memory of the sensor.

Figure 6.3.1. Turbidimetry studies of 5 mg mL⁻¹ solutions of P[(EtOx)₆₂-*ran*-(NonOx)₂₉] with increasing HP α CD/NonOx molar ratios. The heating and cooling ramps are represented by the top (red) and bottom (blue) curves, respectively. Rate: 1 K min⁻¹, $\lambda = 700$ nm. The top picture displays the corresponding samples after being cooled to 0 °C and then stored at room temperature for one day, where only the sample with 3.3 equivalents of HP α CD remained transparent.



Nonetheless, the solutions slowly became opaque at room temperature after 24 hours, indicating the progressive breakage of the inclusion complexes and the formation of larger aggregates indicating a transition for the soluble metastable state to the collapsed thermodynamic state. Interestingly, when 3.3 equivalents of HP α CD were added, the solution remained translucent even after 24 hours (See Figure 6.3.1., top picture).

Next, isothermal turbidimetry studies were performed to assess the stability of the hysteresis window exhibited by these sensors and, thus, the stability of the memory function. A pair of aliquots from three of the solutions described in Figure 6.3.1., with HP α CD contents ranging from 1.9 to 3.3 equivalents was taken. All of the solutions were cooled to 5 °C and thus became transparent. One set of solutions was then heated to 55 °C, resulting in the collapse of the polymer, and consequently a white opaque solution was obtained. Finally, all the samples were brought to 25 °C and the turbidity of the solutions was monitored for 2.5 days. The results are displayed in Figure 6.3.2., showing no changes in time for the heated samples that all remained opaque and did not exhibit further aggregation nor sedimentation. The cooled solutions with 1.9 and 2.7 equivalents of HP α CD, however, lost 50% of transmittance within 10 hours clearly indicating that the host-guest complexation of the HP α CD with the nonyl side chains leads to a metastable solubilized state that is slowly transformed into the thermodynamic collapsed state. Even though the transparency of the sample containing 3.3 equivalents HP α CD also progressively decayed, this occurred at a much slower rate in comparison to the copolymer solutions containing a lower content of HP α CD, indicating that this amount of HP α CD can sufficiently stabilize the metastable soluble state. In fact, only 10% transmittance was lost after 2.5 days, accounting for an 80% transmittance difference with the corresponding aliquot that was previously heated.

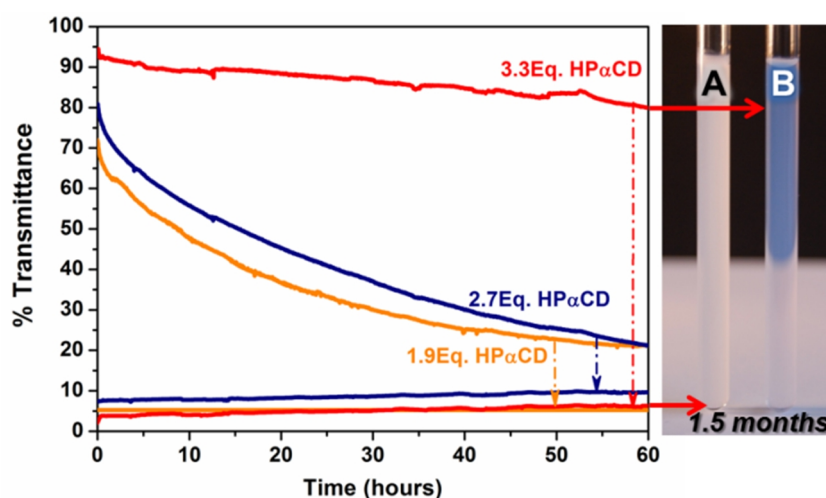


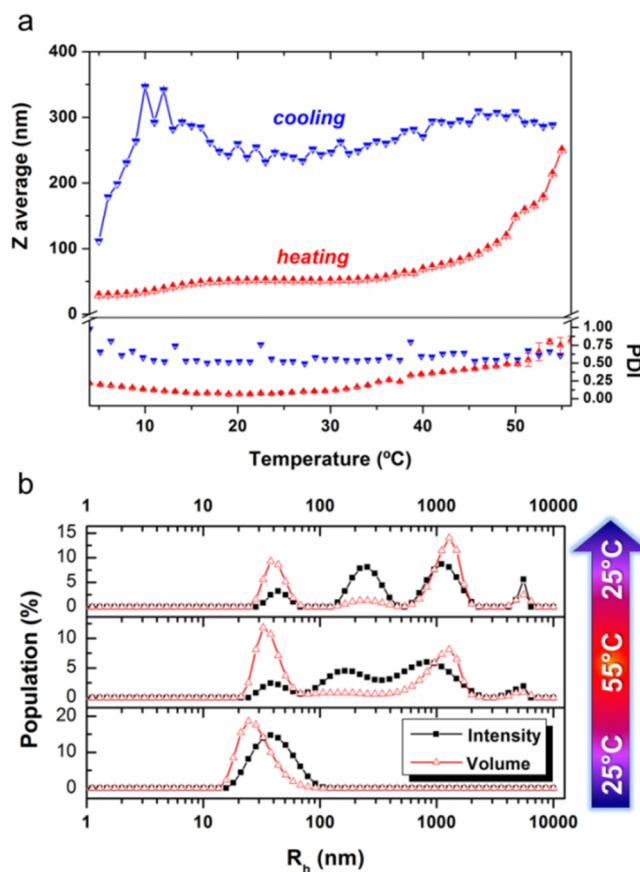
Figure 6.3.2. Evolution of the transmittance in time of PEO x_{62} -ran-PNonO x_{29} copolymer solutions with different HP α CD/NonOx molar ratios at isothermal conditions (25 °C) during 2.5 days. The samples were cooled to ca. 0 °C (top curves) or heated to 55 °C (bottom curves) before starting the measurements. As can be seen, 3.3 equivalents of HP α CD are necessary to assure long-term stability of the metastable supramolecular soluble structures. The picture shows two aliquots of the same PEO x_{62} -ran-PNonO x_{29} solution, one heated to 55 °C (A) and the other cooled to 0 °C (B), after staying for 1.5 months at room temperature. Even after 1.5 months, the difference between both solutions is clearly visible by eye. Polymer concentration: 5 mg mL $^{-1}$, $\lambda = 700$ nm.

After 1.5 months at room temperature, both solutions still showed a stark difference in appearance, clearly visible by eye (see picture in Figure 6.3.2.). The hereby developed temperature

sensor thus allows the observer to keep record of the sample thermal history even six weeks after the temperature-triggered transition occurred. To the best of our knowledge, this system represents the first reported example of a soluble polymeric temperature sensor with such a long-term memory function.

To gain further insights in the topology of the formed aggregates and their evolution with temperature after long equilibration times (heating/cooling rate of approximately 0.01 K min^{-1}), dynamic light scattering measurements of the samples were performed. As can be seen in Figure 6.3.3a, structures of *ca.* 20 nm in size are formed at low temperatures, which evolve to well-defined, stable 50 nm supramolecular nanoparticles at room temperature ($\text{PDI} \approx 0.10$). The presence of these nanoparticles accounts for the translucent appearance of the solution (picture B in Figure 6.3.2.). A concentration of 3.3 equivalents of HP α CD proved to be sufficient for the cavitands to effectively compete with the hydrophobic interactions between the nonyl side chains of the copolymer, preventing the aggregation of the nanoparticles and conferring long-term stability to these kinetically-trapped supramolecular nanostructures for at least 6 weeks.

Figure 6.3.3. *Temperature-dependent Dynamic Light Scattering (DLS) data for a 5 mg mL^{-1} solution of $\text{P}[(\text{EtOx})_{62}\text{-ran-(NonOx)}_{29}]$ and 3.3 equivalents of HP α CD (relative to nonyl side chains). a) Z average and PDI evolution with temperature. \blacktriangle heating; \blacktriangledown cooling. Kinetically-trapped nanoparticles are formed at low temperature and are stable up to $50 \text{ }^\circ\text{C}$ (transparent solution); above this temperature, larger aggregates are formed (opaque solution), that can be brought back in solution only when cooled below $5 \text{ }^\circ\text{C}$ (erasable memory). Four measurements are averaged at every temperature. Approximate heating/cooling rate: $< 0.01 \text{ K min}^{-1}$. b) Size distribution of the sample at $25 \text{ }^\circ\text{C}$, $55 \text{ }^\circ\text{C}$ and back to $25 \text{ }^\circ\text{C}$. At $25 \text{ }^\circ\text{C}$, well-defined ($\text{PDI} \approx 0.10$) stable nanoparticles are observed. Heating to $55 \text{ }^\circ\text{C}$ leads to the appearance of larger particles and aggregates that remain stable when cooling back to $25 \text{ }^\circ\text{C}$.*



Further increase in temperature has little impact on the nanoparticles, up to $40 \text{ }^\circ\text{C}$ when the nanoparticles begin to aggregate resulting in an exponential increase in particle size beyond $50 \text{ }^\circ\text{C}$. As can be seen in Figure 6.3.3b, at $55 \text{ }^\circ\text{C}$ three new populations arise, comprising particles of 200 and 1000 nm, in addition to large thermodynamically stable aggregates. These larger particles are well-defined and remain stable in time, preventing the large aggregates from further growing and, therefore, no macroscopic precipitation occurred, even after a long period of time (picture A in Figure 6.3.2). When performed on a solution containing 2.7 equivalents of HP α CD, similar results were obtained at low temperatures, although the average particle size increased up to $\approx 700 \text{ nm}$ upon heating, instead of $\approx 300 \text{ nm}$ for the sample containing 3.3 equivalents of HP α CD. These

results confirmed the turbidimetry observations that indicated the formation of unstable aggregates at high temperatures for samples containing less than 3.3 equivalents of HP α CD.

The temperature-triggered aggregation of the initially formed nanoparticles could be either related to the LCST of the polymer-cyclodextrin ensemble, that disrupts the host-guest interactions by increasing the hydrophobicity of the environment, or alternatively by the thermal breakage of the host-guest complexes that leads to aggregation of the nonyl chains that are set free. Even though at this stage we cannot conclude which of these two pathways is predominant, later on we will identify the thermal breakage of the cyclodextrin-nonyl host-guest complexes as the driving force behind the nanoparticle aggregation, as was also found in Chapter 5 (*vide infra*).

To understand the mechanism of the supramolecular temperature sensor comprising of P[(EtOx)₆₂-ran-(NonOx)₂₉] with 3.3 equivalents HP α CD, both opaque and transparent aliquots at 25 °C shown in Figure 6.3.2 were analyzed by NMR spectroscopy in D₂O.

In the cooled, transparent sample, quantitative ¹H-NMR spectroscopy revealed that only 20% of the polymeric nonyl side chains could be detected, indicating low polymer chain mobility and hydrophobic aggregation of the remainder of the nonyl side chains, being the driving force for nanoparticle formation (see Figure 6.3.4).

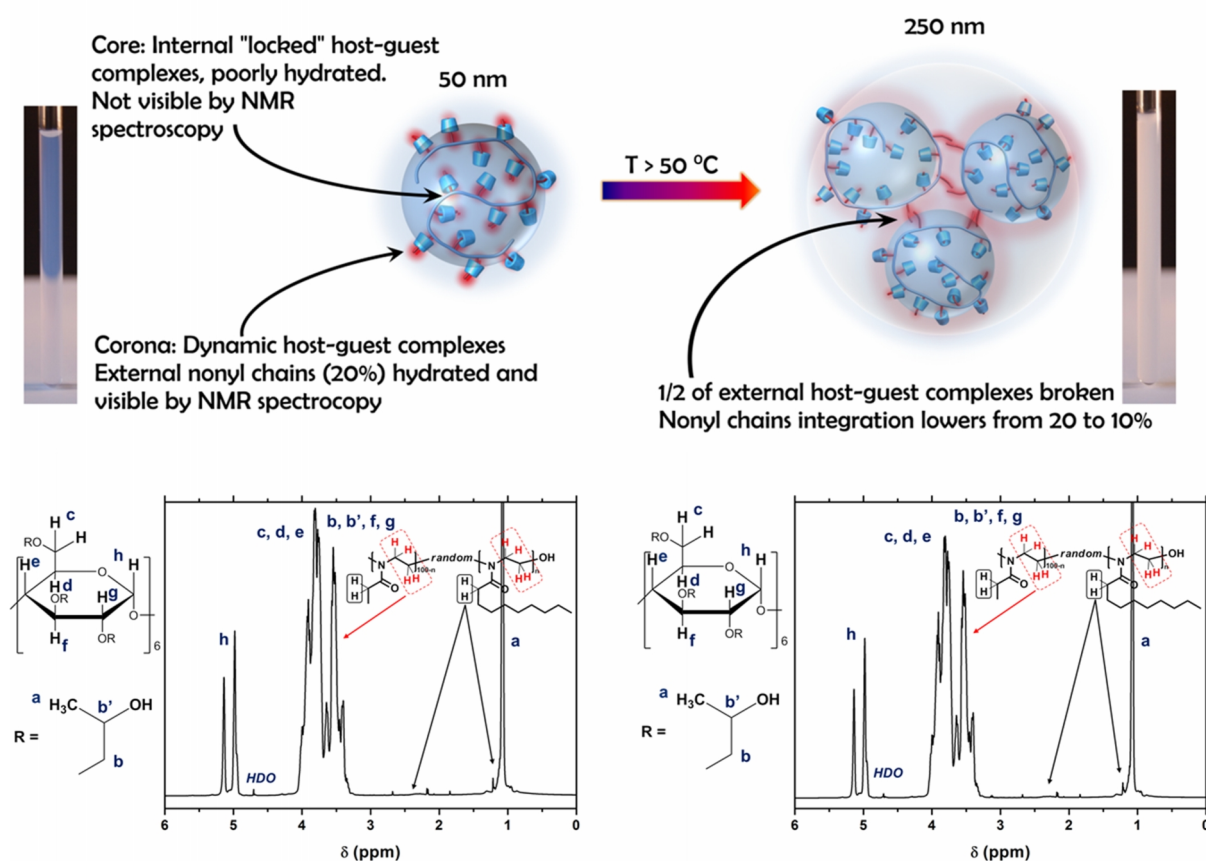


Figure 6.3.4. Quantitative ¹H NMR spectra of P[(EtOx)₆₂-ran-(NonOx)₂₉] (5 mg mL⁻¹) with 3.3 equivalents of HP α CD (water suppression, 500 MHz, D₂O, 298 K). R = H or hydroxypropyl. The left sample had previously been cooled to 5 °C and was translucent, whereas the right sample had previously been heated to 55 °C and therefore was white opaque (see pictures). An interpretation of the quantitative ¹H NMR spectroscopy results is displayed on top.

One third of the HP α CD, *i.e.* equimolar with NonOx, was also micro-phase separated inside the aggregates and consequently could not be detected, indicating the formation of 1:1 host-guest complexes with the nonyl side chains. The nearly complete complexation of nonyl side chains with HP α CD explains the invariability of the copolymer T_{CP} with increasing amounts of cyclodextrin, as was seen in Figure 6.3.1.

When compared with the cooled, transparent sample, the heated sample showed the presence of nearly 10% of additional free HP α CD, while the alkylic NonOx side chains integrated 10% less. This can be ascribed to the breakage of *ca.* 10% of the HP α CD-nonyl inclusion complexes, leading to further hydrophobic nonyl-chain association, driving the aggregation of the supramolecular nanoparticles into larger aggregates. The fact that only a minor percentage of the nonyl side chains lose their inclusion complex with HP α CD, and thus establish hydrophobic interactions with each other, accounts for the relatively limited size of the larger particles formed (200 and 1000 nm) and their resistance to further aggregation in time. In addition, we attempted to assess the size of the nanoparticles by Diffusion Ordered Spectroscopy (DOSY) of both aliquots. However, the low chain mobility and hydration of the copolymer masked its correspondent DOSY signals. The diffusion coefficients calculated for both aliquots were nearly the same ($D = 216 \pm 2 \cdot 10^{-12} \text{ m}^2 \text{ s}^{-1}$ and $D = 212 \pm 2 \cdot 10^{-12} \text{ m}^2 \text{ s}^{-1}$ for the previously cooled and heated sample, respectively) and correspond to a hydrodynamic radius of *ca.* 1 nm, matching with the size of free HP α CD.

In summary, well-defined kinetically-trapped nanoparticles are formed by host-guest complexation between HP α CD and the nonyl side chains of a P[(EtOx) $_{62}$ -*ran*-(NonOx) $_{29}$] copolymer. Temperatures above 50 °C lead to the breakage of a small fraction (10%) of the HP α CD-nonyl inclusion complexes, and the formation of stable aggregates that turn the solution opaque. These host-guest complexes can be re-formed, leading to the recovery of kinetically-trapped small nanoparticles (transparent solution) only when cooled to 1 °C. Therefore, the memory of this system can be erased by cooling to temperatures near 0 °C. A visual representation of the working mechanism of the supramolecular temperature sensor at the nanoscale based on DLS and $^1\text{H-NMR}$ spectroscopy data is displayed in Figure 6.3.4 and Figure 6.3.5.

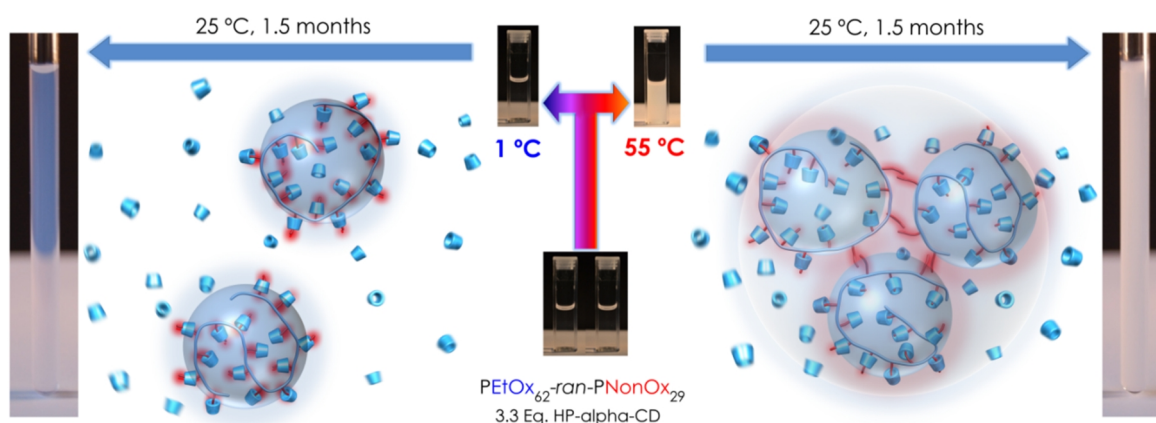
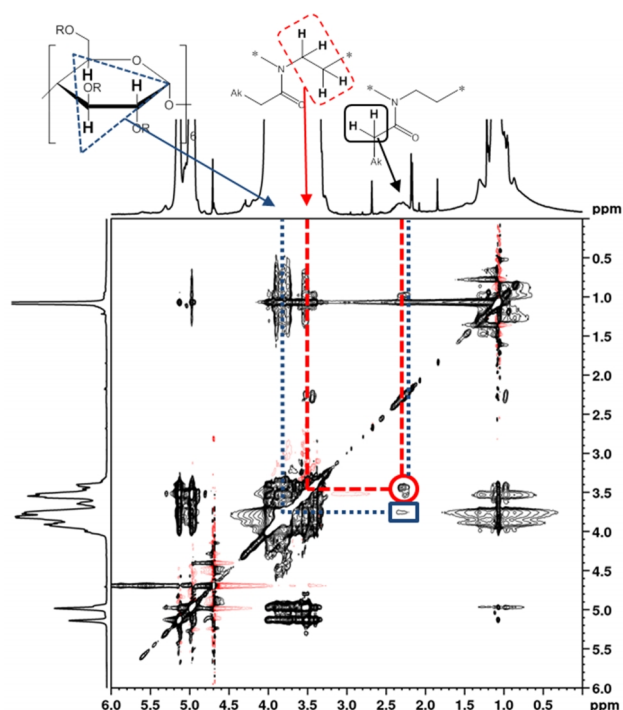


Figure 6.3.5. Schematic representation of the supramolecular nanoparticles formed by host-guest complexation of the P(EtOx)-P(NonOx) copolymer and cyclodextrins, based on interpretation of the experimental data. Two aliquots of the same P[(EtOx) $_{62}$ -*ran*-(NonOx) $_{29}$] solution containing 3.3 equivalents of HP α CD were respectively taken to 55 and 1 °C for one minute. Subsequently, both samples were brought to room temperature and their appearance remained largely unvaried, even after 1.5 months. Polymer concentration: 5 mg mL $^{-1}$. The relative size of cyclodextrins is exaggerated for clarity.

Since the copolymer is insoluble in water in the absence of cyclodextrin, classical titration techniques to calculate complex stoichiometry and stability could not be performed. However, the formation of specific inclusion complexes between HP α CD and polymeric nonyl-side chains could be proven by 2D-NOESY NMR spectroscopy, that showed a clear through-space coupling between the alpha-methylene groups of the poly(2-nonyl-2-oxazoline) amide and the HP α CD glucose-ring protons (see Figure 6.3.6). In addition, it was attempted to solubilize the copolymer with γ CD and HP γ CD, which are known to be poor hosts for linear aliphatic alkyl chains due to their larger cavity size, without success even in saturated solutions of the cavitands. These results thus confirmed that polymer solubilization and the formation of metastable nanoparticles is driven by specific host-guest complex formation between a suitable cavitand and the copolymer nonyl side chains.

Figure 6.3.6. 2D NOESY NMR spectrum of a PEtOx₆₂-ran-PNonOx₂₉ copolymer solution containing 3.3 equivalents of HP α CD (25 °C, D₂O). The sample was cooled to 0 °C before the measurement (see Figure 6.3.2, sample B). The polymeric NonOx signals (from 2.5 to 0.5 ppm) integrate only for 20% of the expected value as a result of their low mobility inside the nanoparticles. The two highlighted NOE signals correspond to the through-space coupling of the polymeric -N(CO)CH₂-(CH₂)₇CH₃ with the polymer backbone (circle) and the HP α CD glucose-ring protons (square), thus indicating a close spatial proximity between HP α CD cyclodextrin rim and the poly(2-oxazoline) side chains. Ak = CH₃ from EtOx and C₈H₁₇ from NonOx. R = H or hydroxypropyl.

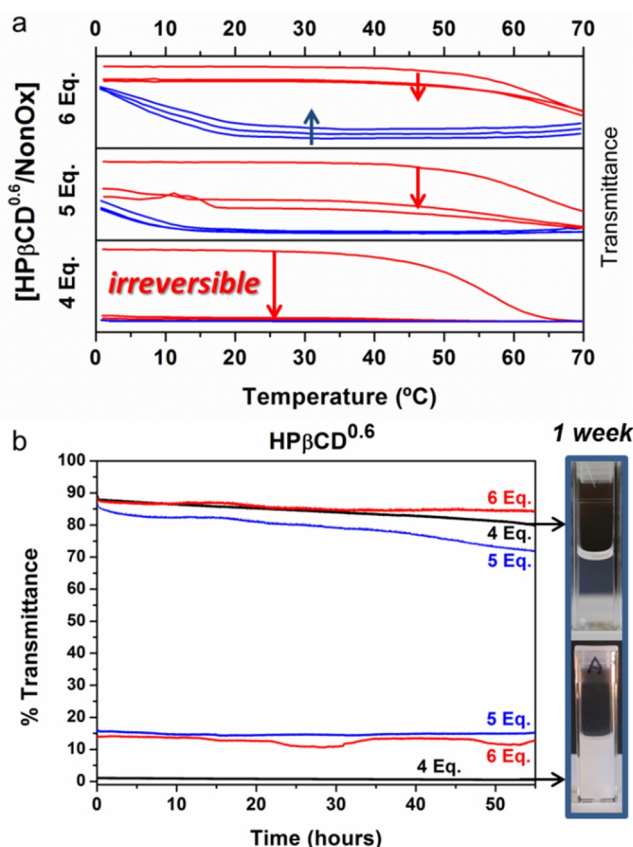


6.4 Poly(2-ethyl-2-oxazoline)₆₂-ran-poly(2-nonyl-2-oxazoline)₂₉ host-guest complexation with HP β CDs

Once a good understanding of the working principle of the supramolecular temperature sensor was obtained, the attention was focused on studying the effect of the cavitand structure on the transition temperature and memory function. HP β CD constitutes an alternative cavitand to HP α CD with a similar chemical structure while having a larger cavity (seven glucose units instead of six). When compared to the HP α CD-nonyl inclusion complex, this extended cavity results in a larger distance between the aliphatic nonyl chain and the hydrophobic inner cavity of the cyclodextrin. Consequently, the enthalpic gain upon complexation is reduced, as does the strength of the association.^[14] Figure 6.4.1a shows the evolution of the transition temperature of P[(EtOx)₆₂-ran-(NonOx)₂₉] with increasing concentrations of HP β CD^{0.6} (DS = 0.6). As expected, the amount of HP β CD^{0.6} required to solubilize the polymer is larger than with the smaller HP α CD^{0.6}, as a result of the lower association constant with the copolymer nonyl chains. The resulting transition temperature of the solution is ~60 °C and is again relatively independent of the host

concentration. In contrast to the previous results with HP α CD, however, the HP β CD-based sensor did not recover its transparency after one full heating/cooling cycle, an effect that is particularly seen when only four equivalents of HP β CD^{0.6} were added. This irreversibility of the transition can be ascribed to the lower association constant between HP β CD^{0.6} and aliphatic chains, preventing the cavitands from competing with the nonyl-nonyl hydrophobic interactions that are established upon thermal agglomeration of the copolymer nanoparticles. If more than the optimal four equivalents of cavitand are added, the solution progressively evolves towards an intermediate equilibrium situation after repeated heating/cooling cycles.

Figure 6.4.1. a) *Transmittance versus temperature plots of 5 mg mL⁻¹ solutions of P[(EtOx)₆₂-ran-(NonOx)₂₉] with increasing HP β CD^{0.6}/NonOx molar ratios. The heating and cooling ramps are represented by the top and bottom curves, respectively (3 consecutive cycles). The transition is optimal when 4 equivalents of HP β CD^{0.6} are used. Rate: 1 K min⁻¹, λ = 700 nm. b) *Evolution of the % transmittance in time of the same copolymer solutions with different HP β CD^{0.6}/NonOx molar ratios at isothermal conditions (25 °C) during 2.5 days. The samples were formerly cooled to 0 °C (top curves) or heated to 70 °C (bottom curves). All the samples exhibit long-term stability of the kinetically trapped supramolecular nanoparticles. The pictures show two aliquots of the same copolymer solution with 4 Eq. HP β CD^{0.6}, one heated to 70 °C (bottom) and other cooled to 0 °C (top) after staying for one week at room temperature.**

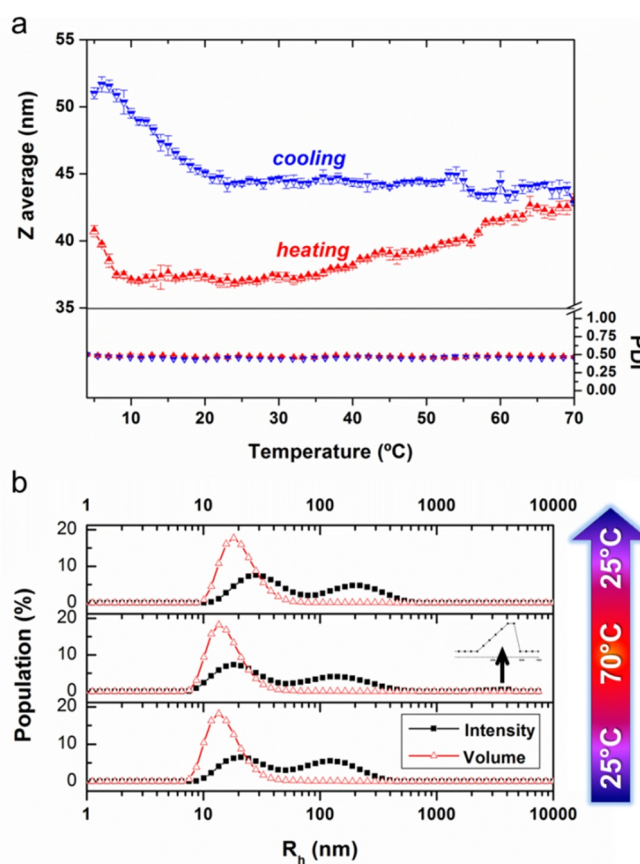


In analogy with the previously studied sensor comprising HP α CD, this HP β CD^{0.6} sensor “remembers” its thermal history after a long period of time (see Figure 6.4.1b). In contrast to the reversible nature of the sensor with HP α CD that allowed erasure of the memory by cooling to 5 °C, this sensor based on HP β CD exhibits an irreversible, permanent memory.

Further analysis of the HP β CD^{0.6} based supramolecular nanoparticles by dynamic light scattering showed the presence of ill-defined nanoparticles at 25 °C, including two populations of *ca.* 20 and 100–200 nm in size (Figure 6.4.2). The stability constant between HP β CD^{0.6} and nonyl chains seems therefore to be insufficient to maintain a single distribution of small defined nanoparticles. Upon heating, larger thermodynamically stable aggregates of *ca.* 4000 nm were irreversibly formed at the expense of the metastable 100–200 nm particles, and these large aggregates partially sedimented. When cooled back to 25 °C, the average size of the particles in solution was larger than before heating, sufficient to scatter light but not to turn the solution completely opaque. The slow heating rate of the DLS experiment (less than 0.01 K min⁻¹) apparently permitted the metastable 100–200 nm nanoparticles to dehydrate and irreversibly associate into large aggregates that precipitated from the solution. This irreversible precipitation was not observed in

the turbidimetry studies, where a heating rate of 1 K min^{-1} was applied, which seems to provide insufficient time for the metastable nanoparticles to re-arrange into large dehydrated aggregates. Turbidimetry studies at an intermediate heating rate of 0.1 K min^{-1} , were also performed and large aggregates were also not observed, as the nanoparticles did not have enough time to form large aggregates and remained trapped in the metastable 100-200 nm sized structures.

Figure 6.4.2. Temperature-dependent Dynamic Light Scattering (DLS) data for a 5 mg mL^{-1} solution of $P[(\text{EtOx})_{62}\text{-ran-(NonOx)}_{29}]$ and 4.0 equivalents of $\text{HP}\beta\text{CD}^{0.6}$ (relative to nonyl side chains). a) Z average and PDI evolution with temperature. \blacktriangle heating; \blacktriangledown cooling. Kinetically-trapped nanoparticles are formed at low temperature and are stable up to $40 \text{ }^\circ\text{C}$ (transparent solution); above this temperature, the particle size increases progressively and remains upon cooling. The increase in size observed below $20 \text{ }^\circ\text{C}$ upon cooling is a result of the copolymer LCST behavior (swelling of the nanoparticles hydrophobic cores). Four measurements are averaged at every temperature. Approximate heating/cooling rate: $< 0.01 \text{ K min}^{-1}$. b) Size distribution of the sample at $25 \text{ }^\circ\text{C}$, $70 \text{ }^\circ\text{C}$ and back to $25 \text{ }^\circ\text{C}$. At $25 \text{ }^\circ\text{C}$, ill-defined kinetically-trapped nanoparticles are observed. Heating to $70 \text{ }^\circ\text{C}$ leads to the appearance of larger particles and large aggregates that precipitate irreversibly. The nanoparticles remain stable when cooling back to $25 \text{ }^\circ\text{C}$.



In summary, $\text{HP}\beta\text{CD}^{0.6}$ is also able to form inclusion complexes with the nonyl side chains of the copolymer, leading to kinetically-trapped nanoparticles.^[15, 16] When the inclusion complexes are disrupted at elevated temperatures, the nonyl chains established efficient hydrophobic interactions that could not be disrupted by the cavitand upon cooling, leading to the irreversible collapse of the copolymer into 100-200 nm metastable particles. As a result, the solution acquired a white opaque appearance that remained stable in time.

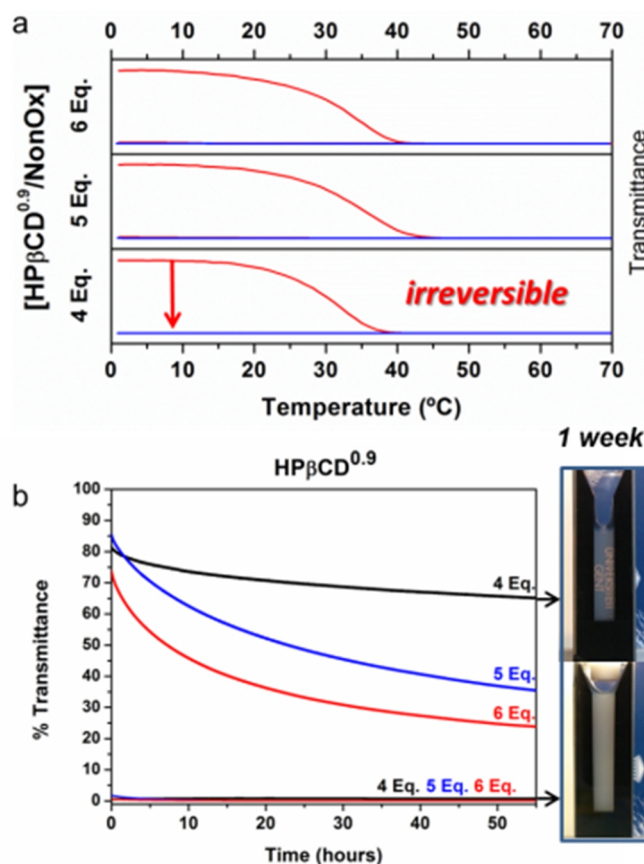
Next, it was hypothesized that the use of a cavitand with a lower association constant with the nonyl side chains would be able to enhance the irreversible coalescence of the copolymer, since a larger number of cavitand-nonyl chains complexes would thermally break during the phase transition, potentially leading to diminished effects of the heating rate.^[16] Interestingly, the binding strength of hydroxypropyl-cyclodextrins can be controlled by tuning the degree of hydroxypropyl substitution. Additional hydroxypropyl groups partially block the cyclodextrin cavity entrance sterically hindering inclusion complex formation, thereby lowering the association constant. In addition, hydroxypropyl substituents alter the cyclodextrin rigidity, resulting in a looser fit with the copolymer nonyl side chains.^[14, 17-19]

Therefore, hydroxypropyl- β -cyclodextrin with an average degree of substitution of 0.9 ($\text{HP}\beta\text{CD}^{0.9}$) was utilized to solubilize the copolymer, causing the transition temperature of the obtained sensor

to decrease to 30 °C, as seen in Figure 6.4.3a. The decrease in transition temperature upon host-guest complexation with a weaker host indicates that the temperature-triggered aggregation of the polymeric nanoparticles is driven by the breakage of the host-guest interactions and not by the LCST transition of the ensemble. Furthermore, this second pathway is disproved as the higher hydrophilicity of the more hydroxypropylated HP β CD^{0.9} should result in a higher transition temperature of the ensemble.

Similarly as with HP β CD^{0.6}, the T-induced aggregation was found to be irreversible, and the polymer could not be brought back in solution once the T_{CP} was reached. However, the copolymer phase transition was more abrupt, and had little dependence on the heating/cooling rate applied, confirming our initial hypothesis that a weaker cavitaand would enhance the copolymer coalescence.

Figure 6.4.3. a) *Transmittance versus temperature plots of 5 mg mL⁻¹ solutions of P[(EtOx)₆₂-ran-(NonOx)₂₉] with increasing HP β CD^{0.9}/NonOx molar ratios. The heating and cooling ramps are represented by the top and bottom curves, respectively (2 consecutive cycles). The transition is optimal when 4 equivalents of HP β CD^{0.9} are used. Rate: 1 K min⁻¹, λ = 700 nm. b) *Evolution of the % transmittance in time of the same copolymer solutions with different HP β CD^{0.9}/NonOx molar ratios at isothermal conditions (15 °C) during 2.5 days. The samples were formerly cooled to 0 °C (top curves) or heated to 70 °C (bottom curves). 4 equivalents of HP β CD^{0.9} provide long-term stability of the kinetically trapped supramolecular nanoparticles, whereas higher amounts produce an accelerated coalescence of the copolymer. The pictures show two aliquots of the same copolymer solution with 4 eq. HP β CD^{0.9}, one heated to 70 °C (bottom) and other cooled to 0 °C (top) after staying for one week at 15 °C. The difference between both sensors appearance remains clearly visible by eye.**

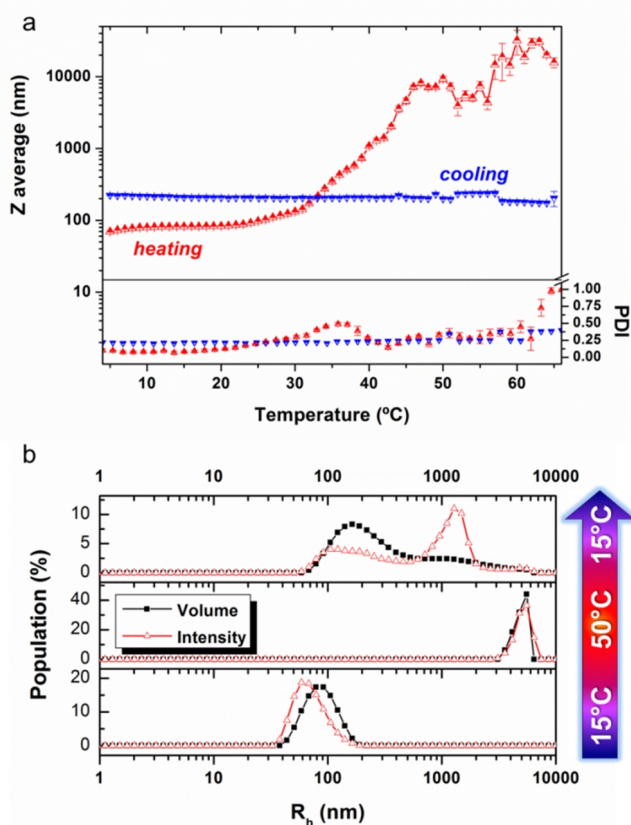


As seen in Figure 6.4.3b, all the solutions that were heated maintained their opacity in time at room temperature, due to the formation of thermodynamically stable aggregates. However, from the cooled solutions, only the copolymer solution with 4 equivalents HP β CD^{0.9} remained transparent for a long period of time while larger amounts of HP β CD^{0.9} accelerated the copolymer collapse from the metastable to the thermodynamic state. A review of the solution history is necessary to interpret this atypical behavior: when the copolymer was initially solubilized from its solid amorphous state at 0 °C in the presence of 4 equivalents of HP β CD^{0.9}, kinetically-trapped nanoparticles were formed. These nanoparticles comprise a hydrophobic core of amorphous copolymer and a hydrophilic corona of cyclodextrin-nonyl inclusion complexes. The addition of increasing concentrations of HP β CD^{0.9} leads to the formation of a larger number of HP β CD^{0.9}-nonyl

inclusion complexes that, upon dynamic breakage, result in a more efficient rearrangement of the copolymer by nanoconfinement. HP β CD^{0.9} might then be unable to compete with the efficient packing of the nonyl chains present in the coalesced copolymers.^[16] Moreover, the observed aggregation could not be ascribed to HP β CD^{0.9} intermolecular interactions due to: 1) substitution of hydroxyl groups by hydroxypropyl groups suppresses cyclodextrin intermolecular hydrogen-bonding and consequently aggregation and 2) cyclodextrin aggregation is inversely proportional to temperature.^[20-22]

To ascertain the topology of the kinetically-trapped nanoparticles, the sensor containing the optimal molar ratio of HP β CD^{0.9} was analyzed by dynamic light scattering (see Figure 6.4.4.). Monodisperse (PDI \approx 0.08) kinetically trapped nanoparticles were observed at low temperatures that remained stable up to 30 °C. Further increase in temperature led to the formation of large thermodynamically stable aggregates that turned the solution opaque. The long exposure of the aggregates (hours) to high temperatures together with the lack of stirring provoked their sedimentation on the bottom of the cuvette during the DLS measurements, and therefore they were not detected during the cooling ramp. This sedimentation was not observed in turbidimetry studies, where the sensor was not exposed to high temperatures for long periods of time (see Figure 6.4.3.).

Figure 6.4.4. *a) Temperature-dependent Dynamic Light Scattering data for a 5 mg mL⁻¹ solution of P[(EtOx)₆₂-ran-(NonOx)₂₉] and 4.0 equivalents of HP β CD^{0.9} (relative to nonyl side chains). a) Z average and PDI evolution with temperature. \blacktriangle heating; \blacktriangledown cooling. Well-defined kinetically-trapped nanoparticles are formed at low temperature and are stable up to 30 °C (transparent solution); above this temperature, the particle size increases exponentially (note the logarithmic scale of the Z average axis). Beyond 50 °C, large aggregates are formed and sediment –count rate decreased by a factor of 20–. Upon cooling, only the most stable aggregates remained in solution. Four measurements are averaged at every temperature. Approximate heating/cooling rate: < 0.01 K min⁻¹. b) Size distribution of the sample at 15 °C, 50 °C and back to 15 °C. At 15 °C, well-defined stable nanoparticles are observed (Z_{ave} = 80 nm, PDI < 0.10). Heating to 50 °C led to the abrupt appearance of large aggregates. Back to 15 °C, both large stable particles and aggregates were present.*



The supramolecular assembly of HP β CD^{0.9} and the nonyl chains of the P[(EtOx)₆₂-ran-(NonOx)₂₉] copolymer thus also results in a temperature sensor with permanent memory function, due to the polymer rearrangement by nanoconfinement induced by the HP β CD^{0.9} hosts.

6.5 A different polymeric supramolecular system: PNIPAM-naphtalene - Blue Box

In collaboration with Prof. Patrice Woisel, from the Unité des Matériaux et Transformations, UMR CNRS 8207 (Université Lille Nord de France, ENSCL) and Prof. Graeme Cook, from the Glasgow Centre for Physical Organic Chemistry (University of Glasgow) et al. †

The described strategy to produce temperature sensors with memory by a supramolecular approach, has been proven to be applicable to other polymeric host-guest systems, even when they are based on a completely different polymer platform and host macromolecule. Our collaborators synthesized a poly(*N*-isopropylacrylamide) (PNIPAM) with hydrophobic dialkoxynaphthalene moieties in the side chain and studied its thermoresponsive properties in solution. The electron-rich dialkoxynaphthalene units can form host-guest complexes with the hydrophilic tetracationic macrocyclic host cyclobis(paraquat-*p*-phenylene) tetrachloride (CBPQT⁴⁺), also known as *blue-box*.^[23] The addition of CBPQT⁴⁺ to a colorless solution of the copolymer in water immediately resulted in the formation of a purple-colored solution indicating the formation of dialkoxynaphthalene- CBPQT⁴⁺ complexes. In addition, the appearance of an absorption band around 520 nm in the UV-vis spectra, which is characteristic for naphthalene – CBPQT⁴⁺ donor-acceptor inclusion complexes, further proved the proposed supramolecular complexation (see Figure 6.5.1). The complexation was also proven by ¹H-NMR spectroscopy and isothermal titration calorimetry revealing an association constant of $K_a = 1.8 (\pm 0.1) 10^4 \text{ M}^{-1}$, and a binding stoichiometry of $N = 4.6 (\pm 0.1)$.^[24]

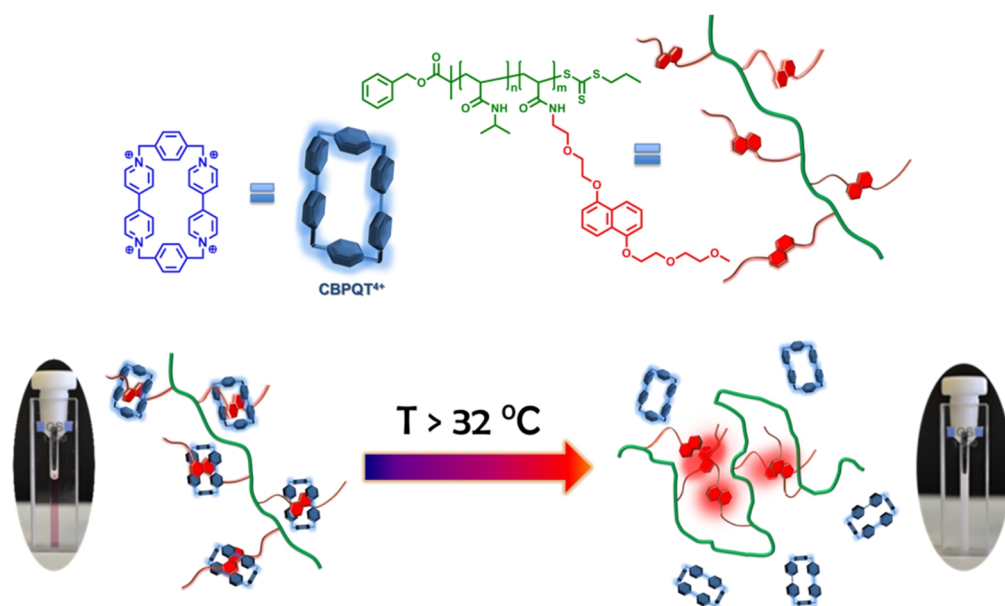


Figure 6.5.1. *Top: Structures of the utilized CBPQT⁴⁺ host and the dialkoxynaphthalene functionalized PNIPAM. Bottom: Schematic representation of the decomplexation of the host-guest assembly during the LCST phase transition (TCP = 32 °C in the presence of 5 equivalents CBPQT⁴⁺). This decomplexation will be the basis for the stability of the hysteresis window associated with the ensemble phase transition.*

This research has been published in: Sambe, L.; de La Rosa, V. R.; Belal, K.; Stoffelbach, F.; Lyskawa, J.; Delattre, F.; Bria, M.; Cooke, G.; Hoogenboom, R.; Woisel, P. *Angew. Chem. Int. Ed.*, **2014**, *53*, 5044–5048.

The host-guest complexation had a strong impact on the Lower Critical Solution Temperature (LCST) behavior of the copolymer. The addition of 5 equivalents of CBPQT⁴⁺ to a solution containing 5 mg mL⁻¹ of PNIPAM₁₉₅-naphthalene₅ copolymer resulted in an increase in the polymer cloud point temperature from 20 °C to 32 °C.

Interestingly, turbidimetry experiments on the PNIPAM₁₉₅-naphthalene₅ copolymer with CBPQT⁴⁺ revealed that the LCST-mediated polymer phase transition of PNIPAM caused a complete disappearance of the purple color. This indicated the complete disassembly of the donor-acceptor complexes, and resembled the behavior of the previously studied PEtOx₆₂-*ran*-PNonOx₂₉ – cyclodextrin system, thus suggesting the possibility of also obtaining a stable hysteresis window and, consequently, a memory function.

Therefore, we recorded two heating-cooling cycles of a solution containing PNIPAM₁₉₅-naphthalene₅ copolymer in the presence of 5 equivalents of CBPQT⁴⁺ (Figure 6.5.2a). Upon heating, the polymer phase transition occurs at 32 °C as discussed previously but, during cooling, redissolution of the polymer only occurred at 21 °C, which is similar to the T_{CP} of the copolymer in the absence of CBPQT⁴⁺. This large hysteresis can be directly ascribed to the destruction of the host-guest complex during precipitation: during heating, the solubility of the supramolecular assembly is determined by the ensemble of the copolymer and the more hydrophilic CBPQT⁴⁺ host while, during cooling, the solubility behavior of the copolymer prevails, as apparently the host-guest complexes can only be reformed when the copolymer goes back in solution.

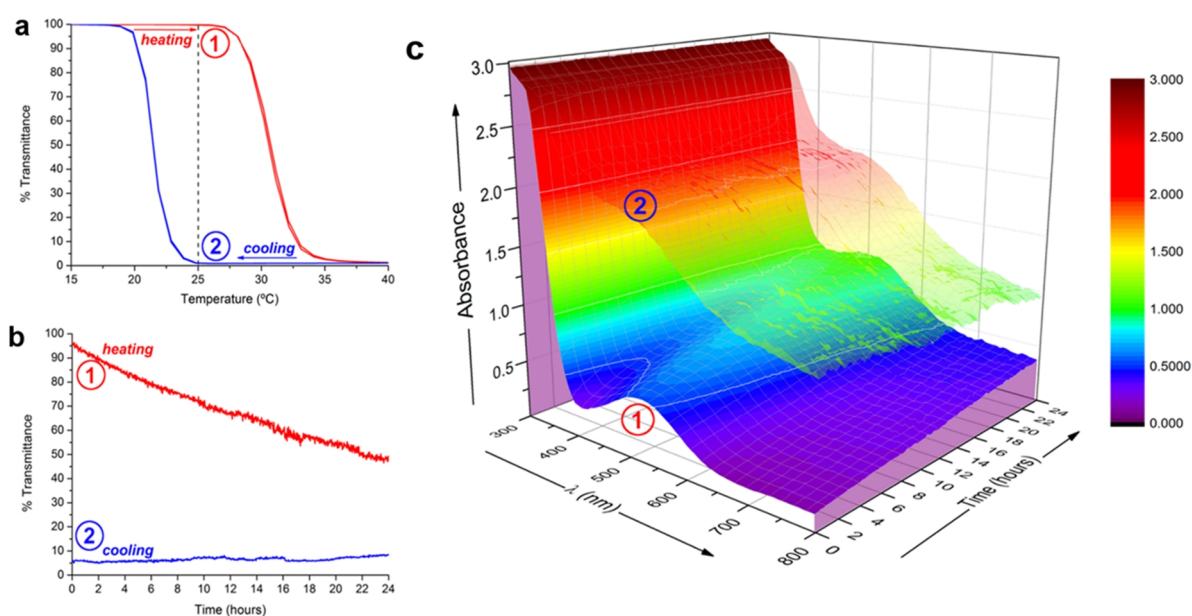


Figure 6.5.2. *UV-vis experiments demonstrating memory-stability. All the memory-stability experiments were performed on aliquots from a solution containing the PNIPAM₁₉₅-naphthalene₅ copolymer (5 mg ml⁻¹) and 5 equivalents of CBPQT⁴⁺. (a) Transmittance versus temperature plot (2 overlapping heating/cooling cycles). The memory-stability experiments were performed at 25 °C (dotted line), within the limits of the hysteresis window. Heating rate: 1 K min⁻¹, $\lambda = 700$ nm. (b) Evolution of transmittance at 700 nm at 25 °C for a sample that was cooled from 45 °C to 25 °C (label (1)) and a sample that was heated from 15 °C to 25 °C (label (2)). (c) Full UV-vis absorbance spectra of the solution at 25 °C corresponding to the heated and cooled samples in b. The spectra were isothermally recorded over a period of 24 hours (1 scan/1.4min.).*

The stability of the temperature memory window was studied *via* isothermal UV-vis turbidity measurements during a period of 24 hours. Therefore, an aqueous solution of the PNIPAM₁₉₅-naphthalene₅ copolymer (5 mg mL⁻¹) and 5 equivalents of CBPQT⁴⁺ was heated beyond the T_{cp} (heating) to become white opaque followed by cooling back to 25 °C, which is within the hysteresis window. This sample was kept for 24 hours at 25 °C revealing that the solution maintained its cloudy appearance (Figure 6.5.2) and no visible changes, such as redissolution or macroscopic precipitation of the collapsed polymeric globules, occurred. This clearly demonstrates that the system has a memory function and that the solution 'remembered' being heated above the T_{cp} by remaining cloudy when cooled back to 25 °C.

Conversely, an aliquot of the same solution was cooled down below the T_{cp} (cooling) resulting in a purple transparent solution. This solution was subsequently heated to 25 °C where the evolution of its UV-vis absorbance was followed for 24 h. In this case, a steady decrease of transmittance could be observed, as the naphthalene-CBPQT⁴⁺ host-guest interactions of the kinetically trapped, metastable, complex were progressively lost and, as a result, the polymer collapsed and aggregated. The disassembly of the naphthalene-CBPQT⁴⁺ complex can be also followed by the progressive flattening of the absorbance band at ca. 520 nm (Figure 6.5.2c). However, this transition from the kinetically trapped soluble polymer to the thermodynamically stable precipitated state was found to be very slow, and the solution still exhibited 70 % transmittance even after 10 hours at 25 °C. The solution still maintained a 50 % transmittance after 24 hours, which is sufficient to be distinguishable by eye from the formerly heated sample.

In conclusion, this PNIPAM-naphthalene thermoresponsive copolymer formed host-guest complexes with an electron deficient CBPQT⁴⁺ host molecule resulting in a (re)programmable temperature sensor with memory function featuring a colorimetric readout.[‡]

Albeit the time-scale of the memory function was far from the results obtained for the P(EtOx)₆₂-*ran*-P(NonOx)₂₉ – cyclodextrin system, it was demonstrated that the developed supramolecular host-guest approach constitutes an effective method to enable memory function in solution polymeric temperature sensors.

6.6 Conclusions

Soluble temperature sensors with an unprecedented long-term thermal memory function were developed by supramolecular assembly of a simple amphiphilic P[(EtOx)₆₂-*ran*-(NonOx)₂₉] copolymer together with a range of suitable hydrophilic cyclodextrins. Kinetically-trapped nanoparticles were formed at low temperature through inclusion-complex formation of hydroxypropylated cyclodextrins and the copolymer pendant nonyl chains. The choice of cyclodextrin and its concentration enabled control over the dynamics of the kinetically-trapped state, permitting to tune the sensor transition temperature and its reversibility.

A similar strategy based on supramolecular host-guest interactions of poly(*N*-isopropylacrylamide) (PNIPAM) with side-chain naphthalene guest moieties and the tetracationic macrocyclic cyclobis(paraquat-*p*-phenylene) (CBPQT⁴⁺) host resulted in a polymeric thermometer thermometer with memory function. In analogy with the poly(2-oxazoline)-cyclodextrin system, the memory feature arises from the large hysteresis of the thermoresponsive LCST phase transition which is

[‡] A multimedia file describing the working mechanism of the sensor can be found online at <http://dx.doi.org/10.1002/anie.201402108>.

based on the formation of a metastable soluble state consisting of the PNIPAM – CBPQT⁴⁺ host-guest complex. (see Figure 6.6.1).

To the best of our knowledge, the hereby developed systems represent the first reported soluble polymeric temperature sensors with a long-term memory function. In the case of the PEOx-PNonOx – cyclodextrin system, the memory time scale allows the observer to keep track of the thermal history of the system even days or weeks after the programmed temperature was surpassed. These developed thermometers with long-term memory function might find use in applications ranging the physical and biological sciences, as water soluble sensors have great potential for *in vivo* thermography.

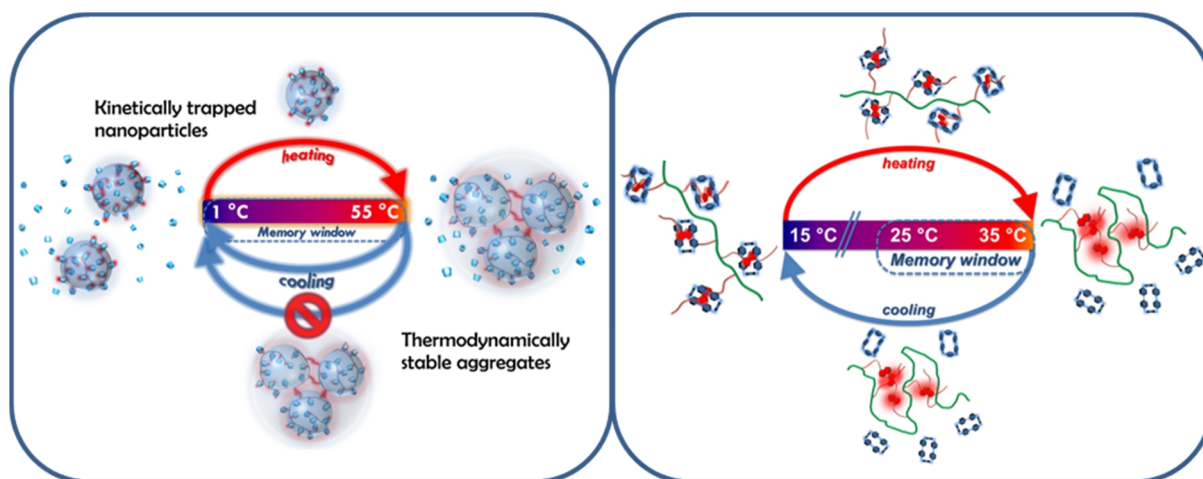


Figure 6.6.1. *Schematic representation of the developed soluble polymeric temperature sensors that are able to store thermal information for a long time, based on the stability of its constituent kinetically-trapped supramolecular nanoparticles. In the case of the PEOx-PNonOx system, the information can be erasable (by cooling), or permanently recorded, depending on the choice of the cyclodextrin host.*

In addition, the analysis of the mechanism behind the sensor long-term memory at the nanoscale sheds light onto the importance of out-of-equilibrium dynamic supramolecular assemblies, which are the foundation of biological supramolecular processes enabling living matter.

6.7 Experimental Section

Materials

Solvents and reagents were purchased from Sigma Aldrich, and used as received unless otherwise specified. Methyl tosylate (MeOTs) was distilled twice under vacuum prior to use. 2-Ethyl-2-oxazoline (EtOx, Aldrich) and 2-nonyl-2-oxazoline (NonOx, kindly donated by Henkel) were distilled over barium oxide (BaO). Acetonitrile (CH₃CN, Acros Organics) was dried over molecular sieves (3Å). All reagents were stored and handled under a dry argon or nitrogen atmosphere. KOH, and tetramethylammonium hydroxide in methanol (25 wt.%) were used as received.

Native γ -cyclodextrin, 2-hydroxypropyl- α -cyclodextrin (degree of substitution, DS = 0.6), 2-hydroxypropyl- β -cyclodextrin (DS = 0.6), 2-hydroxypropyl- β -cyclodextrin (DS = 0.9) were used as received from Aldrich. The degree of hydroxypropyl substitution corresponds to the average

number of hydroxypropyl groups per glucose unit and was confirmed by $^1\text{H-NMR}$ spectroscopy in D_2O (Euriso Top).

Deionized (Milli-Q) water was obtained from a Sartorius Arium 611 with a Sartopore 2 150 (0.45 + 0.2 μm pore size) cartridge filter (resistivity $\geq 18.2 \text{ M}\Omega \text{ cm}$).

Instrumentation

$^1\text{H-NMR}$ spectra were recorded in CDCl_3 on a Bruker Avance 300 MHz spectrometer, to calculate polymer composition, and in D_2O to calculate the hydroxypropyl-cyclodextrins degree of substitution. Quantitative $^1\text{H-NMR}$ and $2\text{D-}^1\text{H-NMR}$ spectra were recorded on a Bruker Avance III Spectrometer operating at a ^1H frequency of 500 MHz, equipped with a 5 mm BBI-Z probe or on a Bruker Avance II Spectrometer operating at a ^1H frequency of 500 MHz, equipped with a 5 mm TXI-Z (^1H , ^{13}C , ^{31}P) 3-channel probe. The quantitative measurements were executed with a relaxation delay of 30 seconds and concentrations were obtained using the ERETIC method. Spectra were all processed using TOPSPIN 3.0.

Size exclusion chromatography (SEC) measurements were performed on an Agilent 1260-series equipped with a 1260 ISO-pump, a 1260 Diode Array Detector (DAD), a 1260 Refractive Index Detector (RID), and a PSS Gram30 column in series with a PSS Gram1000 column inside a 1260 Thermostated Column Compartment (TCC) at 50°C using dimethylacetamide containing 50 mM of LiCl (flow rate of 0.6 mL min^{-1}) as solvent. Molar masses and dispersities were calculated against poly(methyl methacrylate) standards.

Poly[(2-ethyl-2-oxazoline)-*ran*-(2-nonyl-2-oxazoline)] synthesis

The polymerization was performed as previously reported^[10] in a capped vial in a single mode microwave Biotage initiator sixty using temperature control based on an IR temperature sensor. The vial was heated to 120°C for 24 hours and cooled down under vacuum before usage. The vial was loaded with 0.0335 g of MeOTs (0.18 mmol, 1 equivalent), 1.250 g of EtOx (12.6 mmol, 70 equivalents) and 1.065 g of NonOx (5.40 mmol, 30 equivalents), in dry acetonitrile (total monomer concentration of 4M). The polymerization was run for 15 minutes at 140°C , and the polymer was terminated with KOH in methanol, yielding a hydroxyl-terminated polymer. The solvent was evaporated under reduced pressure, and the polymer was subsequently precipitated in diethyl ether from dichloromethane. The pure polymer was then dried in a vacuum oven at 50°C for 24h.

Turbidimetry and dynamic light scattering studies

Turbidimetry measurements were performed in a CARY Bio 100 UV-VIS spectrophotometer equipped with a temperature controller, at a wavelength of 700 nm. Heating/cooling cycles were performed at a rate of 1K min^{-1} or 0.1K min^{-1} with stirring. The polymer concentration was kept at 5 mg mL^{-1} in deionized water. The equivalents of cyclodextrin added were calculated in relation to the equivalents of nonyl side chains.

Dynamic light scattering (DLS) was performed on a Zetasizer Nano-ZS Malvern apparatus (Malvern Instruments Ltd) using disposable PMMA cuvettes. The excitation light source was a He–Ne laser at 633 nm, and the intensity of the scattered light was measured at 173° . This method measures the rate of the intensity fluctuation and the size of the particles is determined through the Stokes–Einstein equation ($d(H) = \sqrt{kT/3\pi\eta D}$) where $d(H)$ is the mean hydrodynamic diameter, k is the Boltzmann constant, T is the absolute temperature, η is the viscosity of the dispersing medium, and D is the apparent diffusion coefficient. Before starting the measurements, samples were equilibrated at the specific temperature for at least 300 s. The samples were analyzed four times,

allowing the calculation of the corresponding Z_{ave} and PDI uncertainties. Samples were filtered through Millipore membranes with a pore size of 0.2 μm prior to measurement.

6.8. References

- [1] J. Kunzleman, T. Chung, P. T. Mather, C. Weder, *J. Mater. Chem.* **2008**, *18*, 1082.
- [2] A. M. DiOrto, X. Luo, K. M. Lee, P. T. Mather, *Soft Matter* **2011**, *7*, 68.
- [3] M. Behl, K. Kratz, U. Noechel, T. Sauter, A. Lendlein, *Proc. Natl. Acad. Sci. U. S. A.* **2013**.
- [4] F. Grillard, P. Poulin, A. Korzhenko, P. Gaillard, C. Zakri, *ACS Macro Lett.* **2014**, 224.
- [5] N. Herzer, H. Guneyusu, D. J. D. Davies, D. Yildirim, A. R. Vaccaro, D. J. Broer, C. W. M. Bastiaansen, A. P. H. J. Schenning, *J. Am. Chem. Soc.* **2012**, *134*, 7608.
- [6] D. J. D. Davies, A. R. Vaccaro, S. M. Morris, N. Herzer, A. P. H. J. Schenning, C. W. M. Bastiaansen, *Adv. Funct. Mater.* **2013**, *23*, 2723.
- [7] T. Tsuji, S. Yoshida, A. Yoshida, S. Uchiyama, *Anal. Chem.* **2013**, *85*, 9815.
- [8] K. Okabe, N. Inada, C. Gota, Y. Harada, T. Funatsu, S. Uchiyama, *Nat. Commun.* **2012**, *3*, 705.
- [9] C. Pietsch, U. S. Schubert, R. Hoogenboom, *Chem. Commun.* **2011**, *47*, 8750.
- [10] M. W. M. Fijten, J. M. Kranenburg, H. M. L. Thijs, R. M. Paulus, B. M. van Lankvelt, J. de Hullu, M. Springintveld, D. J. G. Thielen, C. A. Tweedie, R. Hoogenboom, K. J. Van Vliet, U. S. Schubert, *Macromolecules* **2007**, *40*, 5879.
- [11] G. Castronuovo, V. Elia, A. Iannone, M. Niccoli, F. Velleca, *Carbohydr. Res.* **2000**, *325*, 278.
- [12] D. Hallen, A. Schon, I. Shehatta, I. Wadso, *J. Chem. Soc., Faraday Trans.* **1992**, *88*, 2859.
- [13] Y. Zhao, K. Guo, C. Wang, L. Wang, *Langmuir* **2010**, *26*, 8966.
- [14] S. Concha-Santos, S. Pérez-Casas, P. Brocos, Á. Piñeiro, *J. Chem. Thermodyn.* **2013**, *67*, 112.
- [15] Y. Liu, D. Zhao, R. Ma, D. a. Xiong, Y. An, L. Shi, *Polymer* **2009**, *50*, 855.
- [16] A. E. Tonelli, *Beilstein J. Org. Chem.* **2012**, *8*, 1318.
- [17] C. Schönbeck, P. Westh, J. C. Madsen, K. L. Larsen, L. W. Städe, R. Holm, *Langmuir* **2010**, *26*, 17949.
- [18] H. Chen, H. Ji, *Supramol. Chem.* **2014**, *1*.
- [19] C. Tang, A. Inomata, Y. Sakai, H. Yokoyama, T. Miyoshi, K. Ito, *Macromolecules* **2013**, *46*, 6898.
- [20] C. Yong, C. Washington, W. Smith, *Pharm. Res.* **2008**, *25*, 1092.
- [21] I. Puskás, M. Schrott, M. Malanga, L. Szenté, *J. Inclusion Phenom. Macrocyclic Chem.* **2013**, *75*, 269.
- [22] M. Bonini, S. Rossi, G. Karlsson, M. Almgren, P. Lo Nostro, P. Baglioni, *Langmuir* **2006**, *22*, 1478.
- [23] B. Odell, M. V. Reddington, A. M. Z. Slawin, N. Spencer, J. F. Stoddart, D. J. Williams, *Angew. Chem. Int. Ed. Engl.* **1988**, *27*, 1547.
- [24] L. Samba, V. R. de La Rosa, K. Belal, F. Stoffelbach, J. Lyskawa, F. Delattre, M. Bria, G. Cooke, R. Hoogenboom, P. Woisel, *Angew. Chem. Int. Ed.* **2014**, *53*, 5044.

The control on the synthesis of polymers and macromolecules only allowed researchers in recent history (it should not be forgotten that the mere existence of polymers was still under discussion until well inside last century) to modulate the behavior and assembly of polymeric systems in solution. This has resulted in the dawn of completely new research areas that benefit from the control on nanostructures in solution granted by this new macromolecular tool-box.

This thesis has focused on the development of smart polymers in solution based on the versatile polymer platform that constitute poly(2-alkyl/aryl-2-oxazoline)s (PAOx).

Chapter 2 describes detailed investigations on PAOx hydrolysis to obtain polyethyleneimine (PEI) copolymers. New methods have been developed to synthesize PAOx-PEI quasi-block copolymers by selective partial hydrolysis of double hydrophilic PAOx block copolymers, by rational tuning of the composition of ethanol-water binary solvent mixtures. Future work may be directed towards the use of different alcohols that might be more efficient at shielding the hydrophobic block from the hydronium ions that catalyze the amide hydrolysis. For instance, longer alkylic alcohols could yield high selectivity in the hydrolysis of PAOx block copolymers with a thermoresponsive block, leading to thermoresponsive PAOx-*b*-PEI copolymers and ultimately in thermoresponsive polyplexes. The thermal collapse of the thermoresponsive block might facilitate the release of the poly(nucleic acid)s cargo entrapped by the PEI block.

In the same context, a robust and efficient method was developed to partially hydrolyze PAOx with accurate control over the hydrolysis degree, by using sub-stoichiometric amounts of acid. Although amide hydrolysis is an acid-catalyzed reaction, the recovered hydronium ion upon hydrolysis can be trapped by the basic secondary amine formed, therefore enabling control over the degree of hydrolysis. Moreover, besides achieving a high level of control on the hydrolysis process, the reaction was greatly accelerated by increasing temperature. The partially hydrolyzed polymers were analyzed by size exclusion chromatography (SEC), revealing polymer decomposition beyond 180 °C, that was found to be the optimal temperature to perform the reaction. Therefore, the developed methodology greatly facilitates synthesis of PAOx-PEI copolymers and the use of the secondary amines present in the PEI units as handles for further polymer modification. In addition, the synthesis of PAOx-based hydrogels will benefit from the developed protocol.

In Chapter 3, the effect of temperature and terminating agent was investigated in detail for the synthesis of poly(2-ethyl-2-oxazoline) (PEtOx). In the range from 80 °C to 140 °C, the polymerization was greatly accelerated without the observation of major effects on polymer molecular weight distribution or end-group fidelity. However, the use of high temperatures tends to result in exposure of the polymer living chains to heat in the absence of monomer units, inducing minor chain-coupling reactions. Regarding termination, the widespread termination with potassium hydroxide in methanol was found to result in the occurrence of side reactions leading to a hydrolyzed ester-amine end-group, instead of the intended hydroxyl amide end functionality. Tetramethylammonium hydroxide, however, was found to be an efficient terminating agent leading to quantitative –OH termination. Albeit useful for the synthesis of PEtOx at high temperatures, and for the production of –OH terminated PAOx, this study only partially covered the optimization of PAOx synthesis. Therefore, there is still a necessity of more in depth fundamental studies on the polymerization mechanism of (2-oxazoline)s and the associated intrinsic side reactions.

The obtained PEtOx-OH polymers were used as macroinitiators for the polymerization of polycarbonates, resulting in amphiphilic block copolymers that self-assembled into a variety of

structures in solution, including star-shaped and crew-cut micelles, or polymersomes. The topology of the formed structures could be modulated by the composition of the hydrophobic polycarbonate block, even when the relative length of the hydrophilic and hydrophobic chains was unvaried. The formed micelles and polymersomes have recently been found to be readily incorporated by cells, and research will continue to assess their efficacy as biodegradable drug-delivery carriers.

The thermoresponsive behavior of PAOx was exploited in Chapter 4 in combination with gold nanoparticles (AuNPs). A new synthesis strategy was developed, based on termination of the PAOx living chain with potassium ethyl xanthatogenate, affording xanthate-functional PAOx in a straightforward manner. These functional PAOx were grafted onto AuNPs in a simple way, resulting in dual stimuli-responsive PAOx@AuNP hybrids. Besides serving as highly sensitive solution temperature sensors, the dual responsive character of the PAOx@AuNPs was applied to obtain colorimetric AND logic gates, advancing in the development of smart systems. Importantly, the thermal trigger threshold could be tuned by variation of the PAOx composition. Furthermore, the synthesized xanthate-functional PAOx can be easily converted into thiol-functional PAOx by aminolysis, opening new direct synthetic possibilities for this polymer type, such as the efficient thiol-ene chemistry, which will certainly be subject of further research.

Finally, the last two chapters dealt with the synergetic combination of polymer and supramolecular chemistry. A series of PAOx amphiphilic copolymers, based on 2-ethyl- and 2-nonyl-2-oxazoline (NonOx), were synthesized and their thermoresponsive behavior studied in the presence of different cavitands. The cavitands formed host guest interactions with the copolymer pendant nonyl chains, leading to an increase in the cloud point temperature of the thermoresponsive polymer. Interestingly, the extent of this increase was found to be mainly dependent on the strength of the binding constant between the macromolecular hosts and the polymeric nonyl side chain-guests.

On the other hand, polymer composition had a profound impact on the solubility properties of the copolymer. Inclusion complex formation of cavitands with polymers containing *ca.* 10 % NonOx (in number) formed stretched random coil structures. As the hydrophobic nonyl content increased to *ca.* 20 %, these structures started to fold and arranged into well-defined nanoparticles during the copolymer-cavitand ensemble phase transition. Further increase of the nonyl content to *ca.* 30 % resulted in stronger intramolecular hydrophobic interactions within the copolymer chains and the formation of stable kinetically trapped nanoparticles in solution at low temperature. The nanoparticles aggregated upon increasing temperature, and remained stable even after lowering the temperature below the ensemble T_{CP} , thereby recording thermal information from the solution. Interestingly, by tuning the strength of the macromolecular host used, the reversibility of the phase transition could be controlled, providing sensors with erasable or permanent memory. A similar system was reported based in a completely different supramolecular host-guest system based on cyclobis(paraquat-*p*-phenylene)- PNIPAAm-naphtalene, confirming the broad applicability of this supramolecular polymeric design.

In all, during this thesis we have developed new synthetic methodologies to further expand the scope of PAOx and PEI as a versatile platform in biomedicine and supramolecular chemistry. In addition, we have investigated the subtle balances that modulate polymer self-assembly in solution, and the synergy that results from the combination of polymers with supramolecular hosts.

To summarize, the Bijzonder Onderzoeksfonds (BOF) project under which I had the fortune to be subject, granted me with the research freedom needed to explore a wide variety of topics, from which some could not make it into this thesis, but in all gave me the opportunity to explore the synthesis and characterization of fascinating polymeric and supramolecular systems. I am convinced that, in the coming years, the fast advance in these blooming fields will result in personalized targeted therapies, and will furnish the world around us with smart materials. Hopefully we make the grade!

De evolutie van onze menselijke beschaving wordt gestuurd door de ontwikkeling van nieuwe materialen en manieren om onze omgeving te controleren. Door de geschiedenis heen, overheerste het paradigma om specifieke functionele materialen te ontwikkelen die onveranderlijk bleven onder externe factoren. In dat opzicht, bewandelde de mensheid een tegennatuurlijk pad. Ons huidige inzicht in de werking van de natuur, en de chemische mechanismen die daar ten grondslag aan liggen, heeft tot een meer intelligente benadering van dit paradigma geleid. Onze focus ligt niet langer op het ontwerp van inerte materialen met een specifieke functie, maar op functionele materialen die zich kunnen aanpassen aan een steeds veranderende omgeving.

Dankzij de opkomst van levende en gecontroleerde polymerisatietechnieken zijn we in staat zulke responsieve, functionele materialen te ontwikkelen, vaak geïnspireerd door de werking van natuurlijke systemen. De gecontroleerde synthese van gedefinieerde polymeren heeft tot een beter inzicht in structuur-eigenschap relaties geleid. Meer bepaald, heeft dit inzicht een beter begrip van de conformatie van zulke gedefinieerde polymeerketens op nanoniveau tot stand gebracht, naar analogie van natuurlijke polymeren zoals proteïnen en DNA. Het gebruik van deze gedefinieerde polymeer-gebaseerde materialen hebben al snel een toepassing gevonden in biomedisch onderzoek, zoals gedetailleerd wordt toegelicht in de inleiding van deze dissertatie. Er wordt verwacht dat poly(2-alkyl/aryl-2-oxazoline)s (PAOx) een prominente rol zullen spelen in dit onderzoeksdomein, aangezien reeds werd aangetoond dat deze polymeren kwalitatief beter presteert op vlak van veiligere implantaten, effectievere tabletten, betere weefselverbanden of geavanceerde doelgerichte therapiën.

Ondanks het belang op zoek te gaan naar nieuwe toepassingen en functionaliteiten, is gedetailleerde literatuur, handelend over PAOx polymeersynthese, moleculaire compositie en moleculaire massaverdeling vrij beperkt in recente jaren. Dit staat in schril contrast met het grote aantal publicaties die verschenen zijn rond polyethyleenimine (PEI) synthese. Daarom zal in de loop van deze dissertatie, de synthese en functionalisatie van PAOx in detail bestudeerd worden, met als doel de optimalisatie van de PAOx synthese op een snelle en reproduceerbare wijze. Bovendien wordt de synthese van PEI, door selectieve of gedeeltelijke hydrolyse van PAOx, onderzocht. Dit resulteert in efficiënte methodes om vectoren voor genterapie te verkrijgen, alsook in het toegankelijker maken van de structurele en functionele verscheidenheid van PAOx. Deze onderwerpen worden besproken in hoofdstuk 2 en 3 van deze dissertatie.

Zoals eerder vermeld is inzicht in de structuur-eigenschap relatie, die de conformationele organisatie van polymeren in complexe architecturen op nanoschaal bepaald, erg belangrijk in de ontwikkeling van responsieve, functionele materialen. Daarom wordt in hoofdstuk 3, de samenstelling van amfifiele PAOx-polycarbonaat blok copolymeren gevarieerd om hun zelf-organisatie in oplossing te moduleren. Er werd geopteerd voor een hydrofoob polycarbonaat blok omwille van zijn biocompatibiliteit. Dit resulteerde in een grote variëteit aan morfologiën, gaande van sterachtige, tot 'crew-cut' micellen en polymersomen. De structuur-eigenschap relaties werden onderzocht zodat het ontwerp van nieuwe transportmiddelen voor medicijn afgifte of diagnostiek gerationaliseerd kan worden.

Het tweede deel van deze dissertatie handelt over de ontwikkeling van intelligente materialen die, in oplossing, in staat zijn te reageren op externe stimuli. In hoofdstuk 4 wordt een nieuwe functionalisatie strategie voorgesteld om het oppervlak van gouddeeltjes te modificeren met PAOx. Zulke systemen zijn potentieel interessant in het ontwerp van ultra-gevoelige sensoren. De ontwikkeling van PAOx met xanthaat eindgroepen en hun gebruik in de synthese van PAOx-goud hybride nanodeeltjes worden beschreven. Daarnaast vertonen deze hybride deeltjes een dubbele

responsiviteit afhankelijk van variatie in temperatuur en de aanwezigheid van ionen in de oplossing. Zulke dubbele responsiviteit kan toepassing vinden in colorimetrische logische poorten. Wat interessant is, is dat deze responsiviteit en het thermisch start signaal, getuned kan worden door variaties in de PAOx samenstelling.

De temperatuursafhankelijke respons van PAOx werd verder onderzocht in combinatie met supramoleculaire host-moleculen in waterige oplossing. Voor zover ons bekend is, bestaat er tot op heden verrassend genoeg geen systematische studie die de invloed van zulke supramoleculaire host-moleculen op de fasetransitie van een thermoresponsief polymeer. Reeds bestaande systemen maken over het algemeen gebruik van weinig gedefinieerde polymeren, die gesynthetiseerd werden door middel van vrije radicalaire polymerizaties, waardoor het bepalen van structuur-eigenschap relaties bemoeilijkt wordt. Ook wordt in deze studies zelden de invloed van de macromoleculaire host op de organisatie van het systeem geëvalueerd. Om dit fascinerende onderwerp verder uit te lichten, werden de thermoresponsieve eigenschappen van een reeks goed gedefinieerde, amfifiele PAOx copolymeren in combinatie met verschillende moleculaire host-moleculen systematisch onderzocht. De transitie temperatuur van de copolymeren kon getuned worden in een uitzonderlijk breed temperatuursinterval. Belangrijker nog, deze gedetailleerde studie heeft ons enerzijds toegelaten om structuur-eigenschap relaties te achterhalen, zodat controle kon verkregen worden over de omkeerbaarheid van deze transitie en anderzijds kon de thermische informatie opgeslagen worden in de supramoleculaire structuur. Dit onderzoek, in welke de synergie van polymeer chemie en supramoleculaire chemie benadrukt wordt, is beschreven in hoofdstukken 5 en 6 van deze dissertatie.



Victor Retamero de la Rosa was born in Valladolid (Castilla y León, Spain) in 1984. After finishing his high-school education, he spent one year practicing theatre before starting his studies of Licenciado en Química at the University of Valladolid. During the academic year 2008-2009, he joined Ghent University as exchange student, within the framework of the Erasmus program. Upon finishing his studies in Valladolid, his interest in polymer and supramolecular chemistry brought him back to Ghent University, where he started a PhD program under the supervision of Prof. Richard Hoogenboom. The most important results obtained during this period are described in the present PhD thesis.

To contact Victor:

Email

- Victor.RetameroDeLaRosa@UGent.be
- VictorRdelaRosa@gmail.com

Linked In

- Victor R. de la Rosa, be.linkedin.com/in/victorrdelarosa/

- ◆ *Work included in the thesis
◇ *Work not included in the thesis**
- ◆ de la Rosa, V. R.; Zhang, Z.; de Geest, Bruno G.; Hoogenboom, R., Colorimetric Logic Gates Based on Novel Poly(2-alkyl-2-Oxazoline) Coated Gold Nanoparticles. ***Submitted***
- ◆ de la Rosa, V. R.; Hoogenboom, R., 2014, Solution Polymeric Temperature Sensors with Long-Term Memory Function Powered by Supramolecular Chemistry. *Chem. Eur. J.* **2014**. DOI: 10.1002/chem.201405161
- ◇ Glassner, M.; Lava, K.; de la Rosa, V. R.; Hoogenboom, R. Tuning the LCST of Poly(2-cyclopropyl-2-oxazoline) via Gradient Copolymerization with 2-Ethyl-2-oxazoline. *J. Polym. Sci. A Polym. Chem.* **2014**, *52*, 3118.
- ◆ de la Rosa, V. R.; Bauwens, E.; Monnery, B. D.; De Geest, B. G.; Hoogenboom, R. Fast and accurate partial hydrolysis of poly(2-ethyl-2-oxazoline) into tailored linear polyethylenimine copolymers. *Polym. Chem.* **2014**, *17*, 4957.
- ◆ Sambe, L.; de la Rosa, V. R.; Belal, K.; Stoffelbach, F.; Lyskawa, J.; Delattre, F.; Bria, M.; Cooke, G.; Hoogenboom, R.; Woisel, P. Programmable Polymer-Based Supramolecular Temperature Sensor with a Memory Function. *Angew. Chem. Int. Ed.* **2014**, *53*, 5044.
- ◆ de la Rosa, V. R. Poly(2-oxazoline)s as materials for biomedical applications. *J. Mater. Sci. Mater. Med.* **2014**, *25*, 1211-1225.
- ◇ Goossens, H.; Catak, S.; Glassner, M.; de la Rosa, V. R.; Monnery, B. D.; De Proft, F.; Van Speybroeck, V.; Hoogenboom, R. Cationic Ring-Opening Polymerization of 2-Propyl-2-oxazolines: Understanding Structural Effects on Polymerization Behavior Based on Molecular Modeling. *ACS Macro Lett.* **2013**, *2*, 651-654.
- ◇ Claeys, B.; Coen, R. D.; De Geest, B. G.; de la Rosa, V. R.; Hoogenboom, R.; Carleer, R.; Adriaensens, P.; Remon, J. P.; Vervaet, C. Structural modifications of polymethacrylates: Impact on thermal behavior and release characteristics of glassy solid solutions. *Eur. J. Pharm. Biopharm.* **2013**, *85*, 1206.
- ◆ de la Rosa, V. R.; Bouten, P. J. M.; Hoogenboom, R. First Symposium on Poly(2-oxazoline)s and Related Pseudo-Polypeptide Structures. *Macromol. Chem. Phys.* **2012**, *213*, 2669.
- ◆ van Kuringen, H. P. C.; de la Rosa, V. R.; Fijten, M. W. M.; Heuts, J. P. A.; Hoogenboom, R. Enhanced Selectivity for the Hydrolysis of Block Copoly(2-oxazoline)s in Ethanol–Water Resulting in Linear Poly(ethylene imine) Copolymers. *Macromol. Rapid Commun.* **2012**, *33*, 827.

Four years have passed since I started the journey that has resulted in this thesis. The beginnings were not easy but fortunately I was surrounded by fantastic people that helped me from the start. The list of people that has not only helped me but also made my everyday life enjoyable could fill many pages, I already apologize for those of you that I forgot to include here.

I would like to thank the members of my reading committee, Prof. Filip Du Prez, Prof. Laetitia Mespouille, and Prof. Patrice Woisel, for doing a very detailed revision of my thesis; you really helped me improving the quality of the final manuscript. Patrice, I had a great time with you in Lille; together with David Fournier and Jöel Lyskawa you made my stays at your laboratories feel very short, as I enjoyed and learned there so much. I hope we keep in touch.

It is easy to identify the person that meant the most to me during this period. This thesis would not exist without the support of Prof. Richard Hoogenboom, who trusted on me from the start. He was always available to help me and motivated me every day. He pushed me to my limits but not without being committed to support me. Doing a PhD thesis can be hard sometimes, but he managed to turn my doubts into motivation and self-confidence every time we had a discussion, which is remarkable. After these four years I have undoubtedly grown as a chemist, but also as a person, and much of this as a result of my interaction with Prof. Hoogenboom. Thank you Richard, you have been my mentor, my guide, and whatever goals I reach in the future will be partially thanks to you, without any doubt.

Prof. Hoogenboom also managed to compose a multicolored group of great people that now constitutes the Supramolecular Chemistry Group. We complement each other very well and I always felt in family with all of them. Qilu, we had a tough start as the first ones but we managed very well! Gertjan, the master of the SEC, thanks for your support setting everything up, including the nice posters! Lenny, Bart, Maarten (Jimmy), Maarten (Jimbo), Kathleen, Dingying, Glenn, Zhanyao, Petra, Bryn, Mathias, Samarendra, Bahar, Kanykei, thanks for being such great colleagues, I have really enjoyed sharing the lab with you guys. Bart, thanks for bringing the group together, it is incredible how people from so many different cultures, religions, and nationalities can be brought together by a common dislike of your music! ;-) You should be hired by the UN! Seriously, thanks for being there always when needed. Coffee breaks and lunches with Kanykei, Mathias, Bryn, Dr. Maji and Joachim are something I have in my heart, always great discussions and the right sentence said from Bryn just when someone passed nearby, "fan-tastic!". Thank you Bryn for sharing your endless knowledge of polyoxazolines with me. Mathias, you are the official source of literature for coffee breaks, but also replied always immediately when I could not access an article. This really helped me writing the thesis and working with you has been a great pleasure. Kathleen, thank you for translating the summary of my thesis and for your help, always with a big smile. I would also like to thank the great guys I had the pleasure to mentor during their Master theses: Huub, Florian, Maarten Mees, Eva, Joachim, you all did a great job and I am very happy I will have the chance of working close to some of you in the future. Thanks also to Martin Fijten (TU/e) for his great support with HFIP-SEC (and Dutch carnival!).

I would like to acknowledge Prof. Filip Du Prez for putting me in contact with Prof. Richard Hoogenboom, event that ultimately meant the first seed of this PhD work. Secondly, for letting us use the PCR Group equipment when we were still setting up our labs at the newborn Supramolecular Chemistry Group. In this regard, the support of Bernhard De Meyer was great, and he always had a smile and a helping hand when I needed it. He and the rest of the members of the PCR group were helpful and it has been always great to visit you upstairs. Milan, Lionel, Fabienne, Peter, Otto, Sofie, Sophie, Xander, Kevin, Steven, Frank (thanks for your great support with the MALDI-ToF)... It was great to meet you guys! Of course I could not forget Daniel Frank, honorary member of the Supra group. Our scientific discussions and coffee breaks are memorable. The very few times that we had a beer, and the many that we went to the gym, were also great ;-)

Special thanks go for Prof. Annemieke Madder and the OBC group; (now Dr.) Qilu Zhang and I were the first in sharing the lab with you in the beginnings and you were always helpful in the

times we were new *inhabitants* of the S4 building. Thanks to Jos Van den Begin for his great support during these years and all the great people with whom I shared coffees, PhD student issues, and furthermore great times. Vicky, Kurt, Lieselot, Ellen, Nathalie, Bram, Matthias, Abhishek, Yara, Eva, Margarida, Smita ... thanks guys for making it so pleasant to work in the lab. I could not forget Prof. Johan Winne, an endless source of chemical (and, during coffee breaks Flemish culture) knowledge, and Duchan Laplace, that always helped me with a big smile.

I could not forget to thank Prof. Bruno G. de Geest and his great crew of students (Zhiyue, Benoit, Nane...) with whom it was a pleasure to work. I always enjoyed my visits to the Pharmacy Department and our scientific discussions. Your enthusiasm when you installed a new piece of equipment (or *toy*) was contagious and I always learnt a lot by your side.

The support of the NMR group and in particular Prof. José Martins, and Tim Courtin is highly appreciated. Especially, I would like to acknowledge Freya van den Broek for her priceless help with DOSY and quantitative NMR measurements. We had a lot of interesting discussions, also together with Dr. Davy Sinnaeve, and I would have liked to include our research in this thesis.

Some experiments that also did not make it in this thesis but nevertheless were a very good experience for me were done in collaboration with Prof. Frederic Lynen. Thank you very much for all the time spent with me, I remember that evening packing an HPLC column, a great experience! Thanks also to all the colleagues at the Separation Science Group, in particular Peter for his technical and IT support. Sorry guys for disrupting the analytical calm at the 4th floor!

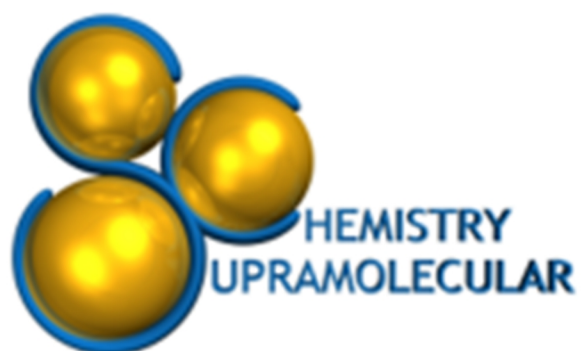
I would also like to thank Prof. Peter Dubruel and the people at the PCB group. Especially Veerle Boterberg for her support and help performing Karl-Fisher and contact angle measurements. And of course, Kenny, Diana(s), Didi, Elke, Myriam... I had a great time with you in Ghent.

A big thank you goes for Prof. Van der Eycken for letting me use some of his equipment and definitely to Jan Goeman, known by some as "the almighty" as he truly helped me any time I had a problem related to science, equipment, analysis... you name it. When I had a problem you were always there, especially after 6-7 PM, when problems usually look even worse!

Thanks to all the admin people that made my way easier through the –especially for a scientist– always obscure world of bureaucracy: Tom Parlevliet, Veerle, Carine, Queenie: thanks a lot! Also to Tom and Paul. Very important the help of the members of the mechanics team, glass-blowing, and electronics that also supported me always (Joris, Marc, Mario, Tim, Theo...). You were there to make some microwave septa for me, Schlenk lines, heating blocks, repair heating plates, pumps, synthesis microwaves, autosamplers... and also gave me priceless technical insights on the equipment I was using and other available. Thank you all for your professional and human quality.

Finally I would like to thank all the people outside the scientific realm that have meant so much for me during these four years. The list of names would go too far to be included here, but you all know I have you in my heart. Lobo, la llegada a Gante no hubiera sido lo mismo sin ti y sin Ali. Koen, Daan, estoy feliz de saber que seréis mis amigos toda la vida. Me ayudasteis muchísimo en mi llegada y nunca lo olvidaré. Amparo, Conchi, Trompi, Miguelito, Julián, María, Paco, Benedicto, Julia, Nuria, Adri, Fernando, Follonero, Yiyus, Eduardo (te voy a echar de menos)... sólo vosotros me llamáis Imagine, y desde luego ¡me dais la vida!. Mis colegas de Pucela, Pako, Chopo, David, Pardo, sois la caña y os echo muchísimo de menos. Por supuesto gracias a mi pequeña Anne-Sophie, por soportar este último año de locura escribiendo la tesis. Espero poder recompensarte por las horas sentado delante del ordenador sin cuidarte como te mereces. Y ya sí, finalmente, mi querida Penélope, y mis padres Begoña y Jose: sin vuestro apoyo incondicional nunca hubiera llegado hasta aquí. Espero haceros felices y que os sintáis orgullosos de mí. Cada día me siento afortunado de teneros a mi lado, aunque estéis lejos. Os tengo siempre en mi mente y mi corazón.

Victor



2014